



Universiteit
Leiden
The Netherlands

Synthesis of chemical tools to study the immune system

Graaff, M.J. van de

Citation

Graaff, M. J. van de. (2023, January 19). *Synthesis of chemical tools to study the immune system*. Retrieved from <https://hdl.handle.net/1887/3512649>

Version: Publisher's Version

License: [Licence agreement concerning inclusion of doctoral thesis in the Institutional Repository of the University of Leiden](#)

Downloaded from: <https://hdl.handle.net/1887/3512649>

Note: To cite this publication please use the final published version (if applicable).

Synthesis of chemical tools to study the immune system

Proefschrift

Ter verkrijging van
de graad van doctor aan de Universiteit Leiden,
op gezag van rector magnificus prof.dr.ir. H. Bijl,
volgens besluit van het college voor promoties
te verdedigen op donderdag 19 januari 2023
klokke 10:00 uur

door

Michel Johan van de Graaff

geboren te Delft

in 1991

Promotores: Prof. dr. S.I. van Kasteren

Prof.dr. H.S. Overkleeft

Promotiecommissie

Overige leden: Prof.dr. J.D.C. Codee

Prof.dr. M. van der Stelt

Dr. D.V. Filippov

Dr. S. Hoogendoorn (Université de
Genève)

Prof.dr. L. Brunsveld (TU Eindhoven)

ISBN: 978-94-6458-821-7

Printed by Ridderprint B.V.

Thesis cover art generated by DALL-E 2

“It is not the mountains ahead to climb that wears you down,
but it is the pebble in your shoe.”

Muhammad Ali

Table of Contents

Chapter 1	1
<i>General introduction</i>	
Chapter 2	15
<i>Conditionally controlled TLR2/6 ligands</i>	
Chapter 3	49
<i>Conditionally controlled intracellular TLR-ligands</i>	
Chapter 4	77
<i>Photo-activatable TLR-ligands</i>	
Chapter 5	107
<i>Summary and Future Prospects</i>	
Nederlandse samenvatting	127
List of publications	129
Curriculum vitae	131
Acknowledgements	132

Chapter 1

General introduction¹

Immune response during host infection and its orchestration

The defense of the host against infection is critically dependent on the *innate* immune system. Mucus, tears, the skin, endothelial cells, and the enzymes of the digestive tract are just a few of the mechanisms with which the host attempts to avoid infection and combat intruders.² This multi-layered system can be seen as the defense of a fortress; with moats, palisades, and wall all contributing to keeping out the invading hordes. Despite these multiple layers, breaches of this defense can still occur. This is where the *adaptive* immune system plays its vital role. The host constantly samples the interior with cells bearing Pattern Recognition Receptors (PRRs); best described as guards patrolling behind the stone buttresses of the fortress.

PRRs recognize Pathogen-Associated Molecular Patterns (PAMPs) that are evolutionary highly conserved.³ They have evolved to recognize molecules that are critical for pathogen survival. A mutation in the PAMPs will almost always result in decreased pathogen viability, which prevents the pathogen to escape detection by mutagenesis. It has become apparent that a wide variety of PAMPs exist, enabling the host to detect a large group of pathogens quickly – without having encountered the pathogen before - via this innate immunity (Figure 1).⁴ PRRs can be divided into two groups: the cytoplasmic receptors and the membrane bound receptors.

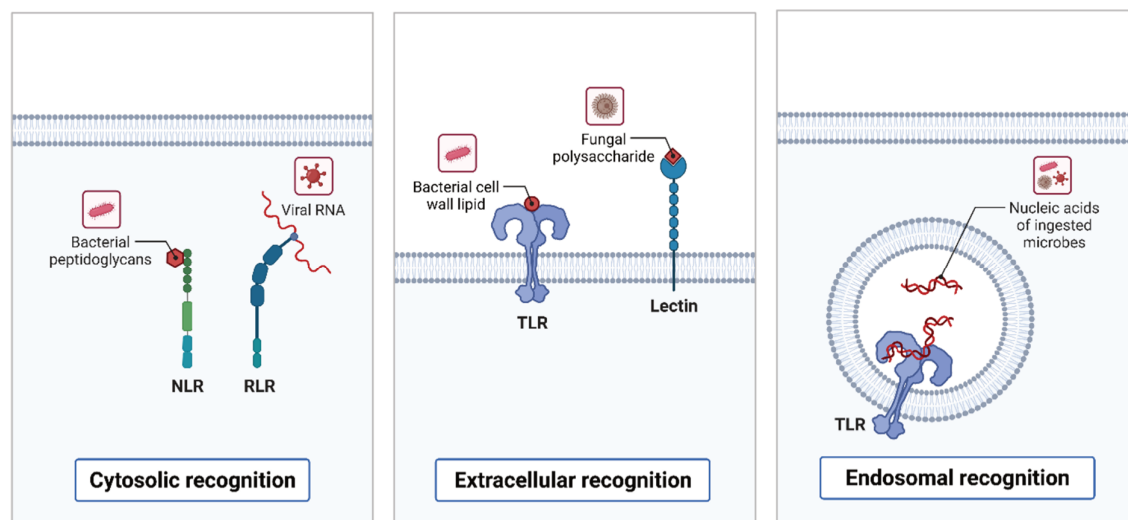


Figure 1. Overview of various PRRs and their respective ligands and cellular localization. Cytosolic recognition is initiated by NLRs and RLRs, whereas the membrane-bound receptors are responsible for either endosomal (TLRs) or extracellular (TLRs and C-type lectins) recognition.

The first group includes the nucleotide-binding oligomerization domain-like I (NLRs)⁵ and retinoic acid-inducible gene-I-like receptors (RLRs)⁶, and the second group includes receptors such as the C-type Lectin Receptors (CLRs)⁷ and the Toll-Like Receptors (TLRs).⁸

Activation of these receptors lead to the start of the immune response, which includes the innate response (e.g., neutrophil recruitment), but also the adaptive immune response, in which a more tailored response to the pathogen is mounted.

For this latter response, the pathogen is proteolytically processed and one or more epitopes are generated from this process and presented on the surface of an antigen presenting cell, which can be sampled by T-cells. The activation of the PRR on the APC then translates to two additional signals: the co-stimulatory signal (upregulation of CD80 and CD86)⁹, and the secretion of cytokines that induce responses appropriate for the pathogen family that induced the initial PRR trigger. Once activated by these three signals, the T-cells can orchestrate the anti-pathogen response, through direct killing of infected cells or the activation of the appropriate other families of immune cells through cytokine signaling. They can also form long-lived memory cells, which allow a faster recognition and immune response during a second infection with the same pathogen.¹⁰ This combination of PRR ligands and a source of epitopes provides the framework within which some modern synthetic vaccines are conceptualized¹¹: one or more ligands for these PRRs are co-delivered with a source of pathogen polypeptide (from whole cell to minimal peptides) that allows the activation of T-cells in a manner appropriate for the pathogen against which the vaccine is aimed; albeit bacterial, viral or tumor.¹² The proper combination of PRR-ligands remains a hurdle and often lies at heart of vaccine failure.¹³

One of the reasons for this is that certain aspects of PRR-biology remain poorly understood. The effect of the location of binding, kinetics, and multivalency of the ligation (when multiple receptors are activated at the same time) on signaling outcomes are not yet known. One PRR can bind multiple ligands at different sites within the receptor leading to different responses, whereas one ligand is able to bind to multiple different PRRs¹⁴ thereby modulating the overall response.¹⁵ PRRs engage in crosstalk and cellular localization of the PRR at the moment of activation can lead to vastly different signaling outputs.¹⁶ Taken together, intracellular – but also intercellular – signaling events within the context of the immune system is quite complex. The toolbox from which the experimental biologist has to pick from to investigate these signaling events is not fitted to deal with such complexity without having to compromise conclusions with significant assumptions. The use of fusion proteins renders many PRRs inactive, and the modification of fluorophores to the ligands – in many cases chemically non-trivial – may also significantly alter the properties of the ligands. The use of inhibitors of specific pathways is also fraught with dangers relating to unexpected side-effects and/or off-targets.¹⁷

The recent emergence of a multidisciplinary approach to answering biological questions aided by design and synthesis of molecules can procure tools that are neatly fitted to the experiment. This thesis describes the process of designing and synthesizing chemical tools that adhere to specific experimental conditions, culminated through continuous feedback from close-collaborating immunobiological experimentalists. This process is contextualized within Toll-Like Receptors, combined with their respective ligands using photo- and/or chemo-protecting groups. The following paragraphs will explore these topics, with a focus on the Toll-Like Receptors, more deeply to aid in appreciating the experiments performed and described throughout this thesis.

Toll-Like Receptors

There are 13 TLR subsets within the mammalian family, of which TLR1 to TLR9 are conserved between humans and mice.¹⁸ Humans have lost the ability to produce TLR11 to TLR13 whereas mice have lost functional TLR10.¹⁹ The structural feats of the TLRs are similar, consisting of an N-terminal ectodomain, one transmembrane domain and a C-terminal cytosolic Toll-interleukin-1 receptor (TIR) domain.²⁰ The ectodomain is characterized by leucine-rich repeats which adopt a structural motif resemblant of horseshoe, and are involved with ligand recognition. The TIR domain is responsible for the recruitment of signaling proteins in the cytosol upon TLR activation.²¹ Based on the predominant cellular localization of the TLRs prior to activation, they can be grouped into two classes: TLR1, TLR2 and TLR4 to TLR6 mainly reside on the plasma membrane, whereas TLR3 and TLR7 to TLR9 are localized intracellularly (Figure 2).¹⁶

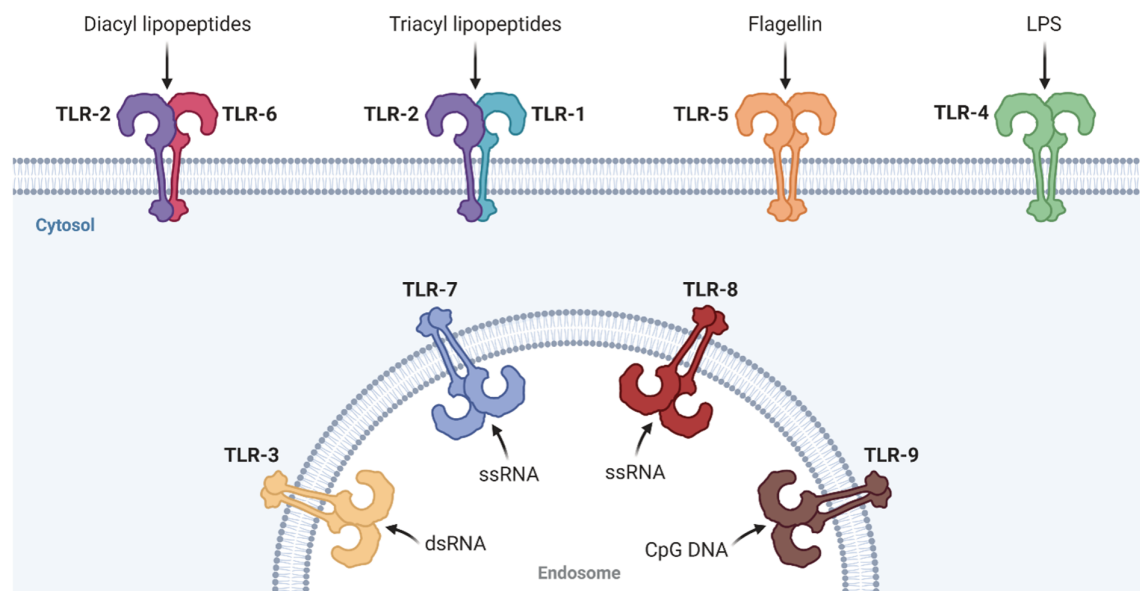


Figure 2. Localizations of TLRs when activated by their respective canonical ligands.

TLRs dimerize upon ligand binding.²⁰ Most TLRs homodimerize, one exception being TLR2 and its interaction partners: it can heterodimerize either with TLR1 or TLR6.^{22,23} PAMP-binding-induced dimerization initiates signal transduction pathways leading to the transcription of genes crucial to host defense. These genes code for pro-inflammatory cytokines and type I interferons (IFN-I).²⁴ Pro-inflammatory cytokine production is induced by the transcription factor nuclear factor κ B (NF- κ B) which translocates to the cell nucleus upon TLR activation.²⁵ Pro-inflammatory cytokines mature cells of the innate immune system and appropriately initiate and organize the adaptive immune response. Production of IFN-I is in turn induced by activation of the members of the interferon regulatory transcription factor (IRF) family.²⁶ IFN-I is involved in a more direct way of inhibiting microbial cell growth, through the transcription of genes with direct antiviral activities.

Plasma membrane-residing TLRs are perpetually exposed to the extracellular environment in which encountering certain PAMPs is more likely. TLR2/1 and TLR2/6 are able to detect the presence of Gram-positive cell wall components such as peptidoglycans and glycolipids as well as viral structural proteins, whereas TLR4/TLR4 can detect Gram-negative cell wall components such as lipopolysaccharide (LPS).^{27–29} TLR5/TLR5 senses the presence of flagellin, another highly evolutionary conserved molecular motif critical for microbial locomotion.³⁰

The TLRs that are exposed to the intracellular environment are sensitive towards nucleic acids derived from microbial origin. The main entry for pathogens is through endocytosis or phagocytosis, and thus these TLRs are found predominantly along these pathways. Presence of these receptors in other subcellular sites may lead to self-sensing of host-derived nucleic acids and may explain why these receptors are restricted to endosomes and phagosomes.³¹ TLR3 senses viral double-stranded RNA³², TLR7 and TLR8 recognize viral single-stranded RNA^{33,34} and TLR9 senses DNA with a high recurrence of unmethylated 5'-Cytosine-Guanine-3' (CpG) motifs.³⁵

Although TLRs are still grouped today as residing in either the plasma membrane or endosomes, it recently became evident that some TLRs have the ability to signal both from the plasma membrane and intracellular vesicles.¹⁶ More interestingly, the cytokine production profile is different when the TLR is activated from these distinct localizations.³⁶ This effect was first discovered for TLR4, which was shown to be able to induce both NF- κ B and IRF activation depending on its localization upon ligand engagement (Figure 3).

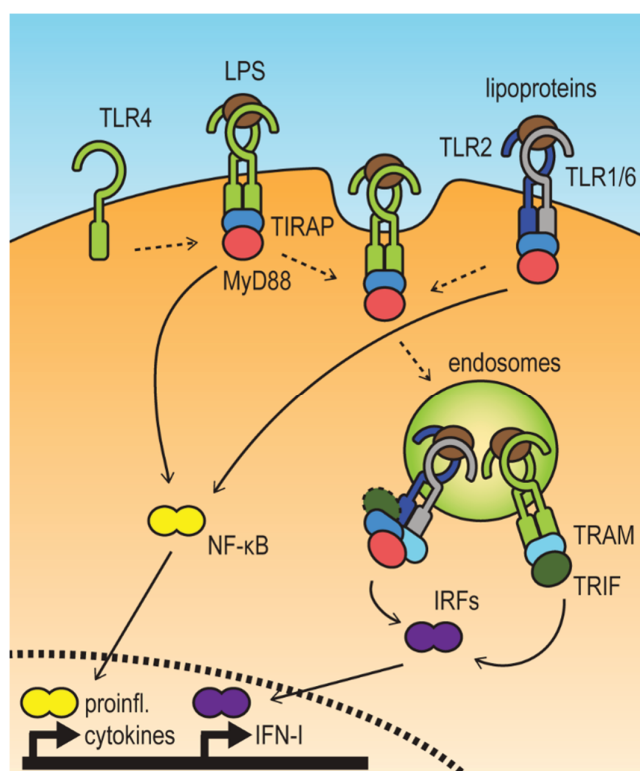


Figure 3. Proposed mechanism for distinct signal transduction pathways for TLR4. Dashed lines represent trafficking pathways; solid lines represent signaling pathways.

Several strategies have since emerged to explore this spatial-dependent activation more deeply. Endocytosis inhibitors restrict trafficking of the TLRs and thus offer insight in sequestered populations of TLRs.^{37,38} Anti-TLR antibodies not only enable the visualization of TLRs during activation-induced translocation of the receptors, but can also prevent ligands to interact with certain receptor populations. Although valuable, these tools come with their disadvantages: specific antibodies against TLRs are difficult to obtain and endocytosis inhibitors do not only affect TLR trafficking events. TLRs have been recombinantly modified with tags against which an antibody *is* available, or fused to fluorescent proteins to address the issue of obtaining anti-TLR antibodies. However, fusion of TLRs with a tag or fluorescent moiety may interfere with receptor signaling and/or ligand binding. Thus, these techniques are not able to observe TLR signaling processes without substantial perturbation of the natural signaling mode-of-action. To study isolated TLR signaling events with minimal alteration to the TLR-signaling platform an alternative strategy is explored in this thesis, namely the use of conditionally controlled ligands: molecules that are only able to activate TLRs when exposed to a non-natural, spatial restricted trigger.

Conditionally controlled ligands

Conditionally controlled TLR ligands are a class of reagents new to field of TLR that show promise of unraveling the above-mentioned spatial – but also temporal – complexity exhibited by the TLR signaling processes. Spatial context can never be imposed when using canonical or synthetic TLR ligands, as they can only activate the TLR-expressing cells in bulk and thus, spatial restrictions have to be implemented in ways that can perturb the system such as co-administering endocytosis inhibitors as described above. A more elegant approach has recently surfaced, in which spatial restrictions have been incorporated as an inherent property of the TLR ligands. This is done by shielding a position within the ligand that is imperative for activation to occur, effectively inactivating the ligand. This protecting group can be conditionally removed; for example, by irradiating a specific volume of the sample with light when using a photolabile protecting group ('photocage') or, as proposed in this thesis, by treating the sample with uncaging reagents that are directed to endosomes or phagosomes when using a chemically labile protecting group ('chemocage').

Photocages

Photocages have been applied (Figure 4) in the design of caged Resiquimod (TLR7/8)³⁹ **1**, Pam₂CSK₄ (TLR2/6)⁴⁰ **2**, pyrimido[5,4-b]-indole **3** (TLR4)⁴¹ and CpG-containing oligodeoxynucleotides (TLR9)⁴² **4**. In the case of compound **2** it was found that the ligand was still able to bind TLR2 but inhibited dimerization with TLR6. This property allows for an even distribution of the ligand prior to activation and enables TLR dimerization and cytokine monitoring within minutes after 'pulling the trigger' (Chapter 2). These chemical tools enabled constraining a volume within the sample to be activated, usually by virtue of a strategically placed mask over the sample. However, the experiment is limited by the scattering of UV photons, as BMDCs rapidly move outside of the irradiation area, and phototoxicity induced by the high-energy UV-irradiation³⁹ necessary for these specific photocages.

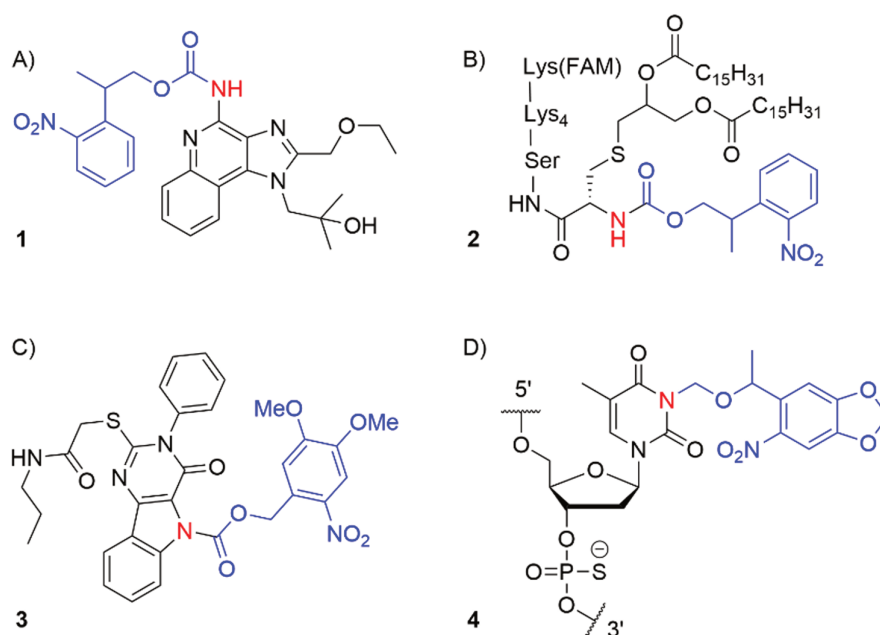


Figure 4. Photocaged TLR ligands. Photocages are indicated in blue whereas the amine critical for activity is indicated in red. A) Resiquimod protected with 2-(2-nitrophenyl)propoxycarbonyl (NPPOC). B) Fluorescein (FAM)-conjugated Pam₂CSK₄K(FAM) protected with NPPOC. C) A pyrimido[5,4-b]-indole protected with nitroveratryloxycarbonyl (NVOC). D) A phosphorothioate-linked thymidine residue as located in a CpG-bearing oligodeoxynucleotide protected with 6-nitropiperonyloxymethyl (NPOM).

Two-photon labile cages pose an obvious answer to some of these limitations, although they would have to be compatible with the synthetic route as the photoprotection step is not usually the final reaction in the synthetic plan. These cages contain highly conjugated systems often with strong electron donor/acceptor couples.⁴³ These properties increase both the number of photons that can be absorbed within a timeframe, and the time within which two photons can arrive in the system to allow electron transition. In such a system, two photons of 700 nm can be absorbed to allow an energetic transition of 350 nm, thus limiting UV-induced phototoxicity. Two photon absorption is quadratically dependent on the light intensity, whereas single photon absorption is linearly dependent on light intensity. This nonlinear scaling means that it will dominate over one photon absorption only at higher intensities. This necessitates the use of ultrashort pulse lasers, as normal LEDs or lasers are unable to reach the photon intensities required to observe significant two-photon absorption. Moreover, the light emitted has to be coherent for 2-photon absorption to occur, a property expressed by lasers but not LEDs. Pulse lasers build up energy over a microsecond timescale and release a pulse of coherent light over an interval in the femtosecond timescale, having a repetition rate of 50-500 MHz. Although these setups are costly, they are capable of irradiating volumes in the femtoliter range.⁴⁴

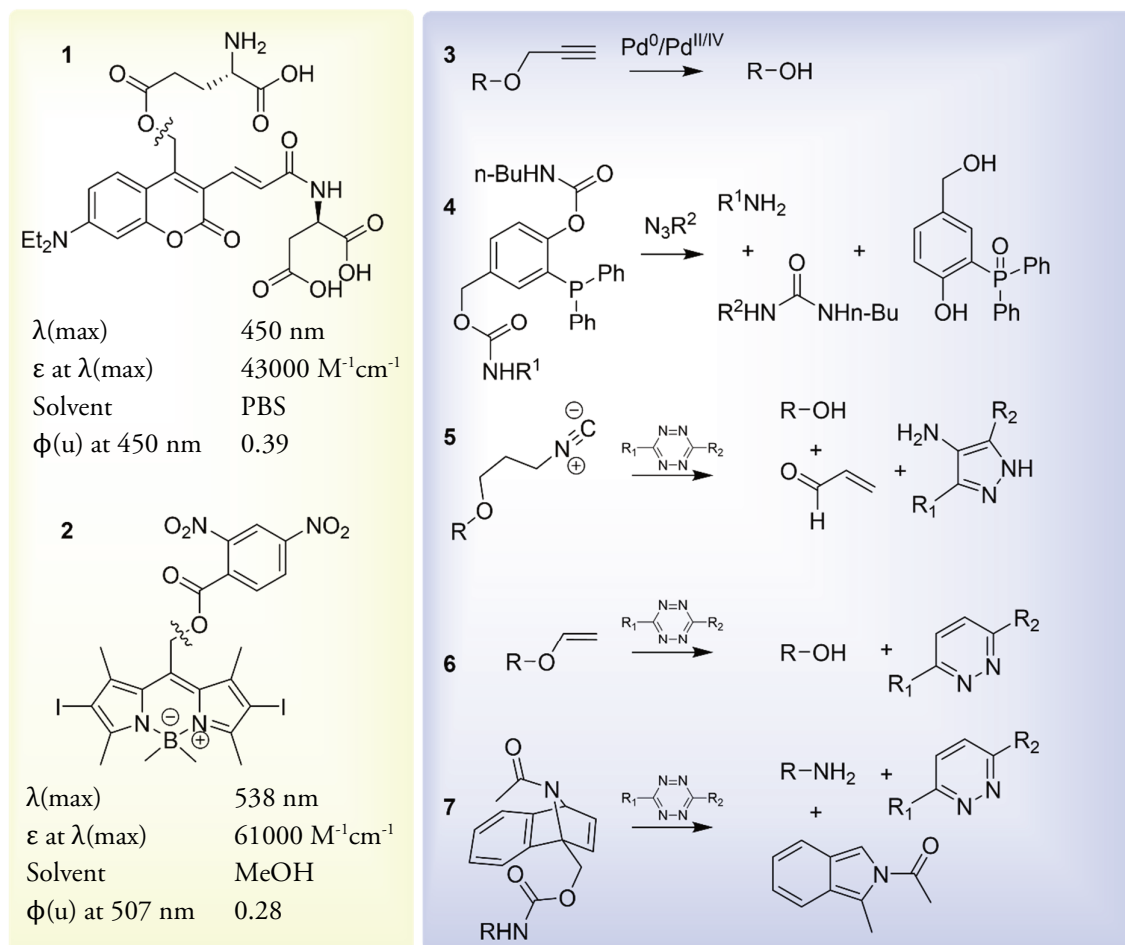
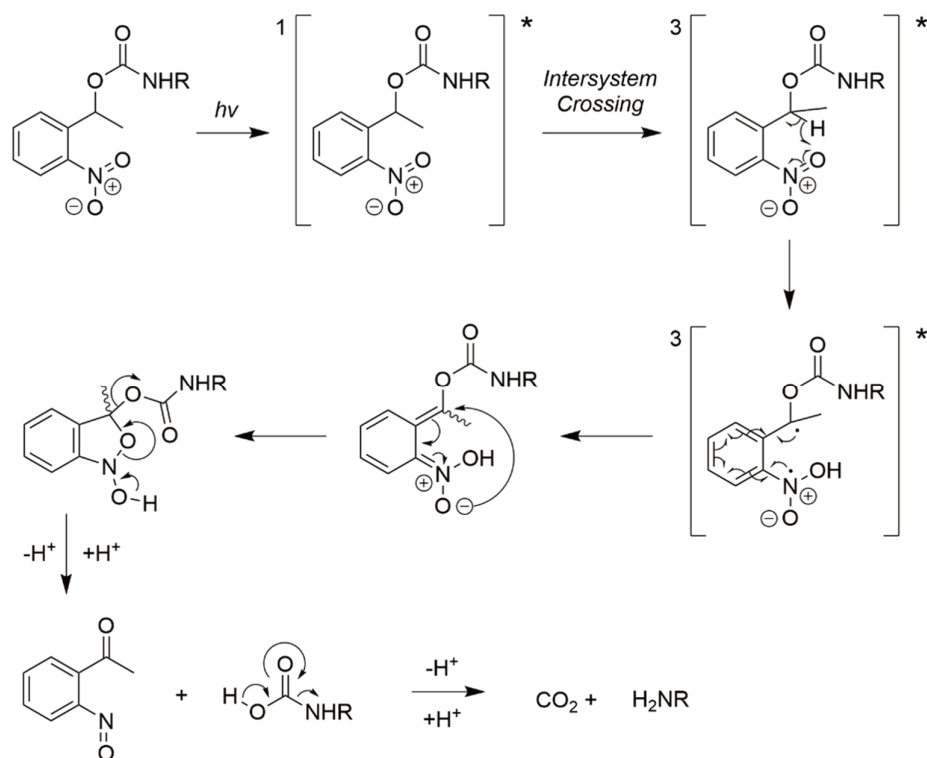


Figure 5. Examples of photo- and chemocages. Yellow box: compound **1** is a coumarin-4-ylmethyl based photocage⁴⁵ and compound **2** is a halogenated BODIPY-derived photocage⁴⁶. Blue box: Several examples of bio-orthogonal chemo-uncaging, including removal of propargyl⁴⁷ by transition metals (**3**), modified Staudinger reactions(**4**)^{48,49} or inverse electron-demand Diels-Alder (IEDDA) reactions employing isocyanides(**5**)⁵⁰, vinyl ethers(**6**)^{51,52}, benzonorbornadienes(**7**)⁵³ with tetrazine derivatives.

Nitrobenzyl cages

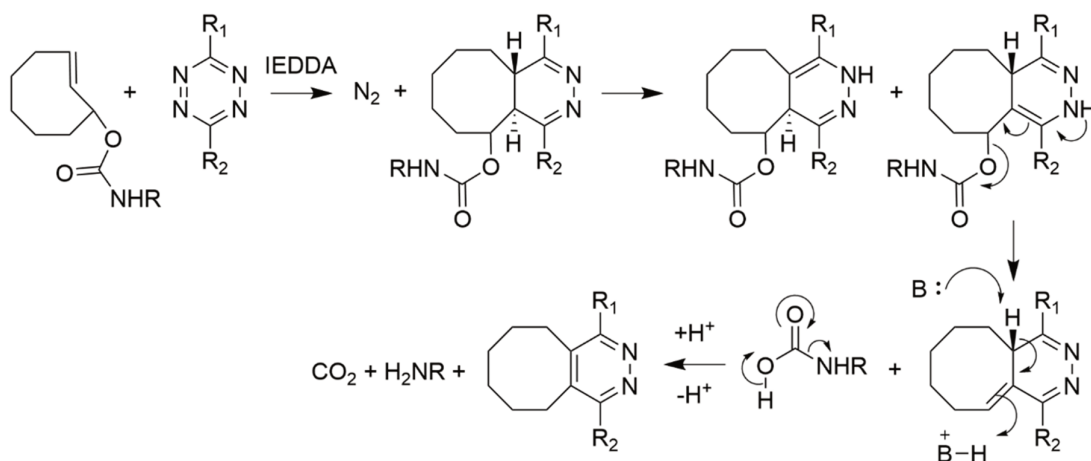
Many conditionally controlled ligands used in biological experiments still make use of 2-nitrobenzyl derived photocages. In the past decade a lot of attention has been focused on photocages with improved photochemical properties over the 2-nitrobenzyl derivatives. These include coumarin-4-ylmethyl⁴⁵-, BODIPY⁴⁶-, arylcarbonylmethyl⁵⁴- and metal⁵⁵-based photoremovable protecting groups (Figure 5). Alternatively, the 2-nitrobenzyl core can be extended with a conjugated ring system to enhance its molar attenuation coefficient ϵ (its efficiency in absorbing photons). This can enable two-photon absorption as it dramatically reduces the light intensities required before significant uncaging occurs.^{56,57} The chemical robustness of these next-generation 2-nitrobenzyl cages make them appealing to use in synthetic routes in which the product has yet to be exposed to multiple reagents. The simplified mechanism with which the 2-nitrobenzyl cages are cleaved can be seen below (Scheme 1) and has been reviewed extensively.^{58–60}



Scheme 1. Deprotection mechanism of benzylic-substituted 2-nitrobenzyls.⁵⁸ Irradiation leads to an excited singlet state, which quickly crosses to an excited triplet state. From here, a hydrogen atom is abstracted from the benzylic carbon to the nitro-group. The radicals rearrange to form the aci-nitro intermediate. This intermediate forms a 5-membered ketal ring which collapses to form the nitroso byproduct and liberates the carbamic acid.

Chemocages

An alternative to photocaging is the use of chemocages. They can be viewed similarly as protecting groups used in organic synthesis, with the important criterion that the uncaging conditions have to be bio-orthogonal. Early examples include removal of alloc⁶¹ or propargyl⁴⁷ by transition metals, modified Staudinger reactions^{48,49} or inverse electron-demand Diels-Alder (IEDDA) reactions employing isocyanides⁵⁰, benzonorbornadienes⁵³, vinyl ethers^{51,52} or cyclooctynes⁶² with tetrazine derivatives. Extra criteria must be added to warrant the use of chemical protecting groups in the context of conditionally controlled TLR ligands. A suitable cage would have to 1) be stable, as TLRs are highly sensitive for small amounts of free, uncaged ligand due to a positive feedback loop exerted by the signaling cascade, 2) uncage quickly, as transcription of the first cytokines start within 15 minutes of activation^{63,64}, and 3) be spatially controllable in its uncaging, in other words its uncaging reagents have to be directable specifically to endosomes. One such reaction was discovered in 2008 by Fox and co-workers: *trans*-cyclooctenes (TCOs) ligate with tetrazines with a rate of 2000 M⁻¹s⁻¹, enabling fast and quantitative reactions at low concentrations.⁶⁵ In 2013, Robillard and co-workers modified the TCO to include a hydroxyl functionality at the 2-position⁶⁶, onto which a payload can be loaded that is released upon tetrazine ligation. The mechanism with which a TCO releases its payload is depicted in Scheme 2.^{67–70}



Scheme 2. The ligation and consequent elimination of 2-O-substituted *trans*-cyclooctenes with tetrazines.

Outline of this thesis

The lack of chemical tools to study spatiotemporal effects in TLR signaling is addressed in Chapter 2. The TLR2/6 ligand Pam₂CSK₄ has been caged with a *trans*-cyclooctene on its N-terminal amine. This resulted in a ligand that binds to TLR2, but only induces activation through heterodimerization with TLR6 when tetrazine is present. This is verified through assessment of functional outcome (cytokine production) as well as visualization of nuclear translocation of fluorescently labeled NF-κB in mouse cells. Interestingly, when the experiment was repeated in human cells, significant TLR2 activity was displayed also in the absence of tetrazine. A variety of modifications on the ligand has been tested and resulted in a ligand that is desensitized to activate TLR2/6 in the absence of tetrazine, even in primary human cells.

Chapter 3 describes the synthesis of several TLR ligands that have a TCO on a position that is critical for TLR activation. The strategy described in Chapter 2 is extended and applied to ligands for TLR7, TLR8 and TLR9. A TCO-caged deoxycytidine has been made amenable for solid-phase oligonucleotide synthesis to produce caged CpG-containing DNA fragments. Lastly, the concept of caged TLR ligands is extended towards an *in vivo* application in which an anti-tumor antibody has been conjugated to a TLR7/8 ligand, Resiquimod, through a bifunctional TCO. Some tetrazine derivatives have been shown to be non-toxic in concentrations necessary to effect dissociation of TCO and its payload⁷¹ and thus potentially can be exploited to initiate TLR downstream signaling within the tumor environment.

In Chapter 4, various known photocages are modified to include a second functionality that enables conjugation to a nucleophile. This effectively led to a light-labile linker, or 'photo-linker'. The second functionality broadens the scope of its utility to be included in-line as a building block in solid-phase peptide and DNA/RNA synthesis to create photolabile peptide or DNA/RNA sequences. Moreover, it also offers a platform to alter some of the photocage's properties such as its aqueous solubility by introducing hydrophilic moieties. One of the next-generation 2-nitrobenzyl

photocages, NPBF⁵⁶, has also been modified such that conjugation to two molecules of interest is now possible.

Chapter 5 offers a summary of the above research and some suggestions for future applications. For example, the above-mentioned modified NPBF linker has been applied in the synthesis of a conjugate able to eradicate chemotherapeutic-resistant multiple-myeloma cells *in vitro*. The linker has also been used as a probe that can tag CD8+ T cells in human primary tumor tissue and enables isolation of cells of interest on a single cell resolution, both upon low-dose photo-irradiation.

References

- (1) Oosenbrug, T.; van de Graaff, M. J.; Rensing, M. E.; van Kasteren, S. I. Chemical Tools for Studying TLR Signaling Dynamics. *Cell Chem. Biol.* **2017**, *24* (7), 801–812.
- (2) Medzhitov, R.; Janeway, Charles S. J. Innate Immune Recognition: Mechanisms and Pathways: Innate Immune Recognition. *Immunol. Rev.* **2000**, *173* (1), 89–97.
- (3) Akira, S.; Takeda, K.; Kaisho, T. Toll-like Receptors: Critical Proteins Linking Innate and Acquired Immunity. *Nat. Immunol.* **2001**, *2* (8), 675–680.
- (4) Kumagai, Y.; Akira, S. Identification and Functions of Pattern-Recognition Receptors. *J. Allergy Clin. Immunol.* **2010**, *125* (5), 985–992.
- (5) Kanneganti, T.-D.; Lamkanfi, M. Intracellular NOD-like Receptors in Host Defense and Disease. *Immunity*, **2007**, *27* (4), 549–559.
- (6) Loo, Y.-M.; Gale, M. Immune Signaling by RIG-I-like Receptors. *Immunity*, **2011**, *34* (5), 680–692.
- (7) Kingeter, L. M.; Lin, X. C-Type Lectin Receptor-Induced NF- κ B Activation in Innate Immune and Inflammatory Responses. *Cell. Mol. Immunol.* **2012**, *9* (2), 105–112.
- (8) Fitzgerald, K. A. Toll-like Receptors and the Control of Immunity. *Cell*, **2020**, *180* (6), 1044–1066.
- (9) Rahman, A. H.; Taylor, D. K.; Turka, L. A. The Contribution of Direct TLR Signaling to T Cell Responses. *Immunol. Res.* **2009**, *45* (1), 25–36.
- (10) Mercier, B. C.; Cottalorda, A.; Coupet, C.-A.; Marvel, J.; Bonnefoy-Bérard, N. TLR2 Engagement on CD8 T Cells Enables Generation of Functional Memory Cells in Response to a Suboptimal TCR Signal. *J. Immunol.* **2009**, *182* (4), 1860–1867.
- (11) Ingale, S.; Wolfert, M. A.; Gaekwad, J.; Buskas, T.; Boons, G.-J. Robust Immune Responses Elicited by a Fully Synthetic Three-Component Vaccine. *Nat. Chem. Biol.* **2007**, *3* (10), 663–667.
- (12) Moyle, P. M.; Dai, W.; Zhang, Y.; Batzloff, M. R.; Good, M. F.; Toth, I. Site-Specific Incorporation of Three Toll-Like Receptor 2 Targeting Adjuvants into Semisynthetic, Molecularly Defined Nanoparticles: Application to Group A Streptococcal Vaccines. *Bioconjug. Chem.* **2014**, *25* (5), 965–978.
- (13) Jones, L. H. Recent Advances in the Molecular Design of Synthetic Vaccines. *Nat. Chem.* **2015**, *7* (12), 952–960.
- (14) Zhang, Z.; Ohto, U.; Shibata, T.; Krayukhina, E.; Taoka, M.; Yamauchi, Y.; Tanji, H.; Isobe, T.; Uchiyama, S.; Miyake, K.; Shimizu, T. Structural Analysis Reveals That Toll-

- like Receptor 7 Is a Dual Receptor for Guanosine and Single-Stranded RNA. *Immunity* **2016**, *45* (4), 737–748.
- (15) Wittmann, A.; Lamprinak, D.; Bowles, K. M.; Katzenellenbogen, E.; Knirel, Y. A.; Whitfield, C.; Nishimura, T.; Matsumoto, N.; Yamamoto, K.; Iwakura, Y.; Saijo, S.; Kawasaki, N. Dectin-2 Recognizes Mannosylated O-Antigens of Human Opportunistic Pathogens and Augments Lipopolysaccharide Activation of Myeloid Cells. *J. Biol. Chem.* **2016**, *291* (34), 17629–17638.
 - (16) McGettrick, A. F.; O'Neill, L. A. Localisation and Trafficking of Toll-like Receptors: An Important Mode of Regulation. *Curr. Opin. Immunol.* **2010**, *22* (1), 20–27.
 - (17) *Exocytosis and Endocytosis*; Ivanov, A. I., Ed.; Methods in molecular biology; Humana Press: Totowa, N.J, **2008**.
 - (18) Rehli, M. Of Mice and Men: Species Variations of Toll-like Receptor Expression. *Trends Immunol.* **2002**, *23* (8), 375–378.
 - (19) Hasan, U.; Chaffois, C.; Gaillard, C.; Saulnier, V.; Merck, E.; Tancredi, S.; Guet, C.; Brière, F.; Vlach, J.; Lebecque, S.; Trinchieri, G.; Bates, E. E. M. Human TLR10 Is a Functional Receptor, Expressed by B Cells and Plasmacytoid Dendritic Cells, Which Activates Gene Transcription through MyD88. *J. Immunol.* **2005**, *174* (5), 2942–2950.
 - (20) Botos, I.; Segal, D. M.; Davies, D. R. The Structural Biology of Toll-like Receptors. *Structure* **2011**, *19* (4), 447–459.
 - (21) Jenkins, K. A.; Mansell, A. TIR-Containing Adaptors in Toll-like Receptor Signalling. *Cytokine* **2010**, *49* (3), 237–244.
 - (22) Kang, J. Y.; Nan, X.; Jin, M. S.; Youn, S.-J.; Ryu, Y. H.; Mah, S.; Han, S. H.; Lee, H.; Paik, S.-G.; Lee, J.-O. Recognition of Lipopeptide Patterns by Toll-like Receptor 2-Toll-like Receptor 6 Heterodimer. *Immunity* **2009**, *31* (6), 873–884.
 - (23) Jin, M. S.; Kim, S. E.; Heo, J. Y.; Lee, M. E.; Kim, H. M.; Paik, S.-G.; Lee, H.; Lee, J.-O. Crystal Structure of the TLR1-TLR2 Heterodimer Induced by Binding of a Tri-Acylated Lipopeptide. *Cell* **2007**, *130* (6), 1071–1082.
 - (24) Tseng, P.-H.; Matsuzawa, A.; Zhang, W.; Mino, T.; Vignali, D. A. A.; Karin, M. Different Modes of Ubiquitination of the Adaptor TRAF3 Selectively Activate the Expression of Type I Interferons and Proinflammatory Cytokines. *Nat. Immunol.* **2010**, *11* (1), 70–75.
 - (25) Li, Q.; Verma, I. M. NF- κ B Regulation in the Immune System. *Nat. Rev. Immunol.* **2002**, *2* (10), 725–734.
 - (26) Honda, K.; Taniguchi, T. IRFs: Master Regulators of Signalling by Toll-like Receptors and Cytosolic Pattern-Recognition Receptors. *Nat. Rev. Immunol.* **2006**, *6* (9), 644–658.
 - (27) Mancini, R. J.; Stutts, L.; Ryu, K. A.; Tom, J. K.; Esser-Kahn, A. P. Directing the Immune System with Chemical Compounds. *ACS Chem. Biol.* **2014**, *9* (5), 1075–1085.
 - (28) Barton, G. M. Viral Recognition by Toll-like Receptors. *Semin. Immunol.* **2007**, *19* (1), 33–40.
 - (29) Thompson, J.; Iwasaki, A. Toll-like Receptors Regulation of Viral Infection and Disease☆. *Adv. Drug Deliv. Rev.* **2008**, *60* (7), 786–794.
 - (30) Hayashi, F.; Smith, K. D.; Ozinsky, A.; Hawn, T. R.; Yi, E. C.; Goodlett, D. R.; Eng, J. K.; Akira, S. The Innate Immune Response to Bacterial α -agellin Is Mediated by Toll-like Receptor 5. **2001**, *410*, 5.

- (31) Lee, B. L.; Barton, G. M. Trafficking of Endosomal Toll-like Receptors. *Trends Cell Biol.* **2014**, *24* (6), 360–369.
- (32) Alexopoulou, L.; Holt, A. C.; Medzhitov, R.; Flavell, R. A. Recognition of Double-Stranded RNA and Activation of NF-KB by Toll-like Receptor 3. *Nature* **2001**, *413* (6857), 732–738.
- (33) Heil, F. Species-Specific Recognition of Single-Stranded RNA via Toll-like Receptor 7 and 8. *Science* **2004**, *303* (5663), 1526–1529.
- (34) Lund, J. M.; Alexopoulou, L.; Sato, A.; Karow, M.; Adams, N. C.; Gale, N. W.; Iwasaki, A.; Flavell, R. A. Recognition of Single-Stranded RNA Viruses by Toll-like Receptor 7. *Proc. Natl. Acad. Sci.* **2004**, *101* (15), 5598–5603.
- (35) Hemmi, H.; Takeuchi, O.; Kawai, T.; Kaisho, T.; Sato, S.; Sanjo, H.; Matsumoto, M.; Hoshino, K.; Wagner, H.; Takeda, K.; Akira, S. A Toll-like Receptor Recognizes Bacterial DNA. *Nature* **2000**, *408* (6813), 740–745.
- (36) Tan, Y.; Kagan, J. C. Microbe-Inducible Trafficking Pathways That Control Toll-like Receptor Signaling: TAN ET AL. *Traffic* **2017**, *18* (1), 6–17.
- (37) Kagan, J. C.; Su, T.; Horng, T.; Chow, A.; Akira, S.; Medzhitov, R. TRAM Couples Endocytosis of Toll-like Receptor 4 to the Induction of Interferon- β . *Nat. Immunol.* **2008**, *9* (4), 361–368.
- (38) Tatematsu, M.; Yoshida, R.; Morioka, Y.; Ishii, N.; Funami, K.; Watanabe, A.; Saeki, K.; Seya, T.; Matsumoto, M. Raftlin Controls Lipopolysaccharide-Induced TLR4 Internalization and TICAM-1 Signaling in a Cell Type-Specific Manner. *J. Immunol.* **2016**, *196* (9), 3865–3876.
- (39) Ryu, K. A.; Stutts, L.; Tom, J. K.; Mancini, R. J.; Esser-Kahn, A. P. Stimulation of Innate Immune Cells by Light-Activated TLR7/8 Agonists. *J. Am. Chem. Soc.* **2014**, *136* (31), 10823–10825.
- (40) Mancini, R. J.; Stutts, L.; Moore, T.; Esser-Kahn, A. P. Controlling the Origins of Inflammation with a Photoactive Lipopeptide Immunopotentiator. *Angew. Chem. Int. Ed.* **2015**, *54* (20), 5962–5965.
- (41) Stutts, L.; Esser-Kahn, A. P. A Light-Controlled TLR4 Agonist and Selectable Activation of Cell Subpopulations. *ChemBioChem* **2015**, *16* (12), 1744–1748.
- (42) Govan, J. M.; Young, D. D.; Lively, M. O.; Deiters, A. Optically Triggered Immune Response through Photocaged Oligonucleotides. *Tetrahedron Lett.* **2015**, *56* (23), 3639–3642.
- (43) Chung, S.-J.; Kim, K.-S.; Lin, T.-C.; He, G. S.; Swiatkiewicz, J.; Prasad, P. N. Cooperative Enhancement of Two-Photon Absorption in Multi-Branched Structures. *J. Phys. Chem. B* **1999**, *103* (49), 10741–10745.
- (44) Brown, E. B.; Shear, J. B.; Adams, S. R.; Tsien, R. Y.; Webb, W. W. Photolysis of Caged Calcium in Femtoliter Volumes Using Two-Photon Excitation. *Biophys. J.* **1999**, *76* (1), 489–499.
- (45) Givens, R. S.; Matuszewski, B.; Athey, P. S.; Stoner, M. R. Photochemistry of Phosphate Esters: An Efficient Method for the Generation of Electrophiles. *6*.
- (46) Umeda, N.; Takahashi, H.; Kamiya, M.; Ueno, T.; Komatsu, T.; Terai, T.; Hanaoka, K.; Nagano, T.; Urano, Y. Boron Dipyrromethene As a Fluorescent Caging Group for Single-Photon Uncaging with Long-Wavelength Visible Light. *ACS Chem. Biol.* **2014**, *9* (10), 2242–2246.

- (47) Li, J.; Yu, J.; Zhao, J.; Wang, J.; Zheng, S.; Lin, S.; Chen, L.; Yang, M.; Jia, S.; Zhang, X.; Chen, P. R. Palladium-Triggered Deprotection Chemistry for Protein Activation in Living Cells. *Nat. Chem.* **2014**, *6* (4), 352–361.
- (48) Azoulay, M.; Tuffin, G.; Sallem, W.; Florent, J.-C. A New Drug-Release Method Using the Staudinger Ligation. *Bioorg. Med. Chem. Lett.* **2006**, *16* (12), 3147–3149.
- (49) van der Gracht, A. M. F.; de Geus, M. A. R.; Camps, M. G. M.; Ruckwardt, T. J.; Sarris, A. J. C.; Bremmers, J.; Maurits, E.; Pawlak, J. B.; Posthoorn, M. M.; Bongers, K. M.; Filippov, D. V.; Overkleeft, H. S.; Robillard, M. S.; Ossendorp, F.; van Kasteren, S. I. Chemical Control over T-Cell Activation *in Vivo* Using Deprotection of *Trans*-Cyclooctene-Modified Epitopes. *ACS Chem. Biol.* **2018**, *13* (6), 1569–1576.
- (50) Tu, J.; Xu, M.; Parvez, S.; Peterson, R. T.; Franzini, R. M. Bioorthogonal Removal of 3-Isocyanopropyl Groups Enables the Controlled Release of Fluorophores and Drugs *in Vivo*. *J. Am. Chem. Soc.* **2018**, *140* (27), 8410–8414.
- (51) Jiménez-Moreno, E.; Guo, Z.; Oliveira, B. L.; Albuquerque, I. S.; Kitowski, A.; Guerreiro, A.; Boutureira, O.; Rodrigues, T.; Jiménez-Osés, G.; Bernardes, G. J. L. Vinyl Ether/Tetrazine Pair for the Traceless Release of Alcohols in Cells. *Angew. Chem. Int. Ed.* **2017**, *56* (1), 243–247.
- (52) Neumann, K.; Jain, S.; Gambardella, A.; Walker, S. E.; Valero, E.; Lilienkampf, A.; Bradley, M. Tetrazine-Responsive Self-Immolative Linkers. *ChemBioChem* **2017**, *18* (1), 91–95.
- (53) Xu, M.; Tu, J.; Franzini, R. M. Rapid and Efficient Tetrazine-Induced Drug Release from Highly Stable Benzonorbornadiene Derivatives. *Chem. Commun.* **2017**, *53* (46), 6271–6274.
- (54) Sheehan, J. C.; Umezawa, K. Phenacyl Photosensitive Blocking Groups. *J. Org. Chem.* **1973**, *38* (21), 3771–3774.
- (55) Zayat, L.; Calero, C.; Alborés, P.; Baraldo, L.; Etchenique, R. A New Strategy for Neurochemical Photodelivery: Metal–Ligand Heterolytic Cleavage. *J. Am. Chem. Soc.* **2003**, *125* (4), 882–883.
- (56) Komori, N.; Jakkampudi, S.; Motoishi, R.; Abe, M.; Kamada, K.; Furukawa, K.; Katan, C.; Sawada, W.; Takahashi, N.; Kasai, H.; Xue, B.; Kobayashi, T. Design and Synthesis of a New Chromophore, 2-(4-Nitrophenyl)Benzofuran, for Two-Photon Uncaging Using near-IR Light. *Chem. Commun.* **2016**, *52* (2), 331–334.
- (57) Momotake, A.; Lindegger, N.; Niggli, E.; Barsotti, R. J.; Ellis-Davies, G. C. R. The Nitrodibenzofuran Chromophore: A New Caging Group for Ultra-Efficient Photolysis in Living Cells. *Nat. Methods* **2006**, *3* (1), 35–40.
- (58) Klán, P.; Šolomek, T.; Bochet, C. G.; Blanc, A.; Givens, R.; Rubina, M.; Popik, V.; Kostikov, A.; Wirz, J. Photoremovable Protecting Groups in Chemistry and Biology: Reaction Mechanisms and Efficacy. *Chem. Rev.* **2013**, *113* (1), 119–191.
- (59) Bardhan, A.; Deiters, A. Development of Photolabile Protecting Groups and Their Application to the Optochemical Control of Cell Signaling. *Curr. Opin. Struct. Biol.* **2019**, *57*, 164–175.
- (60) Il'ichev, Y. V.; Schwörer, M. A.; Wirz, J. Photochemical Reaction Mechanisms of 2-Nitrobenzyl Compounds: Methyl Ethers and Caged ATP. *J. Am. Chem. Soc.* **2004**, *126* (14), 4581–4595.

- (61) Sasmal, P. K.; Streu, C. N.; Meggers, E. Metal Complex Catalysis in Living Biological Systems. *Chem Commun* **2013**, 49 (16), 1581–1587.
- (62) Zheng, Y.; Ji, X.; Yu, B.; Ji, K.; Gallo, D.; Csizmadia, E.; Zhu, M.; Choudhury, M. R.; De La Cruz, L. K. C.; Chittavong, V.; Pan, Z.; Yuan, Z.; Otterbein, L. E.; Wang, B. Enrichment-Triggered Prodrug Activation Demonstrated through Mitochondria-Targeted Delivery of Doxorubicin and Carbon Monoxide. *Nat. Chem.* **2018**, 10 (7), 787–794.
- (63) Lee, R. E. C.; Walker, S. R.; Savery, K.; Frank, D. A.; Gaudet, S. Fold Change of Nuclear NF-KB Determines TNF-Induced Transcription in Single Cells. *Mol. Cell* **2014**, 53 (6), 867–879.
- (64) Lee, T. K.; Denny, E. M.; Sanghvi, J. C.; Gaston, J. E.; Maynard, N. D.; Hughey, J. J.; Covert, M. W. A Noisy Paracrine Signal Determines the Cellular NF-KB Response to Lipopolysaccharide. *Science Signaling*, **2009**, 2 (93), ra65.
- (65) Blackman, M. L.; Royzen, M.; Fox, J. M. Tetrazine Ligation: Fast Bioconjugation Based on Inverse-Electron-Demand Diels–Alder Reactivity. *J. Am. Chem. Soc.* **2008**, 130 (41), 13518–13519.
- (66) Versteegen, R. M.; Rossin, R.; ten Hoeve, W.; Janssen, H. M.; Robillard, M. S. Click to Release: Instantaneous Doxorubicin Elimination upon Tetrazine Ligation. *Angew. Chem. Int. Ed.* **2013**, 52 (52), 14112–14116.
- (67) Li, J.; Chen, P. R. Development and Application of Bond Cleavage Reactions in Bioorthogonal Chemistry. *Nat. Chem. Biol.* **2016**, 12 (3), 129–137.
- (68) Tu, J.; Xu, M.; Franzini, R. M. Dissociative Bioorthogonal Reactions. *ChemBioChem* **2019**, 20 (13), 1615–1627.
- (69) Rossin, R.; Versteegen, R. M.; Wu, J.; Khasanov, A.; Wessels, H. J.; Steenbergen, E. J.; ten Hoeve, W.; Janssen, H. M.; van Onzen, A. H. A. M.; Hudson, P. J.; Robillard, M. S. Chemically Triggered Drug Release from an Antibody-Drug Conjugate Leads to Potent Antitumour Activity in Mice. *Nat. Commun.* **2018**, 9 (1), 1484.
- (70) Rossin, R.; van Duijnhoven, S. M. J.; ten Hoeve, W.; Janssen, H. M.; Kleijn, L. H. J.; Hoebe, F. J. M.; Versteegen, R. M.; Robillard, M. S. Triggered Drug Release from an Antibody–Drug Conjugate Using Fast “Click-to-Release” Chemistry in Mice. *Bioconjug. Chem.* **2016**, 27 (7), 1697–1706.
- (71) Rossin, R.; Versteegen, R. M.; Wu, J.; Khasanov, A.; Wessels, H. J.; Steenbergen, E. J.; ten Hoeve, W.; Janssen, H. M.; van Onzen, A. H. A. M.; Hudson, P. J.; Robillard, M. S. Chemically Triggered Drug Release from an Antibody-Drug Conjugate Leads to Potent Antitumour Activity in Mice. *Nat. Commun.* **2018**, 9 (1), 1484.

Chapter 2

Conditionally controlled TLR2/6 ligands^{1,2}

Introduction

Toll-like receptor 2 (TLR 2) is localized on the surface plasma membrane. Like most TLRs, it is expressed predominantly in dendritic cells and macrophages.³ Agonist binding and heterodimerization with either TLR1 or TLR6 initiates downstream signaling transduction.^{4,5} The acylation pattern of the ligand dictates which dimer is stabilized: Pam₃CSK₄ (Figure 1C) engages the TLR2/1 signaling pathway⁶, whereas Pam₂CSK₄ engages the TLR2/6 signaling pathway.^{4,5}

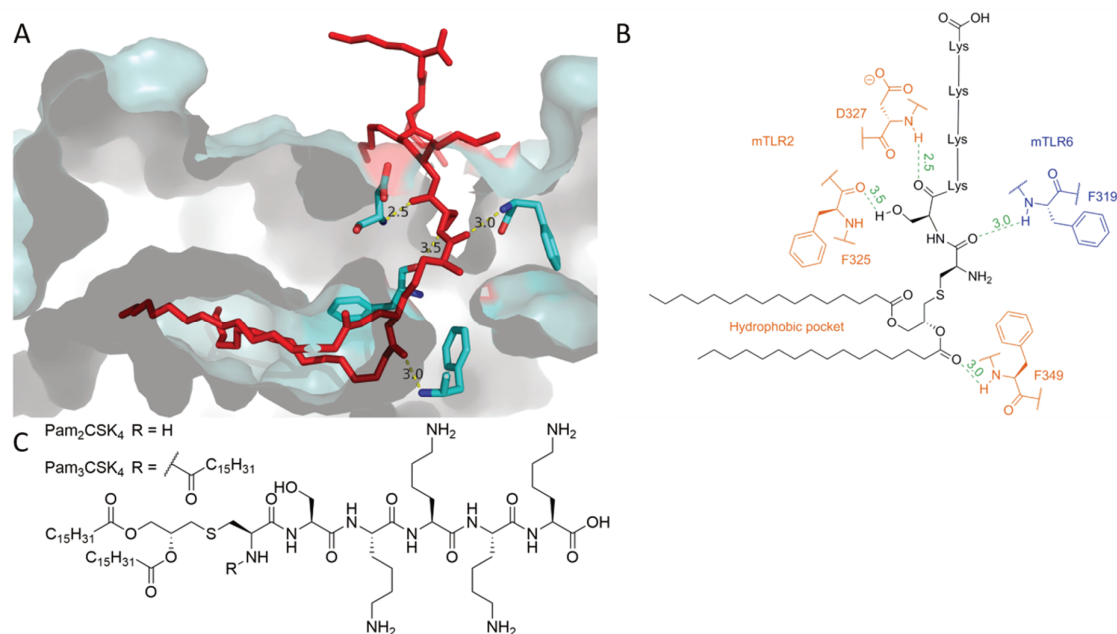


Figure 1. Ligand binding of Pam₂CSK₄ to TLR2/6 A) Surface rendering of the crystal structure of Pam₂CSK₄-bound TLR2/6⁴. Key interacting residues are highlighted with putative hydrogen bond lengths (Å). B) Schematic representation of A). Depicted in orange are TLR2 residues, depicted in blue a TLR6 residue. Green dashed lines represent potential hydrogen bonds with calculated distances noted in Ångström units of length. The four C-terminal lysine residues of the ligand have no interaction with the TLR2/6 complex. The two palmitoyl tails fit inside a hydrophobic pocket present on TLR2. C) Structures of Pam₂CSK₄ and Pam₃CSK₄.

Crystal structure analysis of the TLR2/1-Pam₃CSK₄ complex revealed that two palmitoyl tails of Pam₃CSK₄ are anchored within a hydrophobic pocket inside the TLR2 ectodomain.⁵ The third palmitoyl tail, present on the N-terminus of the ligand, bridges the gap between TLR2 and TLR1 and is anchored within a hydrophobic tunnel of the TLR1 ectodomain, facilitating stabilization of the dimer. When considering the TLR2/6 dimer however, the hydrophobic tunnel in TLR6

(structurally similar to TLR1) is blocked by the side-chains of two phenylalanine residues, precluding anchoring of the palmitoyl tail and thus binding with Pam₃CSK₄.⁴ Instead, another phenylalanine residue (F319, Figure 1B) is located on the dimerization interface, capable of forming a hydrogen bond with the cysteine-serine amide bond in the ligand. For this interaction to occur any acylation on the N-terminus of the ligand is excluded, thus Pam₂CSK₄ gains selectivity for TLR2/6 whereas Pam₃CSK₄ is selective for TLR2/1.

Recently, it became evident that not only the ligand structure can dictate signaling outcome of TLRs, but also the cellular localization in the cell where the receptor is activated.^{7,8} This was first exemplified in the activation of TLR4, signaling events of which induce the production of pro-inflammatory cytokines and type I interferons (IFN-I).⁹ Presence of inhibitors that block endocytosis prevented the production of IFN-I, but not of pro-inflammatory cytokines.^{7,8} The signaling pathways are differentially engaged through recruitment of specific adaptor proteins on the cytosolic domain of TLR dimers. It is now believed the spatially distinct pathways are engaged in a sequential manner, meaning the adaptor molecule responsible for pro-inflammatory cytokine production is displaced by recruitment of the adaptor protein responsible for IFN-I production as the TLR4-ligand complex translocates to endosomes.

The signaling platforms present on cell surface-residing TLR2 resemble that of TLR4, both recruiting TIRAP and MyD88 to activate NF-κB. However, different adaptors are recruited in endosomally localized TLRs. Yet not much is known about the bifurcation of TLR2 signaling, in part due to the lack of chemical tools in the immunologist's repertoire. Until now, endocytosis inhibitors were the prime choice of reagent to probe for spatiotemporal effects, but these can perturb other cellular processes to such extent that experimental outcome cannot be entirely conclusive.¹⁰

A ligand's activity needs to be spatially and temporally controlled in order to accurately decouple spatiotemporal complexity in TLR activation. The aim was therefore to synthesize TLR2/6 ligands that were able to be activated on demand, with the ultimate goal of decoupling endosomal activation from cell surface TLR activation. Mancini *et al.* found that protecting the N-terminal amine of Pam₂CSK₄ with an *ortho*-nitrobenzyl (*o*-NB) derived biologically compatible protecting group – or 'cage' – precludes TLR2/6 dimerization, but not binding to TLR2.¹¹ This enables pretreatment of cells with the caged ligand, priming all the TLR2s for dimerization. Removal of the cage by applying light as an external trigger restored dimerization with TLR6 thus achieving temporal control over TLR activation. Spatial control is limited by the accuracy with which the apparatus can irradiate the sample, the scattering of the UV-photons as well as the minimum irradiation time (as BMDCs rapidly move outside the irradiation area within the minimum timeframe needed to photo-uncage¹²).

Although these limitations can be overcome with two-photon irradiation, where volumes as small as 1 femtoliter can be irradiated with near-IR light¹³, the aim was to explore the use of chemo-labile cages to selectively activate TLRs in endosomes. To this end, a suitable cage would have to 1) be stable, as TLRs are highly sensitive for small amounts of free ligand due to a positive feedback loop exerted by the signaling cascade, 2) uncage quickly, as transcription of the first cytokines start

within 15 minutes of activation^{14,15}, and 3) be spatial controllable in its uncaging: its uncaging reagents have to be directable specifically to endosomes.

One such cage was discovered in 2008 by Prof. Joseph Fox. The Fox lab discovered that *trans*-cyclooctenes (TCOs) ligate with tetrazines with a rate of $2000 \text{ M}^{-1}\text{s}^{-1}$, enabling fast and quantitative reactions at low concentrations (Figure 2).¹⁶ In 2013, Marc Robillard and co-workers modified the TCO to include a hydroxyl functionality at the 2-position that would allow it to function as a bio-compatible release reaction.¹⁷

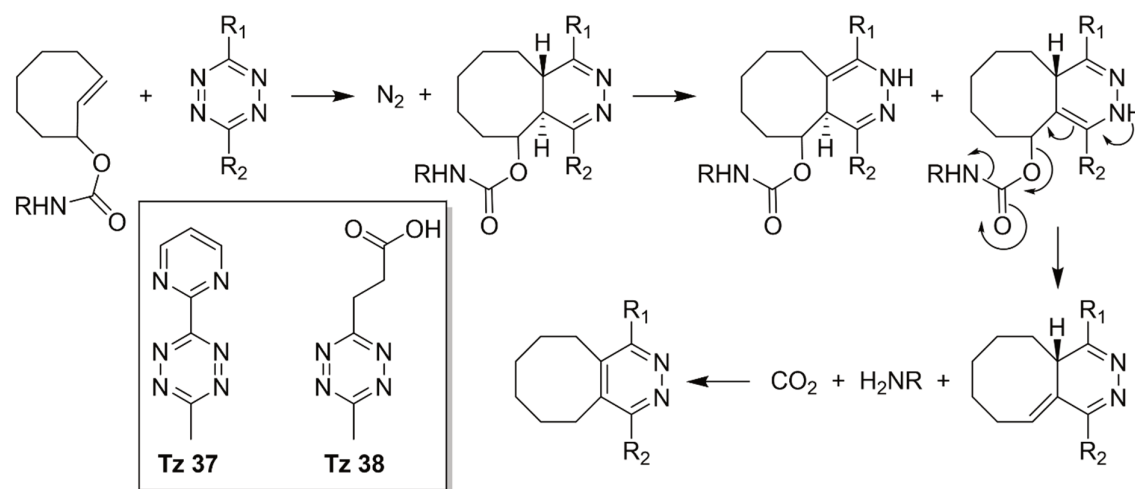


Figure 2. Ligation of a tetrazine and 2-alkoxy-TCO. Inverse electron demand Diels-Alder ligation of the tetrazine with the TCO leads to expulsion of nitrogen and formation of the adduct. Tautomerization leads to two structural isomers of which one is primed for consequent elimination. Structures of tetrazines employed in this chapter are given.

Amines that are coupled to this hydroxyl through a carbamylation are released upon ligation of tetrazine and subsequent tautomerization. As the axial isomer of the hydroxyl is more reactive and less sterically hindered towards elimination, isolation of this isomer comes with a rate constant of $7.9 \times 10^4 \text{ M}^{-1}\text{s}^{-1}$ in water at 20°C . This pioneering work initiated the possibility of bio-orthogonally uncaging quantitatively, in a short timeframe at low concentrations with a reagent that appears non-toxic, even *in vivo*.^{18,19} The tetrazine reaction partner can be modified to alter the reaction kinetics²⁰, or to restrict cell permeability by incorporating ionic substituents or by immobilization onto a surface. For a fast ligation one R-substituent needs to have an electron-withdrawing character, whereas the elimination step is heavily reliant on the second R-substituent to be non-electron-withdrawing. Building on this knowledge, tetrazine **37** (Figure 2) was developed by the group of Peng Chen, to exert the highest uncaging activity in living cells.²⁰ Since then Sarris and co-workers have developed even faster tetrazines, carrying aminoethyl substituents at the para-position.²¹

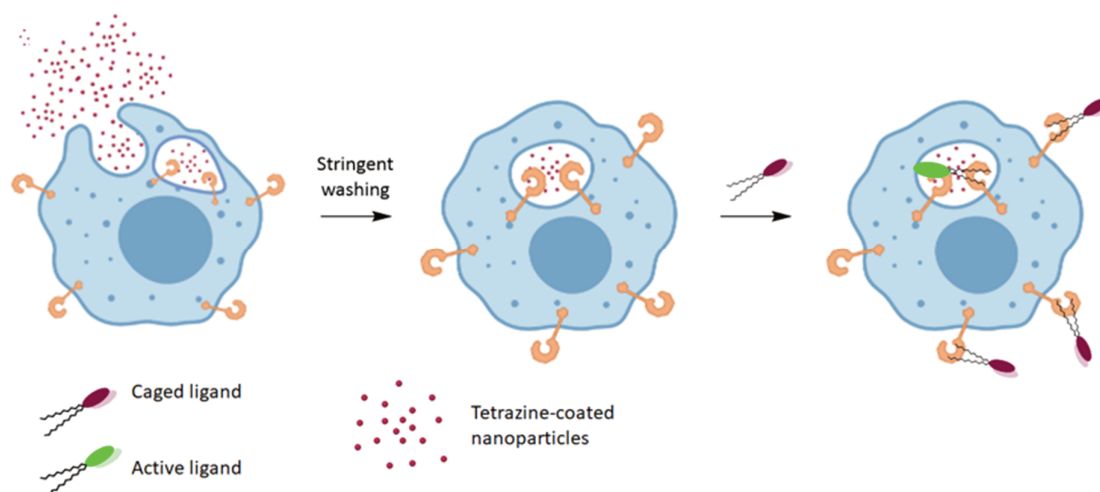
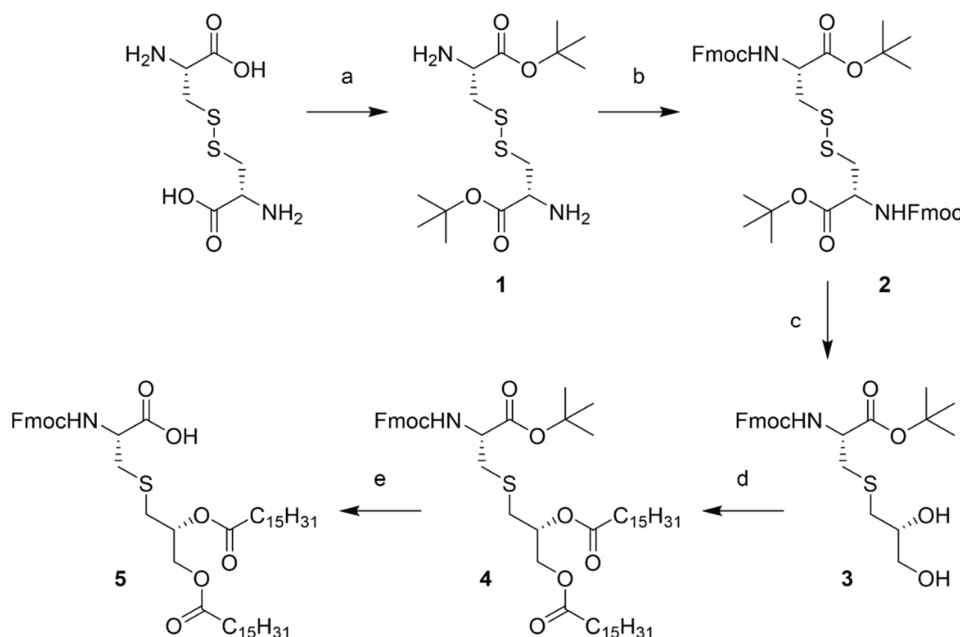


Figure 3. A strategy to activate intracellular TLRs. First the cells are treated with tetrazine-coated nanoparticles which are taken up through phago- and endocytic pathways. After a stringent washing procedure, the cells are treated with TCO-caged TLR-ligand. Liberation of the ligand from its cage should now be prevalent in intracellular vesicles as opposed to the extracellular environment.

It was envisaged that the localization of tetrazines in endosomes by immobilization of tetrazine **38** onto nano-sized amine-coated beads could yield endosome-selective deprotection agents. These beads would be endocytosed by the DC or macrophage, after which a stringent washing procedure would remove all remaining extracellular beads. Treatment with the caged ligand would then result in accumulation of free ligand only inside endosomes carrying the tetrazine beads. Alternatively, were the tetrazine to be sufficiently derivatized with electron-withdrawing groups, the reaction rate of elimination drops to zero whilst maintaining proper ligation kinetics. It was envisaged that decoration of such a tetrazine with cell permeability-restricting entities would lead to a valuable tool to inactivate TCO-bearing species on the cell surface. In other words, treatment of cells that are primed with caged ligand with such a tetrazine would result in permanently inactive *surface-residing only* TLR-ligand complexes. A second treatment with a *cell-permeable* tetrazine would then uncage all endosomally localized ligands. These are two hypothetical examples with which the TCO-tetrazine reaction can be used to spatially control TLR activity. In the context of TLR2/6, the lipopeptide Pam₂CSK₄ had to be functionalized with axial 2-TCO on the N-terminal amine. *Cis*-cyclooctene does not ligate with tetrazine at a significant reaction rate, but the similarity in the chemophysical properties makes it a useful control compound. Thus, both TCO- and CCO-bearing ligands were synthesized in parallel.

Results and Discussion

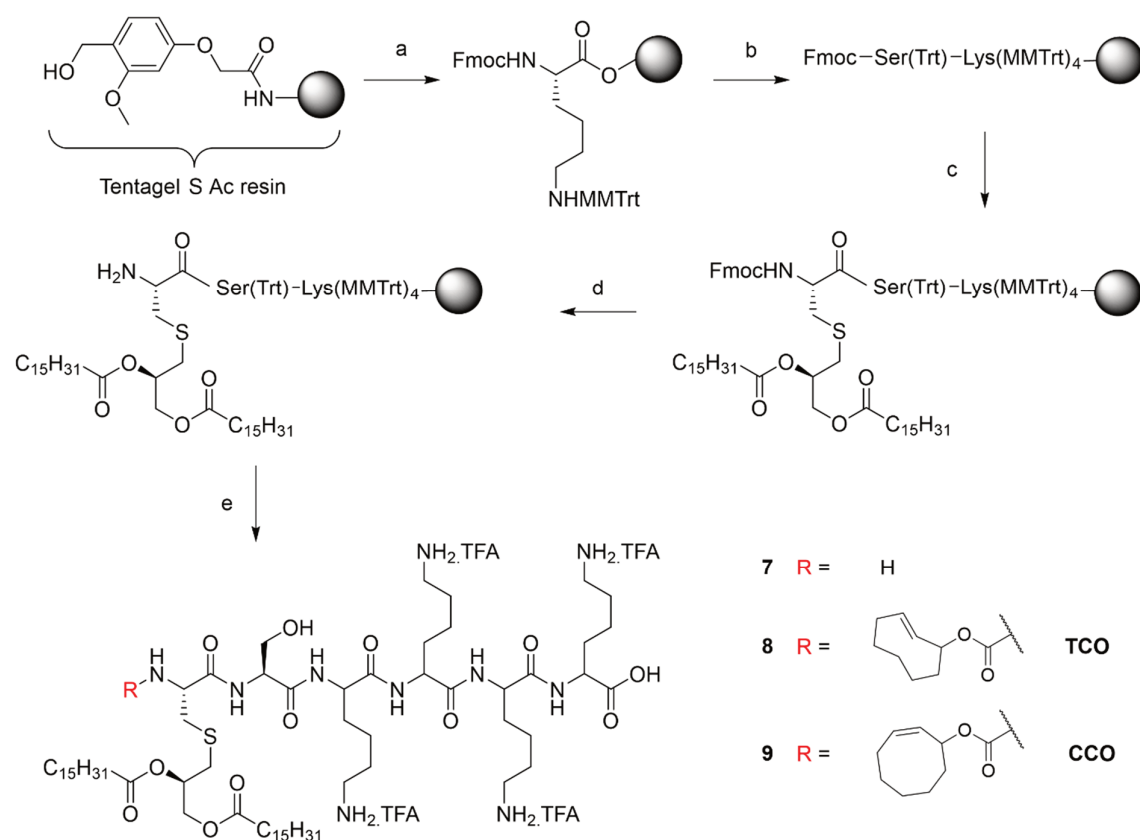
The synthesis of Pam₂CSK₄ and its protected derivatives focused on obtaining chirally pure R-Pam₂Cys, as the S-epimer of Pam₂CSK₄ is significantly less active.²² This building block was obtained on gram-scale starting from relatively cheap starting materials as illustrated in Scheme 1.²³



Scheme 1. Synthesis of chiral pure Fmoc-Pam₂Cys-OH (R-epimer) building block on multi-gram scale. **a)** *t*-butyl acetate, 70% HClO₄, r.t., 75 hrs, qt.; **b)** Fmoc-OSu, N-methyl morpholine, THF, r.t., 2 hrs, 68%; **c)** (i) Zn powder (10 μm), 93:6:1 MeOH:37% HCl (aq.):98% H₂SO₄, r.t., 15 min (ii) R-(+)-glycidol, r.t., 72 hrs, 78%; **d)** Palmitic acid, diisopropylcarbodiimide, DMAP, DCM, r.t., o.n., 95%; **e)** TFA, r.t., 1 hr, qt.

L-Cystine was protected as a *tert*-butyl ester in a transesterification reaction catalyzed by perchloric acid after which a fluorenylmethyl oxycarbonyl was installed on both amines. The disulfide bridge was reduced using activated zinc powder in an acidic environment after which enantiopure R-glycidol was added to alkylate the liberated thiol in a one-pot procedure. The zinc powder was observed to aggregate 10 minutes after the addition of the acidic mixture which corresponded with completion of the disulfide reduction. Interestingly, when the zinc powder was removed at this stage, addition of R-glycidol did not result in any product formation, whilst robust product formation was observed in the flask that did contain zinc. This indicated an – as yet unidentified – functional role of the zinc in the alkylation step. Esterification with palmitic acid, diisopropylcarbodiimide and a catalytic amount of DMAP resulted in di-protected compound **4**. Removal of the *tert*-butyl group with neat TFA yielded Fmoc-Pam₂Cys-OH **5** in a 50% overall yield on a multi-gram scale.

A facile method of synthesizing (caged) Pam₂CSK₄ derivatives is by making use of Fmoc-based solid-phase peptide synthesis (SPPS) as the C→N synthesis allows the introduction of the TCO in the final step. The relatively labile TCO therefore did not have to endure multiple coupling and deprotection steps. However, global deprotection often involves highly concentrated mixtures of TFA, observed to have the potential to isomerize or even eliminate 2-oxo-*trans*-cyclooctenes. Global deprotection strategies involving basic conditions may in turn hydrolyze the palmitoyl esters present on the cysteine residue. Therefore, a strategy was chosen where global deprotection can be carried out in dilute TFA using monomethyltrityl (MMTrt) protecting groups and the highly acid labile S-Ac linker.



Scheme 2. Synthesis of TCO/CCO-caged P_2CSK_4 . Reagents and conditions: **a)** Fmoc-Lys(MMTTrt), diisopropylcarbo-diimide, DMAP, r.t., o.n.; **b)** (i) 20% piperidine in DMF, r.t., 10 min (3x) (ii) amino acid (0.6 M in DMF), HCTU (0.6 M in DMF), DiPEA (0.6 M in DMF), r.t., 2 hrs (iii) 5% acetic anhydride in DMF (containing 0.1 M DiPEA), r.t., 10 min; **c)** (i) 20% piperidine in DMF, r.t., 10 min (3x) (ii) HCTU (0.6 M in DMF), **5** (0.6 M in DMF), DiPEA (0.6 M in DMF), r.t., 2 hrs (iii) 5% acetic anhydride in DMF (containing 0.1 M DiPEA), r.t., 10 min; **d)** 20% piperidine in DMF, r.t., 10 min (3x); **e)** Compound **7**: 20% TFA, 2.5% TIS and 2.5% H_2O in DCM, r.t., 1 hr; Compound **8**: (i) TCO-OSu, DiPEA, DMF, r.t., o.n. (ii) 5% TFA, 2.5% TIS and 2.5% H_2O in DCM, r.t., 1 hr; Compound **9**: (i) CCO-OSu, DiPEA, DMF, r.t., o.n. (ii) 5% TFA, 2.5% TIS and 2.5% H_2O in DCM, r.t., 1 hr.

Using standard Fmoc-based SPPS coupling/deprotection cycles (HCTU / piperidine in DMF), H_2N -Pam₂CS(Trt)(K(MMTTrt))₄ was obtained on resin (Scheme 2). The free amine was treated either with axial TCO-OSu or CCO-OSu and DiPEA. Global deprotection with 5% TFA in DCM appeared sufficient to cleave the product from the resin, although due to the extreme lipophilicity of the product standard precipitation methods failed. Cooling the precipitation solvent to $-20^{\circ}C$ and centrifuging at $4^{\circ}C$ for several hours yielded some precipitation, but not in a consistent manner. Direct injection of the crude deprotection mixture (reconstituted in DMSO after evaporation) on HPLC seemed the only viable strategy to consistently afford product isolation, albeit in poor (4% overall) yield. HPLC using 0.1% TFA as a mobile phase modifier is preferentially avoided due to the aforementioned acidic lability of 2-oxo-TCO. However, basic HPLC buffers such as ammonium carbonate proved impractical, as the deprotonated lysine amines

affected the polarity in favor of hydrophobic interactions to such degree that no suitable gradient system was found that yielded pure product. The ionization in the HPLC-MS was also affected to such degree that no ion threshold count could be reached to initiate sample collection. Therefore, TCO-Pam₂CSK₄ was purified on HPLC using 0.1% TFA as a mobile phase modifier. Care was taken when concentrating the collected fractions, as prolonged concentration at elevated temperatures was observed to lead to isomerization or hydrolysis of the TCO, resulting in contamination of free ligand or permanently silenced ligand in the final product.

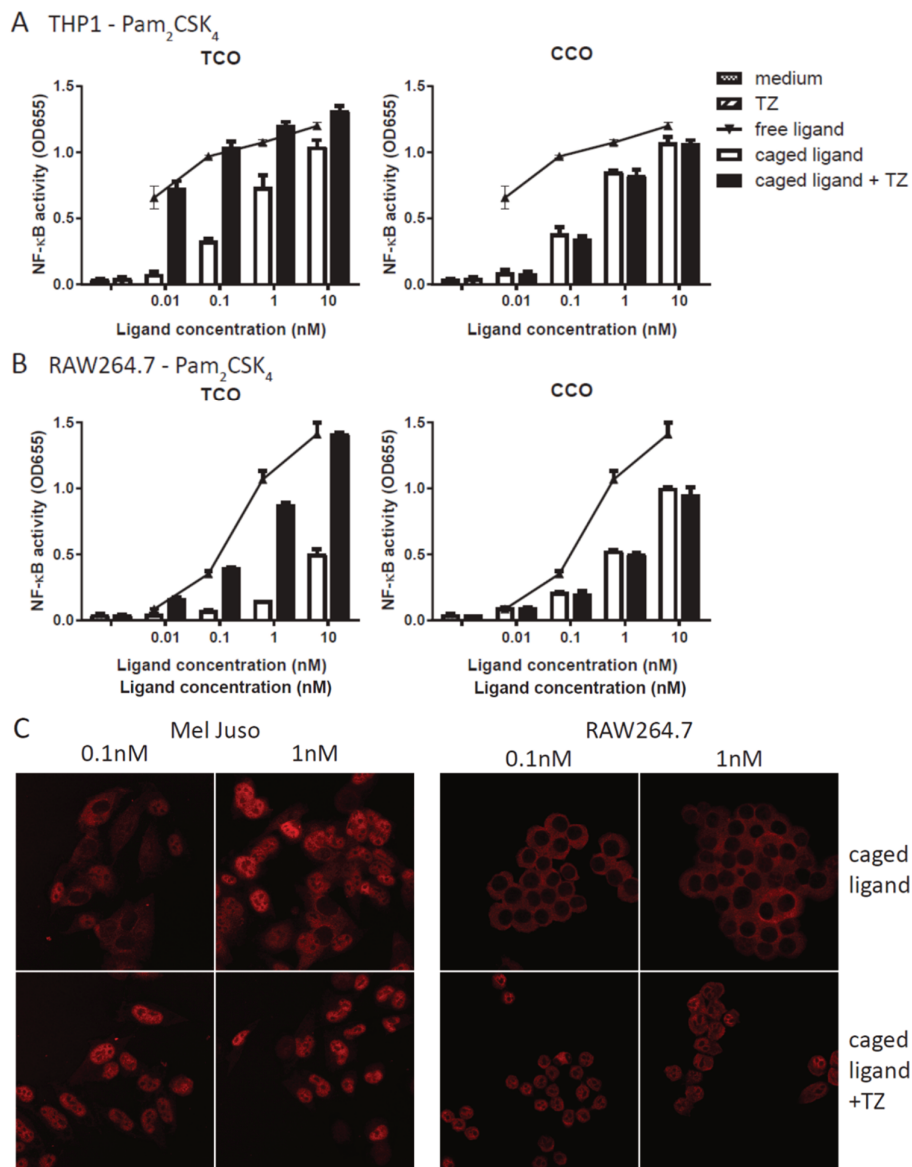


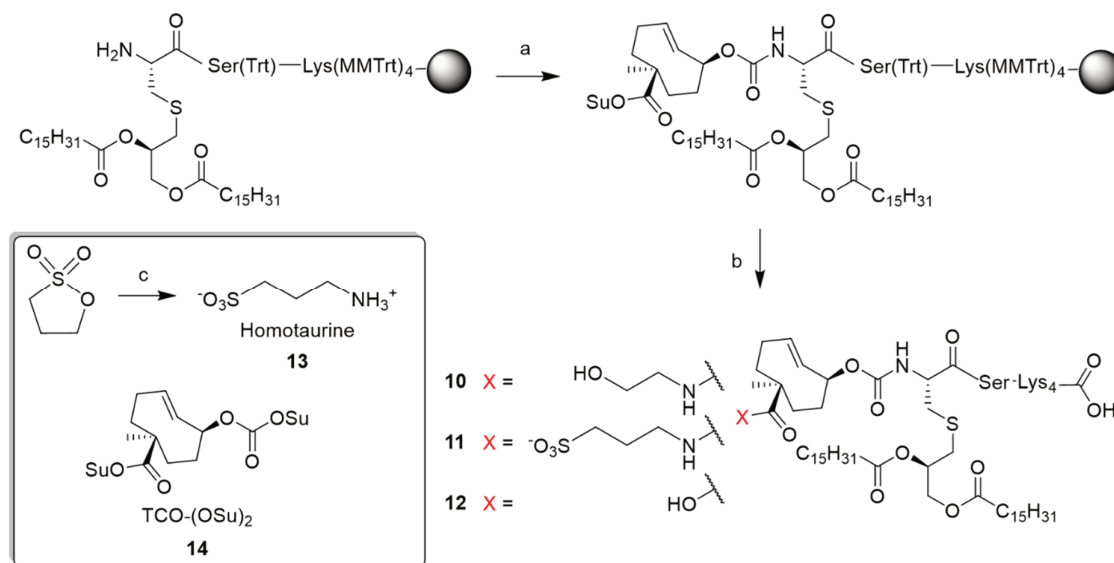
Figure 4. Chemical uncaging of Pam₂CSK₄-TCO induces NF-κB activation both in human THP1-Dual (A) or murine RAW-Blue (B) cells were pre-incubated with the indicated ligands for 45 min. Fresh medium +/- tetrazine was added and after 24hrs NF-κB activity was measured in the culture supernatant using a SEAP colorimetric assay. (C) Cells were pre-incubated with Pam₂CSK₄-TCO for 45 min. Cells were washed and fresh medium +/- tetrazine was added. After 30 min cells were fixed and stained for p65 (NFκB). Experiments were carried out by Timo Oosenbrug (LUMC).

The distinctness of the activation profile between human and mouse TLR2/6 activation was of primary interest. Therefore, the uncaging reaction of compounds **8** and **9** was tested on both a human cell line (THP1-Dual) and murine (RAW264.7) cell line (Figure 4). THP1-Dual is a monocyte cell line containing two inducible reporter constructs: the NF- κ B-pathway can be monitored by activity of Secreted Embryonic Alkaline Phosphatase (SEAP) and simultaneously the IRF-pathway can be monitored by the activity of secreted luciferase (Lucia).

RAW-Blue is a mouse macrophage cell line with a SEAP reporter construct inducible by NF- κ B, expressing all TLR's except TLR5. The cells were incubated either with compounds **8** or **9** for 45 minutes prior to the addition of a 10 μ M solution of tetrazine **37** (Figure 2), or no addition of tetrazine. SEAP levels were measured in the culture supernatant as a measure of NF- κ B activity. The level of NF- κ B activity for the CCO-caged compounds is independent of addition of tetrazine **37**, exhibiting only residual activity of the caged ligand. The TCO-caged ligand does react with the tetrazine, resulting in an increase of NF- κ B activity at every concentration range for both cell types. Interestingly, the RAW macrophages require a 100-fold higher concentration of ligand to achieve the same level of activation when compared to the THP1 cells. The nuclear translocation of NF- κ B was visualized using p65-RFP expressing Mel Juso (human) and RAW264.7 cells under confocal microscopy (Figure 4C). The p65-RFP is a fluorescently labeled subunit of the NF- κ B complex which translocates to the cell nucleus upon TLR2/6 activation. The murine cells exhibited several concentrations in which a favorable window of uncaging existed: activating almost every cell which was inactive prior the addition of tetrazine **37**. Surprisingly, no concentration exhibiting a favorable window of uncaging existed when Mel Juso cells were employed.

It was hypothesized that the *cis/trans*-cyclooctene either undergo hydrophobic-hydrophobic interactions with a hydrophobic patch present on hTLR6 but not mTLR6, or that the cages suffer from insufficient bulk to counteract the dimerization of TLR2/6. Since no crystal structure of hTLR2/hTLR6 is available, it was chosen to append either a small or a large hydrophilic group from the existing cage that would probe which of these effects were causing background activity. For the small-to-medium appendages, linkers containing alcohols, sulfonates or monodisperse ethylene glycols were chosen. For the large appendage, the small protein ubiquitin was chosen. Ubiquitin is an 8.6 kDa water soluble, accessible and thermally stable protein containing seven lysine residues, useable as sites of conjugation.²⁴

Introducing the hydrophilic appendage in TCO-caged Pam₂CSK₄ was facilitated by using the recently published bis-functionalized TCO-(OSu)₂ (compound **14**, Scheme 3).²⁵ Amines react regioselectively with the NHS-carbonate prior to reacting with the sterically hindered NHS-ester.

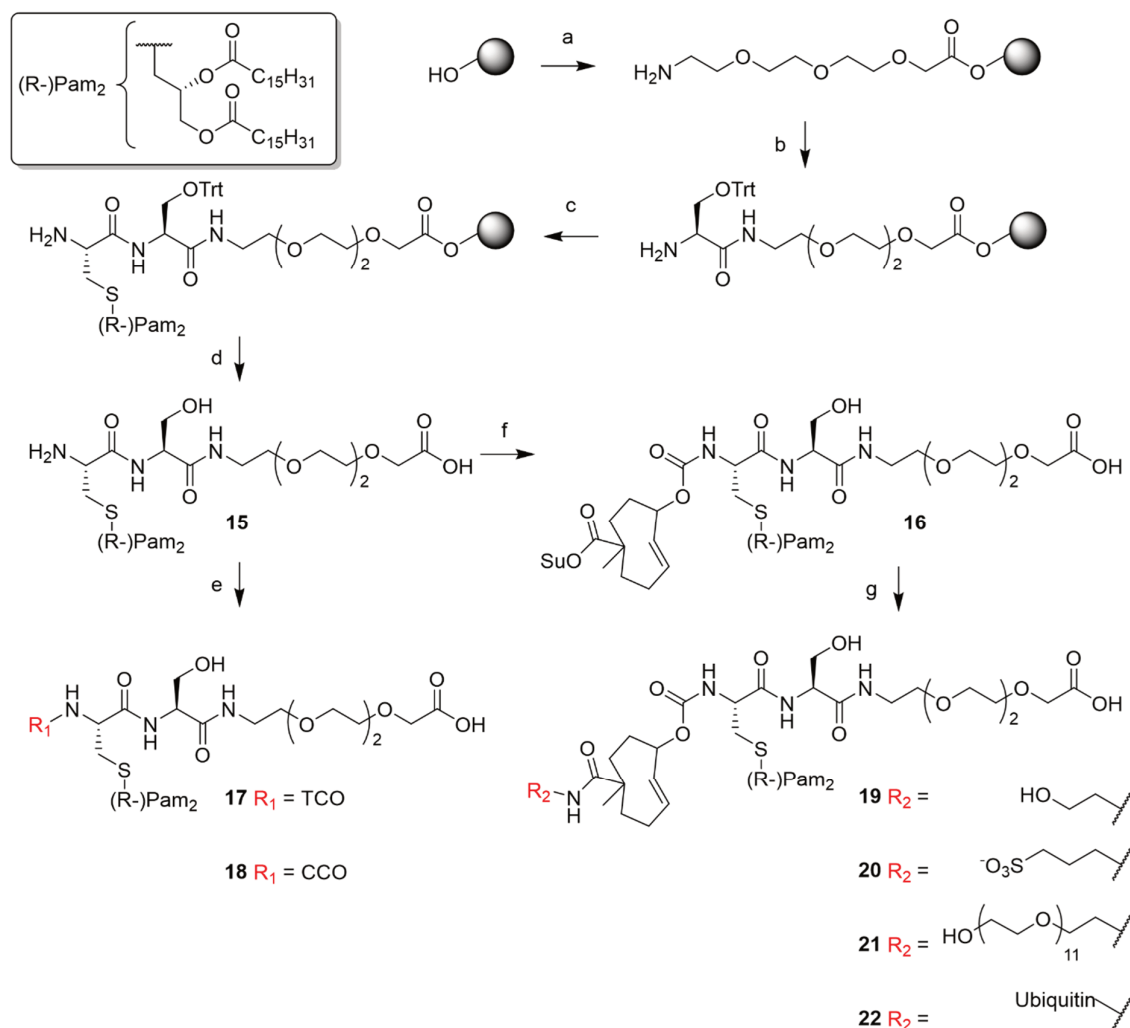


Scheme 3. Synthesis of TCO-caged P₂CSK₄ bearing hydrophilic linkers on the cyclooctene. Reagents and conditions: **a**) TCO-(OSu)₂, DiPEA, DMF, r.t., o.n. **b**) (i) Compound **10**: ethanolamine, DCM, r.t., o.n. (ii) 5% TFA, 2.5% TIS, 2.5% H₂O, DCM, r.t., 30 min; Compounds **11** and **12**: (i) homotaurine **13**, DiPEA, DMSO, r.t., o.n. (ii) 5% TFA, 2.5% TIS, 2.5% H₂O, DCM, r.t., 30 min. **c**) 7N methanolic ammonia, 0°C → r.t.

Three hydrophilic derivatives of TCO-P₂CSK₄ were synthesized on-resin by first reacting the free amine P₂CSK₄ with the bis-functionalized TCO-(OSu)₂ reagent **14** (Scheme 3). When LC-MS indicated complete conversion, the resin was washed and treated with either ethanolamine or homotaurine. Homotaurine itself was synthesized by treating 1,3-propanesultone with methanolic ammonia and subsequent precipitation in diethylether. Conjugation with homotaurine resulted in a mixture of partially hydrolyzed NHS-ester → carboxylic acid (**12**) and product **11** in a 1:1 ratio, whereas conjugation with ethanolamine resulted in quantitative conversion to the respective product. Unfortunately, HPLC purification proved unsuccessful in isolating either of the three products. Also, no formation of product was observed when conjugation with ubiquitin was attempted. This was, however, unsurprising as conjugating a large molecule to an activated ester immobilized on solid phase often suffers from extremely low coupling efficiencies. This construct therefore warranted a solution-phase coupling strategy.

Solution-phase couplings require the lysine side chains to be deprotected after conjugation has taken place. The use of the TCO added the restraint that acid- or base-labile protecting groups could not be used. This quickly leads to a complex synthetic route accompanied with complex purification methods. Therefore, it was decided to substitute the C-terminal tetralysine motif for a triethylene glycol (TEG) linker. This adaptation was postulated to minimally influence the activity of the ligand as the tetralysine moiety does not interact with the mTLR2/mTLR6 dimer in the published crystal structure, and conjugates have been described previously employing this motif.²⁶ Moreover, the two linkers share the same length with heteroatoms (O for TEG and N for Lys₄) in the same position in the carbon backbone. With the lysine primary amines now excluded, the serine alcohol is the only other functional group bearing nucleophilic character. The N-terminal cysteine

amine should outcompete the serine alcohol in terms of nucleophilicity, thus omitting any protecting group usage when the TCO/CCO is introduced in the ligand in a solution-phase coupling strategy.



First, the ligand $P_2CS(TEG)$ was synthesized on-resin for ease of purification of the intermediates (Scheme 4). Then, either CCO-NHS, TCO-NHS or TCO-bis-NHS is reacted with the crude N-terminal amine. The intermediate compound **16** is purified by HPLC and consequently conjugated

with ethanolamine, homotaurine, dodecaethylene glycol or ubiquitin. Dodecaethylene glycol was obtained via a modified procedure from a recent publication describing the synthesis of monodisperse PEG derivatives.²⁷ Interestingly, in all conjugations a minor byproduct was observed which corresponded with a molecular mass reduction of 18 amu, indicating loss of a H₂O molecule. This can be ascribed to the conversion of the serine residue to a dehydroalanine, or by the cyclization with the C-terminal carboxylic acid. It was, however, not investigated further. Also, in the conjugation with homotaurine a major byproduct was observed which again corresponded with the molecular mass of hydrolyzed NHS-ester. Ubiquitin carries seven lysine residues, as well as an N-terminal amine, which can all react with the NHS-ester, so multiple regioisomers as well as a varying ligand-to-protein ratios can be expected. When the reaction mixture was purified with HPLC, ubiquitin carrying one ligand was able to be separated from ubiquitin carrying two or more ligands. Moreover, fractions containing the same molecular mass of mono-conjugated ubiquitin but having a different retention time were isolated, indicating separation of different isoforms of the mono-conjugated ubiquitin.

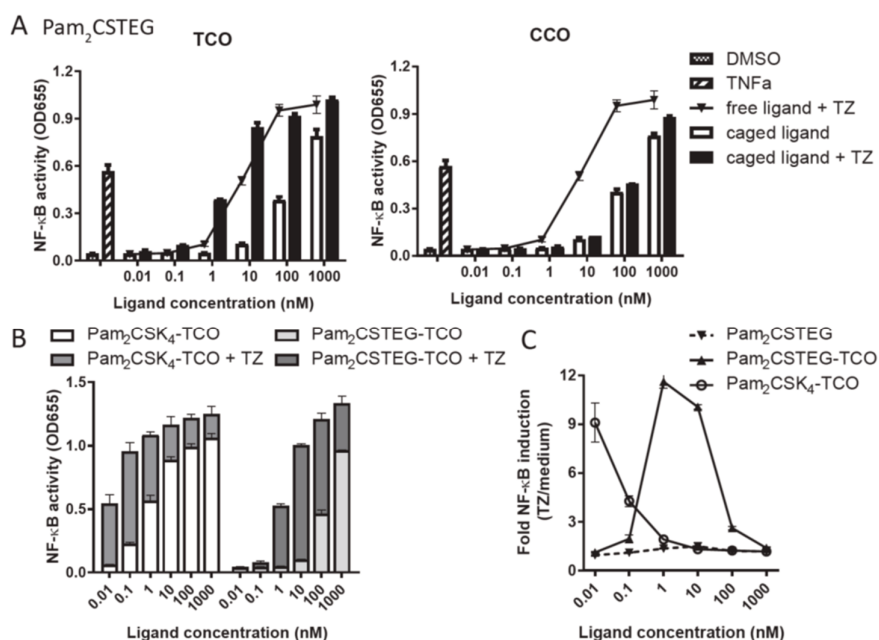


Figure 5. Evaluation of TCO/CCO-caged P₂CS(TEG) in comparison to TCO-caged P₂CSK₄. A/B) THP1-Dual reporter cells were pre-incubated with the indicated ligands for 45min. Fresh medium +/- tetrazine was added and after 24hrs NF-κB activity was measured in the culture supernatant using a SEAP colorimetric assay. C) Fold NF-κB inductions were calculated from the data in (B) by dividing the level of NF-κB activation after decaging (+TZ) over the residual activity in absence of the uncaging reagent. Experiment was carried out by Timo Oosenbrug (LUMC).

First, the effect of substituting the tetralysine linker for the triethylene glycol was assessed by quantifying the NF-κB activity induced by both ligands in THP1-dual reporter cells (Figure 5). P₂CSK₄ was shown to be 100-fold more active than P₂CS(TEG), indicating a beneficial effect of the tetralysine moiety over the TEG elongation. Residual activity in P₂CS(TEG) was still observed, albeit only at higher concentrations. This effect brings about a widening of the concentration range in which a significant fold NF-κB induction exists (Figure 5C).

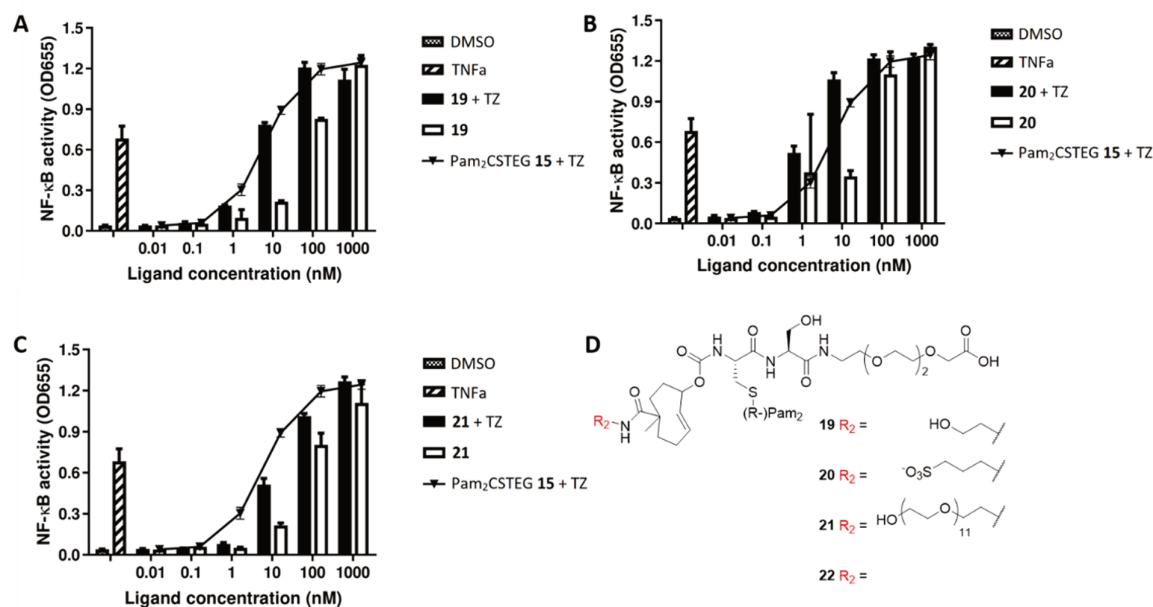


Figure 6. Evaluation of hydrophilically extended TCO-caged P₂CS(TEG) ligands 19-21. THP1-Dual reporter cells were pre-incubated with the indicated ligands for 45min. Fresh medium +/- tetrazine was added and after 24hrs NF-κB activity was measured in the culture supernatant using a SEAP colorimetric assay. Experiments were carried out by Timo Oosenbrug (LUMC).

Evaluation of the hydrophilically extended caged ligands 19-21 (Figure 6) revealed that the hydrophobic nature of the cyclooctene is not responsible for the residual activity observed in the caged versions of P₂CSK₄ and P₂CS(TEG), as there was no effect observed for the varying substitutions in comparison to no substitution.

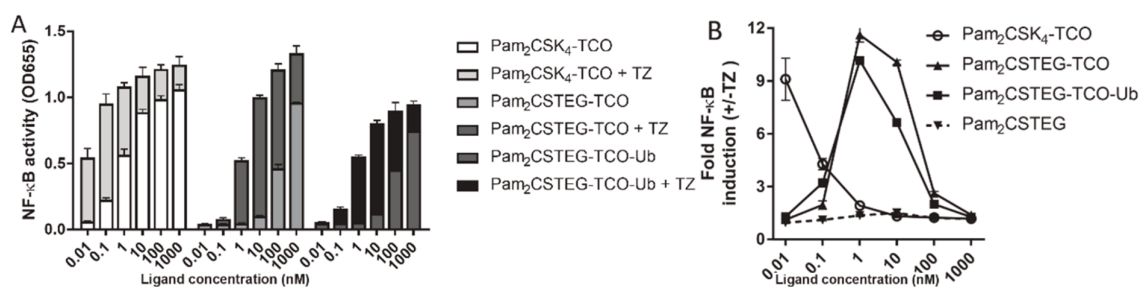


Figure 7. Evaluation of P₂CS(TEG)-TCO-ubiquitin conjugate. A/B) THP1-Dual reporter cells were pre-incubated with the indicated ligands for 45min. Fresh medium +/- tetrazine was added and after 24hrs NF-κB activity was measured in the culture supernatant using an SEAP colorimetric assay. B) Fold NF-κB inductions were calculated from the data in (A) by dividing the level of NF-κB activation after decaging (+TZ) over the residual activity in absence of the uncaging reagent. Experiments were carried out by Timo Oosenbrug (LUMC).

Evaluation of the ubiquitin-conjugated P₂CS(TEG) ligand (Figure 7) revealed that the potential lack of bulk in the cyclooctene cage is not responsible for the residual activity observed in the parent compounds. This is clearly visualized in Figure 7B, where the window of activity of TCO-P₂CS(TEG) overlaps neatly with the window of activity of Ubq-TCO-P₂CS(TEG). Perhaps, it is

the metastable nature of the carbamate linkage, prone to hydrolysis, that causes the residual activity observed throughout all experiments. Upon closer inspection of the results outlined in Figure 7A, it seems that the amount of residual activity throughout all ligands tested corresponds closely to the amount of tetrazine-induced activity observed in a 2 log lower concentration. So, >1% prematurely hydrolyzed ligand can already explain the residual activity observed. This hypothesis can be probed by conjugating the cyclooctenes via a more stable linkage towards hydrolysis, for instance the recently published ether-linked TCO cages^{28,29}. Ironically, the widened window of activity that was created by substituting the C-terminus, a modification needed to enable substitution on the N-terminus, was already sufficient in continuing investigation of spatiotemporal effects in the TLR2/6 system.

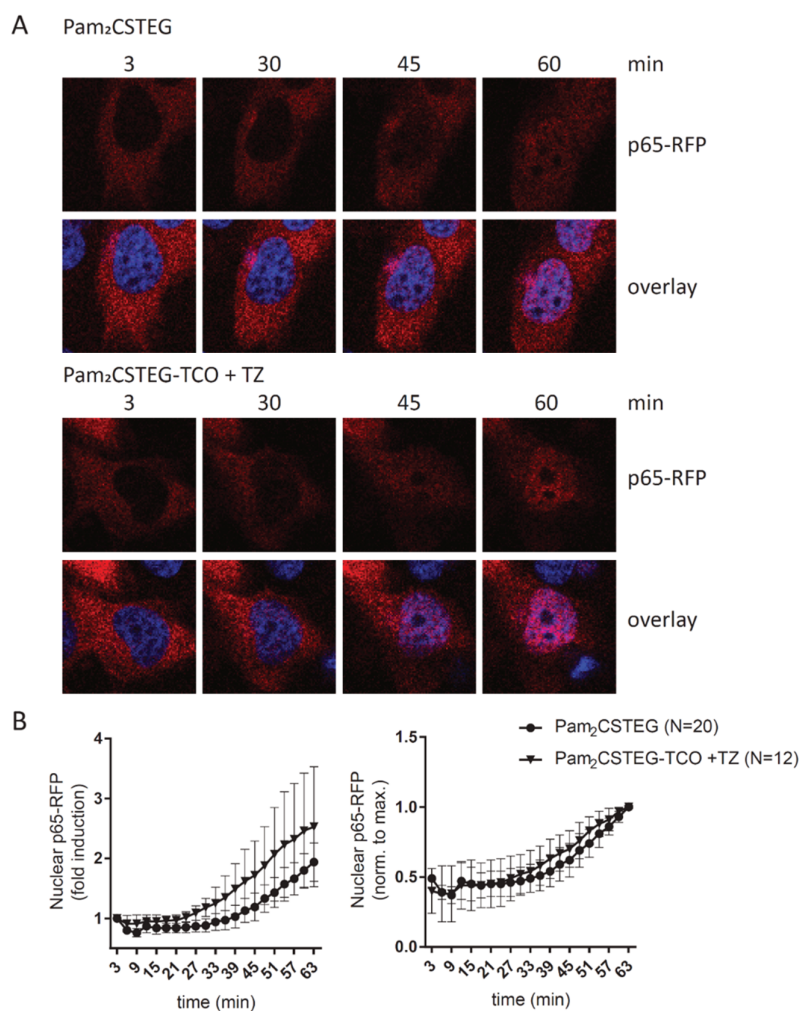


Figure 8. Assessing uncaging speed of TCO-P₂CS(TEG) on live cells. Mel Juso TLR2-YFP p65-RFP cells were pre-incubated for 45 min with 10nM Pam₂CSTEG-TCO. Live cells were imaged after addition of tetrazine (TZ) or after treatment with 10nM free Pam₂CSTEG. A) Representative images of the nuclear translocation of p65-RFP over time. To indicate nuclei, overlays with Hoechst are shown. B) For individual cells the nuclear accumulation of NF-κB was tracked over time. Left: fold increase in nuclear p65-RFP

signal, right: data was normalized per cell to the maximum nuclear p65-RFP signal observed. Experiments were carried out by Timo Oosenbrug (LUMC).

To assess the applicability of the new chemical tool in a temporal-sensitive setting, live cells were primed with TCO-P₂CS(TEG) and treated with tetrazine at t=45min. At this time point, free ligand was added to a separate well and the cells were imaged during the following hour. The Mel Juso cells express p65-RFP, a fluorescently labeled subunit of the NF- κ B complex which translocates to the cell nucleus upon TLR2/6 activation. The increase of the RFP-signal in the nucleus was quantified as a function of time (Figure 8B). Gratifyingly, the speed with which the p65-RFP accumulates in the nucleus after treatment with tetrazine coalesces with the p65-RFP nuclear appearance in the cells treated with free ligand at the same time point (Figure 9). Thus, adding tetrazine at a certain time point in the experiment has the same effect as adding free ligand, underlining the benefit of this fast chemo-uncaging in comparison to photo-uncaging, where the cells are usually irradiated for 15 minutes before signal output can be assessed.

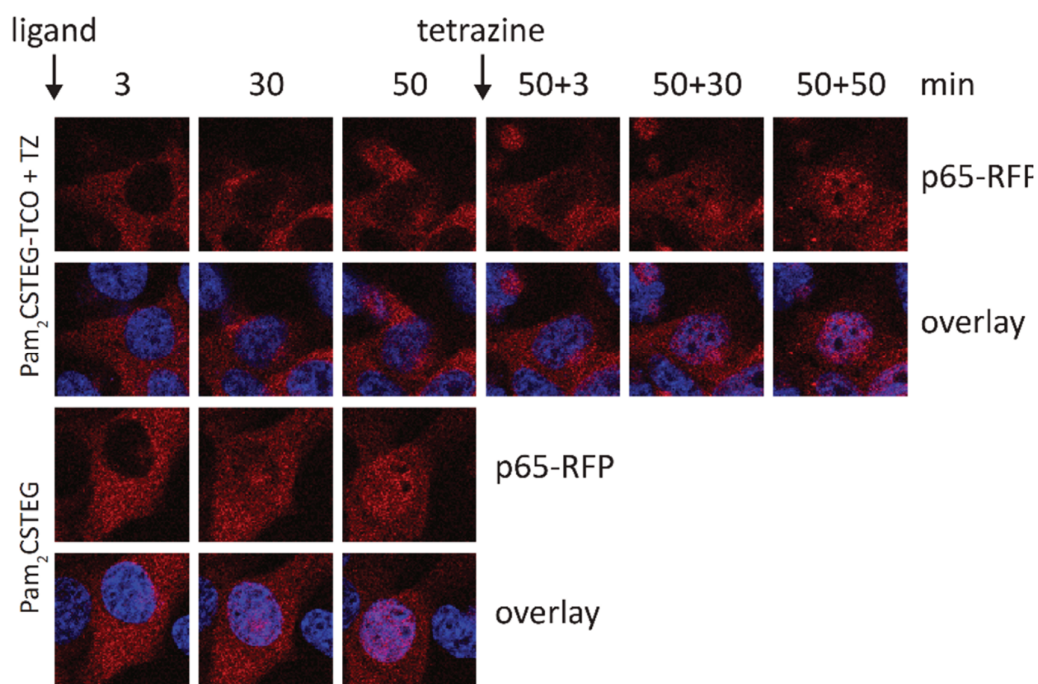


Figure 9. Live human cells respond to TCO-P₂CS(TEG) after tetrazine-mediated uncaging. Live Mel Juso TLR2-YFP p65-RFP cells were imaged over time. Cells were first treated with 10nM caged or free TLR2 ligand. After 50 min the uncaging reagent tetrazine was added and the same cells were imaged for an additional 50 min. To indicate nuclei, overlays with Hoechst are shown. Experiments were carried out by Timo Oosenbrug (LUMC).

It was next investigated whether this approach could be modified to separate two TLR populations: cell surface TLRs and intracellular TLRs. Cell surface-only activation was envisaged through immobilizing a TLR ligand-biotin conjugate on streptavidin-coated wells². However, no tools currently exist to exclusively probe for intracellular activation. For this, either the cell-surface TLR-population has to be selectively inhibited or access to tetrazine reagent has to be limited to only the intracellular TLR-population (Figure 3). Selective inhibition can be achieved by varying the

tetrazine substituents: electron withdrawing moieties have a negligible effect on the ligation, but disfavour the following tautomerisation, thus preventing the elimination. When such a tetrazine is conjugated to a motif limiting cell-permeability, one could selectively silence all the primed cell surface TLRs, while keeping the primed intracellular TLRs intact. Addition of cell-permeable tetrazine would then solely activate intracellular TLR's. Alternatively, the tetrazine can be selectively delivered to endosomes by conjugation to nano-sized beads. Phagocytosis of these beads prior to treatment with chemical tool 17 should lead to accumulation of free ligand inside endosomes containing the nanoparticles only.

Unfortunately, no conjugateable tetrazine is currently described which exerts <1% elimination, so the former strategy cannot be employed without also getting significant cell-surface activation. The latter strategy was therefore selected: amino-modified FluoSpheres (fluorescent 0.2 μm sized polystyrene amine-coated beads, Invitrogen) were decorated with a functional tetrazine (tetrazine 38, Figure 2) through an NHS-coupling. The number of amines present on the polystyrene beads is not known, so presence of functional tetrazine was quantified by reacting the beads with a known amount of fluorescently labelled TCO-caged ligand and subjecting the mixture to LC-MS. It was found that 1 μL of a 0.2% bead stock solution can uncage up to 40 pmol of TCO-caged ligand. A strong solvent effect was observed for the uncaging reaction and cellular uptake: when suspended in water, only 7.5 pmol could be uncaged, whereas addition of an equivolumair amount of DMSO increased this to 40 pmol. Also, cellular uptake of the beads appeared to be highly dependent on the presence of DMSO in the suspension. The hydrophobic character of the tetrazine can have a detrimental effect by virtue of aggregation as well as non-specific binding to plastic pipette tips and plastic wells. DMSO can act as a surfactant on the interface of the tetrazines with the aqueous environment, increasing the amount of available and functional tetrazine for uncaging. Alternatively, tetrazines that are functionalized with a water-soluble linker can be used to decorate the nanobeads to combat this effect. The ability of these nanobeads to uncage TCO-bearing TLR ligands *in vitro* is currently awaiting its assessment.

Conclusion

This Chapter describes the use of *trans*-cyclooctene as a suitable cage for preventing TLR2/6 dimerization when conjugated to a TLR2/6 agonist. When present on the N-terminus of the canonical Pam₂CSK₄ TLR2/6 ligand, conditional induction of TLR2 responses could be validated in various murine cell types through application of a tetrazine derivative. Substitution of the C-terminal tetralysine motif to a triethylene glycol linker yielded an TLR2/6 agonist that was more facile to synthesize and allowed for greater derivatization through the enablement of solution-phase chemistry. Simultaneously, this TCO-caged ligand exerts improved performance in human cells; having a lower background activity in a non-tetrazine milieu. Further reducing this background activity through increased disruption of the dimerization interface was probed with this new ligand by appending linkers of various sizes and polarity to the TCO-cage, leading to the finding the unmodified olefin was sufficient in negating most binding interactions at this site of the ligand. Furthermore, it was shown that the kinetics of the uncaging reaction do not induce a detectable

delay in TLR2 activation, allowing for highly precise temporal control over TLR2 activity. Future work will focus on imposing spatial control on this system, through the site-selective delivery of the uncaging reagents.

Acknowledgements

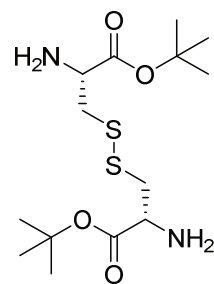
Timo Oosenbrug (LUMC) is acknowledged for the biological evaluation of the compounds described in this Chapter. Mark de Geus is acknowledged for providing *trans*-cyclooctene building blocks, tetrazine derivatives and valuable discussions. RAW Blue macrophages were kindly provided by the laboratory of Professor A. Esser-Kahn (University of Chicago). Dr. Gerbrand J. van der Heden-van Noort (LUMC) is acknowledged for his aid in the purification and characterization of ubiquitin conjugates. Ubiquitin was kindly provided by the laboratory of the late Professor H. Ovaa.

Experimental section

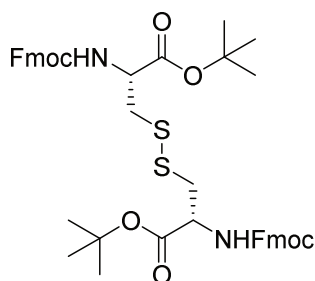
General experimental procedures

General reagents were obtained from Sigma Aldrich, Fluka, and Acros. All reagents were of commercial grade and used as received unless stated otherwise. Solvents used in synthesis were dried and stored over 4Å molecular sieves, except MeOH and ACN which were stored over 3Å molecular sieves. Triethylamine (Et₃N) and Diisopropylethylamine (DiPEA) were stored over KOH pellets. Peptide polymer resins were purchased at Rapp Polymere. Ubiquitin protein was generously provided by the laboratory of the late Dr. H. Ovaa (LUMC, Leiden, The Netherlands). LC-MS analysis was performed on a Finnigan Surveyor HPLC system with a Nucleodur C18 Gravity 3µm 50 x 4.60 mm column (detection at 200-600 nm) coupled to a Finnigan LCQ Advantage Max mass spectrometer with ESI or coupled to a Thermo LCQ Fleet Ion mass spectrometer with ESI. The Method used was 10→90% 13.5 min (0→0.5 min: 10% MeCN; 0.5→8.5 min: 10% to 90% MeCN; 8.5→ 11 min: 90% MeCN; 11→13.5 min: 10% MeCN) unless otherwise stated. High resolution mass spectra (HRMS) were recorded on the following machines: Thermo Scientific Q Exactive HF Orbitrap mass spectrometer equipped with an electrospray ion source in positive-ion mode (source voltage 3.5 kV, sheath gas flow 10, capillary temperature 275 °C) with resolution R = 240.000 at m/z 400 (mass range of 150-6000) correlated to an external calibration, or on a Waters Synapt G2-Si (TOF) equipped with an electrospray ion source in positive mode (source voltage 3.5 kV) and LeuEnk (m/z = 556.2771) as internal lock mass. As an exception, compound **22** was measured on the following apparatus: Waters XEVO-G2 XS Q-TOF mass spectrometer equipped with an electrospray ion source in positive mode (source voltage 3.0 kV, desolvation gas flow 900 L/hr, temperature 250 °C) with resolution R = 22000 (mass range m/z = 50-2000) and 200 pg/uL Leu-Enk (m/z = 556.2771) as a “lock mass”. HPLC purification was performed on a Gilson HPLC system coupled to a Magerey-Nagel Nucleodur C18 Gravity 5 µm 250 ×10mm column, or on an Agilent 1200 HPLC/6130 MS system coupled to a Magerey-Nagel Nucleodur C18 Gravity 5µm 250×10 mm column or on a Waters autopurifier HPCL/MS system coupled to a Phenomenex Gemini 5µm 150×21.2 mm column.

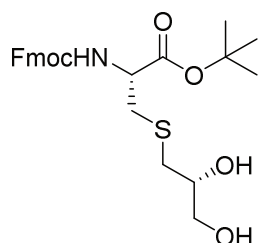
Compound 1



L-Cystine (41.6 mmol, 10.0 g) was dissolved in 70% HClO₄ (aq.) (166 mmol, 14.6 mL). *Tert*-butyl acetate (750 mmol, 100 mL) was added and the reaction was stirred at room temperature for 75 hours. TLC-MS indicated complete conversion of the starting material and the reaction mixture was cooled on ice for 30 minutes. 2M NaOH (aq.) (0.17 mol, 6.8 g in 85 mL) was slowly added and the mixture was washed with Et₂O (3x) and EtOAc (3x). The organic layers were combined, dried (MgSO₄) and concentrated *in vacuo* to yield the title compound (41 mmol, 14 g, qt.). ¹H NMR (400 MHz, CDCl₃) δ = 7.78 (s, 7H), 4.35 (t, J=5.9, 2H), 3.38 (m, 4H), 2.04 (d, J=2.8, 3H), 1.51 (s, 18H). ¹³C NMR (101 MHz, CDCl₃) δ = 177.57, 167.66, 85.12, 53.43, 38.62, 27.95.

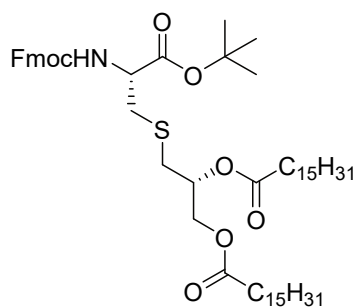
Compound 2

Compound 1 (37 mmol, 13 g) was dissolved in THF (40 mL). Fmoc-OSu (77 mmol, 26 g) and a solution of N-methyl morpholine (112 mmol, 12.3 mL) in THF (20 mL) were added. The mixture was stirred for 2 hours at room temperature when TLC analysis (20% EtOAc in Pnt, $R_f=0.6$) indicated complete conversion of the starting material. The mixture was poured in EtOAc (500 mL) and washed with 0.5M HCl (aq.) (3x) and brine (1x). The organic layers were combined, dried (MgSO_4) and concentrated *in vacuo*. Et_2O (500 mL) was added and the white precipitate was filtered yielding the title compound (18.3 mmol, 14.6 g). The filtrate was concentrated and adsorbed onto Celite. Silica gel column chromatography (10% EtOAc in Pnt \rightarrow 20% EtOAc in Pnt) yielded the title compound (7.2 mmol, 5.8 g, 68% combined yield). ^1H NMR (400 MHz, CDCl_3) δ = 7.79 – 7.69 (m, 4H), 7.57 (d, $J=7.5$, 4H), 7.36 (td, $J=7.4$, 3.0, 4H), 7.27 (t, $J=7.4$, 4H), 5.80 (d, $J=7.8$, 2H), 4.58 (dt, $J=7.9$, 5.3, 2H), 4.35 (dd, $J=7.3$, 2.6, 5H), 4.19 (q, $J=7.3$, 5.6, 2H), 3.20 (qd, $J=14.1$, 5.3, 4H), 1.47 (s, 18H). ^{13}C NMR (101 MHz, CDCl_3) δ = 169.42, 155.80, 143.85, 141.32, 127.75, 127.12, 125.23, 120.02, 83.15, 67.27, 60.46, 54.20, 47.13, 28.05.

Compound 3

Compound 2 (10 mmol, 8.0 g) was dissolved in THF (100 mL). Zinc powder (7 mmol, 0.46 g, 10 μm) and a solution of MeOH:37% HCl (aq.):98% H_2SO_4 (93:6:1, 50 mL) were added and the reaction was stirred for 15 minutes at room temperature. TLC analysis (20% EtOAc in Pnt, $R_f=0.8$) indicated complete conversion of the starting material. R-(+)-glycidol (30 mmol, 2.5 mL) was added and the reaction was stirred for 72 hours at room temperature. TLC analysis (80% EtOAc in Pnt, $R_f=0.5$) indicated complete conversion of the starting material. The mixture was filtered and the filtrate was concentrated *in vacuo*. The concentrate was diluted in DCM and washed with sat. NaHCO_3 (aq.) (5x). The aqueous layers were combined and back-extracted with DCM (3x). The organic layers were combined, dried (MgSO_4) and concentrated *in vacuo*. Silica gel column chromatography (60% EtOAc \rightarrow 70% EtOAc) yielded the title compound (15.5 mmol, 7.35 g, 78%). ^1H NMR (400 MHz, CDCl_3) δ = 7.70 (d, $J=7.5$, 2H), 7.63 – 7.50 (m, 2H), 7.35 (t, $J=7.4$, 2H), 7.31 – 7.21 (m, 3H), 6.14 (d, $J=8.1$, 1H), 4.48 (dt, $J=7.9$, 5.6, 1H), 4.35 (d, $J=7.2$, 2H), 4.18 (t, $J=7.2$, 1H), 3.94 (s, 1H), 3.78 (qd, $J=8.4$, 5.5, 4.9, 1H), 3.65 (dd, $J=11.0$, 3.4, 1H), 3.51 (dd, $J=11.5$, 6.3, 1H), 2.96 (qd, $J=13.9$, 5.6, 2H), 2.81 – 2.49 (m, 2H), 1.45 (s, 9H). ^{13}C NMR (101 MHz, CDCl_3) δ = 169.82, 156.05, 143.69, 143.61, 141.12, 127.61, 126.98, 125.04, 119.87, 82.82, 71.01, 67.07, 65.08, 54.46, 46.92, 36.17, 35.28, 27.85.

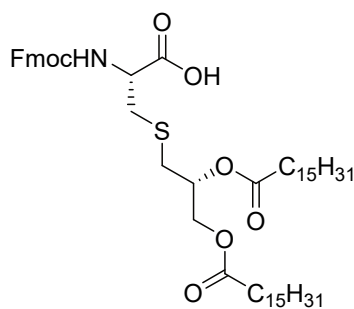
Compound 4



Compound **3** (15.3 mmol, 7.25 g) was dissolved in anhydrous THF (150 mL). Palmitic acid (61 mmol, 16 g), diisopropylcarbodiimide (69 mmol, 11 mL) and DMAP (6.1 mmol, 0.74 g) were added and the reaction was stirred for 2 hours at room temperature. TLC analysis (20% EtOAc in Pnt, $R_f=0.5$) indicated complete conversion of the starting material. Acetic acid (7 mL) was added and the mixture was concentrated *in vacuo*. The concentrate was dissolved in a minimal amount of warm DCM,

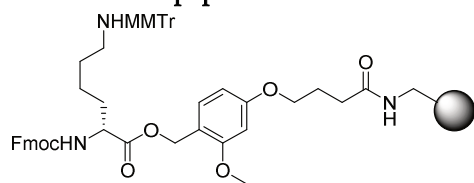
after which the solution was carefully diluted with MeOH ($>10\times V_{DCM}$). The mixture was left overnight at room temperature after which the formed crystals were collected by filtration. The mother liquor was concentrated *in vacuo* and subjected to a second crystallization round. The crystals were combined and washed with cold MeOH, yielding the title compound (14.5 mmol, 13.8 g, 95%). **¹H NMR (400 MHz, CDCl₃)** δ = 7.76 (d, $J=7.5$, 2H), 7.62 (d, $J=7.5$, 2H), 7.40 (t, $J=7.4$, 2H), 7.31 (t, $J=7.4$, 2H), 5.70 (d, $J=7.7$, 1H), 5.16 (qd, $J=6.3$, 3.5, 1H), 4.51 (dt, $J=7.8$, 5.0, 1H), 4.46 – 4.29 (m, 3H), 4.24 (t, $J=7.2$, 1H), 4.16 (dd, $J=11.9$, 5.9, 1H), 3.05 (qd, $J=13.7$, 5.0, 2H), 2.77 (d, $J=6.4$, 2H), 2.30 (q, $J=7.3$, 5H), 1.60 (dq, $J=11.6$, 8.1, 7.2, 4.7, 6H), 1.49 (s, 10H), 1.36 – 1.16 (m, 60H), 0.88 (t, $J=6.8$, 6H). **¹³C NMR (101 MHz, CDCl₃)** δ = 173.48, 173.19, 169.62, 155.86, 143.96, 141.43, 127.86, 127.22, 125.28, 120.13, 83.15, 70.37, 67.36, 63.60, 54.48, 47.26, 35.51, 34.41, 34.22, 33.43, 32.07, 29.85, 29.81, 29.78, 29.64, 29.51, 29.44, 29.27, 28.12, 25.04, 25.01, 22.84, 14.27.

Compound 5

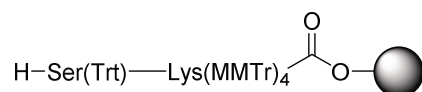


Compound **4** (0.95 mmol, 0.90 g) was dissolved in neat TFA (5 mL) and the mixture was stirred for 1 hour at room temperature. TLC analysis (20% EtOAc in Pnt, $R_f=0.2$) indicated complete conversion of the starting material. The mixture was concentrated *in vacuo* and co-evaporated with toluene (3x) yielding the title compound (0.95 mmol, 0.85 g). **¹H NMR (400 MHz, CDCl₃)** δ = 9.69 (s, 1H), 7.74 (d, $J=7.5$, 2H), 7.60 (d, $J=7.5$, 2H), 7.38 (t, $J=7.5$, 2H), 7.29 (t, $J=7.4$, 2H), 5.92 (d, $J=7.9$, 1H), 5.25 – 5.03

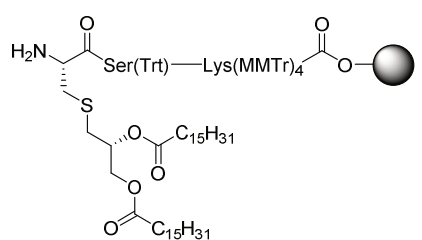
(m, 1H), 4.75 – 4.48 (m, 1H), 4.38 (ddt, $J=16.2$, 12.0, 7.0, 3H), 4.22 (t, $J=7.0$, 1H), 4.15 (dd, $J=12.0$, 6.2, 1H), 3.29 – 2.94 (m, 2H), 2.90 – 2.53 (m, 2H), 2.30 (q, $J=7.7$, 4H), 1.58 (td, $J=7.4$, 4.0, 4H), 1.25 (q, $J=7.8$, 5.1, 52H), 0.88 (t, $J=6.6$, 6H). **¹³C NMR (101 MHz, CDCl₃)** δ = 173.86, 156.34, 143.72, 141.37, 127.85, 127.20, 125.24, 120.08, 70.39, 67.64, 63.72, 47.11, 34.67, 34.40, 34.19, 32.99, 32.04, 29.83, 29.79, 29.76, 29.63, 29.49, 29.41, 29.24, 29.21, 25.00, 24.96, 22.81, 14.24.

Resin-bound peptide 6.1

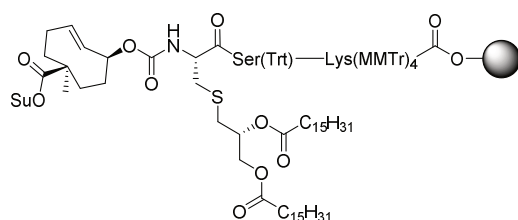
Tentagel S AC resin (0.5 g, 125 μmol) was swollen in DMF and treated with Fmoc-Lys(MMTr)-OH (375 μmol , 241 mg), DIC (375 μmol , 58 μL) and DMAP (cat. amount). The syringe was shaken overnight and consequently washed with DMF (5x), DCM (5x) and Et₂O (3x). Dry weight loading analysis indicated a complete conversion (592 mg, 138 μmol).

Resin-bound peptide 6.2

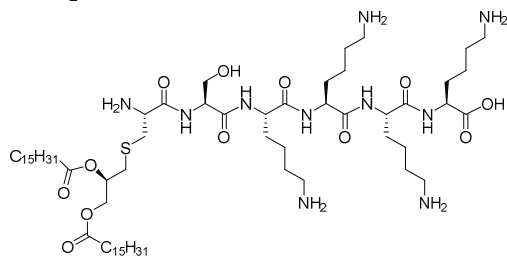
The following SPPS cycle was carried out four times to form the serine-tetralysine pentapeptide: Resin bound lysine **6.1** was swollen in DMF and treated with a solution of 20% piperidine in DMF for 10 min. (4x) and consequently washed with DMF (5x). The resulting resin was treated with HCTU (1 mL, 0.6 M in DMF), amino acid (1 mL, 0.6 M in DMF) and lastly DiPEA (1 mL, 0.6 M in DMF). The syringe was shaken for 2 hours and consequently washed with DMF (5x). A solution of 5% acetic anhydride in 0.1 M DiPEA in DMF was added and the syringe was shaken for 10 min. The resin was washed with DMF (5x), treated with a solution of 20% piperidine in DMF for 10 min. (4x) and consequently washed with DMF (5x).

Resin-bound peptide 6.3

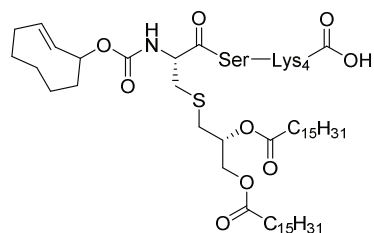
Resin-bound pentapeptide **6.2** was swollen in DMF and treated with HCTU (1 mL, 0.6 M in DMF), Fmoc-*R*-Pam₂Cys-OH (1 mL, 0.6 M in DMF) and lastly DiPEA (1 mL, 0.6 M in DMF). The syringe was shaken for 2 hours and consequently washed with DMF (5x). A solution of 5% acetic anhydride in 0.1 M DiPEA in DMF was added and the syringe was shaken for 10 min. The resin was washed with DMF (5x), treated with a solution of 20% piperidine in DMF for 10 min. (4x) and consequently washed with DMF (5x), DCM (3x) and dried with Et₂O (3x) for prolonged storage.

Resin-bound peptide 6.4

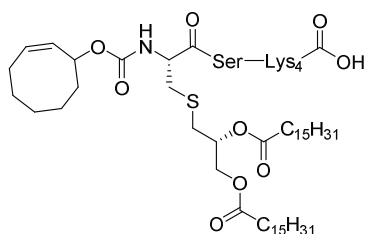
Resin-bound hexapeptide **3** (198 mg, 30 μmol) was swollen in DMF and DiPEA (60 μmol , 11 μL) and bis functionalized TCO-OSu₂ (60 μmol , 25 mg) were added and the reaction syringe was shaken overnight. LC-MS analysis of a small amount of TFA-treated resin indicated complete conversion of the starting material. The resin was washed with DMF (3x) and DCM (3x).

Compound 7

Resin-bound hexapeptide **6.3** (10 μ mol, 45 mg) was swollen in DCM and consequently treated with a solution of 20% TFA, 2.5% TIS and 2.5% H₂O in DCM. The syringe was shaken for 1 hour and emptied in a tube containing a 1:1 mixture of Pnt:Et₂O at -20°C. The resulting precipitation was collected by centrifugation and removal of the supernatant. The crude pellet was purified by reverse-phase HPLC (Gradient: 50% AcN + 90% (H₂O+0.1% TFA) to 90% AcN + 10% (H₂O+0.1% TFA)) to obtain compound **6** (0.65 μ mol, 0.83 mg, 6.5%). **HRMS**: [M+H]⁺ calculated for C₆₅H₁₂₇N₁₀O₁₂S 1271.93502; found 1271.93487

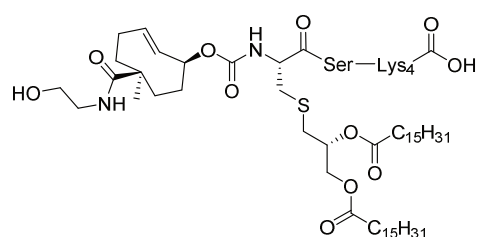
Compound 8

Resin-bound hexapeptide **3** (63 mg, 16 μ mol) was swollen in DMF and DiPEA (20 μ mol, 3.5 μ L) and TCO-OSu (20 μ mol, 5.1 mg) were added and the reaction syringe was shaken overnight. LC-MS analysis of a small amount of TFA-treated resin indicated complete conversion of the starting material. The resin was washed with DMF (3x) and DCM (3x). A solution of 5% TFA, 2.5% TIS, 2.5% H₂O in DCM was added and the reaction vessel was shaken for 15 min. The syringe was emptied in a 0°C solution of 50% Pnt in Et₂O (total volume = 40 mL) and put in a -20°C freezer overnight. The tube was then centrifuged for 90min at 4°C after which a pellet was visible. The tube was decanted and the pellet was purified on HPLC (TFA) to yield compound the title compound (1.2 μ mol, 1.7 mg, 7.5%). **LC-MS (5090, C18, H₂O/AcN + TFA)**: 1424.02 (z=1, simulated), 1423.87 (z=1, observed), 1536.80 (z=1, TFA adduct), 1650.07 (z=1, 2*TFA adduct) **HRMS**: [M+H]⁺ calculated for C₇₄H₁₃₈N₁₀O₁₄S 1424.01875; found 1424.01805

Compound 9

Resin-bound hexapeptide **6.3** (45 mg, 11 μ mol) was swollen in DMF and DiPEA (11 μ mol, 2 μ L) and CCO-OSu (20 μ mol, 5.1 mg) were added and the reaction syringe was shaken overnight. LC-MS analysis of a small amount of TFA-treated resin indicated complete conversion of the starting material. The resin was washed with DMF (3x) and DCM (3x). A solution of 5% TFA, 2.5% TIS, 2.5% H₂O in DCM was added and the reaction vessel was shaken for 15 min. The syringe was emptied in a 0°C solution of 50% Pnt in Et₂O (total volume = 40 mL) and put in a -20°C freezer overnight. The tube was then centrifuged for 90min at 4°C after which a pellet was visible. The tube was decanted and the pellet was purified on HPLC (TFA) to yield compound the title compound (0.31 μ mol, 0.44 mg, 2.8%). **LC-MS (5090, C18, H₂O/AcN + TFA)**: 1424.02 (z=1, simulated), 1423.87 (z=1, observed), 1536.67 (z=1, TFA adduct), 1650.27 (z=1, 2*TFA adduct) **HRMS**: [M+H]⁺ calculated for C₇₄H₁₃₉N₁₀O₁₄S 1424.01875; found 1424.01805

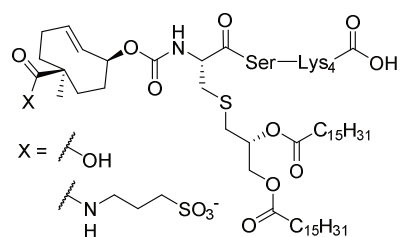
Compound 10



Resin-bound hexapeptide **6.4** (15 μ mol, 100 mg) was swollen in DCM and ethanolamine (75 μ mol, 4.5 μ L) was added. The syringe was shaken overnight after which LC-MS analysis of a small amount of TFA-treated resin indicated complete conversion of the starting material. The resin was washed with DCM (3x).

A solution of 5% TFA, 2.5% TIS, 2.5% H₂O in DCM was added and the reaction vessel was shaken for 30 minutes (repeated 1x). The combined flowthroughs were diluted with toluene and carefully evaporated and co-evaporated with toluene (2x). **LC-MS (5090, C18, H₂O/AcN + TFA):** 1525.06 ($z=1$, simulated), 1524.87 ($z=1$, observed), 1638.80 ($z=1$, TFA adduct), 1751.67 ($z=1$, 2*TFA adduct)

Compounds 11 and 12

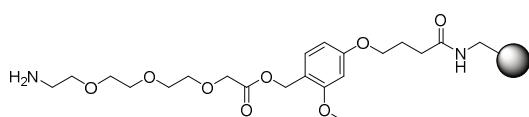


Resin-bound hexapeptide **6.4** (20 μ mol, 140 mg) was swollen in DMSO and homotaurine (100 μ mol, 14 mg) and DiPEA (100 μ mol, 17 μ L) were added. The syringe was shaken overnight after which LC-MS analysis of a small amount of TFA-treated resin indicated complete conversion of the starting material to the product and hydrolyzed NHS-ester.

The resin was washed with DCM (3x). A solution of 5% TFA, 2.5% TIS, 2.5% H₂O in DCM was added and the reaction vessel was shaken for 30 minutes (repeated 1x). The combined flowthroughs were diluted with toluene and carefully evaporated and co-evaporated with toluene (2x). **LC-MS (Homotaurine product, 5090, C18, H₂O/AcN + TFA):** 1602.06 ($z=1$, simulated), 1602.73 ($z=1$, observed), 1715.80 ($z=1$, TFA adduct), 1829.40 ($z=1$, 2*TFA adduct). **LC-MS (Carboxylic acid product, 5090, C18, H₂O/AcN + TFA):** 1481.04 ($z=1$, simulated), 1480.93 ($z=1$, observed), 1593.73 ($z=1$, TFA adduct), 1707.53 ($z=1$, 2*TFA adduct)

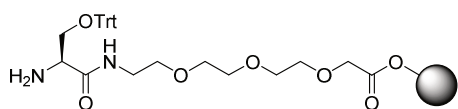
Compound 13

$^+H_3N-CH_2CH_2CH_2-SO_3^-$ 1,3-propanesultone (10 mmol, 1.2 g) was dissolved in 7N methanolic ammonia at 0°C under a nitrogen atmosphere. The mixture was heated to room temperature and stirred for 2 hours. TLC analysis (AcN, $R_f(1,3\text{-propanesultone}) = 0.9$) indicated complete conversion of the starting material. The reaction mixture was poured in Et₂O (200 mL) and centrifuged in 50 mL tubes. The tubes were decanted and the pellet was collected and dried *in vacuo*, yielding the title compound (8.4 mmol, 1.2 g, 84%). **¹H NMR (400 MHz, DMSO-*d*₆)** δ = 7.62 (s, 3H), 2.92 (t, $J=7.0$, 2H), 2.58 (t, $J=6.8$, 2H), 1.87 (p, $J=6.9$, 2H). **¹³C NMR (101 MHz, DMSO)** δ = 48.74, 38.69, 23.30.

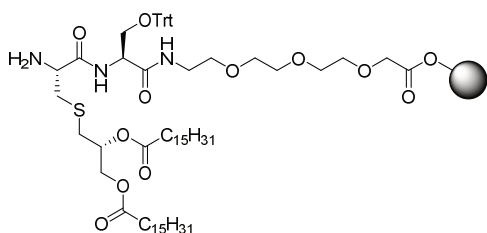
Resin-bound compound 14.1

Tentagel S AC resin (0.5 mmol, 2.0 g) was swollen in dry DCM and treated with diethylene glycol 2-aminoethyl acetic acid (2.5 mmol, 518 mg), DIC (2.5 mmol, 389 μ L) and DMAP (cat.

amount). The reaction syringe was shaken overnight after which the resin was washed with DCM (5x). The resin was treated with a solution of pyridine (2.5 mmol, 201 μ L) in DMF after which a solution of benzoic anhydride (2.5 mmol, 556 mg) in DMF was added and the reaction syringe was shaken for 30 min. The resin was washed with DMF (5x) after which the resin was treated with a solution of 20% piperidine in DMF for 10 min. (4x) and consequently washed with DMF (5x) and DCM (3x).

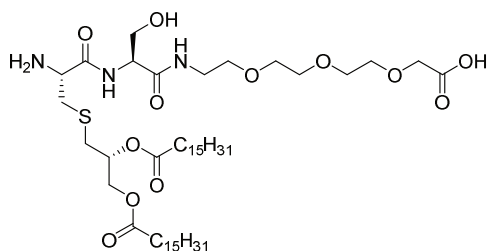
Resin-bound compound 14.2

Resin-bound triethylene glycolamine **14.1** (0.5 mmol) was swollen in DMF. Fmoc-Ser(Trt)-OH (1 mmol, 570 mg), HCTU (1 mmol, 414 mg) and DiPEA (1 mmol, 174 μ L) were added as 1 M solutions in DMF. The reaction syringe was shaken for 4 hours after which the resin was washed with DMF (3x) and DCM (3x). The resin was treated with a solution of 20% piperidine in DMF for 10 min. (4x) and consequently washed with DMF (5x) and DCM (3x).

Resin-bound compound 14.3

Resin-bound compound **14.2** (0.4 mmol, 1.74 g) was swollen in DCM. Compound **5** (0.5 mmol, 447 mg), HCTU (0.5 mmol, 207 mg) and lastly DiPEA (0.5 mmol, 87 μ L) were added as 1 M solutions in DCM. The reaction syringe was shaken for 4 hours after which the resin was washed with DCM (5x). LC-MS

analysis of a small amount of TFA-treated resin indicated complete conversion of the starting compound. The resin was swollen in DMF and treated with a solution of 20% piperidine in DMF for 10 min. (4x) and consequently washed with DMF (5x) and DCM (3x).

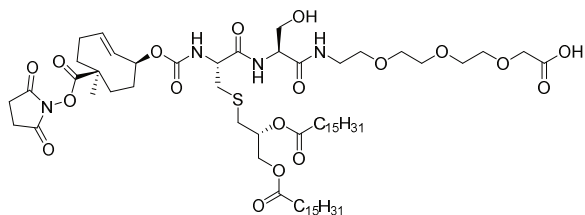
Compound 15

Resin-bound compound **14.3** (0.4 mmol, 2.06 g) was swollen in DCM. A mixture of 20% TFA, 2.5% TIS and 2.5% H₂O in DCM was added and the syringe was shaken for 30 min. The syringe was emptied in a flask containing 50 mL of toluene and the mixture was concentrated *in vacuo*. After co-evaporation with toluene (3x), the crude was purified on HPLC (TFA)

to obtain compound **15** (116 μ mol, 110 mg, 29%). LC-MS (7090, C18, H₂O/AcN + TFA):

948.66 ($z=1$, simulated), 948.47 ($z=1$, observed), 970.53 ($z=1$, Na adduct), 992.47 ($z=1$, 2^*Na adduct) **HRMS**: $[\text{M}+\text{H}]^+$ calculated for $\text{C}_{49}\text{H}_{94}\text{N}_3\text{O}_{12}\text{S}$ 948.65527; found 948.65492

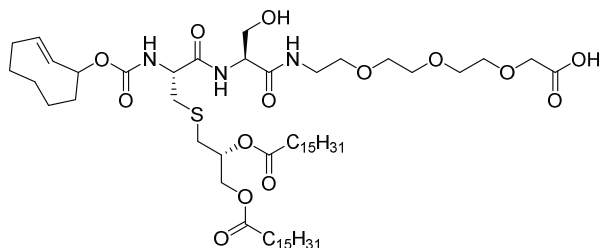
Compound 16



Compound **15** (10 μmol , 9.5 mg) was dissolved in dry DMF (200 μL) in an eppendorf tube (1.5 mL). Dual-functionalized TCO-OSu (20 μmol , 8.4 mg) and DiPEA (20 μmol , 3.5 μL) were added. The tube was shaken for 20 hours after which LC-MS

indicated depletion of the starting material. The crude reaction mixture was used as is for consequent reactions. **LC-MS (5090, DiPhenyl, $\text{H}_2\text{O}/\text{AcN}$ + TFA)**: 1256.74 ($z=1$, simulated), 1255.50 ($z=1$, observed), 1277.67 ($z=1$, Na adduct), 1300.33 ($z=1$, 2^*Na adduct)

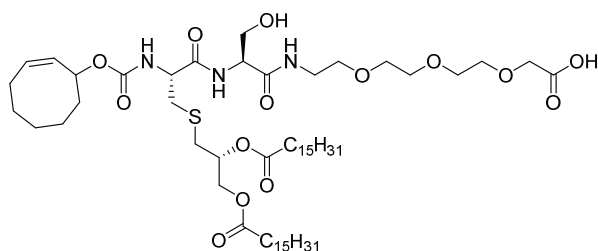
Compound 17



Compound **15** (10 μmol , 9.5 mg) was dissolved in dry DMSO (200 μL) in an eppendorf tube (1.5 mL). TCO-OSu (20 μmol , 5.4 mg) and DiPEA (20 μmol , 3.5 μL) were added. The tube was shaken overnight after which LC-MS (5090,

diphenyl column, TFA) indicated complete conversion of the starting material. The crude mixture was directly injected in the HPLC to obtain compound **17** (1.8 μmol , 2.0 mg, 18%). **LC-MS (5090, DiPhenyl, $\text{H}_2\text{O}/\text{AcN}$ + TFA)**: 1101.72 ($z=1$, simulated), 1100.42 ($z=1$, observed), 1122.67 ($z=1$, Na adduct), 1145.17 ($z=1$, 2^*Na adduct). **HRMS**: $[\text{M}+\text{H}]^+$ calculated for $\text{C}_{58}\text{H}_{106}\text{N}_3\text{O}_{14}\text{S}$ 1100.73900; found 1100.73821

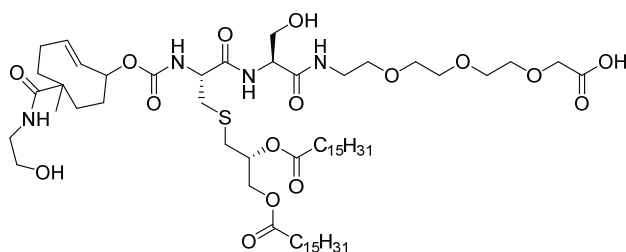
Compound 18



Compound **15** (10 μmol , 9.5 mg) was dissolved in dry DMSO (200 μL) in an eppendorf tube (1.5 mL). CCO-OSu (20 μmol , 5.4 mg) and DiPEA (20 μmol , 3.5 μL) were added. The tube was shaken overnight after which LC-MS (5090, diphenyl column, TFA) indicated complete conversion of the

starting material. The crude mixture was directly injected in the HPLC to obtain compound **18** (2.0 μmol , 2.2 mg, 20%). **LC-MS (5090, DiPhenyl, $\text{H}_2\text{O}/\text{AcN}$ + TFA)**: 1101.72 ($z=1$, simulated), 1100.25 ($z=1$, observed), 1122.58 ($z=1$, Na adduct), 1144.50 ($z=1$, 2^*Na adduct). **HRMS**: $[\text{M}+\text{H}]^+$ calculated for $\text{C}_{58}\text{H}_{106}\text{N}_3\text{O}_{14}\text{S}$ 1100.73900; found 1100.73819

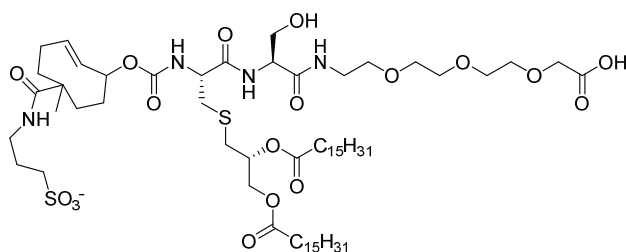
Compound 19



Compound **16** (max. 8.4 μmol in DMF) was put in an eppendorf tube (1.5 mL). Ethanolamine (200 μmol , 12 μL) was added and the tube was shaken overnight at room temperature. LC-MS indicated complete conversion of the starting material. Water (1 mL) was added and the

mixture was lyophilized to extrude DMF. The crude was dissolved in DMSO and purified by HPLC (diphenyl, TFA) to obtain the title compound (1.29 mg, 1.1 μmol , 13%). **LC-MS (5090, DiPhenyl, H₂O/AcN + TFA):** 1201.79 ($z=1$, simulated), 1201.68 ($z=1$, observed). **HRMS:** $[\text{M}+\text{H}]^+$ calculated for $\text{C}_{62}\text{H}_{113}\text{N}_4\text{O}_{16}\text{S}$ 1201.78668; found 1201.78587

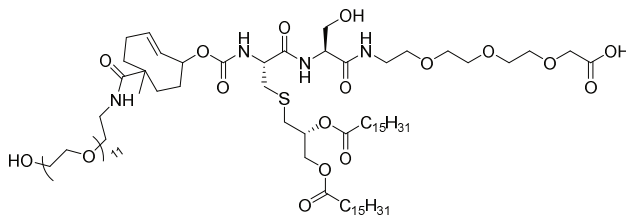
Compound 20



Compound **16** (5 μmol in DMF) was put in an eppendorf tube (1.5 mL). Homotaurine **13** (15 μmol , 2.1 mg) and DiPEA (15 μmol , 2.6 μL) were added and the tube was shaken for 7 days. LC-MS indicated complete conversion of the starting material. Water (1 mL) was added

and the mixture was lyophilized to extrude DMF. The crude was dissolved in DMSO and purified by HPLC (diphenyl, TFA) to obtain the title compound (0.86 μmol , 1.1 mg, 17%). **LC-MS (5090, DiPhenyl, H₂O/AcN + TFA):** 1279.76 ($z=1$, simulated), 1279.42 ($z=1$, observed) **HRMS:** $[\text{M}+\text{H}]^+$ calculated for $\text{C}_{63}\text{H}_{115}\text{N}_4\text{O}_{18}\text{S}_2$ 1279.76423; found 1279.76366

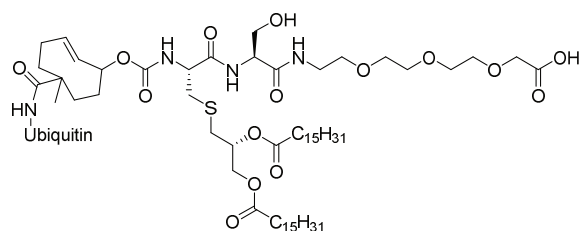
Compound 21



Compound **16** (max. 10 μmol in 200 μL DMF) was put in an eppendorf tube (1.5 mL). Compound **28** (50 μmol , 27 mg) was added and the tube was shaken for 40 hours. LC-MS (5090, diphenyl, TFA) indicated complete conversion of the

starting material. Water (1 mL) was added and the mixture was lyophilized to extrude DMF. The crude was dissolved in DMSO and purified by HPLC (diphenyl, TFA) to obtain compound **21** (1.7 μmol , 2.9 mg, 17%). **LC-MS (5090, DiPhenyl, H₂O/AcN + TFA):** 1685.08 ($z=1$, simulated), 1685.17 ($z=1$, observed), 1707.83 ($z=1$, Na adduct), 843.83 ($z=2$, $\text{M}+2\text{H}$). **HRMS:** $[\text{M}+\text{H}]^+$ calculated for $\text{C}_{84}\text{H}_{157}\text{N}_4\text{O}_{27}\text{S}$ 1686.07504; found 1686.07431

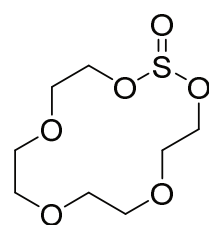
Compound 22



Ubiquitin (0.53 μmol , 4.8 mg, endotoxin-free, Worthington) was dissolved in dry DMSO (160 μL) in an eppendorf tube (1.5 mL). DiPEA (6 μmol , 1 μL) in dry DMSO (20 μL) and compound **16** (0.53 μmol in stock solution) were added. The tube was shaken for

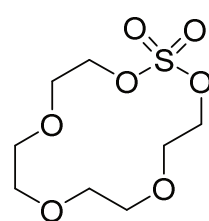
7 days after which HRMS showed formation of single and dual conjugated ubiquitin constructs. The crude was purified on HPLC (1090, C18, TFA) to obtain two separate fractions (A and B) containing products with the mass corresponding to mono-functionalized ubiquitin (Fraction A: 0.65 mg, 67 nmol, 13%; Fraction B: 0.42 mg, 43 nmol, 8.1%). **HRMS:** $[\text{M}+10\text{H}]^{10+}$ calculated for $\text{C}_{438}\text{H}_{734}\text{N}_{108}\text{O}_{133}\text{S}_2$ 971.5438; found 971.5424;

Compound 23



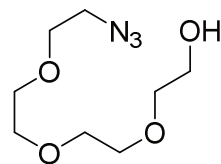
Tetraethylene glycol (5.2 mmol, 1.0 g), DiPEA (25 mmol, 4.4 mL) and DMAP (0.26 mmol, 31 mg) were dissolved in DCM (100 mL) and cooled to 0°C. SOCl_2 (10 mmol, 0.75 mL) was dissolved in DCM, cooled to 0°C and added to the reaction mixture over a period of 1 hour. After addition was complete, the mixture was stirred for another hour at 0°C after which brine was added to the mixture. The water layer was washed with DCM (3x). The organic layers were combined, dried (MgSO_4) and concentrated *in vacuo*. The crude was used *as is* in the following reaction.

Compound 24



Compound **23** (5.2 mmol, 1.2 g) was dissolved in a mixture of acetonitrile (40 mL), DCM (40 mL) and H_2O (60 mL) and cooled to 0°C. NaIO_4 (5.2 mmol, 1.1 g) and $\text{RuCl}_3 \cdot 3\text{H}_2\text{O}$ (0.077 mmol, 20 mg) were added and the mixture stirred for 1 hour at to room temperature. The mixture was transferred to a separatory funnel and the DCM layer was collected. The water layer was washed with DCM (3x). The organic layers were combined, dried (MgSO_4), filtered over Celite and concentrated *in vacuo*. Silica gel column chromatography (50% EtOAc in Pnt, $R_f=0.3$) yielded the title compound (4.7 mmol, 1.2 g, 91% over 2 steps). **^1H NMR (400 MHz, CDCl_3)** δ = 4.53 – 4.43 (m, 4H), 3.84 (dd, $J=5.5, 4.6$, 4H), 3.74 – 3.59 (m, 8H). **^{13}C NMR (101 MHz, CDCl_3)** δ = 72.14, 70.48, 70.39, 68.23.

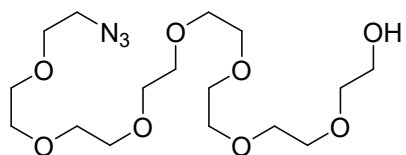
Compound 25



Compound **24** (1.0 mmol, 0.26 g) was dissolved in DMF (5 mL). NaN_3 (1.5 mmol, 0.098 g) was added and the mixture was stirred for 1 hour at 60°C. TLC analysis (50% EtOAc in Pnt, $R_f(\text{starting material})=0.3$) indicated complete conversion of the starting material. The DMF was evaporated *in vacuo* and the concentrate was diluted with THF (5 mL). H_2O (3 mmol, 54

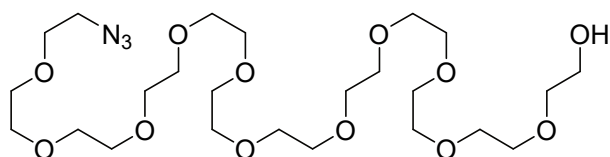
μL) and 98% H_2SO_4 (1.5 mmol, 80 μL) were added and the mixture was stirred for 1 hour at reflux temperature. TLC analysis (100% EtOAc, $R_f=0.4$) indicated complete conversion of the starting material. The mixture was poured into H_2O and washed with DCM (3x). The organic layers were combined, dried (MgSO_4) and concentrated *in vacuo* to yield the title compound (1.0 mmol, 219 mg, qt.). ^1H NMR (400 MHz, CDCl_3) δ = 3.75 – 3.70 (m, 2H), 3.68 (d, $J=2.5$, 11H), 3.63 – 3.58 (m, 2H), 3.40 (dd, $J=5.6$, 4.5, 2H), 3.18 (s, 1H). ^{13}C NMR (101 MHz, CDCl_3) δ = 72.38, 70.45, 70.40, 70.34, 70.10, 69.81, 61.37, 50.43.

Compound 26



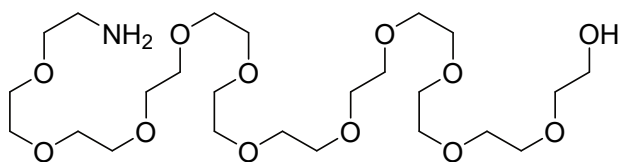
NaH (1.0 mmol, 0.040 g) was suspended in anhydrous THF (10 mL) and cooled to 0°C under a nitrogen atmosphere. To this mixture was added a solution of compound **25** (1.0 mmol, 0.22 g) in anhydrous THF (2.5 mL) and stirred for 15 minutes at 0°C . A solution of compound **24** (0.83 mmol, 0.21 g) in THF (1.7 mL) was added to the reaction mixture and stirred for 2 hours at 0°C . Then the mixture was heated to 50°C for 20 minutes after which TLC analysis (100% EtOAc, $R_f=0.1$) indicated complete conversion of the starting material. H_2O (3 mmol, 54 μL) and 98% H_2SO_4 (1.5 mmol, 80 μL) were added and the mixture was stirred for 1 hour at reflux temperature. The mixture was poured in H_2O and washed with DCM (3x). The organic layers were combined, dried (MgSO_4) and concentrated *in vacuo*. Silica gel column chromatography (DCM \rightarrow 0.75% MeOH in DCM, $\Delta=0.25\%$) yielded the title compound (0.47 mmol, 0.19 g, 56%). ^1H NMR (400 MHz, CDCl_3) δ = 3.75 – 3.71 (m, 2H), 3.71 – 3.63 (m, 26H), 3.63 – 3.58 (m, 2H), 3.39 (t, $J=5.1$, 2H), 2.92 (s, 1H). ^{13}C NMR (101 MHz, CDCl_3) δ = 72.51, 70.64, 70.61, 70.58, 70.56, 70.51, 70.49, 70.28, 69.99, 61.62, 50.62.

Compound 27



NaH (0.5 mmol, 0.020 g) was suspended in anhydrous THF (5 mL) and cooled to 0°C under a nitrogen atmosphere. To this mixture was added a solution of compound **26** (0.47 mmol, 0.19 g) in anhydrous THF (2.5 mL) and stirred for 15 minutes at 0°C . A solution of compound **24** (0.60 mmol, 0.15 g) in THF (1.2 mL) was added to the reaction mixture and stirred for 2 hours at 0°C . Then the mixture was heated to 50°C for 20 minutes after which TLC analysis (7% MeOH in DCM, $R_f=0.5$ (slightly below compound **26**)) indicated complete conversion of the starting material. H_2O (1.4 mmol, 25 μL) and 98% H_2SO_4 (1.1 mmol, 60 μL) were added and the mixture was stirred for 1 hour at reflux temperature. The mixture was poured in H_2O and washed with DCM (3x). The organic layers were combined, dried (MgSO_4) and concentrated *in vacuo*. Silica gel column chromatography (DCM \rightarrow 1% MeOH in DCM, $\Delta=0.25\%$) yielded the title compound (0.27 mmol, 0.15 g, 57%). ^1H NMR (400 MHz, CDCl_3) δ = 3.77 – 3.57 (m, 44H), 3.39 (t, $J=5.1$, 2H), 3.01 (s, 2H). ^{13}C NMR (101 MHz, CDCl_3) δ = 72.49, 70.57, 70.55, 70.52, 70.44, 70.40, 70.18, 69.93, 61.52, 50.55.

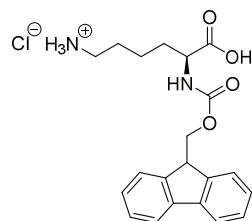
Compound 28



Compound **27** (0.27 mmol, 154 mg) was dissolved in anhydrous THF (2 mL) under an nitrogen atmosphere and cooled to 0°C. Triphenylphosphine (0.35 mmol, 0.091 mg) was added and the mixture was

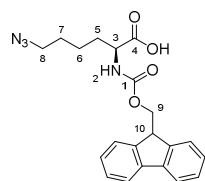
stirred for 18 hours at room temperature. H₂O (0.70 mmol, 13 μ L) was added and the reaction was stirred for 48 hours. H₂O (7 mL) was added and the white precipitate was removed by filtration. The water layer was washed with toluene (3x). The organic layers were discarded and the water layer was concentrated *in vacuo* to yield the title compound (0.20 mmol, 0.11 g, 74%). **¹H NMR (400 MHz, CDCl₃)** δ = 3.79 – 3.55 (m, 47H), 3.51 (t, *J*=5.2, 2H), 2.86 (t, *J*=5.2, 2H), 2.20 (s, 3H). **¹³C NMR (101 MHz, CDCl₃)** δ = 73.27, 72.61, 70.54, 70.50, 70.28, 70.23, 61.46, 41.68.

Compound 29

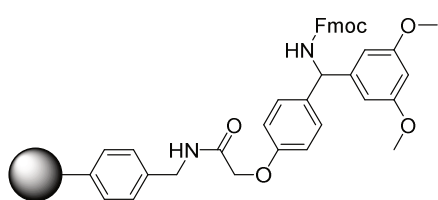


Fmoc-Lys(Boc)-OH (21.3 mmol, 10.0 g) was slowly added to dry 5M HCl in EA (150 mL). The solution was stirred for 30 min, after which the formed crash was isolated by filtration. The residue was washed with EA (3x) to yield the title compound (19.7 mmol, 7.98 g, 92%). **HRMS:** $[M+H]^+$ calculated for C₂₁H₂₅N₂O₄ 369.18088; found 369.18035 **IR(cm⁻¹)**= 3320 (1° N-H, stretch), 2918 (O-H, stretch), 1690 (C=O, stretch)

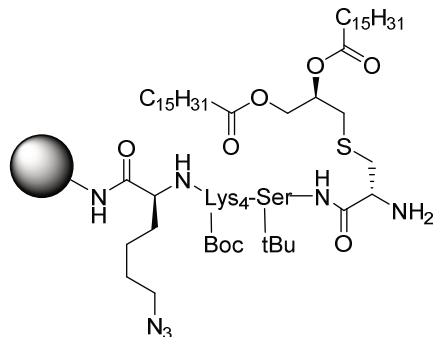
Compound 30



Compound **29** (19,7 mmol, 7,98 g) was dissolved in 8:2 MeOH:H₂O (150 mL). CuSO₄ (0.5 mmol, 80 mg), NaHCO₃ (90 mmol, 7.56 g) and HCl.imidazole-1-sulfonyl azide (0.5 mmol, 80 mg), NaHCO₃ (90 mmol, 7.56 g) and HCl.imidazole-1-sulfonyl azide (24 mmol, 5.0 g) was added. After overnight stirring, 3M HCl (aq) (30 mL) was added to acidify the solution to pH=2. The methanol was evaporated *in vacuo* and the mixture was diluted with EA and consequently washed with 10% KHSO₄ (aq) (3x) and brine (1x). The solution was dried (MgSO₄), filtrated and concentrated. The crude was adsorbed on Celite and purified by silica gel column chromatography (9:1 Pnt:EA \rightarrow 5:5 Pnt:EA, Δ =5%) to yield the title compound (14.8 mmol, 5.84 g, 75%). **HRMS:** $[M+H]^+$ calculated for C₂₁H₂₂N₄O₄ 395.17138; found 395.17120 **IR(cm⁻¹)**= 2949 (C-H, stretch), 2093 (N=N=N, stretch), 1694 (C=O, stretch). **¹H NMR (400 MHz, CDCl₃)** δ 9.38 (s, 1H, COOH), 7.74 (d, *J* = 7.5 Hz, 2H, C-H Fmoc), 7.59 (d, *J* = 5.8 Hz, 2H, C-H Fmoc), 7.38 (t, *J* = 7.4 Hz, 2H, C-H Fmoc), 7.29 (m, 2H, C-H Fmoc), 5.47 (d, *J* = 33.8 Hz, 1H, N₂), 4.51 (m, 1H, C₉), 4.39 (m, 2H, C₃₊₉), 4.20 (t, *J* = 6.8 Hz, 1H, C₁₀), 3.22 (m, 2H, C₈), 1.99 – 1.82 (m, 0.5H, C₅), 1.80 – 1.65 (m, 0.5H, C₅), 1.58 (m, 2H, C₆), 1.52 – 1.38 (m, 2H, C₇). **¹³C NMR (101 MHz, CDCl₃)** δ 176.38 (C₄), 156.31 (C₁), 143.82 (C_q Fmoc), 141.35 (C_q Fmoc), 127.83 (C-H Fmoc), 127.15 (C-H Fmoc), 125.12 (C-H Fmoc), 120.09 (C-H Fmoc), 67.19 (C₉), 53.62 (C₃), 51.09 (C₈), 47.14 (C₁₀), 31.81 (C₅), 28.38 (C₆), 22.51 (C₇).

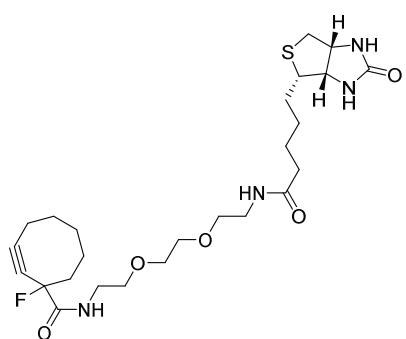
Structure of resin linker used (Rink amide)

Rink amide resin(100-200 mesh, 0.7 mmole/g) was purchased from www.rapp-polymere.com.

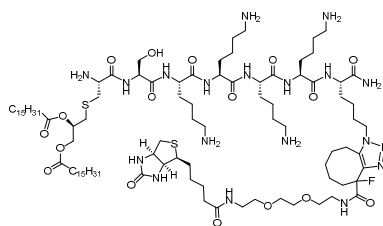
Resin-bound compound 31

Rink amide resin (200 μmol) was treated with a solution of 20% piperidine in DMF (4x) for 10 min. and consequently washed with DMF (5x). This was followed by a coupling cycle procedure consisting of the following. The resin was treated with HCTU (1 mL, 0.6M in DMF), Fmoc-Cys(R-Pam₂)-OH (1mL, 0.6M in DMF) and lastly DiPEA (1mL, 0.6M in DMF). The reaction was shaken for 2 hours and consequently washed with DMF (5x). A solution of 5%

acetic anhydride in 0.1M DiPEA in DMF was added and the syringe was shaken for 10 min. The resin was washed with DMF (5x) after which the resin was treated with a solution of 20% piperidine in DMF (4x) for 10 min. and consequently washed with DMF (5x).The coupling cycle was then started over by coupling the next amino acid. The first amino acid used in the coupling cycle was compound 30. The last amino acid used in the coupling cycle was compound 5.

Compound 32

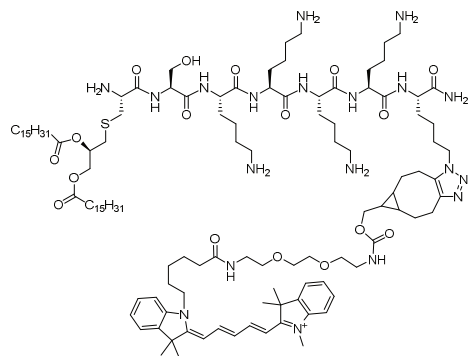
Compound 32 was synthesized in-house³⁰ via a literature procedure.³¹

Compound 33

Resin-bound compound 31 (48 mg, 10 μmol) was swollen in a reaction syringe in DCM for 1 hour. Excess solvent was removed after which a solution of 95% TFA, 2.5% H₂O, 2.5% TIS was added. The reaction syringe was shaken for 2 hours after which the syringe was emptied in a tube containing cold diethyl ether. The tube was centrifuged to collect the

precipitation as a pellet suspended in diethyl ether. The pellet was dried over nitrogen gas and consequently dissolved in DMSO (1 mL). Of this solution 900 μL was taken and put in an Eppendorf tube. Compound **32** (4.7 mg, 9 μmol) was added and the tube was shaken over 3 days when LC-MS showed complete conversion of the peptide starting material. The crude was purified by reverse-phase HPLC (Gradient: 10% AcN + 90% (H_2O +0.1% TFA) to 90% AcN + 10% (H_2O +0.1% TFA)) to obtain compound **33** (0.20 μmol , 0.39 mg, 2%) **HRMS**: $[\text{M}+2\text{H}]^{2+}$ calculated for $\text{C}_{96}\text{H}_{178}\text{FN}_{19}\text{O}_{17}\text{S}_2$ 976.6552; found 976.6570

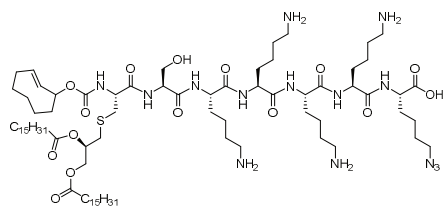
Compound 34



Resin-bound compound **31** (48 mg, 10 μmol) was swollen in a reaction syringe in DCM for 1 hour. Excess solvent was removed after which a solution of 95% TFA, 2.5% H_2O , 2.5% TIS was added. The reaction syringe was shaken for 2 hours after which the syringe was emptied in a tube containing cold diethyl ether. The tube was centrifuged to collect the precipitation as a pellet suspended in diethyl ether. The pellet was dried over nitrogen gas and consequently dissolved in DMSO

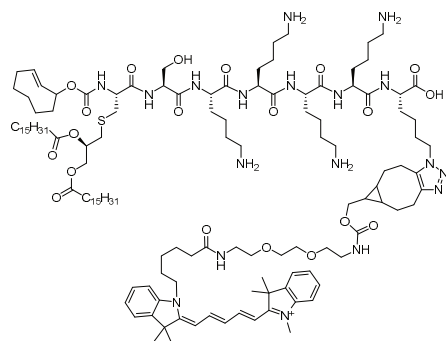
(1 mL). Of this solution, 100 μL was put in an Eppendorf tube (1.5 mL). BCN-Cy5 (1 μmol , 0.81 mg) was added and the tube was shaken for 3 days at room temperature. LC-MS analysis indicated complete conversion of the starting material. The crude was purified by reverse-phase HPLC to yield the title compound (0.20 μmol , 0.44 mg, 20% overall yield) **LC-MS (1090, C18, H_2O /AcN + TFA)**: 1107.27 ($z=2$, simulated), 1107.73 ($z=2$, observed), 1164.13 ($z=2$, TFA adduct), 1221.00 ($z=2$, 2*TFA adduct), 1277.53 ($z=2$, 3*TFA adduct). **HRMS**: $[\text{M}+3\text{H}]^{4+}$ calculated for $\text{C}_{120}\text{H}_{205}\text{N}_{19}\text{O}_{17}\text{S}$ 554.38726; found 554.38633

Compound 35



Resin-bound compound **31** (40 mg, 10 μmol) was swollen in DMF and DiPEA (50 μmol , 9 μL) and TCO-OSu (50 μmol , 13 mg) were added and the reaction syringe was shaken overnight. LC-MS analysis of a small amount of TFA-treated resin indicated complete conversion of the

starting material. The resin was washed with DMF (3x) and DCM (3x). A solution of 5% TFA, 2.5% TIS, 2.5% H_2O in DCM was added and the reaction vessel was shaken for 15 min. The syringe was emptied in a 0°C solution of Et_2O (total volume = 30 mL) and put in a -20°C freezer overnight. The tube was then centrifuged for 90 min at 4°C after which a pellet was visible. The tube was decanted and the pellet dried to yield the title compound (2.3 μmol , 3.3 mg, 23%).

Compound 36

A solution of compound **35** (max. 2.3 μmol , 3.3 mg) in anhydrous DMSO (200 μL) was put in an Eppendorf tube (1.5 mL). BCN-Cy5 (1.1 μmol , 0.90 mg) was added and the tube was shaken for 3 days at room temperature. LC-MS analysis indicated complete conversion of the starting material. The mixture was diluted with DMSO (500 μL) and a mixture of 1:1:1 *t*-BuOH:AcN:H₂O (500 μL). The crude was purified by reverse-phase HPLC to yield the title

compound (0.60 μmol , 1.4 mg, 26% overall yield). **HRMS**: $[\text{M}+3\text{H}]^{3+}$ calculated for C₁₂₉H₂₁₅N₁₈O₂₀S 789.86993; found 789.86841

References

- (1) van de Graaff, M. J.; Oosenbrug, T.; Marqvorsen, M. H. S.; Nascimento, C. R.; de Geus, M. A. R.; Manoury, B.; Rensing, M. E.; van Kasteren, S. I. Conditionally Controlling Human TLR2 Activity via Trans-Cyclooctene Caged Ligands. *Bioconjugate Chem.* **2020**, *31* (6), 1685–1692.
- (2) Oosenbrug, T.; van de Graaff, M. J.; Haks, M. C.; van Kasteren, S.; Rensing, M. E. An Alternative Model for Type I Interferon Induction Downstream of Human TLR2. *J. Biol. Chem.* **2020**, *295* (42), 14325–14342.
- (3) Flo, T. H.; Halaas, Ø.; Torp, S.; Ryan, L.; Lien, E.; Dybdahl, B.; Sundan, A.; Espevik, T. Differential Expression of Toll-like Receptor 2 in Human Cells. *J. Leukoc. Biol.* **2001**, *69* (3), 474–481.
- (4) Kang, J. Y.; Nan, X.; Jin, M. S.; Youn, S.-J.; Ryu, Y. H.; Mah, S.; Han, S. H.; Lee, H.; Paik, S.-G.; Lee, J.-O. Recognition of Lipopeptide Patterns by Toll-like Receptor 2-Toll-like Receptor 6 Heterodimer. *Immunity* **2009**, *31* (6), 873–884.
- (5) Jin, M. S.; Kim, S. E.; Heo, J. Y.; Lee, M. E.; Kim, H. M.; Paik, S.-G.; Lee, H.; Lee, J.-O. Crystal Structure of the TLR1-TLR2 Heterodimer Induced by Binding of a Tri-Acylated Lipopeptide. *Cell* **2007**, *130* (6), 1071–1082.
- (6) Aliprantis, A. O. Cell Activation and Apoptosis by Bacterial Lipoproteins Through Toll-like Receptor-2. *Science* **1999**, *285* (5428), 736–739.
- (7) Kagan, J. C.; Su, T.; Horng, T.; Chow, A.; Akira, S.; Medzhitov, R. TRAM Couples Endocytosis of Toll-like Receptor 4 to the Induction of Interferon- β . *Nat Immunol* **2008**, *9* (4), 361–368.
- (8) Tatematsu, M.; Yoshida, R.; Morioka, Y.; Ishii, N.; Funami, K.; Watanabe, A.; Saeki, K.; Seya, T.; Matsumoto, M. Raftlin Controls Lipopolysaccharide-Induced TLR4 Internalization and TICAM-1 Signaling in a Cell Type-Specific Manner. *J.I.* **2016**, *196* (9), 3865–3876.
- (9) Lu, Y.-C.; Yeh, W.-C.; Ohashi, P. S. LPS/TLR4 Signal Transduction Pathway. *Cytokine* **2008**, *42* (2), 145–151.
- (10) Dutta, D.; Donaldson, J. G. Search for Inhibitors of Endocytosis: Intended Specificity and Unintended Consequences. *Cellular Logistics* **2012**, *2* (4), 203–208.
- (11) Mancini, R. J.; Stutts, L.; Moore, T.; Esser-Kahn, A. P. Controlling the Origins of Inflammation with a Photoactive Lipopeptide Immunopotentiator. *Angew. Chem. Int. Ed.* **2015**, *54* (20), 5962–5965.
- (12) Ryu, K. A.; Stutts, L.; Tom, J. K.; Mancini, R. J.; Esser-Kahn, A. P. Stimulation of Innate Immune Cells by Light-Activated TLR7/8 Agonists. *J. Am. Chem. Soc.* **2014**, *136* (31), 10823–10825.
- (13) Denk, W. Two-Photon Scanning Photochemical Microscopy: Mapping Ligand-Gated Ion Channel Distributions. *Proceedings of the National Academy of Sciences* **1994**, *91* (14), 6629–6633.
- (14) Lee, R. E. C.; Walker, S. R.; Savery, K.; Frank, D. A.; Gaudet, S. Fold Change of Nuclear NF-KB Determines TNF-Induced Transcription in Single Cells. *Molecular Cell* **2014**, *53* (6), 867–879.
- (15) Lee, T. K.; Denny, E. M.; Sanghvi, J. C.; Gaston, J. E.; Maynard, N. D.; Hughey, J. J.; Covert, M. W. A Noisy Paracrine Signal Determines the Cellular NF-KB Response to Lipopolysaccharide. *Science Signaling*, **2009**, *2* (93), ra65.

- (16) Blackman, M. L.; Royzen, M.; Fox, J. M. Tetrazine Ligation: Fast Bioconjugation Based on Inverse-Electron-Demand Diels–Alder Reactivity. *J. Am. Chem. Soc.* **2008**, *130* (41), 13518–13519.
- (17) Versteegen, R. M.; Rossin, R.; ten Hoeve, W.; Janssen, H. M.; Robillard, M. S. Click to Release: Instantaneous Doxorubicin Elimination upon Tetrazine Ligation. *Angew. Chem. Int. Ed.* **2013**, *52* (52), 14112–14116.
- (18) van der Gracht, A. M. F.; de Geus, M. A. R.; Camps, M. G. M.; Ruckwardt, T. J.; Sarris, A. J. C.; Bremmers, J.; Maurits, E.; Pawlak, J. B.; Posthoorn, M. M.; Bongers, K. M.; Filippov, D. V.; Overkleeft, H. S.; Robillard, M. S.; Ossendorp, F.; van Kasteren, S. I. Chemical Control over T-Cell Activation *in Vivo* Using Deprotection of *Trans* -Cyclooctene-Modified Epitopes. *ACS Chem. Biol.* **2018**, *13* (6), 1569–1576.
- (19) Rossin, R.; Versteegen, R. M.; Wu, J.; Khasanov, A.; Wessels, H. J.; Steenbergen, E. J.; ten Hoeve, W.; Janssen, H. M.; van Onzen, A. H. A. M.; Hudson, P. J.; Robillard, M. S. Chemically Triggered Drug Release from an Antibody-Drug Conjugate Leads to Potent Antitumour Activity in Mice. *Nat Commun* **2018**, *9* (1), 1484.
- (20) Fan, X.; Ge, Y.; Lin, F.; Yang, Y.; Zhang, G.; Ngai, W. S. C.; Lin, Z.; Zheng, S.; Wang, J.; Zhao, J.; Li, J.; Chen, P. R. Optimized Tetrazine Derivatives for Rapid Bioorthogonal Decaging in Living Cells. *Angew. Chem. Int. Ed.* **2016**, *55* (45), 14046–14050.
- (21) Sarris, A. J. C.; Hansen, T.; de Geus, M. A. R.; Maurits, E.; Doelman, W.; Overkleeft, H. S.; Codée, J. D. C.; Filippov, D. V.; van Kasteren, S. I. Fast and PH-Independent Elimination of *Trans* -Cyclooctene by Using Aminoethyl-Functionalized Tetrazines. *Chem. Eur. J.* **2018**, *24* (68), 18075–18081.
- (22) Omueti, K. O.; Beyer, J. M.; Johnson, C. M.; Lyle, E. A.; Tapping, R. I. Domain Exchange between Human Toll-like Receptors 1 and 6 Reveals a Region Required for Lipopeptide Discrimination. *J. Biol. Chem.* **2005**, *280* (44), 36616–36625.
- (23) Metzger, J. W.; Wiesmüller, K.-H.; Jung, G. Synthesis of N α -Fmoc Protected Derivatives of S-(2,3-Dihydroxypropyl)-Cysteine and Their Application in Peptide Synthesis. *International Journal of Peptide and Protein Research* **2009**, *38* (6), 545–554.
- (24) El Oualid, F.; Merckx, R.; Ekkebus, R.; Hameed, D. S.; Smit, J. J.; de Jong, A.; Hilkmann, H.; Sixma, T. K.; Ovaa, H. Chemical Synthesis of Ubiquitin, Ubiquitin-Based Probes, and Diubiquitin. *Angew. Chem. Int. Ed.* **2010**, *49* (52), 10149–10153.
- (25) Rossin, R.; van Duijnhoven, S. M. J.; ten Hoeve, W.; Janssen, H. M.; Kleijn, L. H. J.; Hoebe, F. J. M.; Versteegen, R. M.; Robillard, M. S. Triggered Drug Release from an Antibody–Drug Conjugate Using Fast “Click-to-Release” Chemistry in Mice. *Bioconjugate Chem.* **2016**, *27* (7), 1697–1706.
- (26) Wilkinson, B. L.; Day, S.; Malins, L. R.; Apostolopoulos, V.; Payne, R. J. Self-Adjuvanting Multicomponent Cancer Vaccine Candidates Combining Per-Glycosylated MUC1 Glycopeptides and the Toll-like Receptor 2 Agonist Pam3CysSer. *Angew. Chem. Int. Ed.* **2011**, *50* (7), 1635–1639.
- (27) Zhang, H.; Li, X.; Shi, Q.; Li, Y.; Xia, G.; Chen, L.; Yang, Z.; Jiang, Z.-X. Highly Efficient Synthesis of Monodisperse Poly(Ethylene Glycols) and Derivatives through Macrocyclization of Oligo(Ethylene Glycols). *Angew. Chem. Int. Ed.* **2015**, *54* (12), 3763–3767.
- (28) Versteegen, R. M.; ten Hoeve, W.; Rossin, R.; de Geus, M. A. R.; Janssen, H. M.; Robillard, M. S. Click-to-Release from *Trans* -Cyclooctenes: Mechanistic Insights and

- Expansion of Scope from Established Carbamate to Remarkable Ether Cleavage. *Angew. Chem. Int. Ed.* **2018**, *57* (33), 10494–10499.
- (29) de Geus, M. A. R.; Groenewold, G. J. M.; Maurits, E.; Araman, C.; van Kasteren, S. I. Synthetic Methodology towards Allylic *Trans* -Cyclooctene-Ethers Enables Modification of Carbohydrates: Bioorthogonal Manipulation of the *Lac* Repressor. *Chem. Sci.* **2020**, *11* (37), 10175–10179.
- (30) Van Der Linden, W. A.; Li, N.; Hoogendoorn, S.; Ruben, M.; Verdoes, M.; Guo, J.; Boons, G. J.; Van Der Marel, G. A.; Florea, B. I.; Overkleeft, H. S. Two-Step Bioorthogonal Activity-Based Proteasome Profiling Using Copper-Free Click Reagents: A Comparative Study. *Bioorganic and Medicinal Chemistry* **2012**, *20* (2), 662–666.
- (31) Schultz, M. K.; Parameswarappa, S. G.; Pigge, F. C. Synthesis of a DOTA-Biotin Conjugate for Radionuclide Chelation via Cu-Free Click Chemistry. *Organic Letters* **2010**, *12* (10), 2398–2401.

Chapter 3

Conditionally controlled intracellular TLR-ligands¹

Introduction

Chapter 2 introduced the concept of bioorthogonally protected TLR ligands and revealed that a trans-cyclooctene protecting group gave control over TLR2/6 receptor dimer-mediated signaling. The aim of the research described in Chapter 2 was to make use of caged TLR2/6 ligands as tools to reveal where intracellular TLR2/6 signaling occurred, and whether TLR2/6 dimers located at the cell surface provided a pro-inflammatory signal different from that following intracellular activation. TLR2/6 is not the only receptor for which such a signaling duality has been postulated.² TLR4, for example, has been shown to induce NF- κ B when activated at the cell surface, yet signals in an IRF-dependent manner when ligated from within the endosome.³

One sub-family of TLRs resides exclusively in endosomes and lysosomes. This family, encompassing TLR3, TLR7, TLR8, and TLR9, bind nucleic acids (NAs) of non-host origin. TLR3 recognizes double-stranded RNA (dsRNA)⁴, TLR7 and 8 recognize single-stranded RNA (ssRNA)^{5,6} and TLR9 recognizes DNA with recurring motifs of unmethylated cytosine-phosphodiester-guanine (CpG) in the 5'→3' direction.⁷ For this purely endo-lysosomal family of receptors a signaling duality has also been hypothesized: namely that signaling from early endosomes and late endosomes/lysosomes is different.⁸ Indeed, evidence exists that TLR9 signaling from the late endosomal compartment leads to NF-KB activation, whereas its signaling from earlier endosomal compartments induces IRF-signaling.^{9,10} For TLR3, TLR7, and TLR8, no evidence supporting the existence of signaling duality has yet been reported.

Furthermore, it remains to be elucidated *how* this dichotomous TLR9 signaling arises: whether the NF-KB-activating signaling cascade occurs only when an unligated TLR9-receptor encounters its ligand in the late endosome/lysosome, or whether the signaling adapters associated with the TLR9 simply change during the maturation from an early endosome to a late endosome when the receptor encountered its ligand in this early endosome.

It was envisaged that conditional ligands could be used to probe this compartment-specific behavior. Such tools would be useful to unravel TLR9 signaling, but also to determine whether other endosomal TLRs displayed this dichotomous signaling. In an attempt to address these questions, the Esser-Kahn group has published a photocaged variant of the TLR 7/8-ligand Resiquimod (also 'R848'), namely, NPPOC-Resiquimod (Figure 1 – the photolabile groups in the caged TLR ligands depicted in Figure 1 are highlighted in blue).¹¹

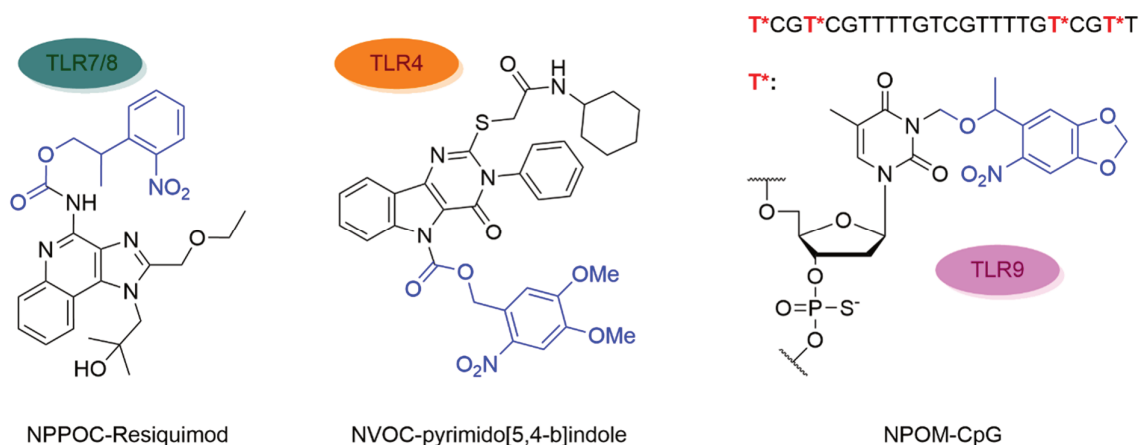


Figure 1. Previously reported conditional ligands for intracellular TLRs: a resiquimod derivative that has a 2-(2-nitrophenyl)-propoxycarbonyl (NPPOC) cage conditionally controls TLR7/8 activity,¹¹ a pyrimido[5,4-b]indole derivative caged with N-veratryloxycarbonyl (NVOC) conditionally controls TLR4 activity,¹² and a CpG sequence carrying four 6-nitropiperonyloxymethyl (NPOM)-modified T residues (indicated in red).¹³

Control over TLR7/8 activity can be achieved upon UV-irradiation of model cell lines and of primary dendritic cells pretreated with NPPOC-Resiquimod. The same laboratory also produced a photocaged variant of a TLR4 ligand, NVOC-pyrimido[5,4-b]indole (Figure 1).¹² The group of Deiters reported a photocaged TLR9 ligand, 24-meric CpG carrying four NPOM-groups (Figure 1).¹³ Treatment of TLR9-expressing HEK293T cells with NPOM-CpG followed by UV-irradiation showed that TLR9 activity could also be controlled with light. A modest three-fold induction of TLR9 activity was observed after irradiation with 360 nm light. This is possibly due to multiple thymidines requiring caging to abolish the binding to TLR9.

The photo-deprotection experiments with the three ligands shown in Figure 1 were the first examples of the use of conditional ligands to study pattern recognition receptors. However, the experimental methods described in these papers are limited in their use for distinguishing between different endosomal compartments. The low spatial resolution of the UV-source (>7 mm²) and the migration of cells during the 10-minute irradiation window prevents this.¹¹

In order to achieve sub-cellular activation of TLR-ligands, it was envisaged that a chemical, rather than a photochemical, deprotection strategy would be of use. Recently, tetrazines have been reported that were targeted to specific organelles and were used for a sub-cellular ligation reaction.¹⁴ Applying such a strategy to the study of TLR-ligands was envisaged to offer a solution for unraveling the potential signaling dichotomy of the TLRs that are present in more than one sub-cellular location: if deprotection could be limited to, for example, an early endosome, the contribution of signaling from this compartment could be isolated.

In this Chapter, the syntheses of trans-cyclooctene-protected ligands for TLR4, the TLR 7/8 combination and TLR9 are described (Figure 2). The produced reagents can be combined with the tetrazine-mediated uncaging strategy described in Chapter 2.

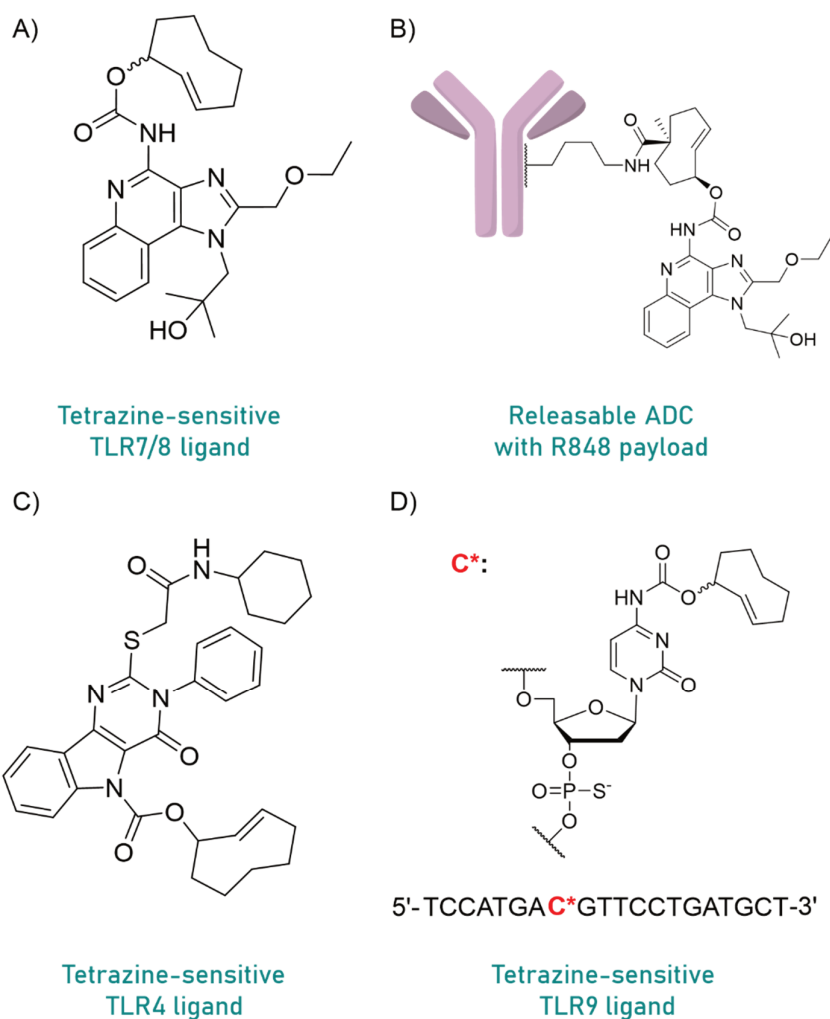


Figure 2. TCO-caged TLR ligands subject of the studies described in this Chapter. A) R848 caged with a TCO on its exocyclic amine. B) An antibody-drug-conjugate (ADC) bearing an R848 payload through a tetrazine-sensitive immolative linker. C) A pyrimido[5,4-b]indole-based synthetic TLR4 ligand caged with a TCO on the endocyclic amine of the indole. D) A 20-mer oligodeoxynucleotide bearing a single CpG motif, of which its deoxycytidine is caged with a TCO on the exocyclic amine.

Results and Discussion

Towards a chemo-controllable TLR9-agonist

The synthesis of a tetrazine-controllable TLR9 ligand was undertaken first. It was envisaged to first introduce a TCO-moiety on the exocyclic amine of a cytidine building block and then use this reagent in a phosphoramidite/DMTr on-resin oligonucleotide synthesis strategy.¹⁵ This strategy was based on the observation that the cytidine in the singly-present CpG-motif (Figure 2, **C***) is engaged in both strong van der Waals interactions and hydrogen bonding as revealed by the co-crystal structure of ODN1668 (a CpG class B ODN with phosphorothioate linkages) in complex with the extracellular domain of bovine TLR9.¹⁶ It was postulated, based on the above interactions, that protection of the exocyclic amine on one of the cytidines of the TLR9-binding 12-mer fragment of ODN1668 (Scheme 2, compound **11**) would yield a compound that does not bind TLR9.

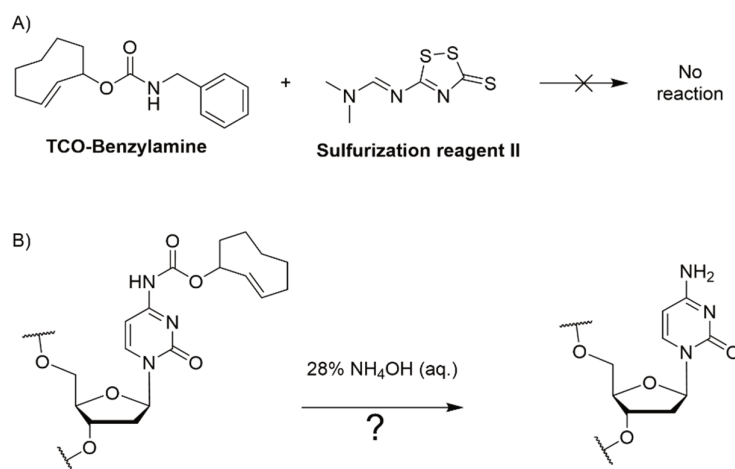
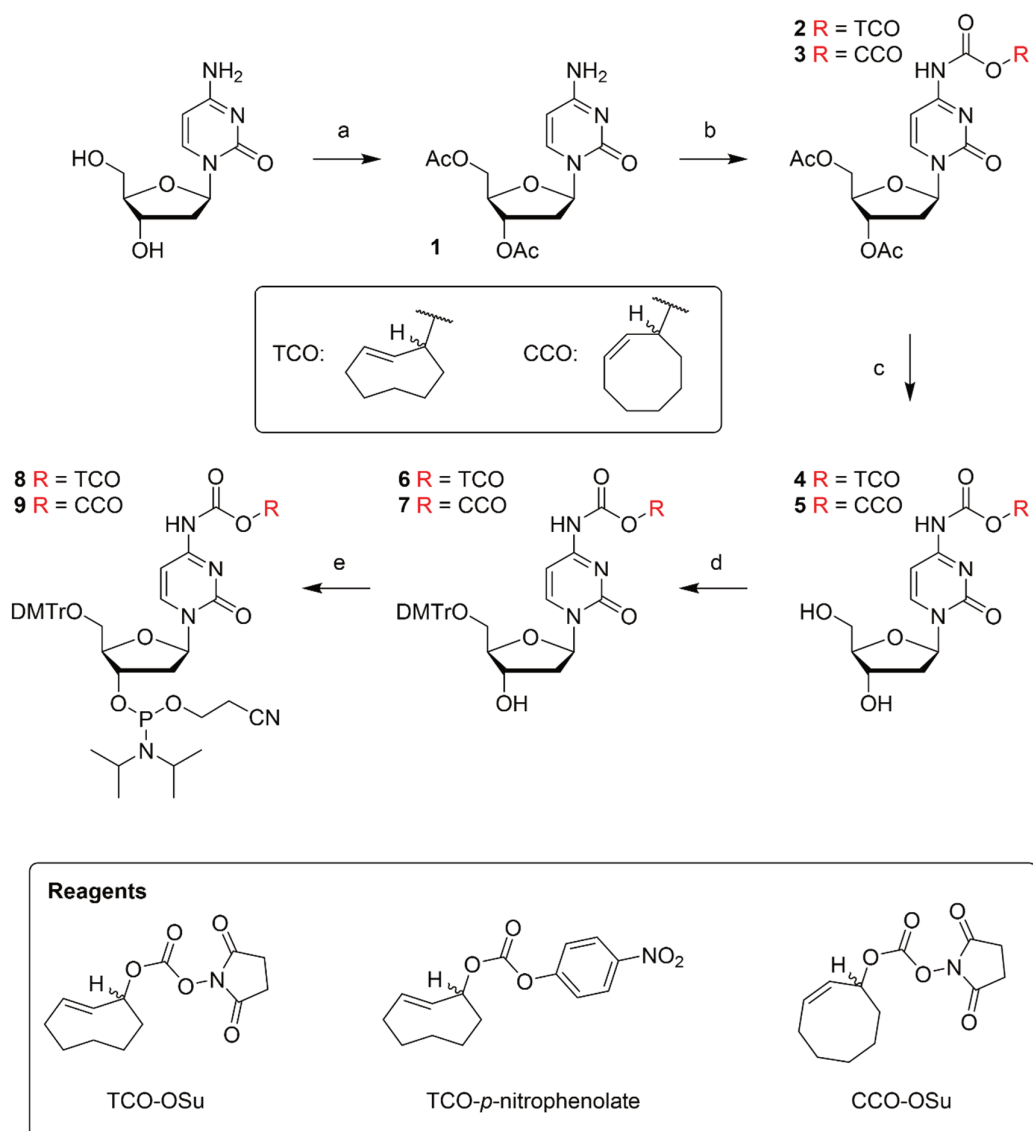


Figure 3. Potential hurdles during ODN synthesis using a TCO-caged deoxycytidine. A) Sulfurization reagents needed to oxidize the phosphites to phosphorothioates may react with the trans-configured olefin, though this was not observed when exposing TCO-benzylamine to this reagent. B) Hydrolysis of the TCO may occur during global deprotection to a significant extent.

ODN1668 contains phosphorothioate esters for increased biological stability.¹⁵ Synthesis of the TCO-protected variant **12** (Scheme 2) requires the TCO-caged cytidine to be stable to repeated cycles of sulfurization and acidic detritylation, as well as to concentrated aqueous ammonium hydroxide used in the final global deprotection step. To first assess whether this is the case, the model TCO-benzylamine was exposed to sulfurization reagent II (Figure 3A). 30-minute exposure of TCO-benzylamine to a 10-fold excess of sulfurization reagent II did not yield any degradation products and TCO-benzylamine could be recovered in >99% yield after work-up and purification.

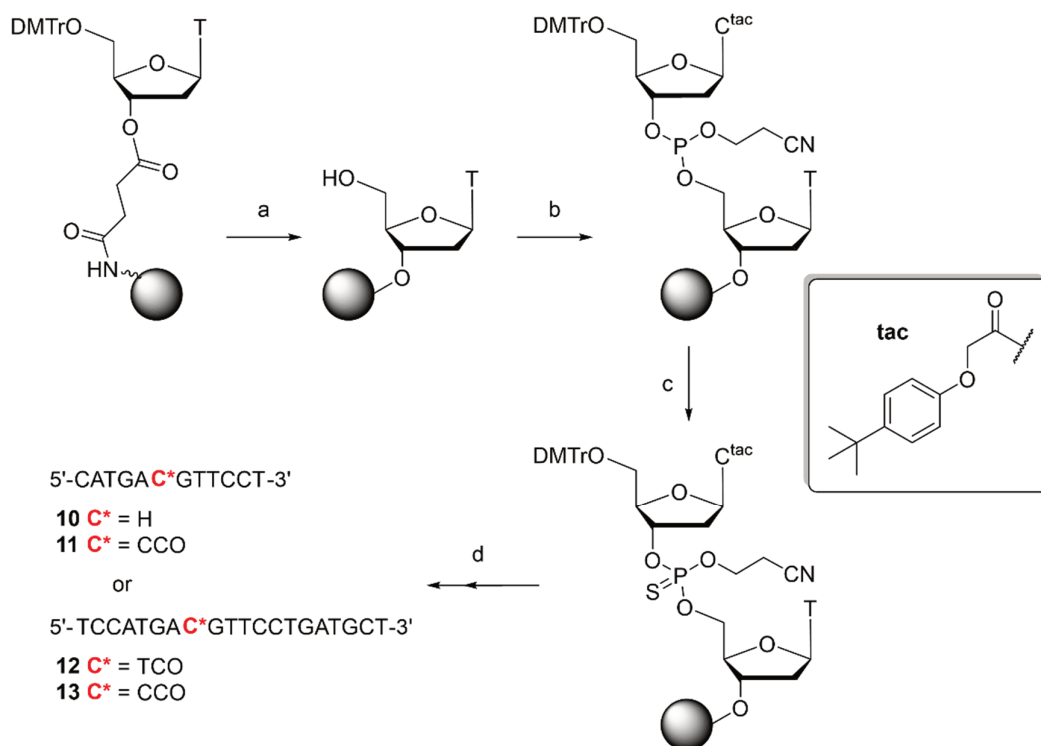


Scheme 1. Synthesis of trans- and cis-cyclooctene protected building blocks for solid phase DNA synthesis starting from deoxycytidine. Reagents and conditions: **a**) 30% Acetyl chloride in CHCl_3 , acetic acid, 40°C , o.n., qt.; **b**) Compound **2**: TCO-*p*-nitrophenolate, DiPEA, DMAP, acetonitrile, 40°C , 7 days, 90%; compound **3**: CCO-*p*-nitrophenolate, DiPEA, DMAP, acetonitrile, 40°C , 7 days, 84%; **c**) K_2CO_3 , MeOH, r.t., 2 hrs, qt.; **d**) DMTrCl, pyridine, r.t., o.n., 77% (Compound **6**), 72% (Compound **7**); **e**) 2-cyanoethyl N,N-diisopropylchlorophosphoramidite, DiPEA, DCM, $0^\circ\text{C} \rightarrow$ r.t., 15 min, 71% (compound **8**), 88% (compound **9**).

Next, the synthesis of the phosphoramidite/DMTr-protected TCO-cytidine **8** was attempted. First the 3'- and 5'-hydroxyl-groups on the deoxycytidine were protected as acetates (reaction **a**, Scheme 1). Next the reaction between TCO-OSu and CCO-OSu and the exocyclic amine on the nucleobase (**1**) was attempted using various bases (DiPEA, DBU, LiHMDS) as catalysts. All failed to yield the desired product. When *p*-nitrophenolate-activated TCO carbonate was used as a TCO-donor, in presence of a catalytic amount of DMAP the reaction proceeded to yield **3** in 90% after 7 days at 40°C . H-NMR spectroscopy showed that no trans-to-cis conversion of the TCO-group

had taken place during this time. Deacetylation was achieved using potassium carbonate in methanol. This resulted in the formation of product **4** in quantitative yield. Interestingly, quenching of the potassium carbonate with Amberlite H⁺ prior to evaporation resulted in a loss of product. The mixture was therefore concentrated without quenching, which prevented the loss of product and did not result in hydrolysis of the carbamate.

Before proceeding with the synthesis of **8**, the stability of the TCO-carbamate to 28% NH₄OH (aq.) was assessed, as these are the conditions used in the final deprotection during solid phase oligonucleotide synthesis (Figure 3). Compound **4** was incubated for 60 minutes at room temperature, followed by concentration at 45°C. This led to partial hydrolysis (10%) of the TCO, as determined by LC-MS. It was therefore decided to employ 4-tert-butylphenoxyacetyl-protected (tac, scheme 2) nucleotide building blocks during ODN synthesis, known for their fast deprotection in comparison to standard benzoyl/isobutyl/acetyl-protected building blocks, to limit the hydro- and aminolysis of the TCO during NH₄OH (aq.) treatment.¹⁷ Exposure to the shorter deprotection conditions required when using these protecting groups did not result in hydrolysis of **4**. Introduction of the DMTr-protecting group onto the 5-position of **4**, followed by phosphitylation proceeded to yield **8** in 41% over 5 steps. The CCO-modified control compound **9** was synthesized in the same manner in a 47% yield over 5 steps.



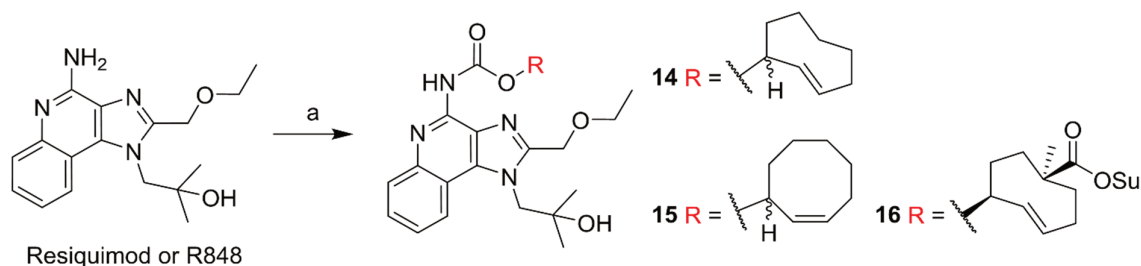
Scheme 2. Synthesis of cyclooctene-caged ODN1668 12- and 20-mer derivatives. Reagents and conditions: **a)** 5% dichloroacetic acid in toluene, r.t., 3 min (1x); **b)** (i) DMTr-dC^{tac}-PAM (3 eq.), r.t., acetonitrile, 3 min (2x) (ii) 4-tert-butylphenoxyacetyl anhydride, acetonitrile, r.t., 30 sec (1x); **c)** Sulfurization reagent II (10 eq.), acetonitrile, r.t., 1 min (1x); **d)** Repeat steps **a-c** with the respective deoxynucleoside phosphoramidite building blocks: DMTr-dG^{tac}-PAM, DMTr-dT-PAM, DMTr-dA^{tac}-PAM. At position C*, either building block **8** or **9** was used as the deoxynucleoside phosphoramidite.

Building block **9** was next used in the synthesis of a the TCO-protected 12-mer oligonucleotide **11**.¹⁶ The parent unprotected motif **10** was also synthesized (Scheme 2). The oligonucleotides were subsequently cleaved from the resin, purified and desalted as reported.¹⁵ MALDI-analysis confirmed the molecular weight of the products.

Next, the ability of **10** and **11** to activate TLR9 was assessed on murine bone marrow-derived dendritic cells (BMDCs). Neither the protected nor unprotected 12-mers induced cytokine expression in these cells. This could be due to the lower levels of TLR9 (and its trafficking adapter Unc93B1) expression in BMDCs, compared to the transfected HEK293T-cell lines used in the aforementioned publication that shows the activation of TLR9 by non-caged 12-mer **10**.¹⁶ In an attempt to achieve a higher NF- κ B activity in BMDCs, the full length 20-mer CpG was synthesized with either a TCO (**12**) or CCO (**13**) on the deoxycytidine indicated in red in Scheme 2. These compounds are currently awaiting their biological evaluation.

A Chemo-controllable TLR7/8-Agonist

Next, the synthesis of the TCO-modified TLR7/8 ligand Resiquimod was attempted (Scheme 3). Previous studies using the *O*-nitrobenzyl-protected variant of the same ligand (NPPOC-Resiquimod, Figure 1) had shown that modification of the exocyclic amine could block TLR7/8 ligation.¹¹



Scheme 3. Synthesis of trans- and cis-cyclooctene protected resiquimod. Reagents and conditions: **a)** Compound **14**: TCO-OSu, DiPEA, 1:1 DMF:DCM, r.t., 5 days, 43%; Compound **15**: CCO-OSu, DiPEA, 1:1 DMF:DCM, r.t., 5 days, 71%; Compound **16**: TCO-(OSu)₂, DiPEA, 1:2 DMF:DCM, r.t., 10 days, 24%

14 Was synthesized by reacting Resiquimod with TCO-OSu to yield the TCO-carbamate **14** (Scheme 3) in 14% yield after 5 days reaction time. The CCO-carbamate-modified control compound **15** was made in the same manner in a 71% yield. Resiquimod modified with a more soluble bifunctional TCO-carbamate (**16**) was made in a 24% yield. The ability of **14** (R848-TCO) and **15** (R848-CCO) to activate TLR7 and/or TLR8 was assessed by quantifying their ability to induce TNF- α and IL-6 production in murine BMDMs (Figure 4).

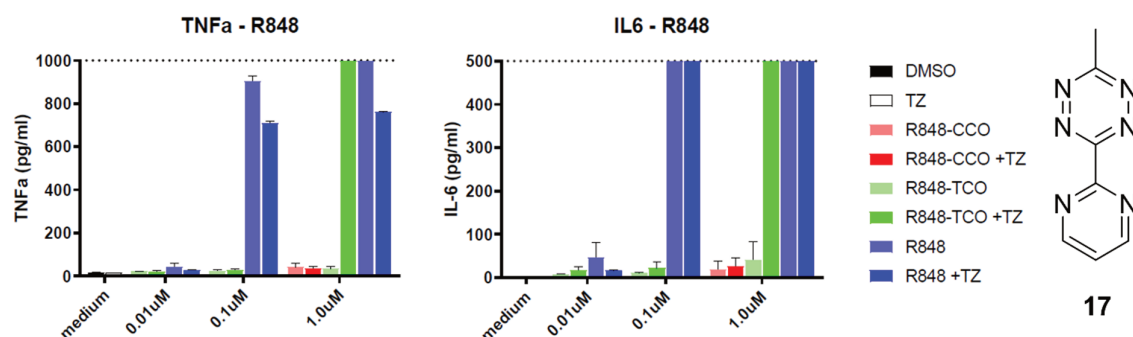


Figure 4. Biological evaluation of compounds **14** and **15**: R848-TCO and R848-CCO, respectively. TNF- α and interleukin 6 (IL6) concentrations were measured in medium containing murine bone marrow-derived macrophages (BMDMs). R848-TCO only elicits a response when co-administering tetrazine **17** at 1 μ M, whereas R848-CCO is irresponsive at the same concentration.

14 Did not induce cytokine production at 0.01-1 μ M (light green bars). Upon addition of tetrazine **17** (Figure 4), activity was restored to a 1 μ M ligand concentration for both secretion of TNF- α and IL6. Future work includes testing this ligand at >1 μ M concentrations in conjunction with tetrazines directed to either the extracellular environment or the endo-lysosomal pathway to selectively activate the populations of TLR7/8 that are residing in various locations in or on the cell.

Synthesis of R848-TCO Conjugates

TLR-ligands have been suggested as chemotherapeutics against numerous cancers by inducing a robust immune response against tumor-associated antigens. Resiquimod is clinically approved for the treatment of cutaneous T cell lymphoma as well as herpes-derived skin lesions. These treatments are, however, all limited by topical application as systemic application of TLR ligands can induce cytokine storms and carry the potential to induce septic shock.¹⁸ It was therefore envisaged that the second OSu-functionality present in **16** (Scheme 3) could be used to conjugate the ligand to an antibody to produce an antibody-drug conjugate (ADC). The ligand's activity would be blocked by the TCO, and 'released' *in vivo* after targeting it to a tumour via the antibody.^{19–22}

In order to produce this R848-based ADC, the protocol described by Rossin *et al.*²³ for modifying antibodies with TCO-modified chemotherapeutics TCO-OSu was used to modify the model protein, egg white protein ovalbumin (OVA). OVA was reacted with compound **16** (Figure 5) for 2 hours in a mixture of PBS, propyleneglycol, and DMF (7:2:1). After size-based separation over a 30 kDa cutoff filter ($m_{\text{ovalbumin}} = 42.7$ kDa), the product was analyzed using a fluorogenic BODIPY-labeled tetrazine (synthesized in-house by Alexi Sarris).²⁴ A single band in the BODIPY channel was observed indicating successful TCO-conjugation, although the modification yield remains to be determined (Figure 5A).

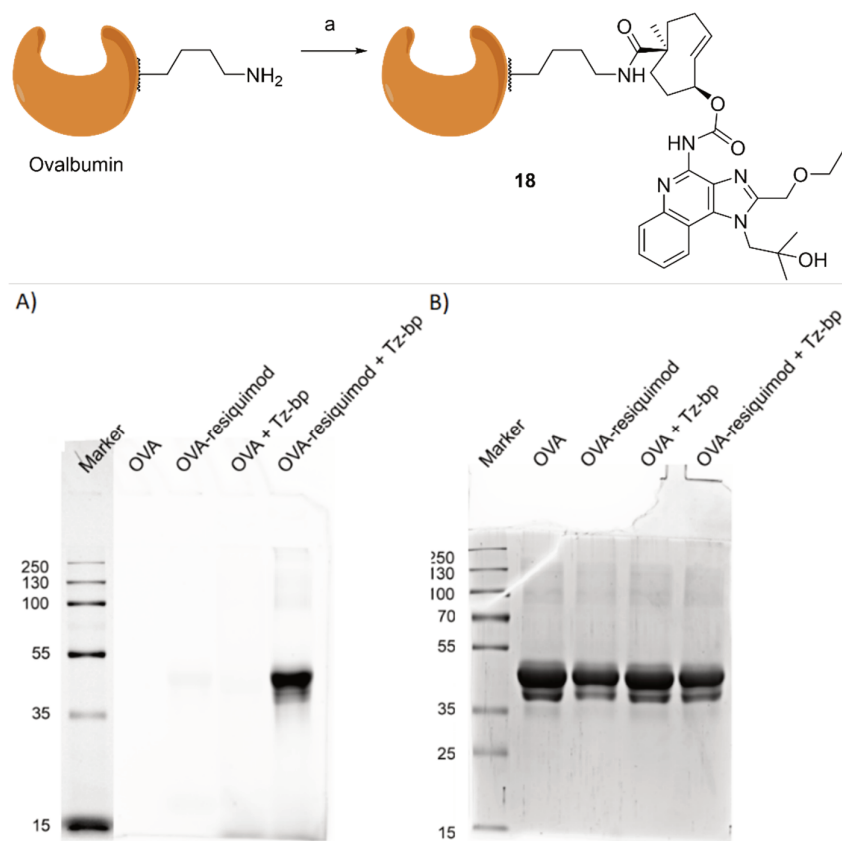
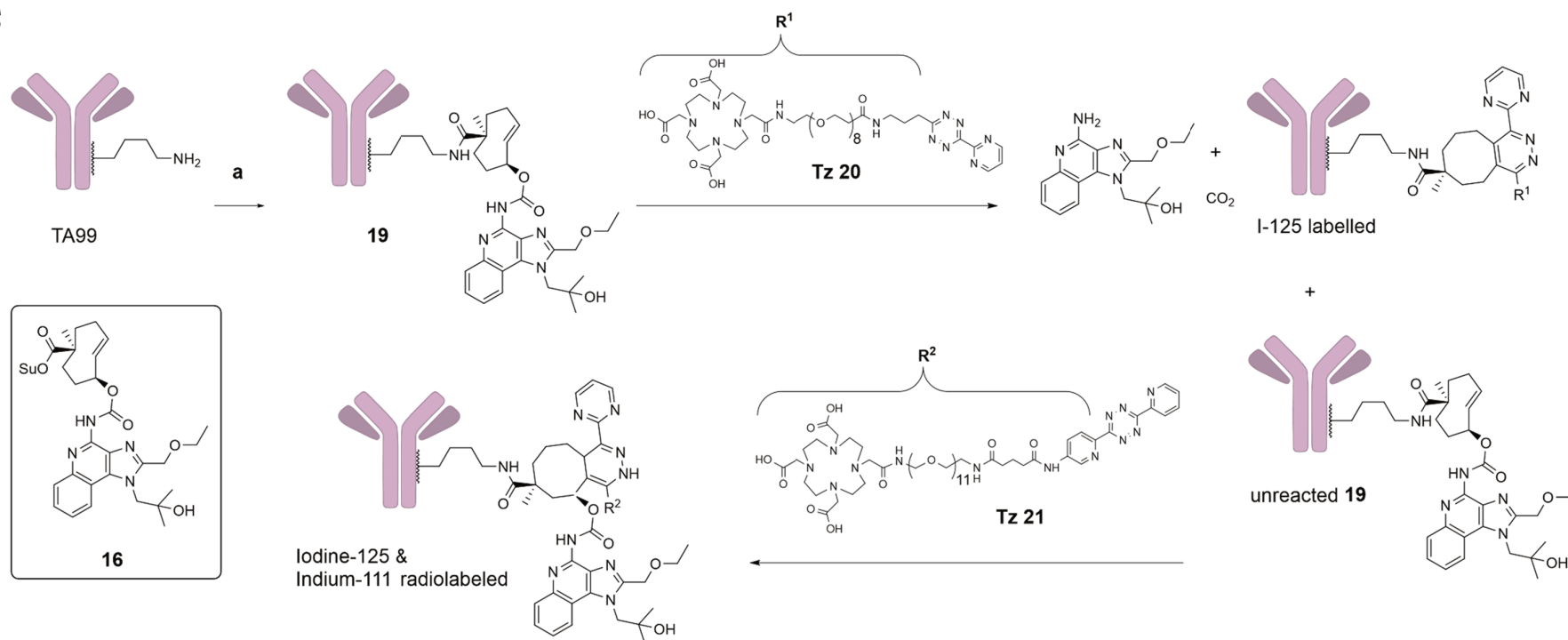


Figure 5. Conjugation of ovalbumin to R848 through a bis-functionalized TCO linker. SDS-PAGE analysis of caged ovalbumin (OVA) was used to verify conjugation as well as trans-configuration of the TCO. A) Fluorescence in the BODIPY channel. Only OVA-TCO-R848 gives rise to a signal when treated with a BODIPY-tetrazine (Tz-bp), indicating product formation. B) Coomassie staining indicating near-equal loading of proteins in each lane. Reagents and conditions: **a)** Compound **16**, 1M Na₂CO₃·(aq.), 7:2:1 PBS:propylene glycol:DMF (v:v:v).

With these conditions in hand, the conjugation of **16** to the tumor-targeting antibody TA99 was attempted.²⁵ This monoclonal antibody binds tyrosinase-related protein 1 (TYPR1) that is often upregulated in melanoma cells.²⁶ The conjugation procedure yielded conjugate **19** after purification using a PD-10 column (Scheme 4, reaction a). Release of Resiquimod from conjugate **19** was assessed in an *in vitro* experiment, in which THP1-Dual cells were treated with the conjugate either in the presence or absence of tetrazine **20** (Figure 6A). Pure Resiquimod was used as a positive control, and PBS buffer as a negative control. After overnight incubation the production of secreted embryonic alkaline phosphatase (SEAP) was quantified as a measure of NF-κB activity (Figure 6). Activity of Resiquimod was fully recovered upon co-incubation with tetrazine.



Scheme 4. Conjugation of antibody TA99 with **16** and consequent release with tetrazine (Tz) **20**. Tz **20** is able to both click and release R448. Tz **21** is first radiolabeled with Indium-111 and, due to the two pyridine substituents, clicks very efficiently but releases R448 poorly. Thus Tz **20** is used release R448 from the ADC and Tz **21** is used to quantify unreacted ADC using radiolabelling. Reagents and condition: **a**) TA99 in PBS (5 mg/mL), compound **16** (10 mM in DMF) in 7:2:1 PBS:propylene glycol:DMF at pH=9 as adjusted with 1M Na₂CO₃, 2h, RT.

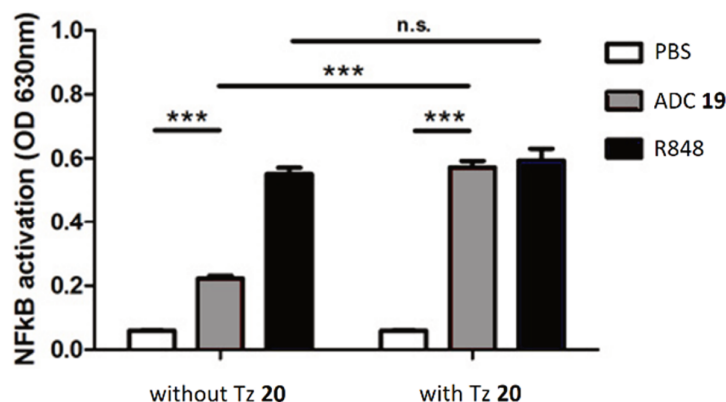


Figure 6. THP1-Dual cells were treated with antibody-drug conjugate (ADC) **19** either in the presence or absence of Tz activator **20**. PBS buffer was used as a negative control and free R848 agonist as a positive control. After overnight incubation NF-κB activity was measured through quantification of SEAP production. Experiment was carried out by Raffaella Rossin (Tagworks Pharmaceuticals).

Behavior of conjugate **19** was next assessed *in vivo* by the company Tagworks. Native TA99 and conjugate **19** were radiolabeled through acylation with radio-iodinated N-succinimidyl-3[4-hydroxyphenyl]propionate (Bolton-Hunter method).²⁷ One group (n=4) of female C57BL/6 mice bearing a subcutaneous B16-F10 melanoma was injected with the radiolabelled native TA99 (5 mg/kg, 0.3 MBq/mouse) and euthanized 48h post-mAb injection (Figure 7A). Three more groups (n=4) of mice were treated with radiolabelled conjugate **19**, of which one group was euthanized 48h post-mAb injection, and two groups were injected with a clearing agent (**CA**, Figure 7C) 48h post-mAb injection. This clearing agent, a conjugate of tetrazine with galactose-albumin, is known to increase the tumour-to-blood ratio of TCO-bearing antibodies by reacting only with freely-circulating antibodies.²⁸ Two hours after **CA** injection one group was injected with activating tetrazine **20**. Three hours after **CA** injection both groups were injected with Indium-111 labelled tetrazine probe **21** (Figure 7B). This probe reacts very efficiently with TCO-groups, but releases drug payloads very poorly (Scheme 4) and was therefore used to quantify the conjugates **19** that have not reacted with tetrazine **20**.

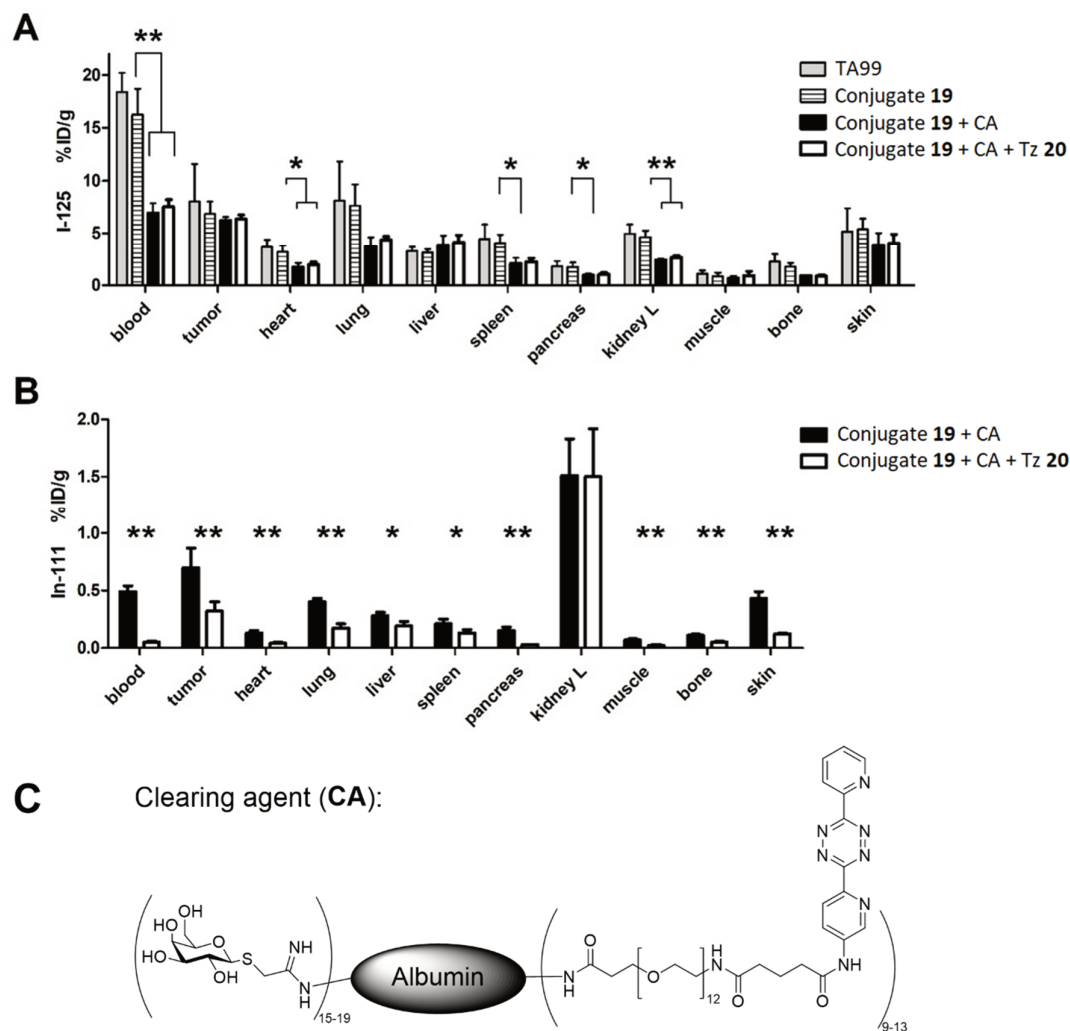


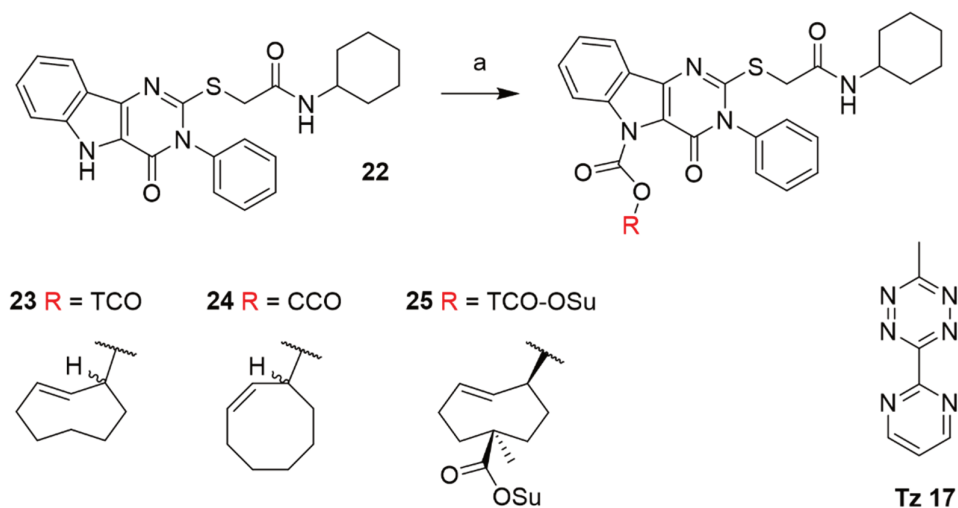
Figure 7. In vivo performance of native TA99 and conjugate 19 and its distribution throughout female C57BL/6 mice bearing a subcutaneous B16-F10 melanoma. A) Native TA99 and conjugate 19 were radiolabelled with ^{125}I , whereas tetrazine 21 was radiolabelled with ^{111}In . The study contained four groups of mice each subject to the order of reagents as presented in the key. ^{125}I isotope signal indicates presence of the TA99 antibody in the specified organ. B) The groups of mice receiving both the conjugate and clearing agent were also injected with ^{111}In -radiolabelled tetrazine 21 one hour after receiving activating tetrazine 20. ^{111}In isotope signal indicates presence of unreacted ADC conjugate 19 prior to the second injection. Significance calculated through a one-way ANOVA Bonferroni post-hoc test, *:p<0.05; **:p<0.01. Experiment was carried out by Raffaella Rossin (Tagworks Pharmaceuticals). C) Clearing agent (CA) consisting of a polygalactosylated albumin-polytetrazine conjugate.

The results outlined in Figure 7A show that conjugate 19 exerts similar target affinity compared to native TA99. A high uptake in blood and blood-rich organs was observed as well as tumoral tissue and the skin. Application of the clearing agent significantly reduced the conjugate uptake in blood and blood-rich organs, whilst maintaining target-specific uptake in the skin and tumoral tissue. Figure 7B shows a measure of reaction inefficiency between Tz activator 20 and conjugate 19, as

unreacted conjugates will react with Indium-111-labelled Tz probe **21**. Uptake of the probe in all tissues, except for the kidney, is significantly lower (Student's t-test) after administration of Tz activator **20**, confirming that reaction between Tz activator **20** and mAb conjugate **19** has taken place. The strong uptake of the probe in the kidney can be explained by the clearance of circulating **19** due to addition of the clearing agent (**CA**). These results suggest the approach is feasible, and further immunological evaluations are required to test immune activating properties of the constructs.

A Chemo-controllable TLR4-Agonist

In a final application of TCO-chemistry to TLR-activation studies, a TCO-modified TLR4 ligand was synthesized. The canonical ligand for TLR4 is lipopolysaccharide²⁹, which is only accessible through isolation from the outer membrane of gram-negative bacteria as a highly heterogeneous mixture. This – and the absence of a unique reactive site in the molecule – precluded its use as starting material for this approach. Our attention was therefore directed to a synthetic pyrimido[5,4-*b*]indole based TLR4 ligand **22** (Scheme 5).³⁰ The activity of this ligand is dependent on a critical heterocyclic amine.³⁰ It was envisaged that this amine could be protected as a TCO-carbamate to allow tetrazine-mediated control over ligand activity.



Scheme 5. Synthesis of a TCO- or CCO-protected pyrimido[5,4-*b*]indole derivative. Reagents and conditions: a) Compound **23**: (i) NaH, THF, r.t., 30 min (ii) TCO-OSu, THF, r.t., o.n., 51%; Compound **24**: (i) NaH, THF, r.t., 30 min (ii) CCO-OSu, THF, r.t., o.n., 63%; Compound **25**: (i) NaH, THF, r.t., 30 min (ii) TCO-(OSu)₂, THF, r.t., o.n.

As endocyclic indolamines are poor nucleophiles, deprotonation with strong bases was performed prior to reaction with the TCO-OSu reagent. Suspending the starting material in THF followed by addition of an excess of sodium hydride led to the formation of a clear yellow solution. Addition of TCO-OSu to this solution resulted in near-quantitative conversion to the product within minutes. Purification was achieved using silica gel column chromatography and yielded TCO-, CCO- and OSu-TCO-modified indoles **23-25** in 50-63% yield (Scheme 5).

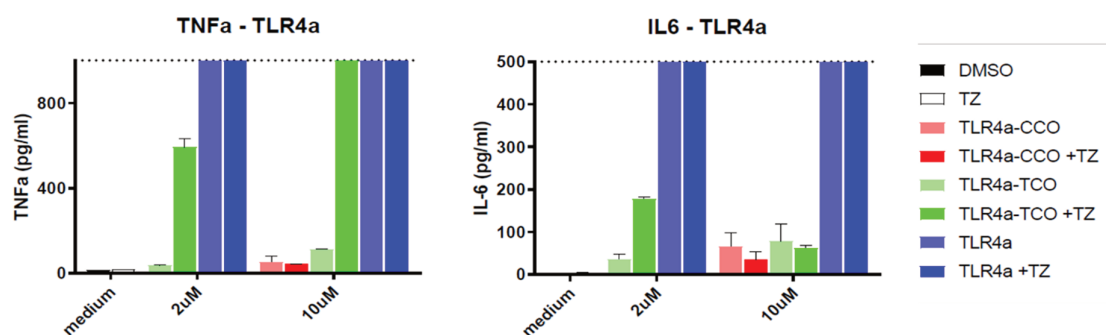
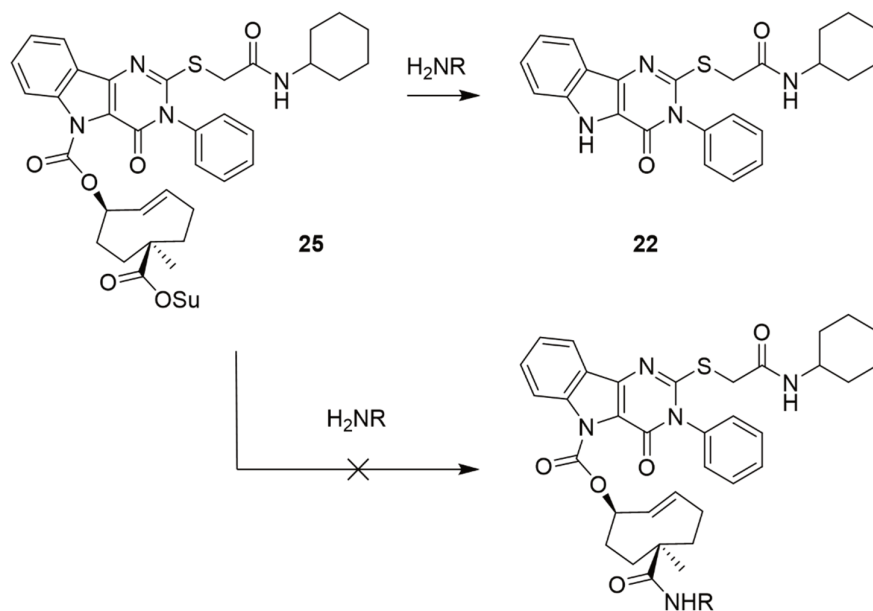


Figure 8. Biological evaluation of compounds **23** and **24**: TLR4a-TCO and TLR4a-CCO, respectively. TNF- α and interleukin 6 (IL6) concentrations were measured in medium containing murine bone marrow-derived macrophages (BMDMs) after treatment with the indicated compounds. TLR4a-TCO **23** only elicits a response when co-administering tetrazine **17**, whereas TLR4a-CCO **24** is irresponsive at the same concentrations. IL6 production appears hampered at higher concentrations.

To assess the suitability of **23-25** as reagents to study TLR4-activation, murine bone marrow-derived macrophages (BMDMs) were treated with either free ligand **22**, TCO-caged ligand **23**, or CCO-caged ligand **24** at 2 or 10 μ M in the presence or absence of tetrazine (Figure 8). **23** showed a strongly diminished (<10%) production of TNF- α and IL-6 in absence of the deprotecting tetrazine. Addition of tetrazine **17** resulted in the production of both cytokines, albeit at lower levels than for the unmodified ligand (60 and 20% respectively). Future work could involve employing this ligand at the window-of-activity concentration in conjunction with tetrazines directed to the endo-lysosomal pathway to selectively activate the intracellular population of TLR4.



Scheme 6. Aminolysis of compound **25**. Addition of amine-containing linkers resulted in regeneration of the free ligand **22**, as opposed to substitution of the succinimide ester.

The synthesis of a conjugatable variant of this caged ligand was also attempted using the previously reported bis-functionalized TCO-(OSu)₂ reagent.²³ Using the procedure outlined in Scheme 5, compound **25** was observed by LC-MS, whilst keeping the succinimidyl ester at position 5 intact. Unfortunately, addition of various amine-containing linkers (e.g. ethanol amine, dodecaethylene glycolamine) resulted in quantitative aminolysis of the TCO from the indole (Scheme 6).

This lability of the indole-carbamate could prevent the biological use of **23** as it might give rise to premature TLR4 activation. The use of an ether-based conjugation-strategy could potentially solve this issue.^{31–33}

Conclusion

In this Chapter the concept of *trans*-cyclooctene as bioorthogonal protecting groups was applied to ligands specific for TLRs residing in intracellular compartments. Deoxycytidine was caged with a CCO or a TCO on the exocyclic amine of the nucleobase. These building blocks were made amenable for DMTr/phosphoramidite solid-phase oligonucleotide synthesis and used to procure a caged 12-meric and 20-meric caged CpG ODN. Although the 12-mer was unable to induce TLR9 activation on BMDMs, it is known that the 20-mer is, and the caged 20-mer is currently awaiting biological evaluation.

The same TCO-caging strategy was applied on Resiquimod, which showed a recovery of functionality after treatment with tetrazine in BMDMs marked by the production of TNF- α and IL6. Substitution of a second functionality on TCO was feasible when present on Resiquimod, enabling the synthesis of an antibody-drug conjugate able to release Resiquimod in sites where the antibody accumulates, for example the tumoral environment. This was assessed and confirmed in an *in vivo* murine experiment employing TA99 as the antibody targeting melanocytes.

Lastly, a synthetic TLR4 ligand was successfully caged with a TCO. This yielded a compound of which its activity towards TLR4 could be controlled by the addition of tetrazine.

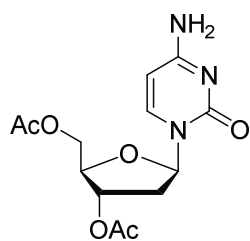
Acknowledgements

Timo Oosenbrug is acknowledged for the biological evaluation of compounds **14** and **15** (Figure 4) and compounds **23** and **24** (Figure 9) described in this Chapter. Nico Meeuwenoord is acknowledged for his aid in the synthesis and purification of DNA fragments. Thuur van Onzen, Raffaella Rossin and Marc Robillard (Tagworks Pharmaceuticals) are acknowledged for the synthesis, purification, and the biological evaluation of the antibody-drug conjugate **19**.

Experimental Section

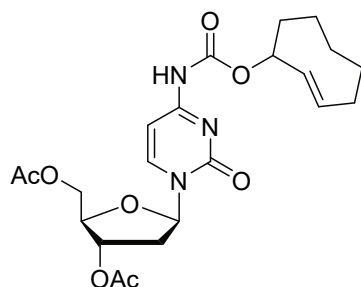
General reagents were obtained from Sigma Aldrich, Fluka, and Acros. All reagents were of commercial grade and used as received unless stated otherwise. Solvents used in synthesis were dried and stored over 4Å molecular sieves, except MeOH and ACN which were stored over 3Å molecular sieves. Triethylamine (Et₃N) and Diisopropylethylamine (DiPEA) were stored over KOH pellets. LC-MS analysis was performed on a Finnigan Surveyor HPLC system with a Nucleodur C18 Gravity 3µm 50 x 4.60 mm column (detection at 200-600 nm) coupled to a Finnigan LCQ Advantage Max mass spectrometer with ESI or coupled to a Thermo LCQ Fleet Ion mass spectrometer with ESI. The Method used was 10→90% 13.5 min (0→0.5 min: 10% MeCN; 0.5→8.5 min: 10% to 90% MeCN; 8.5→11 min: 90% MeCN; 11→13.5 min: 10% MeCN) unless otherwise stated. High resolution mass spectra (HRMS) were recorded on the following machines: Thermo Scientific Q Exactive HF Orbitrap mass spectrometer equipped with an electrospray ion source in positive-ion mode (source voltage 3.5 kV, sheath gas flow 10, capillary temperature 275 °C) with resolution R = 240.000 at m/z 400 (mass range of 150-6000) correlated to an external calibration, or on a Waters Synapt G2-Si (TOF) equipped with an electrospray ion source in positive mode (source voltage 3.5 kV) and LeuEnk (m/z = 556.2771) as internal lock mass. HPLC purification was performed on a Gilson HPLC system coupled to a Magerey-Nagel Nucleodur C18 Gravity 5 µm 250 ×10mm column, or on an Agilent 1200 HPLC/6130 MS system coupled to a Magerey-Nagel Nucleodur C18 Gravity 5µm 250×10 mm column or on a Waters autopurifier HPCL/MS system coupled to a Phenomenex Gemini 5µm 150×21.2 mm column.

Compound 1



The following synthesis was adopted from literature procedure.²⁸ Acetic acid (20mL) was added to a flask charged with deoxycytidine (10 mmol, 2.3 g) and stirred vigorously. A solution of acetyl chloride (6 mL) in CHCl₃ (14 mL) was added to the suspension and the reaction was stirred overnight. The reaction mixture was concentrated *in vacuo* to yield the title compound as a white solid (10 mmol, 3.1 g, qt.) **¹H NMR (400 MHz, DMSO-*d*₆)** δ = 9.98 (d, *J*=13.7, 1H), 8.86 (d, *J*=9.7, 1H), 7.99 (dd, *J*=7.9, 1.3, 1H), 6.27 – 6.19 (m, 1H), 6.08 (t, *J*=6.8, 1H), 5.19 (dt, *J*=6.3, 3.3, 1H), 4.31 – 4.20 (m, 3H), 2.50 – 2.36 (m, 2H), 2.05 (d, *J*=9.9, 6H). **¹³C NMR (101 MHz, DMSO-*d*₆)** δ = 170.47, 160.02, 147.38, 144.77, 94.74, 86.66, 82.39, 74.13, 63.97, 37.01, 21.21, 21.06.

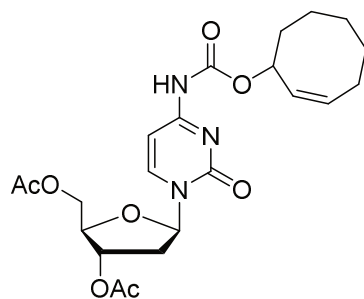
Compound 2



Compound 1 (1.3 mmol, 0.40 g) was dissolved in acetonitrile (2 mL). *Trans*-cyclooctene-2-oxycarbonyl paranitrophenolate (0.67 mmol, 0.20 g), DiPEA (2.6 mmol, 0.45 mL) and DMAP (0.67 mmol, 82 mg) were added and the mixture was stirred for 7 days at 40°C. TLC analysis (10% MeOH in DCM, $R_f=0.8$) indicated complete conversion of the starting material. The reaction mixture was cooled to room temperature, diluted with EtOAc and washed with 0.1 M HCl (aq.) (3x). The combined aqueous

layers were back-extracted with EtOAc (1x). The organic layers were combined and washed with a saturated solution of NaHCO_3 (aq.) (3x). The combined aqueous layers were back-extracted with EtOAc (1x). The organic layers were combined, washed with brine (1x), dried over MgSO_4 and concentrated *in vacuo*. Silica gel column chromatography (DCM \rightarrow 1% MeOH in DCM \rightarrow 2% MeOH in DCM) yielded the pure title compound (0.60 mmol, 0.28 g, 90%). **^1H NMR (400 MHz, CDCl_3)** δ = 7.97 (d, $J=7.5$, 1H), 6.26 (ddd, $J=8.2$, 5.6, 2.9, 1H), 5.86 (ddd, $J=15.9$, 11.0, 3.6, 1H), 5.55 (dt, $J=16.5$, 2.1, 1H), 5.42 (s, 1H), 5.31 (s, 1H), 5.22 (d, $J=6.2$, 1H), 4.37 (s, 3H), 2.86 – 2.76 (m, 1H), 2.50 (dd, $J=9.9$, 4.6, 1H), 2.10 (d, $J=11.4$, 8H), 2.03 (d, $J=10.5$, 1H), 2.02 – 1.91 (m, 1H), 1.89 (dq, $J=11.1$, 5.0, 1H), 1.82 – 1.63 (m, 2H), 1.50 (td, $J=12.8$, 4.2, 1H), 1.31 (s, 1H), 1.26 (d, $J=2.7$, 1H), 1.16 – 1.03 (m, 1H), 0.92 – 0.75 (m, 1H). **^{13}C NMR (101 MHz, CDCl_3)** δ = 170.52, 132.88, 129.96, 87.38, 83.07, 75.96, 74.31, 74.26, 63.79, 40.55, 39.15, 36.05, 35.99, 29.07, 24.15, 21.02, 20.92.

Compound 3

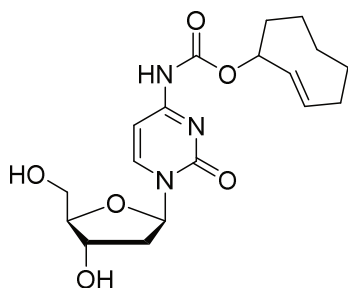


Compound 1 (1.0 mmol, 0.31 g) was dissolved in acetonitrile (2 mL). *Cis*-cyclooctene-2-oxycarbonyl paranitrophenolate (0.54 mmol, 0.16 g), DiPEA (2.0 mmol, 0.35 mL) and DMAP (0.50 mmol, 61 mg) were added and the mixture was stirred for 7 days at 40°C. TLC analysis (10% MeOH in DCM, $R_f=0.8$) indicated complete conversion of the starting material. The reaction mixture was cooled to room temperature, diluted with EtOAc and washed with 0.1 M HCl (aq.) (3x). The combined aqueous

layers were back-extracted with EtOAc (1x). The organic layers were combined and washed with a saturated solution of NaHCO_3 (aq.) (3x). The combined aqueous layers were back-extracted with EtOAc (1x). The organic layers were combined, washed with brine (1x), dried over MgSO_4 and concentrated *in vacuo*. Silica gel column chromatography (DCM \rightarrow 1% MeOH in DCM \rightarrow 2% MeOH in DCM) yielded the pure title compound (0.45 mmol, 0.21 g, 84%). **^1H NMR (400 MHz, CDCl_3)** δ = 7.96 (d, $J=7.6$, 1H), 7.87 (s, 1H), 7.29 (dd, $J=7.7$, 1.5, 1H), 6.26 (ddd, $J=7.5$, 5.5, 1.7, 1H), 5.79 – 5.60 (m, 2H), 5.57 – 5.48 (m, 1H), 5.22 (dd, $J=6.4$, 2.3, 1H), 4.36 (d, $J=1.8$, 3H), 2.82 (ddd, $J=14.4$, 5.7, 2.3, 1H), 2.33 – 2.23 (m, 1H), 2.23 – 2.12 (m, 1H), 2.16 – 2.04 (m, 7H), 1.98 (qd, $J=8.1$, 5.1, 2H), 1.77 – 1.48 (m, 2H), 1.42 (tdt, $J=9.5$, 6.5, 3.4, 1H). **^{13}C NMR (101 MHz, CDCl_3)** δ = 170.52, 170.33, 162.60, 154.88, 152.03, 143.01, 130.51, 129.87, 95.00,

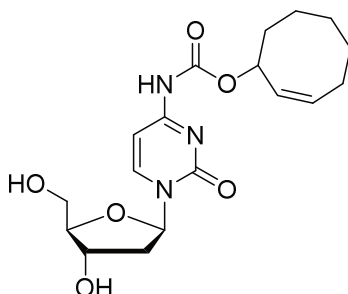
87.35, 83.02, 82.99, 75.08, 74.29, 74.23, 63.77, 39.10, 35.05, 28.81, 26.46, 25.85, 23.28, 20.99, 20.88.

Compound 4



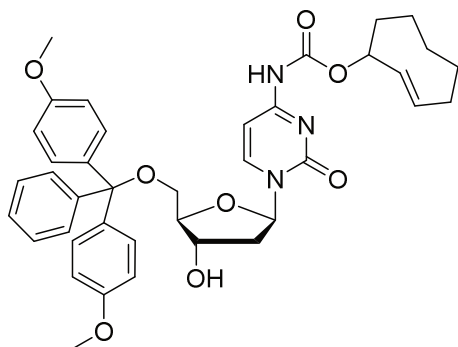
Compound **2** (0.60 mmol, 0.28 g) was dissolved in MeOH (5 mL). K_2CO_3 (0.30 mmol, 41 mg) was added and the reaction was stirred at room temperature for 30 minutes. TLC analysis (5% MeOH in DCM, $R_f=0.2$) indicated complete conversion of the starting material. The reaction mixture was concentrated *in vacuo* and was used *as is* in the following reaction.

Compound 5



Compound **3** (0.41 mmol, 0.19 g) was dissolved in MeOH (4 mL). K_2CO_3 (0.20 mmol, 28 mg) was added and the reaction was stirred at room temperature for 30 minutes. TLC analysis (5% MeOH in DCM, $R_f=0.2$) indicated complete conversion of the starting material. The reaction mixture was concentrated *in vacuo* and was used *as is* in the following reaction.

Compound 6

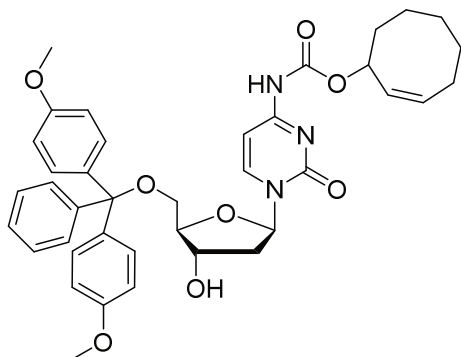


Compound **4** (0.60 mmol, 0.23 g) was dissolved in pyridine (4 mL). DMTr-Cl (1.80 mmol, 610 mg) was added and the reaction mixture was stirred overnight at room temperature. TLC analysis (10% MeOH in DCM, $R_f=0.7$) indicated complete conversion of the starting material. The mixture was concentrated *in vacuo*, diluted with EtOAc and consequently washed with H_2O (3x). The combined aqueous layers were back-extracted with EtOAc (1x). The organic layers were combined, washed

with brine, dried over $MgSO_4$ and concentrated *in vacuo*. Silica gel column chromatography (DCM \rightarrow 0.5% MeOH in DCM \rightarrow 2% MeOH in DCM) yielded the pure title compound (0.46 mmol, 0.31 g, 77% over two steps). 1H NMR (400 MHz, $CDCl_3$) δ = 8.21 (dd, $J=7.5, 1.2$, 1H), 7.75 (s, 1H), 7.43 – 7.35 (m, 2H), 7.34 – 7.26 (m, 7H), 7.26 – 7.19 (m, 1H), 7.02 (dd, $J=7.5, 2.0$, 1H), 6.89 – 6.80 (m, 4H), 6.27 (t, $J=5.8$, 1H), 5.89 – 5.77 (m, 1H), 5.53 (dd, $J=16.4, 2.5$, 1H), 5.39 (d, $J=5.2$, 1H), 4.50 (d, $J=5.4$, 1H), 4.14 (q, $J=3.7$, 1H), 3.83 – 3.77 (m, 6H), 3.49 (dd, $J=10.8, 3.2$, 1H), 3.44 – 3.36 (m, 1H), 2.72 (dt, $J=11.9, 5.7$, 1H), 2.48 (d, $J=10.7$, 1H), 2.25 (ddd, $J=13.6, 6.8, 4.3$, 1H), 2.15 – 1.95 (m, 3H), 1.95 – 1.83 (m, 1H), 1.75 (d, $J=13.6$, 1H), 1.71 (s, 4H), 1.28 (s, 1H), 1.26 (d, $J=2.6$, 1H), 1.13 – 1.00 (m, 1H), 0.82 (td, $J=19.0, 18.6, 9.8$, 1H). ^{13}C NMR (101 MHz, $CDCl_3$) δ = 144.26, 128.26, 128.24, 128.16, 130.22, 127.22, 94.82, 113.47, 87.24,

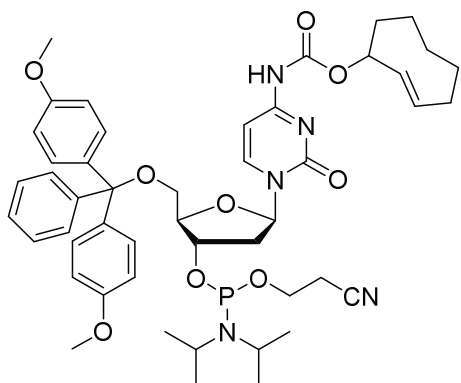
132.86, 129.92, 130.15, 75.69, 71.08, 71.15, 86.44, 55.44, 62.85, 62.73, 42.36, 36.04, 41.97, 36.10, 35.36, 29.85, 23.97, 29.21.

Compound 7



Compound **5** (0.41 mmol, 0.16 g) was dissolved in pyridine (4 mL). DMTr-Cl (1.23 mmol, 420 mg) was added and the reaction mixture was stirred overnight at room temperature. TLC analysis (10% MeOH in DCM, $R_f=0.7$) indicated complete conversion of the starting material. The mixture was concentrated *in vacuo*, diluted with EtOAc and consequently washed with H₂O (3x). The combined aqueous layers were back-extracted with EtOAc (1x). The organic layers were combined, washed with brine, dried over MgSO₄ and concentrated *in vacuo*. Silica gel column chromatography (DCM \rightarrow 0.5% MeOH in DCM \rightarrow 2% MeOH in DCM) yielded the pure title compound (0.29 mmol, 0.20 g, 72% over two steps). ¹H NMR (400 MHz, CDCl₃) δ = 8.25 (d, $J=7.5$, 1H), 7.43 – 7.36 (m, 2H), 7.33 – 7.16 (m, 7H), 7.04 – 6.98 (m, 1H), 6.87 – 6.79 (m, 4H), 6.28 (t, $J=5.8$, 1H), 5.75 – 5.61 (m, 1H), 5.60 (q, $J=5.5$, 1H), 5.53 – 5.43 (m, 1H), 4.54 (q, $J=5.2$, 1H), 4.19 (q, $J=3.7$, 1H), 3.77 (dd, $J=2.5$, 1.3, 6H), 3.45 (dd, $J=12.4$, 2.0, 1H), 3.39 (dd, $J=10.7$, 3.9, 1H), 2.81 – 2.71 (m, 1H), 2.30 – 2.19 (m, 1H), 2.23 – 2.07 (m, 1H), 1.92 (td, $J=11.4$, 10.5, 6.2, 1H), 1.74 – 1.45 (m, 5H), 1.40 (dddd, $J=12.3$, 9.5, 6.4, 3.2, 1H), 1.04 (d, $J=6.7$, 3H). ¹³C NMR (101 MHz, CDCl₃) δ = 162.45, 158.63, 158.60, 155.43, 151.98, 144.38, 144.16, 144.12, 135.69, 135.50, 130.19, 130.08, 129.97, 128.22, 128.03, 127.10, 113.32, 94.95, 87.32, 86.85, 86.56, 77.37, 74.69, 70.74, 62.80, 55.25, 42.13, 35.02, 34.97, 28.79, 26.41, 25.83, 23.26, 20.45.

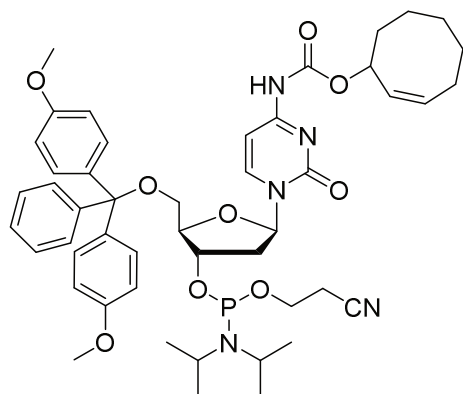
Compound 8



Compound **6** (0.11 mmol, 74 mg) was dissolved in anhydrous DCM (1 mL) and cooled to 0°C. DiPEA (0.50 mmol, 87 μ L) and then 2-Cyanoethyl N,N-diisopropylchloro-phosphoramidite (0.16 mmol, 36 μ L) was added and the mixture was stirred for 10 minutes at room temperature. TLC analysis (5% MeOH in DCM, $R_f=0.7$) indicated complete conversion of the starting material. The reaction mixture was diluted with DCM and washed with a 5% solution of NaHCO₃ (aq.) (3x). The organic layers were combined, dried (Na₂SO₄) and concentrated *in vacuo*. Silica gel column chromatography (Si neutralized with 2% TEA in DCM before adsorbing; DCM \rightarrow 0.5% MeOH in DCM) yielded the pure title compound (78 μ mol, 69 mg, 71%). ¹H NMR (400 MHz, CDCl₃) δ = 8.28 – 8.18 (dd, $J=7.6$, 1H), 7.69 (s, 1H), 7.44 – 7.35 (m, 2H), 7.35 – 7.21 (m, 13H), 7.20 – 7.11 (m, 8H), 6.94 (ddd, $J=7.1$, 4.3, 2.3, 1H), 6.84 (ddd, $J=8.9$, 5.3, 1.8, 5H), 6.31 – 6.22 (m, 1H), 5.89 – 5.75 (m, 1H), 5.52 (d, $J=16.5$, 1H), 5.41 – 5.36 (m, 1H), 5.28 (s, 1H), 4.61 (s, 1H), 4.25 – 4.18 (m, 1H), 3.89 – 3.69 (m, 8H), 3.68 –

3.53 (m, 2H), 3.58 (s, 3H), 3.55 – 3.43 (m, 1H), 3.38 (td, $J=10.7, 3.6$, 1H), 2.63 (dt, $J=12.9, 6.3$, 1H), 2.46 (dt, $J=16.6, 5.8$, 2H), 2.35 (s, 8H), 2.28 (ddd, $J=13.8, 6.8, 4.1$, 1H), 2.15 – 1.94 (m, 2H), 1.87 (d, $J=9.8$, 2H), 1.79 – 1.70 (m, 1H), 1.52 (t, $J=15.1$, 1H), 1.27 (s, 3H), 1.36 – 1.13 (m, 14H), 1.07 (d, $J=6.8$, 4H), 0.91 – 0.73 (m, 2H). ^{31}P NMR (162 MHz, CDCl_3) δ = 148.74, 148.68, 148.45, 148.10, 148.07.

Compound 9



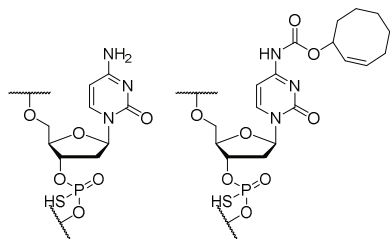
Compound 7 (0.17 mmol, 0.12 g) was dissolved in anhydrous DCM (2 mL) and cooled to 0°C. DiPEA (0.50 mmol, 87 μL) and then 2-Cyanoethyl N,N-diisopropylchlorophosphoramidite (0.21 mmol, 48 μL) was added and the mixture was stirred for 10 minutes at room temperature. TLC analysis (5% MeOH in DCM, $R_f=0.7$) indicated complete conversion of the starting material. The reaction mixture was diluted with DCM and washed with a 5% solution of NaHCO_3 (aq.) (3x). The organic layers were combined, dried (Na_2SO_4) and

concentrated *in vacuo*. Silica gel column chromatography (Si neutralized with 2% TEA in DCM before adsorbing; DCM \rightarrow 0.5% MeOH in DCM) yielded the pure title compound (0.15 mmol, 0.13 g, 88%). ^1H NMR (400 MHz, CDCl_3) δ = 8.30 – 8.20 (dd, $J=7.5, 2.2$, 1H), 7.52 (s, 1H), 7.40 (dt, $J=8.2, 1.3$, 2H), 7.35 – 7.21 (m, 7H), 6.95 (d, $J=7.5$, 1H), 6.89 – 6.81 (m, 4H), 6.25 (t, $J=5.7$, 1H), 5.77 – 5.65 (m, 1H), 5.62 (d, $J=7.9$, 1H), 5.55 – 5.45 (m, 1H), 4.64 (dq, $J=10.2, 5.5$, 4.9, 1H), 4.20 (dt, $J=5.4, 3.1$, 1H), 3.83 – 3.78 (m, 6H), 3.71 – 3.48 (m, 4H), 3.39 (dd, $J=10.8, 3.3$, 1H), 2.71 (dtd, $J=12.1, 6.6, 1.8$, 1H), 2.44 (t, $J=6.4$, 2H), 2.36 – 2.20 (m, 1H), 2.20 – 2.10 (m, 1H), 1.96 (s, 1H), 2.02 – 1.88 (m, 1H), 1.69 (dtd, $J=14.3, 10.3, 9.4, 5.2$, 1H), 1.58 (h, $J=6.3, 5.9$, 3H), 1.41 (dddd, $J=12.6, 9.9, 6.7, 3.2$, 1H), 1.25 (dd, $J=6.8, 4.6$, 1H), 1.17 (t, $J=6.5$, 12H). ^{31}P NMR (162 MHz, CDCl_3) δ = 149.31, 149.28, 148.66.

General method for synthesizing oligonucleotides:

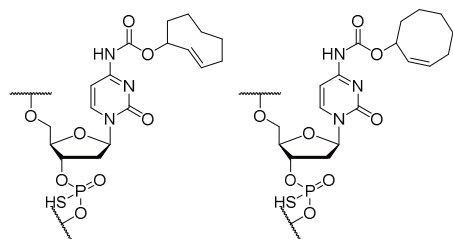
5'-CATGAC*GTTCT-3'

10 C* = 11 C* =



5'-TCCATGAC*GTTCTGATGCT-3'

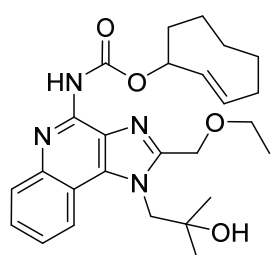
12 C* = 13 C* =



Resin: Controlled Pore Glass (CPG) resin pre-loaded with a deoxythymidine via a succinyl linker (bought from Proligo® Reagents). For a typical oligonucleotide synthesis, 10 μmol of preloaded nucleotide was started with. **Solvent:** Anhydrous acetonitrile (DNA synthesis grade) **Atmosphere:** All steps are carried out under an argon atmosphere. **Reagents:** 2-Cyanoethyl N,N-diisopropyl phosphoramidites protected with 4-*t*-butylphenoxyacetyl (tac) on exocyclic amines of the nucleobases. Bought as a 0.1 M solution in acetonitrile from Proligo® Reagents. IUPAC name for "Sulfurization Reagent II" is 3-((N,N-dimethylaminomethylidene)amino)-3H-1,2,4-dithiazole-5-thione. A 0.25 M solution of 5-(Ethylthio)-1H-tetrazole (ETT) was used as the activator in the coupling steps. **Detritylation:** For the first detritylation, the resin was washed three times with acetonitrile. Then, the resin was treated with a solution of 5% dichloroacetic acid in toluene (3 min, 1x). The resin was washed with acetonitrile (3x). **Coupling:** Two cycles were carried out

consisting of the following: a solution of 0.1 M phosphoramidite in acetonitrile (30 μmol , 300 μL , 3 eq.) was added to the resin. A solution of 0.25 M ETT in acetonitrile (120 μmol , 480 μL , 12 eq.) was added and the resin was shaken for 3 min. After two cycles were carried out and the resin was washed with acetonitrile, a solution of 0.1 M sulfurization reagent II in 6:4 pyridine:acetonitrile (100 μmol , 1 mL, 10 eq.) was added and the resin was shaken for 1 min. (1x). **Deprotection:** The final DMTr group was removed according to the detritylation procedure. The resin was then treated with a solution of 28% NH_4OH (aq.) and shaken for 30 min. The suspension was filtered and the resin was washed with H_2O (3x). The filtrates were combined and concentrated *in vacuo*. The resulting residu was purified using an anion exchange column followed by a desalting procedure.

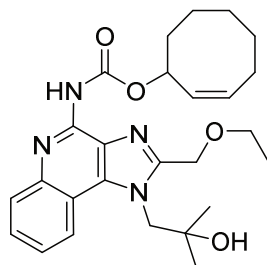
Compound 14



Resiquimod (32 μmol , 10 mg) was dissolved in DMF (200 μL) in an eppendorf tube (1.5 mL). DiPEA (70 μmol , 12 μL), TCO-OSu (35 μmol , 9 mg) and DMAP (3 μmol , 0.4 mg) were added. The tube was shaken for 7 days at 50°C when no further conversion was observed by LC-MS analysis. A solution of 50% brine in H_2O was added to the reaction mixture and washed with DCM (3x). The combined organic layers were evaporated *in vacuo* and reconstituted in DMSO. Purification with RP-HPLC yielded the title compound (13 μmol , 5.9 mg, 41%) as well as unreacted Resiquimod (17 μmol , 5.3 mg, 53%). **LC-MS (1090, C18, $\text{H}_2\text{O}/\text{AcN}$ + TFA):** 467.27 ($z=1$, simulated), 467.07

($z=1$, observed), 932.67 ($z=1$, dimer) **HRMS**: $[M+H]^+$ calculated for $C_{26}H_{35}N_4O_4$ 467.26528; found 467.26530

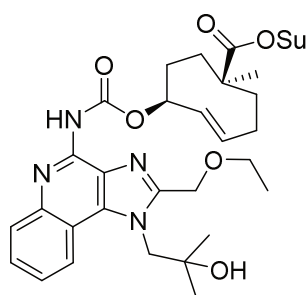
Compound 15



Resiquimod (18 μ mol, 5.7 mg) was dissolved in DMSO (180 μ L) in an eppendorf tube (1.5 mL). DiPEA (27 μ mol, 4.7 μ L) and CCO-OSu (27 μ mol, 7.2 mg) were added. The tube was shaken for 7 days at room temperature when no further conversion was observed by LC-MS analysis. A solution of 50% brine in H_2O was added to the reaction mixture and washed with DCM (3x). The combined organic layers were evaporated *in vacuo* and reconstituted in DMSO. Purification with silica

gel column chromatography (loaded in a Pasteur pipette, DCM \rightarrow 0.5% MeOH in DCM \rightarrow 1% MeOH in DCM) yielded the title compound (5.6 μ mol, 2.6 mg, 31%). **LC-MS (1090, C18, H_2O /AcN + TFA)**: 467.27 ($z=1$, simulated), 467.25 ($z=1$, observed), 932.67 ($z=1$, dimer) **HRMS**: $[M+H]^+$ calculated for $C_{26}H_{35}N_4O_4$ 467.26528; found 467.26522 **1H NMR (400 MHz, $CDCl_3$)** δ = 8.31 (s, 1H), 8.23 (d, $J=8.5$, 1H), 8.15 (d, $J=8.3$, 1H), 7.63 (t, $J=7.7$, 1H), 7.49 (t, $J=7.6$, 1H), 5.85 (s, 1H), 5.79 – 5.68 (m, 1H), 5.67 – 5.59 (m, 1H), 5.33 (s, 1H), 4.94 (s, 2H), 4.82 (s, 2H), 3.70 (q, $J=7.0$, 2H), 3.20 (s, 1H), 2.64 (s, 1H), 2.35 (d, $J=11.9$, 1H), 2.15 (s, 3H), 1.73 (s, 1H), 1.44 (s, 1H), 1.36 (s, 7H), 1.33 – 1.25 (m, 6H).

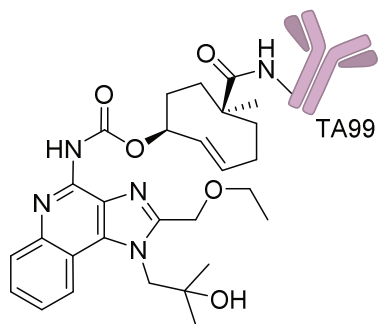
Compound 16



Resiquimod (32 μ mol, 10 mg) was dissolved in anhydrous DMF (200 μ L) in an eppendorf tube. DiPEA (153 μ mol, 28 μ L) and TCO-(OSu)₂ (40 μ mol, 17 mg) were added and the tube was shaken for 10 days at room temperature. LC-MS analysis indicated >50% conversion of the starting material. Water was added to the reaction mixture and the product was extracted with DCM (3x). The organic layers were combined, dried ($MgSO_4$) and concentrated *in vacuo*. The product was purified using silica gel column chromatography (loaded

in a Pasteur pipette, 50% EtOAc in Pnt \rightarrow 80% EtOAc in Pnt) yielding the title compound (7.8 μ mol, 3.6 mg, 24%). **HRMS**: $[M+H]^+$ calculated for $C_{32}H_{40}N_5O_8$ 662.28714; found 622.28713. **1H NMR (400 MHz, $CDCl_3$)** δ = 8.15 (t, 2H, ArH), 7.61 (t, 1H, ArH), 7.48 (t, 1H, ArH), 6.20 (m, 1H, NH), 5.70 (m, 1H, $NHCOOCH$), 5.48 (s, 1H, trans-alkene H), 5.34 (s, 1H, trans-alkene H), 4.95 (s, 2H, CCH_2N), 4.81 (s, 2H, CCH_2O), 3.68 (q, 2H, OCH_2CH_3), 2.83 (d, 4H, CCH_2CH_2C), 2.50-0.77 (m, 21H, aliphatic protons).

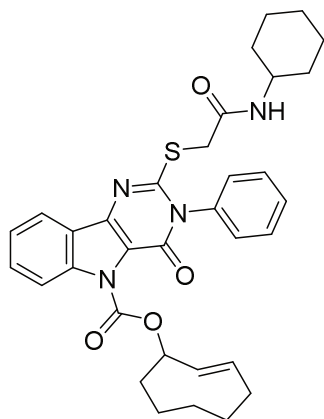
Compound 19



(PBS:propylene glycol) (3x) and purified using a PD-10 column. A ratio of 1.7 R848-TCO per antibody was determined by a tetrazine titration and SDS-PAGE analysis.

Anti-glycoprotein 75 (gp-75) mAb TA99 (1.25 mg, 5 mg/mL in PBS) was reacted with compound **16** (30 mM in DMF, 80 eq.) in a solution of 7:2:1 (PBS:propylene glycol:DMF, total volume of 330 μ L). A pH of 9 was maintained by careful adjustment with a 1 M solution of Na_2CO_3 (aq.). The reaction vessel was wrapped in aluminium foil and shaken for 2 hours. The reaction was transferred to an Amicon Ultra-15 centrifugal device (50 kDa cut-off), washed with a solution of 7.5:2.5

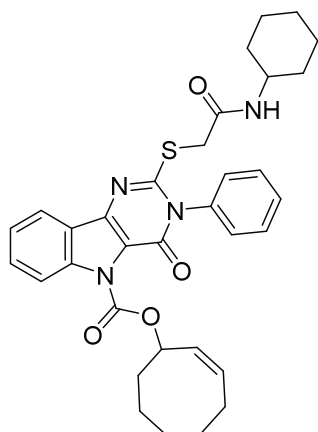
Compound 23



were dried (MgSO_4) and concentrated *in vacuo*. Purification with silica gel column chromatography (loaded in a Pasteur pipette; $\text{DCM} \rightarrow 5\%$ acetonitrile in DCM; TLC analysis $R_f=0.7$ in 10% acetonitrile in DCM) yielded the title compound (5.1 μ mol, 3.0 mg, 51%). **LC-MS (5090, C18, $\text{H}_2\text{O}/\text{AcN} + \text{TFA}$):** 585.25 ($z=1$, simulated), 585.17 ($z=1$, observed), 1191.00 ($z=1$, dimer with sodium cation). **HRMS:** $[\text{M}+\text{H}]^+$ calculated for $\text{C}_{33}\text{H}_{37}\text{N}_4\text{O}_4\text{S}$ 585.25300; found 585.25280

The following procedure was modified from literature¹²: *N*-Cyclohexyl-2-((4-oxo-3-phenyl-4,5-dihydro-3*H*-pyrimido[5,4-*b*]indol-2-yl)thio)acetamide.HCl (As received from the laboratory of Prof. A.P. Esser-Kahn) (10 μ mol, 4.3 mg) was suspended in THF (100 μ L) in an eppendorf tube (1.5 mL). NaH (50 μ mol, 2 mg) was added which dissolved the indole and turned the solution yellow. After shaking for 30 minutes at room temperature, TCO-OSu (12.5 μ mol, 3.34 mg) was added and the mixture was shaken for another 10 minutes. LC-MS analysis indicated near quantitative conversion of the starting material. H_2O was added to the mixture and the product was extracted with DCM (5x). The combined organic layers

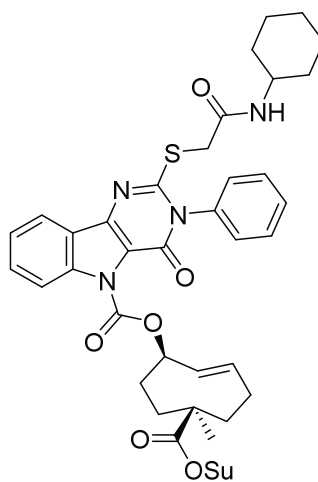
Compound 24



The following procedure was modified from literature¹²: *N*-Cyclohexyl-2-((4-oxo-3-phenyl-4,5-dihydro-3*H*-pyrimido[5,4-*b*]indol-2-yl)thio)-acetamide.HCl³⁰ (As received from the laboratory of Prof. A.P. Esser-Kahn) (10 μ mol, 4.3 mg) was suspended in THF (100 μ L) in an eppendorf tube (1.5 mL). NaH (50 μ mol, 2 mg) was added which dissolved the indole and turned the solution yellow. After shaking for 30 minutes at room temperature, CCO-OSu (12.5 μ mol, 3.34 mg) was added and the mixture was shaken for another 10 minutes. LC-MS analysis indicated near quantitative conversion of the starting material. H₂O was added to the mixture and the product was extracted with DCM (5x). The combined organic layers

were dried (MgSO₄) and concentrated *in vacuo*. Purification with silica gel column chromatography (loaded in a Pasteur pipette, DCM \rightarrow 2.5% acetonitrile in DCM \rightarrow 5% acetonitrile in DCM; TLC analysis R_f=0.7 in 10% acetonitrile in DCM) yielded the title compound (6.3 μ mol, 3.7 mg, 63%). **LC-MS (5090, C18, H₂O/AcN + TFA)**: 585.25 (*z*=1, simulated), 585.13 (*z*=1, observed), 1191.27 (*z*=1, dimer with sodium cation), 1776.00 (*z*=1, trimer with sodium cation). **HRMS**: [M+H]⁺ calculated for C₃₃H₃₇N₄O₄S 585.25300; found 585.25254

Compound 25



The following procedure was modified from literature¹²: *N*-Cyclohexyl-2-((4-oxo-3-phenyl-4,5-dihydro-3*H*-pyrimido[5,4-*b*]indol-2-yl)thio)acetamide.HCl³⁰ (As received from the laboratory of Prof. A.P. Esser-Kahn) (5 μ mol, 2 mg) was suspended in THF (100 μ L) in an eppendorf tube (1.5 mL). NaH (25 μ mol, 1 mg) was added which dissolved the indole and turned the solution yellow. After shaking for 30 minutes at room temperature, TCO-(OSu)₂ (12.5 μ mol, 5.3 mg) was added and the mixture was shaken for another 60 minutes. LC-MS analysis indicated near quantitative conversion of the starting material. The crude mixture was used *as is* to conjugate amine-containing linkers. **LC-MS (5090, C18, H₂O/AcN + TFA)**: 740.27 (*z*=1, simulated), 740.07 (*z*=1, observed), 1478.93 (*z*=1, dimer), 1502.00 (*z*=1, dimer with sodium cation)

References

- (1) Tetrazines for High Click Conjugation Yield in Vivo and High Click Release Yield, US Patent Application #20210299286 Tagworks Pharmaceuticals B.V. (Co-Inventor).
- (2) Barbalat, R.; Lau, L.; Locksley, R. M.; Barton, G. M. Toll-like Receptor 2 on Inflammatory Monocytes Induces Type I Interferon in Response to Viral but Not Bacterial Ligands. *Nat Immunol* **2009**, *10* (11), 1200–1207.
- (3) McGettrick, A. F.; O'Neill, L. A. Localisation and Trafficking of Toll-like Receptors: An Important Mode of Regulation. *Current Opinion in Immunology* **2010**, *22* (1), 20–27.
- (4) Alexopoulou, L.; Holt, A. C.; Medzhitov, R.; Flavell, R. A. Recognition of Double-Stranded RNA and Activation of NF-KB by Toll-like Receptor 3. *Nature* **2001**, *413* (6857), 732–738.
- (5) Lund, J. M.; Alexopoulou, L.; Sato, A.; Karow, M.; Adams, N. C.; Gale, N. W.; Iwasaki, A.; Flavell, R. A. Recognition of Single-Stranded RNA Viruses by Toll-like Receptor 7. *Proceedings of the National Academy of Sciences* **2004**, *101* (15), 5598–5603.
- (6) Heil, F. Species-Specific Recognition of Single-Stranded RNA via Toll-like Receptor 7 and 8. *Science* **2004**, *303* (5663), 1526–1529.
- (7) Hemmi, H.; Takeuchi, O.; Kawai, T.; Kaisho, T.; Sato, S.; Sanjo, H.; Matsumoto, M.; Hoshino, K.; Wagner, H.; Takeda, K.; Akira, S. A Toll-like Receptor Recognizes Bacterial DNA. *Nature* **2000**, *408* (6813), 740–745.
- (8) Honda, K.; Ohba, Y.; Yanai, H.; Negishi, H.; Mizutani, T.; Takaoka, A.; Taya, C.; Taniguchi, T. Spatiotemporal Regulation of MyD88–IRF-7 Signalling for Robust Type-I Interferon Induction. *Nature* **2005**, *434* (7036), 1035–1040.
- (9) Lee, B. L.; Barton, G. M. Trafficking of Endosomal Toll-like Receptors. *Trends in Cell Biology* **2014**, *24* (6), 360–369.
- (10) Combes, A.; Camosseto, V.; N'Guessan, P.; Argüello, R. J.; Mussard, J.; Caux, C.; Bendriss-Vermare, N.; Pierre, P.; Gatti, E. BAD-LAMP Controls TLR9 Trafficking and Signalling in Human Plasmacytoid Dendritic Cells. *Nat Commun* **2017**, *8* (1), 913.
- (11) Ryu, K. A.; Stutts, L.; Tom, J. K.; Mancini, R. J.; Esser-Kahn, A. P. Stimulation of Innate Immune Cells by Light-Activated TLR7/8 Agonists. *J. Am. Chem. Soc.* **2014**, *136* (31), 10823–10825.
- (12) Stutts, L.; Esser-Kahn, A. P. A Light-Controlled TLR4 Agonist and Selectable Activation of Cell Subpopulations. *ChemBioChem* **2015**, *16* (12), 1744–1748.
- (13) Govan, J. M.; Young, D. D.; Lively, M. O.; Deiters, A. Optically Triggered Immune Response through Photocaged Oligonucleotides. *Tetrahedron Letters* **2015**, *56* (23), 3639–3642.
- (14) Dzajak, R.; Galeta, J.; Vázquez, A.; Kozák, J.; Matoušová, M.; Fulka, H.; Dračinský, M.; Vrabec, M. Structurally Redesigned Bioorthogonal Reagents for Mitochondria-Specific Prodrug Activation. *JACS Au* **2021**, *1* (1), 23–30.
- (15) Uhlmann, E.; Vollmer, J. Recent Advances in the Development of Immunostimulatory Oligonucleotides. *Curr. opin. drug discov. dev.* **2003**, *6* (2), 204–217.
- (16) Ohto, U.; Shibata, T.; Tanji, H.; Ishida, H.; Krayukhina, E.; Uchiyama, S.; Miyake, K.; Shimizu, T. Structural Basis of CpG and Inhibitory DNA Recognition by Toll-like Receptor 9. *Nature* **2015**, *520* (7549), 702–705.

- (17) Sinhaa, N. D. Labile Exocyclic Amine Protection of Nucleosides in DNA, RNA and Oligonucleotide Analog Synthesis Facilitating N-Deacylation, Minimizing Depurination and Chain Degradation. *Biochimie*, **1993**, 75 (1-2), 13–23.
- (18) Salomão, R.; Martins, P. S.; Brunialti, M. K. C.; Fernandes, M. da L.; Martos, L. S. W.; Mendes, M. E.; Gomes, N. E.; Rigato, O. TLR Signaling pathway in patients with sepsis. *Shock* **2008**, 30 (7), 73–77.
- (19) van der Gracht, A. M. F.; de Geus, M. A. R.; Camps, M. G. M.; Ruckwardt, T. J.; Sarris, A. J. C.; Bremmers, J.; Maurits, E.; Pawlak, J. B.; Posthoorn, M. M.; Bongers, K. M.; Filippov, D. V.; Overkleeft, H. S.; Robillard, M. S.; Ossendorp, F.; van Kasteren, S. I. Chemical Control over T-Cell Activation *in Vivo* Using Deprotection of *Trans* -Cyclooctene-Modified Epitopes. *ACS Chem. Biol.* **2018**, 13 (6), 1569–1576.
- (20) Rossin, R.; van den Bosch, S. M.; ten Hoeve, W.; Carvelli, M.; Versteegen, R. M.; Lub, J.; Robillard, M. S. Highly Reactive *Trans* -Cyclooctene Tags with Improved Stability for Diels–Alder Chemistry in Living Systems. *Bioconjugate Chem.* **2013**, 24 (7), 1210–1217.
- (21) Rossin, R.; Renart Verkerk, P.; van den Bosch, S. M.; Vulders, R. C. M.; Verel, I.; Lub, J.; Robillard, M. S. In Vivo Chemistry for Pretargeted Tumor Imaging in Live Mice. *Angewandte Chemie International Edition* **2010**, 49 (19), 3375–3378.
- (22) Rossin, R.; Versteegen, R. M.; Wu, J.; Khasanov, A.; Wessels, H. J.; Steenbergen, E. J.; ten Hoeve, W.; Janssen, H. M.; van Onzen, A. H. A. M.; Hudson, P. J.; Robillard, M. S. Chemically Triggered Drug Release from an Antibody-Drug Conjugate Leads to Potent Antitumour Activity in Mice. *Nat Commun* **2018**, 9 (1), 1484.
- (23) Rossin, R.; van Duijnhoven, S. M. J.; ten Hoeve, W.; Janssen, H. M.; Kleijn, L. H. J.; Hoeben, F. J. M.; Versteegen, R. M.; Robillard, M. S. Triggered Drug Release from an Antibody–Drug Conjugate Using Fast “Click-to-Release” Chemistry in Mice. *Bioconjugate Chem.* **2016**, 27 (7), 1697–1706.
- (24) Geus, M. A. R.; Maurits, E.; Sarris, A. J. C.; Hansen, T.; Kloet, M. S.; Kamphorst, K.; Hoeve, W.; Robillard, M. S.; Pannwitz, A.; Bonnet, S. A.; Codée, J. D. C.; Filippov, D. V.; Overkleeft, H. S.; Kasteren, S. I. Fluorogenic Bifunctional *Trans* -Cyclooctenes as Efficient Tools for Investigating Click-to-Release Kinetics. *Chem. Eur. J.* **2020**, 26 (44), 9900–9904.
- (25) Bevaart, L.; Jansen, M. J. H.; van Vugt, M. J.; Verbeek, J. S.; van de Winkel, J. G. J.; Leusen, J. H. W. The High-Affinity IgG Receptor, FcγRI, Plays a Central Role in Antibody Therapy of Experimental Melanoma. *Cancer Res* **2006**, 66 (3), 1261–1264.
- (26) Journe, F.; Boufker, H. I.; Van Kempen, L.; Galibert, M.-D.; Wiedig, M.; Salès, F.; Theunis, A.; Nonclercq, D.; Frau, A.; Laurent, G.; Awada, A.; Ghanem, G. TYRP1 mRNA Expression in Melanoma Metastases Correlates with Clinical Outcome. *Br J Cancer* **2011**, 105 (11), 1726–1732.
- (27) Bolton, A. E.; Hunter, W. M. The Labelling of Proteins to High Specific Radioactivities by Conjugation to a 125I-Containing Acylating Agent. **1973**, 133, 10.
- (28) Rossin, R.; Lappchen, T.; van den Bosch, S. M.; Laforest, R.; Robillard, M. S. Diels-Alder Reaction for Tumor Pretargeting: In Vivo Chemistry Can Boost Tumor Radiation Dose Compared with Directly Labeled Antibody. *Journal of Nuclear Medicine* **2013**, 54 (11), 1989–1995.
- (29) Park, B. S.; Lee, J.-O. Recognition of Lipopolysaccharide Pattern by TLR4 Complexes. *Exp Mol Med* **2013**, 45 (12), e66–e66.

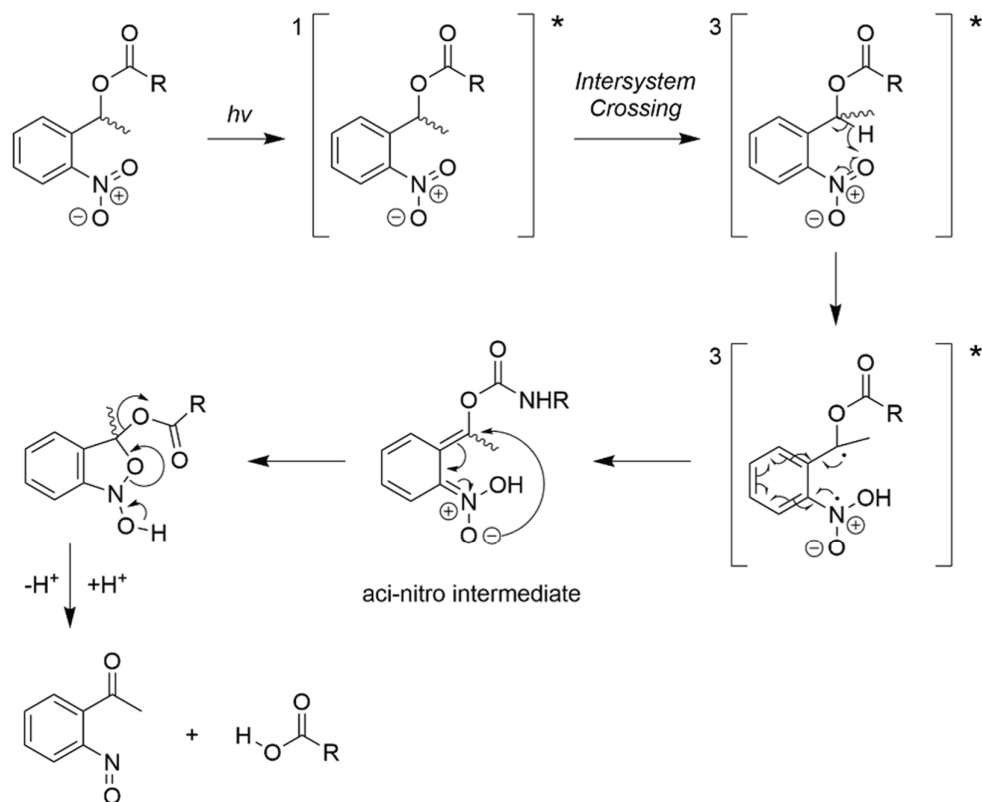
- (30) Chan, M.; Hayashi, T.; Mathewson, R. D.; Nour, A.; Hayashi, Y.; Yao, S.; Tawatao, R. I.; Crain, B.; Tsigelny, I. F.; Kouznetsova, V. L.; Messer, K.; Pu, M.; Corr, M.; Carson, D. A.; Cottam, H. B. Identification of Substituted Pyrimido[5,4- *b*]Indoles as Selective Toll-Like Receptor 4 Ligands. *J. Med. Chem.* **2013**, *56* (11), 4206–4223.
- (31) Lusic, H.; Deiters, A. A New Photocaging Group for Aromatic N-Heterocycles. *New York* **2006**, No. 13, 4.
- (32) Versteegen, R. M.; ten Hoeve, W.; Rossin, R.; de Geus, M. A. R.; Janssen, H. M.; Robillard, M. S. Click-to-Release from *Trans* -Cyclooctenes: Mechanistic Insights and Expansion of Scope from Established Carbamate to Remarkable Ether Cleavage. *Angew. Chem. Int. Ed.* **2018**, *57* (33), 10494–10499.
- (33) de Geus, M. A. R.; Groenewold, G. J. M.; Maurits, E.; Araman, C.; van Kasteren, S. I. Synthetic Methodology towards Allylic *Trans* -Cyclooctene-Ethers Enables Modification of Carbohydrates: Bioorthogonal Manipulation of the *Lac* Repressor. *Chem. Sci.* **2020**, *11* (37), 10175–10179.

Chapter 4

Photo-activatable TLR-ligands¹

Introduction

The *ortho*-nitrobenzyl group (oNB) was reported as a photo-labile protecting group for use in organic synthesis in 1966². Its discovery has since spawned a large body of literature on the use of light-sensitive protecting groups in organic synthesis³⁻⁶. Initially, the oNB group (Scheme 1) was used as an ester-protecting group that could be removed with 350-380 nm light.² The mechanism leading to liberation of the carboxylic acid is thought to be as follows.⁶ Upon irradiation, an excited singlet state is generated, which quickly crosses to an excited triplet state. From this triplet state, a hydrogen atom is abstracted from the benzylic carbon by the nitro-group. The radical species rearranges to form the *aci*-nitro intermediate. This intermediate then forms a 5-membered ketal ring, which collapses to form the nitroso product and the liberated carboxylic acid.



Scheme 1. Deprotection mechanism of benzylic-substituted 2-nitrobenzyls.⁶

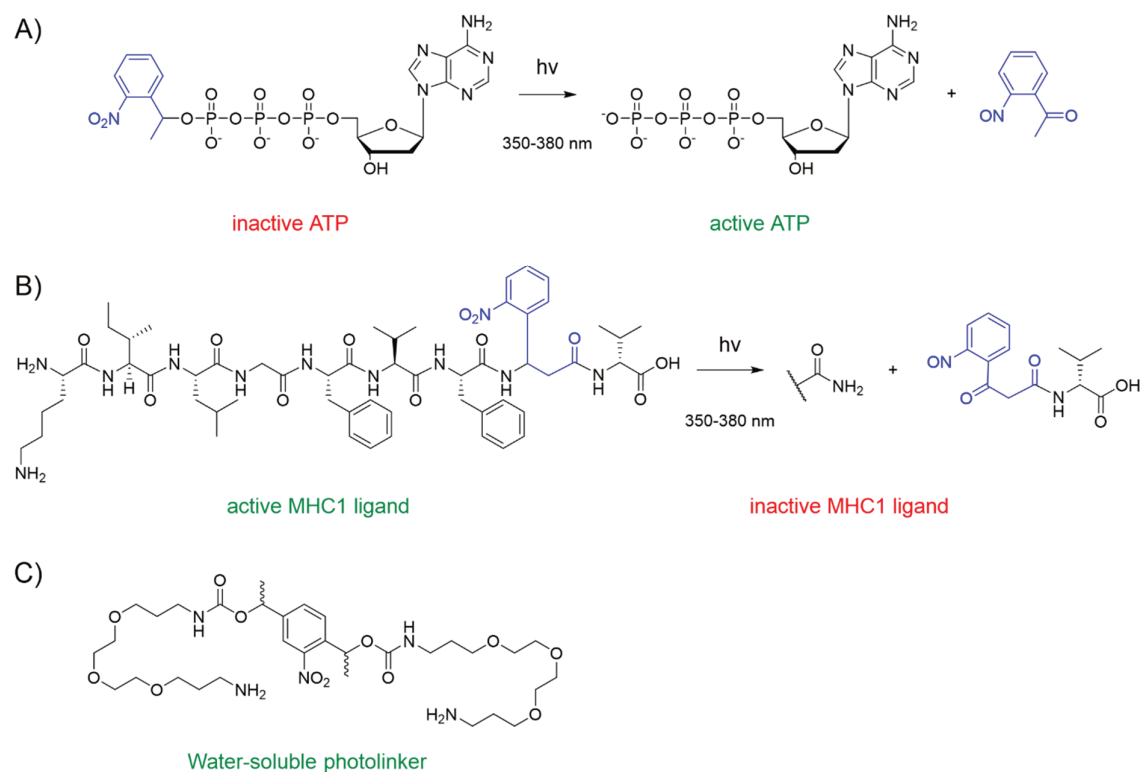
The oNB is able to release a wide varieties on functionalities upon UV-irradiation, including alcohols⁷, amines⁸, amides⁸, carbamates⁷, carboxylic acids², phosphates⁹ and carbonic acids⁷. The oNB protecting group can be used orthogonally with various other protecting groups and has been used in the synthesis of many organic compounds.^{4,10}

This orthogonality was picked up quickly by biochemists in 1977^{9,11}, as it was postulated that this orthogonality to a wide range of chemistries could translate to bioorthogonality of the deprotection reaction. In cells, this is a major issue, due to the wide variety of chemical functionalities present in biological samples that make selective chemistry very difficult.¹² In 1977, Engels¹¹ and Hoffman⁹ found that the oNB-group could be used in this context as well. They reported the light-induced activation of oNB-protected adenosine triphosphate (Scheme 2A). In these experiments the oNB was used to ‘mask’

or ‘cage’ the activity of a biologically active species. The strategy therefore became known as ‘photocaging’¹³. Since these initial experiments, photocages have been used extensively in biology (reviewed here¹⁴), and various different chemistries have been developed to do so. Coumarin-4-ylmethyl¹⁵-, BODIPY¹⁶-, arylcarbonylmethyl¹⁷- and metal¹⁸-based structures have all been employed to this end (see also Chapter 1). These photocages have been used to study a vast array of biological processes, and that involve the (un)caging of a range of metabolites¹⁹, carbohydrates²⁰, proteins²¹, (oligo-)nucleotides,^{22,23} peptides²⁴, and other (small) molecules.²⁵ In all these examples the photocage was used to mask a biologically active agent that was unmasked upon irradiation with light of a specific wavelength.

In recent years, photocages have also been adapted to achieve the opposite to activating: terminating the biological activity of a molecule upon irradiation. This concept was, for example, exploited to generate empty MHC class I molecules.⁸ MHC class I is an unstable complex by itself, but is stabilized by the presence of a peptide with the right size and amino acid composition. A peptide that included a photocage within the amino acid sequence was used to generate stable MHC-peptide complexes (Scheme 2B). UV irradiation of these complexes bearing the depicted nonapeptide led to dissociation of the resulting heptapeptide, due to the strict length requirements for the peptide ligands. This enabled to loading of epitopes of choice in a high-throughput manner on MHC class I molecules.

Photocages with one photolabile and one or more photo-stable connections (photolinkers) not only find their use in creating a fissile feature in a biomolecule to silence biological activity upon irradiation, but can also temporarily introduce features into a molecule. For example, the use of a PEG-modified nitrobenzyl-cage was used to enhance the aqueous-solubility of the photocage, to enable its application in affinity supports in proteomics (Scheme 2C).²⁶



Scheme 2. First examples of a nitrobenzyl being employed in a biological system as a photocage (A)⁹ and photolinker (B).⁸ One of the first reported examples of a solubilized version of a nitrobenzyl photolinker (C).

Despite the numerous applications, the oNB group has some intrinsic shortcomings. The first of these is that its excitation wavelength is in the UV-range (350-380 nm).⁷ This part of the electromagnetic spectrum is toxic to most living cells, as nucleobases and certain amino acids can absorb these wavelengths to form reactive species, leading to, for instance, DNA damage.²⁷ Secondly, the absorbance – the efficiency with which the oNB absorbs photons – is quite low. This efficiency is intrinsic to each photocage and can be described as the molar attenuation coefficient, ϵ , and is usually given at the wavelength at which the system absorbs the most light, λ_{max} . Given the concentration of the photocage, c , and the pathlength of light, l , the amount of light absorbed in a solution, A , is described by the Lambert-Beer law as $A = \epsilon \cdot c \cdot l$. From this equation it follows that the amount of light absorbed is linearly correlated to the ϵ , which for oNB-based photocages is low. The final problem with the oNB-group relates to the spatial resolution with which a sample can be deprotected, making it sub-optimal to investigate biological processes such as TLR-signaling.²⁸ This is in part due to the Abbe-limit of detection that is intrinsic to the wavelength of light used for the deprotection.²⁹

The shortcomings described above have in part been addressed by making analogues of oNB that contain the orthonitrophenyl-group in, for example, an extended conjugated system (Figure 1, NDBF, NPBF). This modification yielded photocages with increased ϵ -value compared to the parent-oNB group, and show uncaging with the decreased photo-toxic irradiation of up to 420 nm.¹ Further extension of the aromatic system, and the inclusion of a second nitrobenzyl-group,

yielded the bisstyrylthiophene group with the λ_{\max} shifted to 440 nm and a ϵ -value of 250 times higher than oNB.

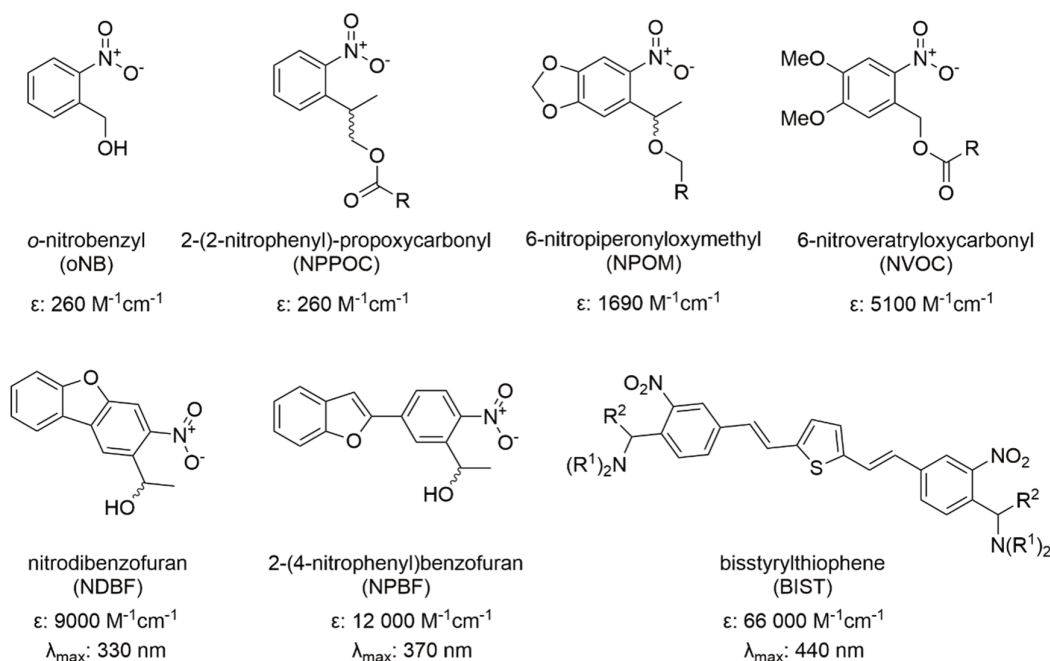


Figure 1. Several derivatives of the oNB-photocage. The NPPOC group has a similar ϵ -value as the oNB group, but has faster uncaging kinetics³⁰. The NPOM-group was developed by the group of Deiters to cage aromatic N-heterocycles which otherwise would hydrolyze quickly in an aqueous pH=7.5 environment³¹. The NVOC-group already has a significant higher absorption coefficient than the oNB-cage³² and has therefore been employed extensively. The NDBF-group has a much-improved ϵ -value and its quantum yield of photolysis is 0.7³³, and was thus useable to study cardiac muscle contraction using 2PE. The NPBF-group was synthesized later as an iteration on the NDBF-group to improve its use in 2-photon absorption³⁴ even further. BIST is a very efficient absorber of light and due to its extended conjugated system it can be cleaved using blue or violet light. It is currently the most-sensitive o-nitrobenzyl-based photocage for single and two-photon uncaging.

These approaches in part solved the issues with wavelength and non-wavelength dependent phototoxicity. They did not, however, address the problem of low uncaging resolution. This can be addressed by using photocages that are sensitive to 2-photon excitation (2PE). In such a 2PE phenomenon, a fluorophore/photocage is excited not by one photon of a given wavelength, but by two photons of double the wavelength. For example, instead of using 1 photon of 350 nm to excite a molecule, 2 photons of 700 nm are absorbed (as energy scales linearly with wavelength according to $E = h \cdot c / \lambda$). This requires however an extremely high photon density, as the likelihood of two absorption events to occur simultaneously is very low. Such a high photon density necessitates the use of non-phototoxic wavelengths in the (near-)infrared.

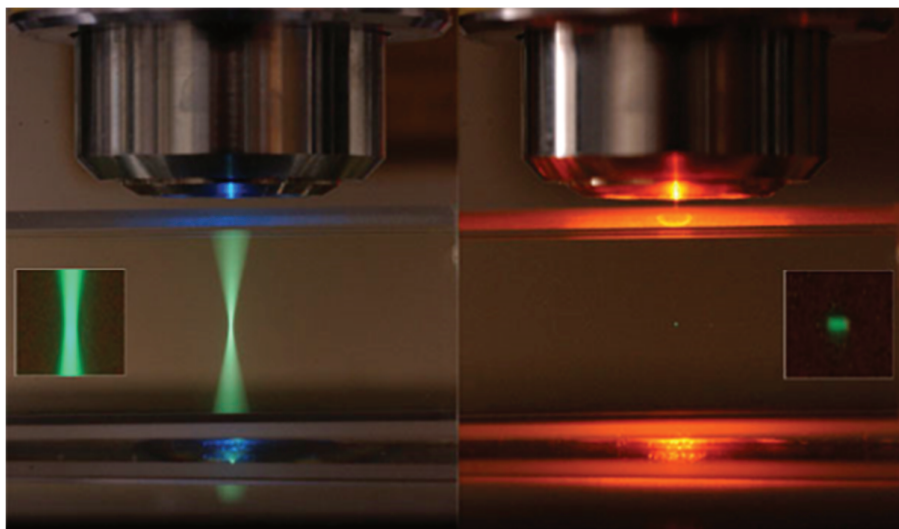


Figure 2. Signal-versus-noise when using single-photon excitation (left-hand side) and two-photon excitation (right hand side). Excitation outside the focal point is much more prominent in single-photon excitation, leading to loss of accuracy when investigating signal-sensitive systems.

Because of the use of lower energetic wavelengths phototoxicity is limited, and tissue penetration is enhanced.³⁵ The main advantage of 2PE is the high spatial resolution that can be obtained (Figure 2). Long wavelengths scatter less and two-photon absorption is extremely unlikely outside the focal point, thus reducing the background signal when compared to single-photon excitation. These effects enable the irradiation of single cells and even volumes in the femtoliter range (which would correspond to the volume of single endosomes).^{36,37}

In one-photon excitation, the probability of photon absorption is linearly proportional to the light intensity. But in 2PE, two photons are required to be simultaneously absorbed and thus the probability of this absorption process is proportional to the square of the light intensity.³⁸ For example in 1PE, the portion of caged biomolecules outside the focal point receiving *half* the amount of photons as those in the focal point are uncaged at *half* the rate. But in 2PE, caged biomolecules outside the focal point receiving *half* the amount of photons are uncaged at a *quarter* of the rate. Uncaging outside the region of interest therefore exponentially drops as the distance from the focal point increases. 2PE-uncaging may therefore assist in the unraveling of spatial-dependent signaling events exhibited by the TLR-system.

In this Chapter, the synthesis of 1P- and 2P-sensitive TLR-ligands is described. The oNB-cage and the NPBF-cage were introduced onto TLR-ligands to control their biological activity (Figure 3). Firstly, a TLR 7 ligand was protected with the 1P-sensitive NVOC (Figure 3, compound 4). A solubilized analogue was also made (Figure 3, compound 3). TLR2/6 ligands bearing the NPBF-photocage on the N-terminal amine were also synthesized and evaluated (Figure 3, 1 and 2).

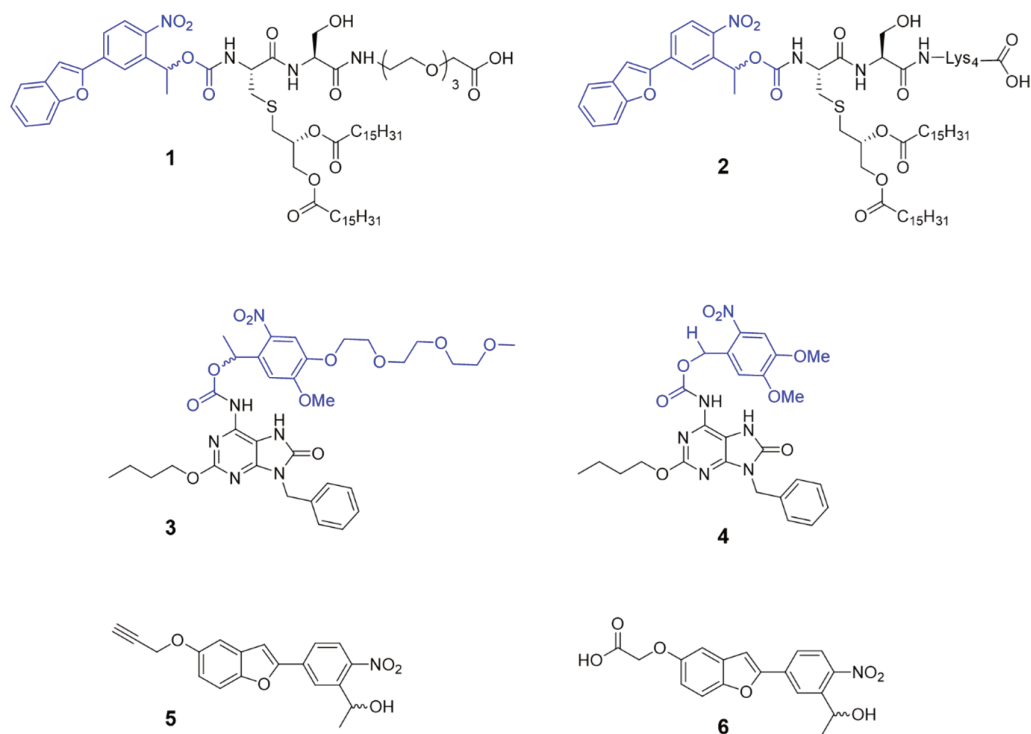
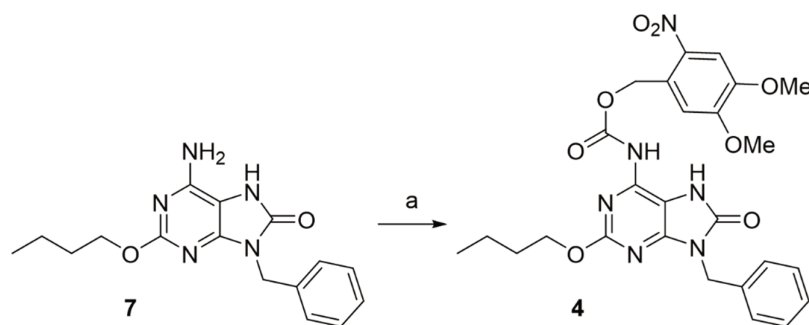


Figure 3. Target compounds described in this Chapter. For compounds 1-4, photocages are depicted in blue whereas the TLR-ligands are depicted in black. Compounds 5 and 6 are bis-functionalized derivatives of the NPBF photocage.

Results and discussion

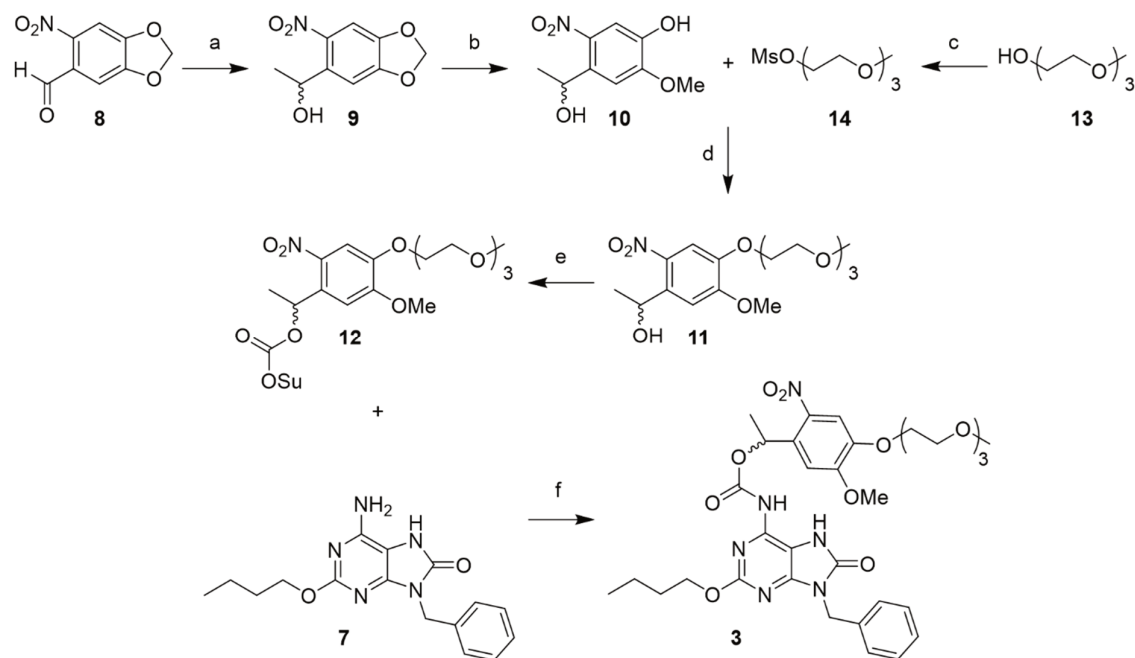
Photocaged TLR7 ligands

9-benzyl-8-oxo-2-butoxyadenine (Scheme 3, compound 7) is a potent TLR7 agonist (see also Chapter 3)³⁹ of which the activity can be blocked by protecting the exocyclic amine. A photocaged variant was made by reacting 7 with 6-nitroveratryloxycarbonyl (NVOC)-chloroformate (Scheme 3).



Scheme 3. a) NVOC-Cl, DMAP, dioxane, 50°C, o.n., 19%

Unfortunately, compound 4 was insoluble in aqueous and cell growth media (dilution of the DMSO stock resulted in precipitation in these solvents). It was hypothesized to occur due to the hydrophobic nature of both the TLR-ligand and the photocage. It was therefore opted to use a photo-destructible linker and use the second functionality within the cage to introduce moieties that improve aqueous solubility. A variant of the NVOC-photocage was synthesized in which triethylene glycol was appended to the nitrobenzene photocage (12, Scheme 4), using an intermediate described by Teague et al.⁴⁰ 6-Nitropiperonal was first reacted with the nucleophilic methylation reagent trimethyl aluminum, resulting in a racemic mixture of compound 9. Then a regioselective nucleophilic aromatic displacement with sodium methoxide was carried out affording compound 10. The phenol functionality could be selectively reacted over the benzylic alcohol under mildly basic conditions with the mesylate of triethyleneglycol monomethylether (14) to yield the solubilized photocage 11.

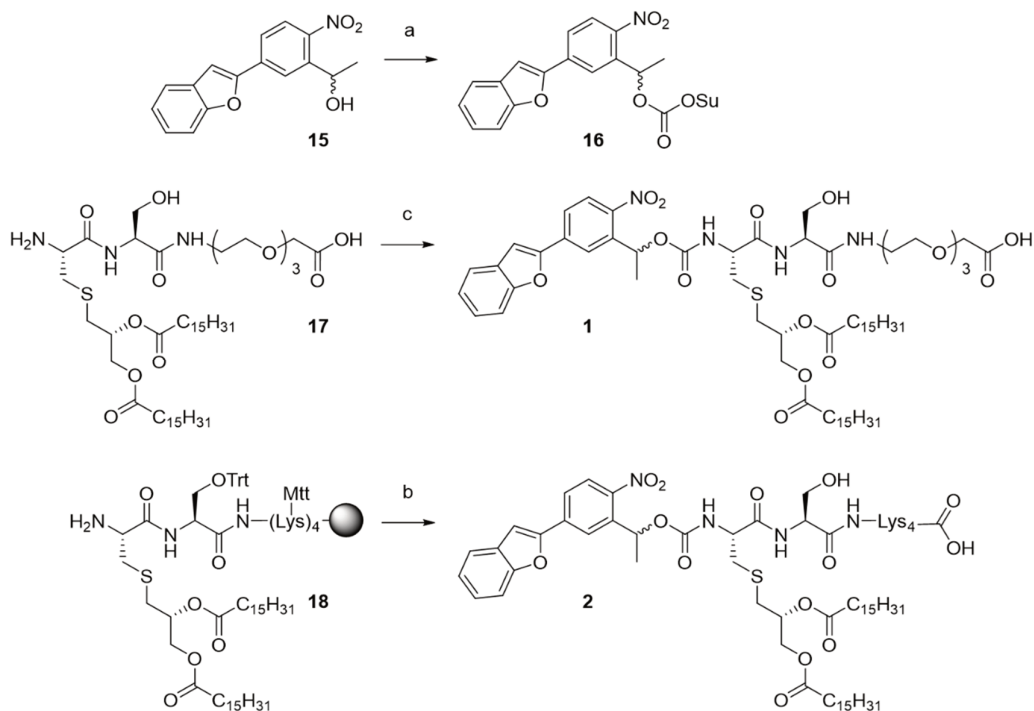


Scheme 4. a) 2M Al_2Me_6 in hexanes, DCM, r.t., qt. b) NaOMe, 1:2 MeOH:DMSO, 120°C, 2 hrs, 72% c) MsCl, TEA, DCM, 0°→RT, 1h, qt. d) K_2CO_3 , DMF, 100°C, 2 hrs, 92% e) N,N'-disuccinimidyl carbonate, TEA, DMAP, DCM, r.t., o.n., 70% f) Compound 12, TEA, DMAP, dioxane, 50°C, o.n., 27%.

Compound 11 was activated with N,N'-disuccinimidyl carbonate to give 12 which was used to modify to exocyclic amine of 7, albeit in modest yields and requiring long reaction times and elevated temperatures. The resulting compound 3 was indeed soluble in aqueous media in the μM -range, and is currently awaiting biological assessment.

Two-photon labile caged TLR 2/6 ligands

It was next explored whether a 2P-sensitive photocage could be used to cage a TLR2/6 ligand. For this the NPBF was chosen as the preferred group, due to its favourable deprotection properties. First, NPBF-OH was synthesized from literature procedure without further modification.³⁴ Next, it was activated with N,N'-disuccinimidyl carbonate to form NPBF-OSu (16, Scheme 5). 16 was then reacted with P_2CSTEG 17 to yield 1, and with on-resin P_2CSK_4 18 to yield NPBF- P_2CSK_4 2. Interestingly, when a *p*-nitrophenylcarbonate activated form of NPBF was first used to attempt to cage 17, no product formation was observed. Instead, two products formed of which one had a mass 18u lower than the starting material and the other mass 18u less than the expected product. This indicated a loss of a water molecule in both the starting material and the product during the reaction. It is suggested that the C-terminal carboxylate is able to attack the activated 4-nitrophenyl carbonate of NPBF, forming a mixed anhydride.



Scheme 5. a) N,N'-disuccinimidyl carbonate, TEA, DMAP, DCM, r.t., o.n., 29% b) i) Compound 23, DiPEA, DMF, r.t., o.n. ii) 20% TFA in DCM, r.t., 5 min (3x), 30% overall yield c) Compound 16, DiPEA, DMF, r.t., o.n., 63%.

An intramolecular cyclization with the serine alcohol or an amide then leads to a byproduct with a mass 18u lower than the parent compound. The formation of this by-product could be circumvented using the less-reactive OSu-ester of NPBH. Indeed, no byproduct formation was observed when NPBH-OSu was used to cage P₂CS_{TEG} instead of the *p*-nitrophenylcarbonate activated NPBH to obtain compound 1.

Compound 1 was very poorly soluble in aqueous media, and showed high adherence to plastic surfaces. Compound 2, however, did not show these issues and therefore was used to assess the ability of NPBH to effectively shield the activity of Pam₂CSK₄ towards the TLR2/6 dimeric receptor (Figure 4). No activity of the caged ligand towards TLR2/6-bearing THP1 cells is observed when shielded from light, except when ligand concentration is high. Only upon exposure of the treated cells with 360 nm light is NF-κB activity recovered.

Residual activity of the caged ligand at higher concentrations was also observed for the TCO-caged ligands in Chapter 2, and was addressed with the use of the C-terminally TEG-extended Pam₂CS ligands. Functionalization of NPBH with solubilizing moieties may enable the use of the TEG-extended ligand 1, and was therefore investigated further, as water solubility appeared to be a continuous bottleneck for caged TLR-ligands. Compound 2 may find its use in the localized activation of human and murine TLR2/6-bearing cells.

THP1 Dual

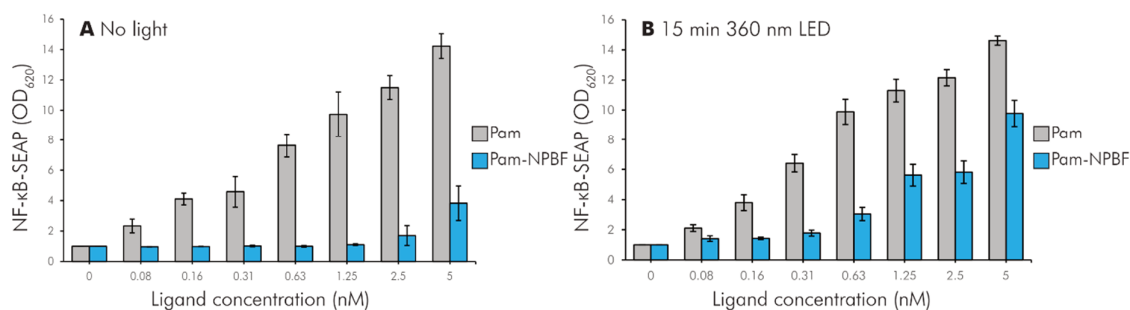
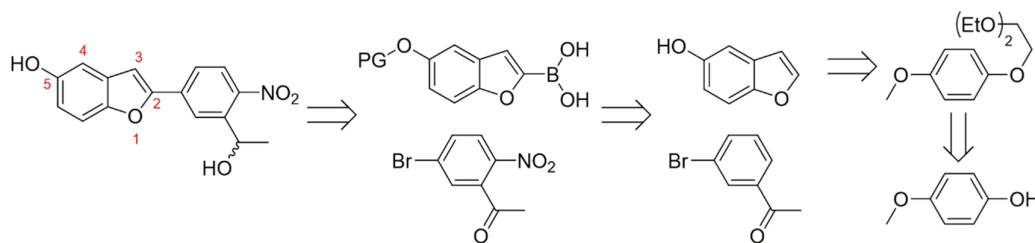


Figure 4. Activation of the NF- κ B cascade in THP1 Dual cells by free ligand Pam₂CSK₄ or NPBF-caged Pam₂CSK₄ **2**, as measured through the SEAP reporter produced upon NF- κ B activation. Cells were either irradiated with 360 nm light for 15 min through a 96-well plate LED array (B), or shielded from light for the same amount of time (A). At higher concentrations (>2.5 nM) caged ligand displays residual activity as reported in Chapter 2 for TCO-caged Pam₂CSK₄, but effectively shields the ligands activity towards TLR2/6 and concentrations below that. Experiment was carried out by Anya Savina (LIC).

Bis-functionalized NPBF-linker: rationalization, retrosynthetic analysis and synthesis

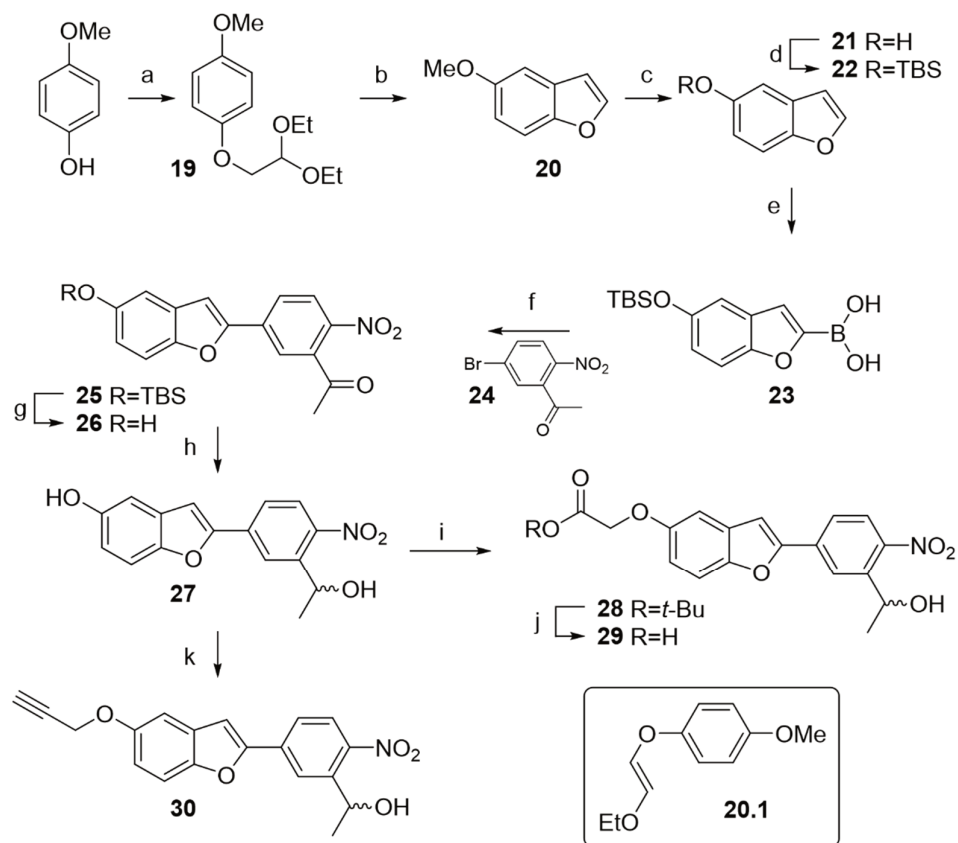
As the PEG-modified NVOC-TLR7 showed, the secondary functionalization of a (photo)cage can be used to allow the alteration of the biophysical properties of the molecule in a removable manner. It was postulated that the NPBF-core could serve as a platform to insert a such a secondary functionality. If – in an analogous fashion to the oNB-linkers described above – a phenol could be introduced in the backbone, it would enable the chemoselective functionalization of the phenol prior to the modification benzylic alcohol of the cage. The resulting ether functionality would also exert an electron-donating effect on the aromatic system, which is known to increase the molar attenuation coefficient thus improving absorbance at λ_{max} .⁴¹ NPBF contains multiple potential sites for introducing a phenol group. However, literature precedence exists for the functionalization of the 5-position (Scheme 6).⁴² Additionally, having the electron-donating group (-OR) on the opposing side of the electron-withdrawing group (-NO₂) may also enhance the 2PA cross section by creating a push-pull structure through a permanent dipole moment change.⁴³



Scheme 6. Retrosynthetic analysis of NPBF diol **27**.

Scheme 6 depicts the retrosynthetic analysis of this 5-hydroxy-NPBF. The C-C bond between the benzofuran and the nitrophenyl could be formed through a Suzuki cross-coupling reaction. The nitrophenyl can be afforded by regioselective nitration of 3'-bromoacetophenone. 5-Hydroxybenzofuran can be obtained by cyclization of aryloxyacetaldehyde acetal catalyzed by

polyphosphoric acid, thus effecting 4-methoxyphenol and 3'-bromoacetophenone as the core starting materials.



Scheme 7. a) Bromoacetaldehyde diethyl acetal, KOH, NMP, 70°C, 15 hrs, 90% **b**) Polyphosphoric acid, toluene, 110°C, 2 hrs, 33% **c**) i) BBr₃, DCM, -78°C → r.t., 2 hrs, 89% **d**) tert-butyldimethylsilyl chloride, imidazole, toluene, DMF, r.t., 1 hr, 70% **e**) i) *n*-BuLi in hexanes, THF, -78°C, 1 hr ii) triisopropyl borate, -78°C, 30 min → r.t., 30 min **f**) Pd(PPh₃)₄, K₂CO₃, 1:1 H₂O:THF, 66°C, 18 hrs, 61% + 14% **26** over 3 steps **g**) 70% HF in pyridine, THF, r.t., 2 hrs, 93% **h**) NaBH₄, MeOH, r.t., 1 hr, qt. **i**) *tert*-butyl bromoacetate, K₂CO₃, DMF, 70°C, 3 hrs, 72% **j**) TFA, DCM, r.t., 30 min, qt. **k**) i) Propargyl bromide, K₂CO₃, DMF, r.t., o.n., 98%

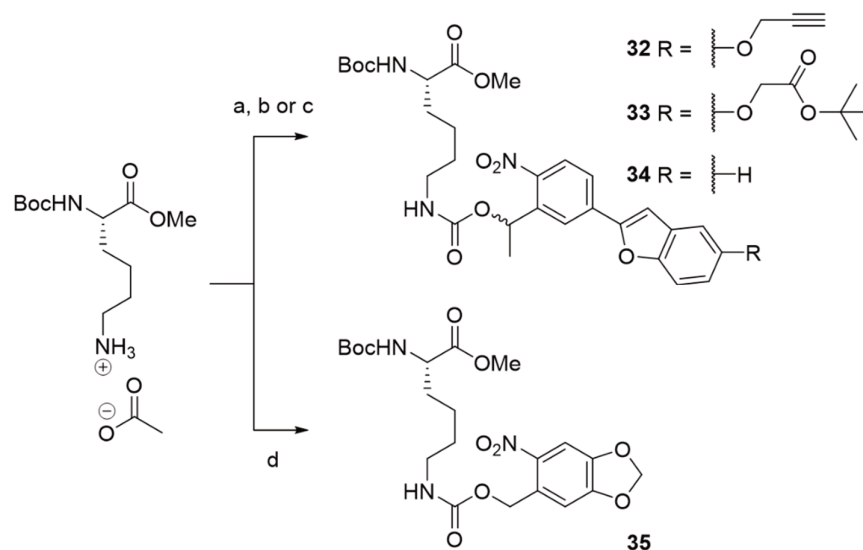
Scheme 7 describes the synthesis towards bis-functionalized NPBF as well as its decoration with an alkyne and carboxylic acid linker. 4-Methoxyphenol was reacted with bromoacetaldehyde diethyl acetal using potassium hydroxide as a base in NMP, a high-yielding reaction that successfully afforded **19** on a 60 g scale. The subsequent cyclization towards **20** proceeded in yields varying from 33-42%, depending on the scale of the reaction. The major byproduct was identified as a singly-eliminated ethoxide, forming the non-cyclized E-alkene **20.1**. The polyphosphoric acid reagent was somewhat unpractical to handle, but was facilitated by the use aqueous NaOH. It is interesting to note that 5-methoxybenzofuran has an extremely sweet and fruity odour and care had to be taken when handling the chemical outside the fume hood. The 5'-O-methyl proved an insufficient protecting group for the subsequent boronation and Suzuki-coupling. **20** was therefore demethylated using boron-tribromide in DCM at -78°C. This reaction did not proceed with the reported substoichiometric amounts of BBr₃ to full demethylation⁴⁴, so instead a molar equivalent

was used. A *tert*-butyldimethyl silyl group was installed on the 5'-OH as a protecting group after which the 2'-position was lithiated using *n*-BuLi. Addition of triisopropyl borate to the solution afforded compound **23**, which is used best as a crude material.

In parallel, 3'-bromoacetophenone was nitrated using a solution of cold sulfuric acid and potassium nitrate to yield **24**. When the temperature exceeds -10°C, formation of the bis-nitrated compound starts to play a significant role thus warranting close monitoring of the reaction temperature. Suzuki cross-coupling of **23** with **24** using Pd(PPh₃)₄ afforded a mixture of the product **25** as well as the desilylated product **26**. Purification by column chromatography to remove the palladium species before proceeding turned out to be imperative. When the crude mixture was moved forward to the desilylation reaction (using an HF.pyridine solution), an elusive palladium impurity was formed that defied removal by column chromatography or crystallization. This impurity led to the rapid total degradation when ketone **26** was reduced with NaBH₄ in the following step. In the absence of this impurity the reduction proceeds smoothly and with diol **27** in hand, the 5'-OH can generally be decorated with various linkers using potassium carbonate in DMF at ambient-to-elevated temperatures (r.t. – 70°C) to obtain carboxylate **29** or propargyl **30**.

Photochemical characterization

The newly introduced phenolic alkyl-ether-substituent was postulated to have an impact on the photochemical properties of the NPBF-core. Three model compounds were synthesized to investigate this hypothesis. Boc-Lys-OMe was functionalized on the side chain amine either with NPBF-*t*-butyl ester **28**, NPBF-Alkyne **30** or NPBF **15** (Scheme 7, 8). The three derivatives were then tested to determine whether the functional groups had an effect on the photochemistry of the NPBF.



Scheme 8. Reagents and conditions: **a)** Compound **31**, DiPEA, DMF, r.t., 15 min, 66% **b)** Compound **28**, N,N'-disuccinimidyl carbonate, DiPEA, AcN, r.t., 16h, 55% **c)** Compound **16**, DiPEA, DMF, r.t., 16h, 78% **d)** Compound **36**, N,N'-disuccinimidyl carbonate, DiPEA, AcN, r.t., 1h, 75%.

First, the molar attenuation coefficient ϵ and λ_{\max} were determined through a serial dilution in an UV-Vis spectrometer (Table 1). The presence of the newly introduced functionality is accompanied with an increase of the ϵ of roughly 30%, with the λ_{\max} only minimally altered. The small difference

Table 1. Molar attenuation coefficient ϵ measured at the λ_{\max} of each model compound including standard deviation σ ($n=3$).

Compound	ϵ	σ	λ_{\max}
32	16 635	88	362 nm
33	17 119	59	365 nm
34	12 945	24	357 nm
35	4248	14	349 nm

between the alkyne- and ester-modified species suggest the increase in ϵ is caused by the electron-donating properties of the -OR substitution, rather than any secondary effects of the functional groups.

Next, the kinetics of uncaging were investigated to check whether substitution has affected this. A UV-Vis spectrum was taken at timepoint $t = 0$, after which the cell was irradiated with a 375 nm light source at a constant distance and power setting for 10 seconds ($c \approx 50 \mu\text{M}$ in a mixture of 1:1:1 AcN:*t*-BuOH:H₂O). After each irradiation interval a UV-Vis spectrum was recorded and after 1 minute of cumulative irradiation time the spectra were compounded (Figure 5). Concentrations were normalized with respect to each compound's molar attenuation coefficient ϵ , such that each cuvette has the same absorption value at 360 nm at $t=0$. Then, the absorbance at $\lambda = 450$ nm was plotted against the irradiation time, enabling the determination of the rate with which the nitroso ketone-side product is formed and thus lysine is uncaged (Figure 6).

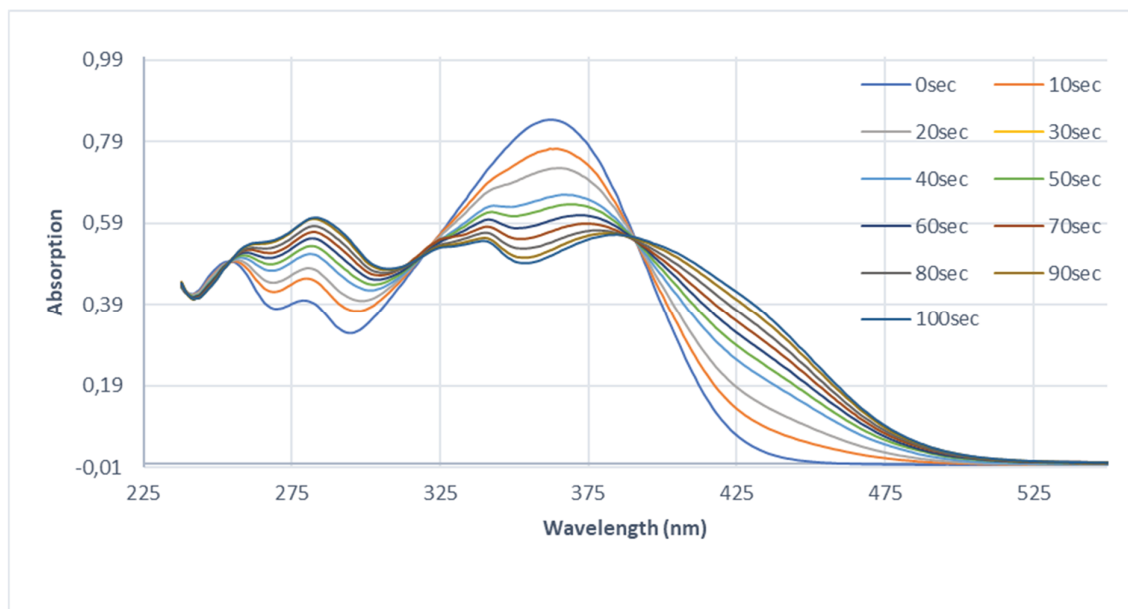


Figure 5. Example of an irradiation experiment with compound **33**. After every 10 seconds of irradiating the light source is switched off and a UV-Vis spectrum (235 – 550 nm, $d=1$ nm) is recorded. After a cumulative time of 100 seconds of irradiation the spectra are compounded.

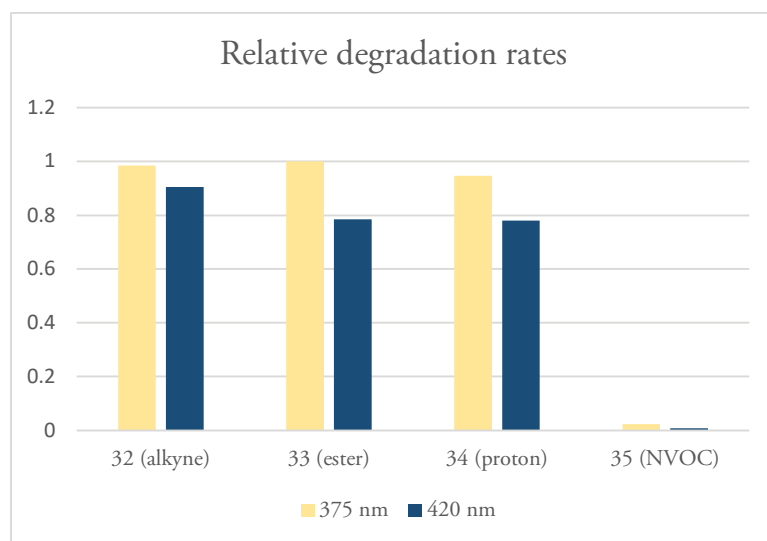


Figure 6. Relative uncaging rates at 375 nm or 420 nm irradiation.

Figure 6 depicts the relative uncaging rates for the model lysine compounds when the number of photons absorbed at the λ_{max} is the same for each sample at $t = 0$. There is no significant difference between the three NPBF-derivatives in regards to uncaging kinetics, meaning the newly introduced substitution does not impact the mechanism with which the photouncaging occurs in a significant manner. The rate at 420 nm appears to match the rate at 375 nm. However, these data were not corrected for the power output difference between the 375 nm LED and 420 nm LED, with the latter being approximately 4-fold brighter than the former. The NPBF-linker can thus be exploited to generate photocaged TLR ligands that are increasingly soluble in aqueous media and useable in two-photon excitation experiments.

Conclusion

In this Chapter the synthesis of various photosensitive TLR-ligands was described. In order to circumvent the poor solubility of these constructs, solubilized variants of the photoprotecting groups oNB and NPBF were developed. The 2-photon sensitive NPBF-derivatives bearing an alkyne or carboxylic acid were of particular interest due to their increase in molar extinction coefficient and the ability to use this compound as a photolinker.

Acknowledgements

Dr. Andrea Pannwitz is acknowledged for her aid in the photochemical characterization of compounds 32-35. Dr. Michael Meijer is acknowledged for his aid in the photoreactor design.

Experimental section

Photochemical characterization

The irradiation experiments on the UV-Vis to characterize compounds **32-35** were performed using a custom-made experimental setup. LEDs were ordered from Roithner Lasertechnik GmbH (High Power Single Chip, H2A1 Series, 1W). Power output was measured using a radiometer on distances and settings relevant to irradiation experiments: 3 mW/cm² for 375 nm LED and 13 mW/cm² for 420 nm LED. LEDs were mounted on an aluminum heatsink that were fitted on plastic adapters (Figure 7). These adapters were custom made for two flask sizes as well as a cuvette for UV-Vis measurements. Power output could be adapted between 50 mA-350mA in steps of 50. Spread of wavelengths emitted by the LEDs as a function of power output has been recorded by the supplier and is available online (Figure 8).

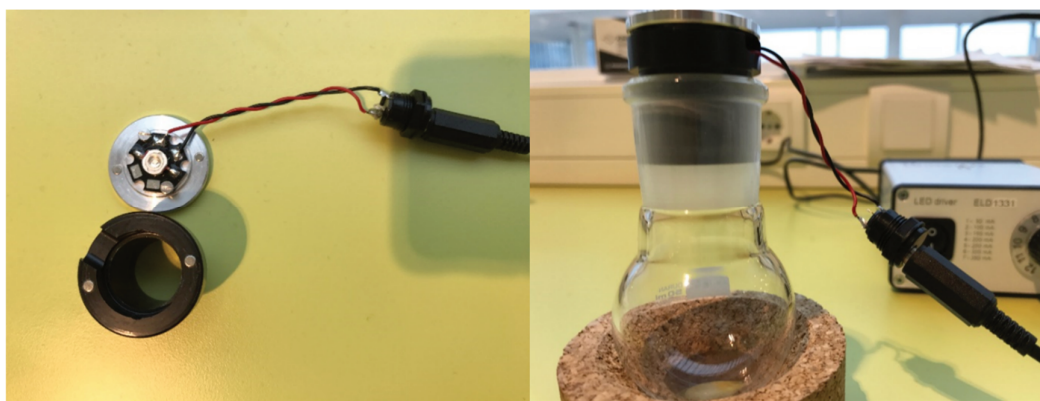


Figure 7. Custom-made photoreactor setup. A hexagonal LED is mounted on an aluminum heatsink. Magnets assist alignment and secure the LED on the black plastic adapter. Adapters have been made that fit on either flasks or a cuvette.

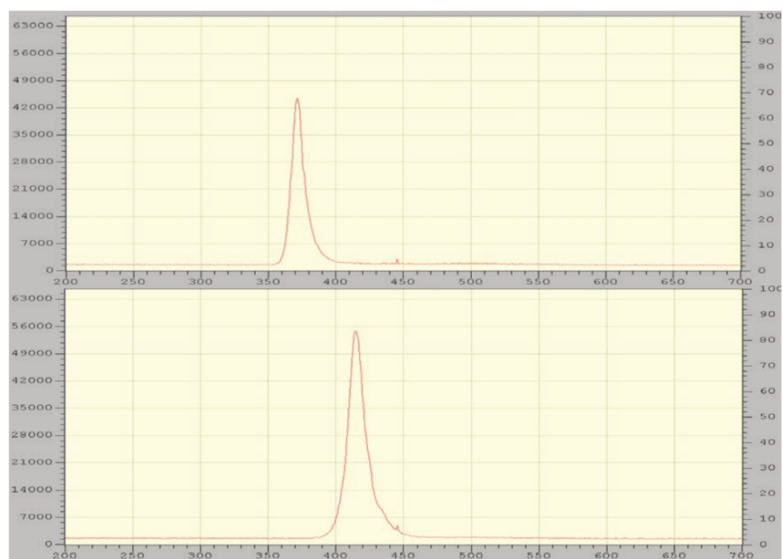
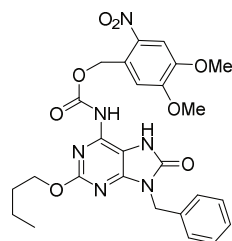


Figure 8. Normalized output power vs wavelength of the two LEDs employed in this chapter: 375 nm (top) and 420 nm (bottom). Spectra were copied from the data sheets available on the Roithner Lasertechnik website.

General methods

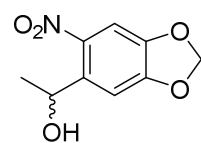
Commercially acquired reagents and solvents were used as received. Anhydrous solvents were prepared with activated 3 Å or 4 Å molecular sieves. All reaction progress was monitored by TLC analysis on Merck aluminum plates pre-coated with silica gel 60 and F254 fluorescent indicator; 254 nm UV light was used to check for compounds, and TLC plates were developed by charring (at approximately 150 °C) plates that were sprayed with permanganate stain (20 g/L KMnO₄ and 10 g/L K₂CO₃ in H₂O), unless stated otherwise. R_f values reported consider the compound being synthesized. Screening Devices silica gel (40-63 µm particle size and 60 Å pore diameter) was used during column chromatography. ¹H and ¹³C NMR spectra were recorded on Bruker AV-400 (400 MHz) and AV-500 (500 MHz) spectrometers. Chemical shifts are reported as δ-values in ppm relative to tetramethylsilane (which was added to CDCl₃) or residual solvent peaks. The ¹³C spectra are proton decoupled. LC-MS checks for all compounds were performed on a Finnigan Surveyor HPLC system with a Gemini C18 50 x 4.60 mm column, which was coupled to a Finnigan LCQ Advantage Max mass spectrometer. LC-MS samples were prepared by dissolving compounds in a tBuOH:ACN:H₂O mixture (1:1:1 by volume).

Compound 4



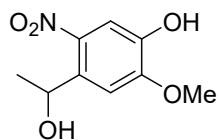
Compound 7 (50 µmol, 16 mg) was dissolved in dioxane (500 µL). DMAP (100 µmol, 12.2 mg) and NVOC-Cl (55 µmol, 16 mg) were added and the reaction was allowed to stir overnight at 50°C. LC-MS indicated over 90% conversion after which the reaction mixture was diluted with DMSO and purified by reverse phase HPLC (C18, TFA, acetonitrile/water) to afford the title compound (9.4 µmol, 5.2 mg) in a 19% yield.

Compound 9



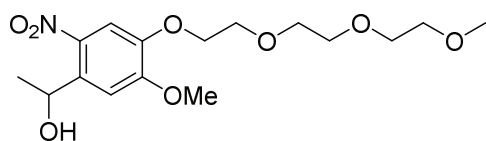
6-nitropiperonal **8** (50 mmol, 9.75 g) was dissolved in anhydrous DCM (500 mL) under a nitrogen atmosphere. Trimethylaluminum (28 mL, 2M in hexanes) was added dropwise at room temperature. After the addition was completed TLC analysis (20% EtOAc in Pnt, R_f=0.3) indicated complete conversion of the starting material. The leftover reagent was quenched by the careful addition of 1M HCl (aq.). The reaction mixture was washed with H₂O (3x), brine (1x), dried over MgSO₄ and concentrated *in vacuo* affording the title compound (49.8 mmol, 10.5 g) in a quantitative yield. ¹H NMR (400 MHz, MeOD) δ 7.42 (s, 1H), 7.26 (s, 1H), 6.12 (dd, *J* = 4.9, 0.9 Hz, 2H), 5.34 (q, *J* = 6.3 Hz, 1H), 1.44 (d, *J* = 6.3 Hz, 3H). ¹³C NMR (101 MHz, MeOD) δ 148.33, 141.21, 107.13, 105.58, 104.62, 66.31, 25.21.

Compound 10



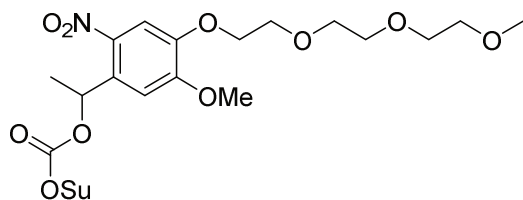
Compound **9** (49.8 mmol, 10.5 g) was dissolved in a mixture of 1:2 (v/v) anhydrous MeOH:DMSO ($V_{\text{total}}=100$ mL) under a nitrogen atmosphere. Sodium methoxide (150 mmol, 7.95 g) was added after which the reaction mixture was heated to 120°C. After 2 hours TLC analysis (30% EtOAc in Pnt, $R_f=0.2$) indicated complete conversion of the starting material. The mixture was cooled down to room temperature after which 1M HCl (aq.) was added to quench leftover reagents. The mixture was washed with EtOAc (3x). The organic layers were combined and washed with brine (1x), dried (MgSO_4) and concentrated *in vacuo*. The crude was adsorbed unto Celite and purified by silica gel column chromatography (20% EtOAc in Pnt \rightarrow 50% EtOAc in Pnt, $\Delta=10\%$) to afford the title compound (35.8 mmol, 7.63 g) in a 72% yield. ^1H NMR (400 MHz, DMSO) δ 9.92 (s, 1H), 7.41 (s, 1H), 7.31 (s, 1H), 5.41 (d, $J = 4.3$ Hz, 1H), 5.24 (dd, $J = 6.1, 4.4$ Hz, 1H), 3.89 (s, 3H), 1.35 (d, $J = 6.2$ Hz, 3H). ^{13}C NMR (101 MHz, DMSO) δ 152.61, 145.11, 138.86, 136.53, 110.66, 109.27, 63.91, 55.96, 25.26.

Compound 11



Compound **10** (9.50 mmol, 2.02 g) was dissolved in DMF (50 mL). K_2CO_3 (10 mmol, 1.4 g) and compound **14** (10.0 mmol, 2.42 g) were added and the mixture was heated to 100 °C for 2 hours. TLC analysis (80% EtOAc in Pnt, $R_f=0.2$) indicated complete conversion of the starting material. The reaction mixture was poured in 1M HCl (aq.) and washed with EtOAc (3x). The organic layers were combined and washed with H_2O (3x), dried (MgSO_4), filtered and concentrated *in vacuo*. The crude was diluted with a small amount of 1:1 EtOAc:Pnt (v/v) and purified by silica gel column chromatography (50% EtOAc in Pnt) to afford the title compound (8.71 mmol, 3.13 mg) in a 92% yield. ^1H NMR (400 MHz, CDCl_3) δ 7.63 (s, 1H), 7.30 (s, 1H), 5.55 (q, $J = 6.3$ Hz, 1H), 4.27 – 4.20 (m, 2H), 3.97 (s, 3H), 3.91 (dd, $J = 9.4, 4.4$ Hz, 2H), 3.73 (tt, $J = 8.8, 4.2$ Hz, 2H), 3.70 – 3.61 (m, 4H), 3.54 (dd, $J = 5.7, 3.6$ Hz, 2H), 3.37 (s, 3H), 1.54 (d, $J = 6.3$ Hz, 3H). ^{13}C NMR (101 MHz, CDCl_3) δ 154.29, 147.03, 139.51, 137.41, 109.75, 108.82, 72.01, 71.01, 70.75, 70.66, 69.57, 69.08, 65.78, 59.14, 56.42, 24.43.

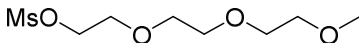
Compound 12



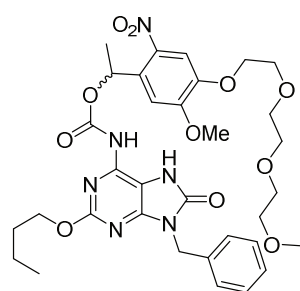
Compound **11** (0.57 mmol, 0.20 g) was dissolved in anhydrous DCM (5 mL) under a nitrogen atmosphere. Triethylamine (0.63 mmol, 87 μL) and N,N' -disuccinimidyl carbonate (1.87 mmol, 483 mg) and DMAP (0.07 mmol, 9 mg) were added and the mixture was allowed to stir at room temperature overnight. TLC analysis (80% EtOAc in Pnt, triethylamine-neutralized, $R_f=0.4$, purple under 365 nm UV) indicated complete conversion of the starting material. The crude was adsorbed onto Celite and purified by silica gel column chromatography (triethylamine-neutralized, 60% EtOAc in Pnt \rightarrow 80% EtOAc in Pnt) to afford the title compound (0.40 mmol, 0.20 g) in a 70% yield. ^1H NMR (400 MHz, CDCl_3) δ

7.72 (s, 1H), 7.07 (s, 1H), 6.49 (q, $J = 6.3$ Hz, 1H), 4.25 (dd, $J = 10.9, 6.0$ Hz, 2H), 4.04 (s, 3H), 3.95 – 3.88 (m, 2H), 3.77 – 3.71 (m, 2H), 3.66 (ddd, $J = 15.6, 7.1, 4.4$ Hz, 4H), 3.55 (dd, $J = 5.6, 3.6$ Hz, 2H), 3.37 (s, 3H), 2.80 (s, 4H), 1.76 (d, $J = 6.4$ Hz, 3H). **^{13}C NMR (101 MHz, CDCl_3) δ** 168.61, 154.64, 150.56, 147.73, 139.09, 131.31, 109.65, 107.35, 76.52, 71.87, 70.88, 70.60, 70.52, 69.37, 68.99, 58.99, 56.49, 25.39, 21.88.

Compound 14

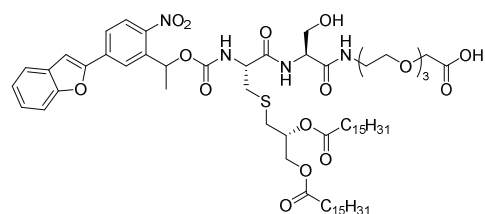
 Triethylene glycol monomethyl ether **13** (10.0 mmol, 1.61 mL) was dissolved in anhydrous DCM (10 mL). Triethylamine (20.0 mmol, 2.77 mL) was added and the mixture was cooled to 0°C. Mesyl chloride (12.0 mmol, 932 μL) was added carefully after which the mixture was allowed to stir for 1 hour at room temperature. TLC analysis (85% EtOAc in Pnt, $R_f=0.3$) indicated complete conversion of the starting material. The mixture was diluted with DCM and washed with 1M HCl (aq.) (3x) and consequently a saturated solution of NaHCO_3 (aq.) (3x). The organic layer was dried (MgSO_4), filtered and concentrated *in vacuo* to afford the title compound (10.0 mmol, 2.42 g) in a quantitative yield. **^1H NMR (400 MHz, CDCl_3) δ** 4.41 – 4.33 (m, 1H), 3.80 – 3.73 (m, 1H), 3.72 – 3.59 (m, 3H), 3.56 – 3.49 (m, 1H), 3.37 (s, 1H), 3.08 (s, 1H). **^{13}C NMR (101 MHz, CDCl_3) δ** 71.87, 70.59, 70.51, 69.36, 68.99, 59.01, 37.68.

Compound 3



Compound **7** (50 μmol , 16 mg) was dissolved in dioxane (100 μL). Triethylamine (150 μmol , 21 μL), DMAP (8 μmol , 1 mg) and compound **12** (55 μmol , 29 mg) were added and the reaction was allowed to shake overnight at 50°C. LC-MS indicated over 90% conversion after which the reaction mixture was diluted with DMSO and purified by reverse phase HPLC (C18, TFA, acetonitrile/water) to afford the title compound (13.5 μmol , 9.4 mg) in a 27% yield.

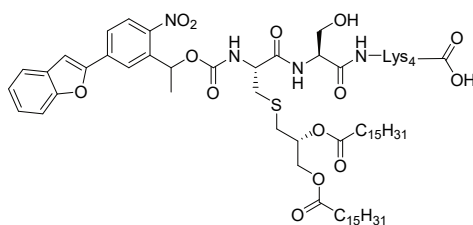
Compound 1



Compound **17** (2.4 μmol , 2.3 mg, synthesis described in Chapter 2) was dissolved in DMF (500 μL). DiPEA (10 μmol , 1.8 μL) and compound **16** (5.9 μmol , 2.5 mg) were added and the reaction was allowed to shake overnight at room temperature. LC-MS analysis indicated complete conversion of the starting material.

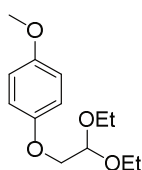
The mixture was concentrated *in vacuo* and co-evaporated with toluene (3x). The crude was dissolved in DCM and purified by silica gel column chromatography (DCM \rightarrow 1% MeOH in DCM \rightarrow 10% MeOH in DCM) to afford the *tert*-butyl protected intermediate product. The product was dissolved in DCM (1 mL) and TFA was added (1 mL) and the reaction was stirred for 2 hours at room temperature. TLC analysis (5% MeOH in DCM, $R_f=0.3$) indicated complete conversion of the reaction and the mixture was concentrated *in vacuo* to afford the title compound (1.5 μmol , 1.9 mg) in a 63% yield.

Compound 2



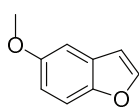
Resin-bound hexapeptide (10 μmol , 45 mg, synthesis described in Chapter 2) was swollen in DMF. DiPEA (11 μmol , 2.0 μL) and compound **16** (50 μmol , 21 mg) were added and the reaction was allowed to shake overnight at room temperature. A small amount of TFA-treated resin analyzed by LC-MS indicated complete conversion of the starting material. The resin was washed with DMF (3x) and treated with a solution of 20% TFA in DCM. The solution was dropped in a mixture of 1:1 Et₂O:Pnt (v/v) at -30°C. The product was allowed to precipitate overnight at -30°C after which the precipitate was collected by centrifugation. The precipitate was dissolved in DMSO and purified by reverse-phase HPLC (C18, TFA, acetonitrile/water) to afford the title compound (3.0 μmol , 4.7 mg) in a 30% overall yield.

Compound 19



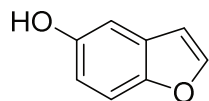
A procedure from literature^[1] was modified as follows: 4-methoxyphenol (300 mmol, 37.2 g) was dissolved in NMP (300 mL, 1 M) followed by addition of potassium hydroxide (600 mmol, 33.6 g) at r.t.. Bromoacetaldehyde diethyl acetal (7.5 mmol, 1.13 mL) was added slowly and the reaction was stirred at 70°C for 15 h. TLC analysis indicated complete conversion of the starting material (10% Et₂O in Pnt, R_f=0.7). The reaction mixture was poured in H₂O and extracted with Et₂O (3x). The combined organic layers were washed with brine (1x), dried over MgSO₄ and concentrated *in vacuo*. Purification by silica gel column chromatography (5% Et₂O \rightarrow 10% Et₂O in Pnt) yielded compound **19** (270 mmol, 64.9 g, 90%). ¹H NMR (400 MHz, Chloroform-*d*) δ 6.90 – 6.76 (m, 4H), 4.80 (t, *J*=5.2, 1H), 3.95 (d, *J*=5.2, 2H), 3.80 – 3.68 (m, 2H), 3.72 (s, 3H), 3.61 (dq, *J*=9.4, 7.0, 2H), 1.23 (t, *J*=7.1, 6H). ¹³C NMR (101 MHz, CDCl₃) δ 153.94, 152.71, 115.53, 114.46, 100.49, 69.13, 62.36, 55.48, 15.26.

Compound 20



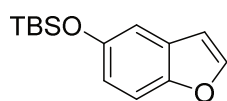
A procedure from literature^[2] was modified as follows: Polyphosphoric acid (60 g, H₃PO₄ basis, 115%) was dissolved in toluene (600 mL) and the mixture was heated to 110°C under vigorous stirring. Compound **19** (255 mmol, 61.3 g) was dissolved in toluene (160 mL, 1.6 M) and was dropwise added to the solution over the course of 1 hour. After stirring for 1 hour at reflux temperature TLC indicated complete conversion of the starting material (5% Et₂O in Pnt, R_f=0.8). The mixture was cooled to r.t., decanted in 1 M NaOH (aq) and extracted with toluene. The combined organic layers were washed with brine (1x), dried over MgSO₄ and concentrated *in vacuo*. Purification by silica gel column chromatography (Pnt \rightarrow 2% Et₂O in Pnt) yielded compound **20** (83.1 mmol, 12.3 g, 33%). ¹H NMR (400 MHz, Chloroform-*d*) δ = 7.59 (dd, *J*=2.2, 0.5, 1H), 7.39 (ddd, *J*=8.9, 1.0, 0.5, 1H), 7.05 (d, *J*=2.6, 1H), 6.90 (ddd, *J*=8.9, 2.6, 0.5, 1H), 6.70 (dd, *J*=2.2, 0.9, 1H), 3.84 (s, 3H). ¹³C NMR (101 MHz, CDCl₃) δ = 145.86, 128.08, 113.20, 111.93, 106.82, 103.61, 56.03.

Compound 21



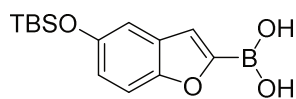
A procedure from literature^[3] was modified as follows: Compound **20** (5.7 mmol, 849 mg) was dissolved in anhydrous DCM (8.1 mL, 0.7 M) under a nitrogen atmosphere. The mixture was cooled to -78°C after which a 1 M solution of BBr₃ in DCM (6.8 mmol, 6.8 mL) was slowly added. The mixture was stirred at -78°C for 1 hour and then heated to r.t. and stirred for an additional hour. TLC analysis indicated complete conversion of the starting material (20% EtOAc in Pnt, R_f=0.7). The reaction was quenched with saturated solution of NaHCO₃ (aq.), poured in H₂O and extracted with EtOAc (3x). The combined organic layers were washed with brine (1x), dried over MgSO₄ and concentrated *in vacuo*. Purification with silica gel column chromatography (5% EtOAc → 10% EtOAc in Pnt) yielded compound **21** (5.11 mmol, 0.685 g, 89%). ¹H NMR (400 MHz, Chloroform-*d*) δ = 7.59 (dd, *J*=2.2, 0.5, 1H), 7.35 (ddd, *J*=8.8, 1.0, 0.5, 1H), 7.01 (dd, *J*=2.6, 0.6, 1H), 6.81 (ddd, *J*=8.8, 2.6, 0.5, 1H), 6.67 (dd, *J*=2.2, 0.9, 1H), 4.89 (s, 1H). ¹³C NMR (101 MHz, CDCl₃) δ = 146.12, 113.05, 111.92, 106.56, 106.21.

Compound 22



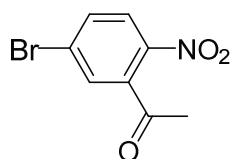
Compound **21** (3.73 mmol, 0.501 g) was dissolved in anhydrous DMF (3.8 mL, 1 M) under a nitrogen atmosphere. A 50 wt% solution of *tert*-butyldimethylsilyl chloride in toluene (11.3 mmol, 3.9 mL, 2.9 M) was added followed by the addition of imidazole (18.7 mmol, 1.27 g). The mixture was stirred for 1 hour at r.t.. TLC analysis indicated complete conversion of the starting material (1% Et₂O in Pnt, R_f= 0.7). The mixture was then poured in H₂O and extracted with Et₂O (3x). The combined organic layers were washed with brine (1x), dried over MgSO₄ and concentrate *in vacuo*. Purification with silica gel column chromatography (Pnt → 1% Et₂O in Pnt) yielded compound **22** (2.62 mmol, 0.65 g, 70.2%). ¹H NMR (400 MHz, Chloroform-*d*) δ = 7.60 (d, *J*=2.1, 1H), 7.38 (dd, *J*=8.8, 0.9, 1H), 7.06 (d, *J*=2.5, 1H), 6.85 (dd, *J*=8.8, 2.4, 1H), 6.69 (dd, *J*=2.2, 0.9, 1H), 1.05 (d, *J*=0.9, 10H), 0.24 (d, *J*=0.8, 6H). ¹³C NMR (101 MHz, CDCl₃) δ = 151.50, 150.46, 145.75, 128.22, 117.63, 111.61, 111.10, 106.69, 30.45, 25.88, 18.35, -4.33.

Compound 23



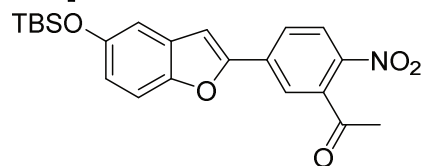
Compound **22** (3.65 mmol, 0.906 g) was dissolved in anhydrous THF (20 mL, 0.2 M) under a nitrogen atmosphere and cooled to -78°C. A 1.6 M solution of *n*-butyllithium in hexanes (8.0 mmol, 5.02 mL) was added dropwise and the mixture was stirred for 1 hour. Triisopropyl borate (4.4 mmol, 1.0 mL) was added dropwise and the mixture was stirred for another 30 min. The mixture was then heated to r.t. and stirred for an additional 30 min. The reaction mixture was quenched with a 2 M solution of HCl (aq.) (4 mL, 8 mmol), poured in H₂O and extracted with EtOAc (3x). The combined organic layers were washed with H₂O (1x) and brine (1x), dried over MgSO₄ and concentrated *in vacuo*. The crude product **23** was used as is in the following reaction.

Compound 24

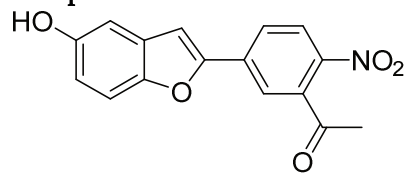


KNO_3 (24.0 mmol, 2.42 g) was loaded into a flask and cooled down to -20°C . H_2SO_4 (21.75 mL, 98%) was added and the mixture was stirred for 30 min. 3'-bromoacetophenone (20 mmol, 3.98 g, 2.64 mL) was slowly added. The reaction mixture was heated up to -10°C and stirred for another 2 h. The reaction mixture was poured into crushed ice and extracted with DCM (3x). The combined organic layers were washed with brine (1x), dried over MgSO_4 and concentrated *in vacuo*. The crude was dissolved in a minimal amount of Et_2O after which Pnt was added until a precipitation was visible. The suspension was gently warmed until the precipitate dissolved again. The product was allowed to crystallize out of solution until no more formation of crystals was observed. The crystals were collected and washed with cold Pnt yielding compound **24** (9.8 mmol, 2.4 g, 49%). ^1H NMR (400 MHz, Chloroform-*d*) δ = 8.00 (d, J =8.7, 1H), 7.74 (dd, J =8.7, 2.1, 1H), 7.55 (d, J =2.1, 1H), 2.56 (s, 3H). ^{13}C NMR (101 MHz, CDCl_3) δ = 133.75, 130.47, 126.05, 30.37.

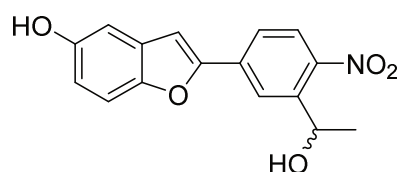
Compound 25



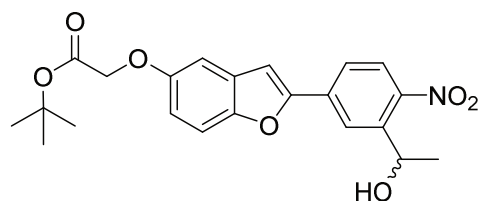
Compound **23** (4.62 mmol, 1.35 g) and compound **24** (3.65 mmol, 0.89 g) were dissolved in a 1:1 mixture of THF and H_2O (42 mL) under a nitrogen atmosphere. The flask was wrapped in aluminum foil and K_2CO_3 (5.48 mmol, 0.757 g) and $\text{Pd}(\text{Ph}_3)_4$ (0.23 mmol, 0.266 g) were added. The mixture was heated to 66°C and refluxed for 18 h. TLC analysis indicated complete conversion of the starting material (10% Et_2O in Pnt, R_f =0.3). The reaction mixture was quenched using a saturated solution of NH_4Cl (aq.), poured in H_2O and extracted with EtOAc (3x). The combined organic layers were washed with brine (1x), dried over MgSO_4 and concentrated *in vacuo*. The crude mixture consists of partially desilylated product, so the crude mixture can be used as is in the following reaction. Purification with silica gel column chromatography (5% Et_2O \rightarrow 30% Et_2O in Pnt) yielded compound **25** (2.23 mmol, 0.919 g, 61%). Increasing the polarity of the eluent (30% Et_2O in Pnt \rightarrow 30% EtOAc in Pnt) yielded prematurely desilylated compound **26** (0.51 mmol, 0.15 g, 14%). ^1H NMR (400 MHz, Chloroform-*d*) δ = 8.09 (d, J =8.6, 1H), 7.87 (dd, J =8.6, 1.9, 1H), 7.76 (d, J =1.8, 1H), 7.36 (dt, J =8.9, 0.8, 1H), 7.13 (d, J =0.9, 1H), 7.05 (d, J =2.4, 1H), 6.89 (dd, J =8.8, 2.5, 1H), 2.61 (s, 3H), 1.04 (d, J =0.7, 13H), 0.25 (d, J =0.7, 7H). ^{13}C NMR (101 MHz, CDCl_3) δ = 199.76, 152.82, 152.03, 150.87, 144.03, 139.06, 136.13, 129.17, 125.65, 125.14, 122.72, 119.69, 111.72, 111.24, 105.94, 30.24, 25.69, 18.18, -4.48.

Compound 26

Compound **25** (0.66 mmol, 0.27 g) was dissolved in anhydrous THF (7 mL) under a nitrogen atmosphere. A solution of 70% HF in Pyridine (0.7 mL, 10 vol%) was added and the reaction was stirred at r.t. for 2 h. TLC analysis indicated complete conversion of the starting material (30% EtOAc in Pnt, $R_f=0.2$). The reaction was quenched with a saturated solution of NaHCO_3 (aq.) until no CO_2 release was observed. The mixture was poured into H_2O and extracted with EtOAc (3x). The combined organic layers were washed with brine (1x), dried over MgSO_4 and concentrated *in vacuo*. Purification with silica gel column chromatography (15% EtOAc \rightarrow 30% EtOAc in Pnt) yielded compound **26** (0.62 mmol, 0.18 g, 93%). ^1H NMR (400 MHz, $\text{DMSO}-d_6$) δ = 9.40 (s, 1H), 8.22 (d, $J=8.4$, 1H), 8.17 – 8.09 (m, 2H), 7.67 (s, 1H), 7.47 (d, $J=8.8$, 1H), 7.01 (d, $J=2.5$, 1H), 6.86 (dd, $J=8.9$, 2.5, 1H), 2.63 (s, 3H). ^{13}C NMR (101 MHz, DMSO) δ = 199.78, 153.96, 152.61, 149.26, 144.26, 138.03, 135.30, 129.18, 126.15, 125.61, 123.21, 115.36, 111.85, 106.77, 105.83, 30.06.

Compound 27

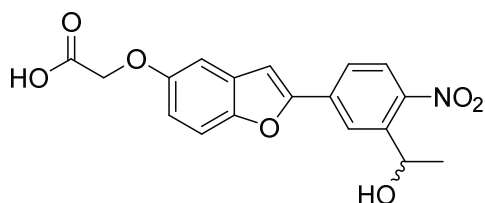
Compound **26** (0.36 mmol, 0.106 g) was dissolved in methanol (3.6 mL, 0.1 M) and the mixture was cooled down to 0°C. NaBH_4 (0.54 mmol, 0.020 g) was added in portions. After addition the mixture was heated to r.t. and stirred for 1 hour. TLC analysis indicated full conversion of the starting material (30% EtOAc in Pnt, $R_f=0.2$). The mixture was concentrated *in vacuo* after which it was poured in H_2O and extracted with EtOAc (3x). The combined organic layers were washed with brine (1x) and dried over MgSO_4 . Concentration *in vacuo* yielded compound **27** (0.36 mmol, 108 mg, 100%). ^1H NMR (400 MHz, $\text{DMSO}-d_6$) δ = 9.36 (s, 1H), 8.29 (d, $J=1.9$, 1H), 8.04 (d, $J=8.5$, 1H), 7.96 (dd, $J=8.5$, 1.9, 1H), 7.57 (d, $J=0.9$, 1H), 7.49 (d, $J=8.9$, 1H), 7.00 (d, $J=2.4$, 1H), 6.83 (dd, $J=8.8$, 2.5, 1H), 5.66 (d, $J=4.3$, 1H), 5.30 – 5.20 (m, 1H), 1.43 (d, $J=6.3$, 3H). ^{13}C NMR (101 MHz, DMSO) δ = 153.85, 146.24, 143.61, 143.61, 134.44, 129.31, 125.17, 123.70, 123.04, 114.82, 111.77, 105.74, 105.50, 64.01, 25.09.

Compound 28

Compound **27** (0.154 g; 0.51 mmol) was dissolved in dry DMF (1.7 mL) in nitrogen atmosphere. K_2CO_3 (0.62 mmol, 0.083 g) and *t*-butyl bromoacetate (0.95 mmol, 0.14 mL) were added and the reaction was stirred at 70°C for 3 h. TLC analysis indicated complete conversion of the starting material (30% EtOAc in Pnt, $R_f=0.8$). The reaction mixture was poured into H_2O and extracted with EtOAc (3x). The combined organic layers were washed with H_2O (1x) and brine (1x), dried over MgSO_4 and concentrated *in vacuo*. Purification with silica gel column chromatography (20% EtOAc in Pnt) yielded compound **28** (0.36 mmol, 0.149 g, 72%). ^1H NMR (300 MHz, $\text{Chloroform}-d$) δ = 8.25 (d, $J=2.0$, 1H), 7.96 (d, $J=8.6$, 1H), 7.72 (dd, $J=8.6$, 1.9, 1H), 7.43 – 7.33 (m, 1H), 7.06 (d, $J=0.9$, 1H), 7.00 –

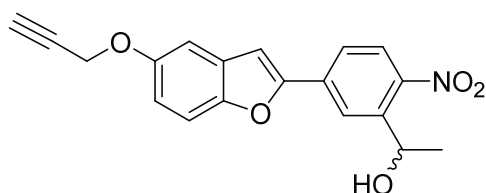
6.89 (m, 2H), 5.52 (q, $J=6.3$, 1H), 4.51 (s, 2H), 3.02 (s, 1H), 1.60 (d, $J=6.3$, 3H), 1.50 (s, 9H). ^{13}C NMR (75 MHz, CDCl_3) δ = 168.35, 154.62, 154.30, 150.83, 146.41, 142.82, 135.33, 129.24, 125.38, 123.69, 123.61, 115.11, 112.10, 105.10, 104.91, 82.62, 66.63, 65.70, 53.56, 28.11, 24.57.

Compound 29

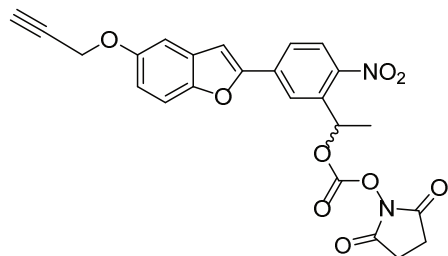


Compound **28** (0.21 mmol, 0.086 g) was dissolved in DCM (2 mL). Trifluoroacetic acid (2 mL) was added and the reaction was stirred at r.t. for 30 min. TLC analysis indicated complete conversion of the starting material (30% EtOAc in Pnt, $R_f=0.1$). The mixture was concentrated *in vacuo*. Co-evaporation with DCM (3x), toluene (3x) and CHCl_3 (1x) yielded compound **29** (0.21 mmol, 0.075 g, quant.). ^1H -NMR (400 MHz, $\text{DMSO}-d_6$) δ = 13.03 (s, 1H), 8.32 (d, $J = 1.7$ Hz, 1H), 8.05 (d, $J = 8.6$ Hz, 1H), 8.00 (dd, $J = 8.6$, 1.8 Hz, 1H), 7.65 (s, 1H), 7.62 (d, $J = 9.1$ Hz, 1H), 7.19 (d, $J = 2.6$ Hz, 1H), 7.01 (dd, $J = 8.9$, 2.6 Hz, 1H), 5.66 (s, 1H), 5.25 (q, $J = 6.3$ Hz, 1H), 4.73 (s, 2H), 1.44 (d, $J = 6.3$ Hz, 3H). ^{13}C -NMR (100 MHz, $\text{DMSO}-d_6$): δ 170.36, 154.52, 153.93, 149.96, 143.60, 134.22, 129.11, 125.17, 123.88, 123.17, 115.02, 112.09, 105.68, 104.86, 65.19, 64.02, 25.09.

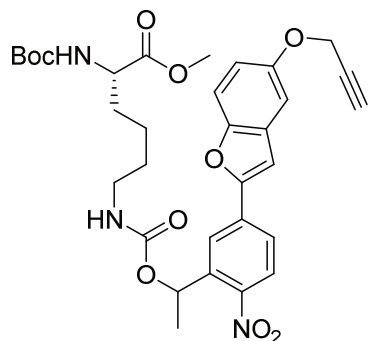
Compound 30



Compound **27** (0.50 mmol, 0.15 g) was dissolved in DMF (0.2 M, 2.5 mL). K_2CO_3 (1.92 mmol, 0.265 g) was added and the reaction mixture was stirred for 1 hour at r.t.. Propargyl bromide (1.2 mmol, 108 μL) was added to the reaction and the mixture was stirred overnight. TLC analysis indicated full conversion the starting material (30% EtOAc in Pnt, $R_f=0.7$). The reaction was quenched with a saturated solution of NH_4Cl (aq.) and extracted with EtOAc (3x). The combined organic layers were washed with brine (1x) and concentrated *in vacuo*. Purification with silica gel column chromatography (10% EtOAc \rightarrow 15% EtOAc in Pnt) yielded compound **30** (0.49 mmol, 0.16 g, 98%). ^1H NMR (400 MHz, $\text{Acetone}-d_6$) δ = 8.40 (d, $J=2.0$, 1H), 7.97 (d, $J=8.6$, 1H), 7.89 (dd, $J=8.5$, 2.0, 1H), 7.50 (d, $J=9.0$, 1H), 7.43 (d, $J=0.9$, 1H), 7.24 (d, $J=2.6$, 1H), 7.01 (dd, $J=9.0$, 2.6, 1H), 5.44 (qd, $J=6.3$, 4.3, 1H), 4.78 (dd, $J=5.4$, 3.3, 3H), 3.07 (t, $J=2.4$, 1H), 1.51 (d, $J=6.3$, 3H). ^{13}C NMR (101 MHz, $\text{Acetone}-d_6$) δ = 155.31, 151.46, 147.54, 144.47, 135.62, 130.29, 129.66, 125.82, 124.45, 124.30, 116.12, 112.69, 112.20, 106.20, 105.94, 79.84, 77.00, 65.57, 65.47, 57.00, 25.45, 25.39.

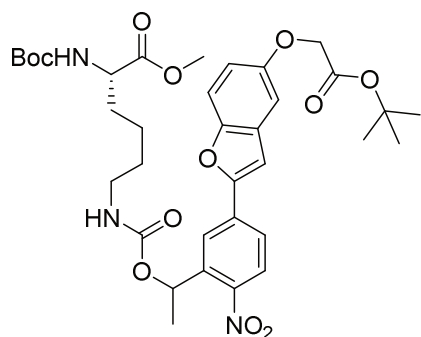
Compound 31

Compound **30** (0.42 mmol, 0.151 g) was dissolved in anhydrous DMF (2.2 mL, 0.2 M) under a nitrogen atmosphere. Disuccinimidyl carbonate (0.63 mmol, 0.16 g) and triethylamine (1.3 mmol, 0.18 mL) were added and the reaction mixture was stirred at r.t. overnight. TLC analysis indicated complete conversion of the starting material (30% EtOAc in Pnt, $R_f=0.4$). The mixture was concentrated *in vacuo* and diluted with H₂O. The aqueous layer was extracted with DCM (3x) after which the combined organic layers were washed with brine (1x), dried over MgSO₄ and concentrated *in vacuo*. The crude product was adsorbed on Celite. Purification with silica gel column chromatography (DCM \rightarrow 0.25% MeOH in DCM) yielded compound **31** (0.30 mmol, 143 mg, 71%). **¹H-NMR (400 MHz, DMSO-*d*₆):** δ = 8.21 (d, J = 1.7, 1H), 8.19 (d, J = 8.7, 1H), 8.14 (dd, J = 8.6, 1.8, 1H), 7.80 (s, 1H), 7.65 (d, J = 9.0, 1H), 7.32 (d, J = 2.6, 1H), 7.06 (dd, J = 9.0, 2.6, 1H), 6.34 (q, J = 6.4, 1H), 4.86 (d, J = 2.3, 2H), 3.59 (t, J = 2.3, 1H), 2.79 (d, J = 14.0, 4H), 1.81 (d, J = 6.5, 2H).

Compound 32

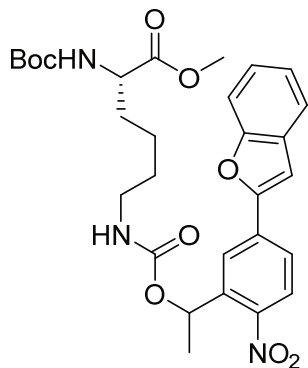
Compound **31** (0.09 mmol, 0.056 g) was dissolved in DMF (1 mL). Boc-Lys-OMe.HOAc (0.5 mmol, 0.130 g) and DiPEA (1 mmol, 174 μ L) was added. The reaction mixture was stirred for 15 min at r.t.. TLC analysis indicated complete conversion of the starting material (5% MeOH in DCM, $R_f=0.6$). The reaction mixture was poured in a 50% brine solution which was washed with EtOAc (3x). The combined organic layers were washed with 0.1M HCl (aq.) (2x), brine (3x), dried (MgSO₄) and concentrated *in vacuo*. Purification with silica gel column chromatography (DCM \rightarrow 0.5% MeOH in DCM) yielded compound **32** (0.059 mmol, 0.037 g, 66%). **¹H NMR (400 MHz, Chloroform-*d*):** δ = 8.08 – 8.00 (m, 2H), 7.82 (dt, $J=8.5$, 1.8, 1H), 7.47 (d, $J=8.9$, 1H), 7.18 (t, $J=3.3$, 2H), 7.03 (ddd, $J=9.0$, 2.6, 1.0, 1H), 6.33 (qd, $J=6.4$, 3.4, 1H), 5.06 (d, $J=8.4$, 1H), 5.00 (d, $J=6.9$, 1H), 4.75 (d, $J=2.4$, 2H), 4.27 (d, $J=7.0$, 1H), 3.70 (d, $J=5.1$, 3H), 3.13 (ddd, $J=35.2$, 13.1, 6.8, 1H), 3.13 (s, 1H), 2.56 (t, $J=2.4$, 1H), 1.74 (s, 1H), 1.68 (dd, $J=6.5$, 1.8, 3H), 1.44 (d, $J=5.0$, 11H), 1.36 (td, $J=10.1$, 9.0, 4.0, 2H), 1.26 (s, 1H). **¹³C NMR (101 MHz, CDCl₃)** δ = 155.43, 154.35, 150.98, 146.66, 140.18, 135.39, 129.30, 125.56, 124.17, 123.09, 115.56, 112.16, 105.53, 105.05, 78.74, 75.75, 56.79, 53.15, 52.42, 40.77, 32.60, 28.43, 22.52, 22.37.

Compound 33



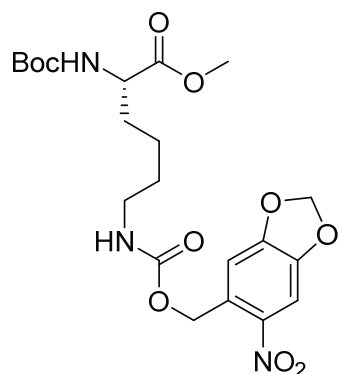
Compound **28** (0.17 mmol, 0.070 g) was dissolved in acetonitrile (1 mL). *N,N'*-disuccinimidyl carbonate (0.50 mmol, 0.13 g) and DiPEA (0.30 mmol, 52 μ L) were added and the mixture was stirred for 16 h at r.t.. The reaction mixture was poured in a 50% brine solution which was washed with EtOAc (3x). The combined organic layers were washed with brine (1x), dried (MgSO_4) and concentrated *in vacuo*. The concentrate was reconstituted in DMF (2 mL) and boc-Lys-OMe.HOAc (0.50 mmol, 0.13 g) and DiPEA (1.0 mmol, 174 μ L) was added. The reaction mixture was stirred for 15 min at r.t.. TLC analysis indicated complete conversion of the starting material (5% MeOH in DCM, R_f =0.6). The reaction mixture was poured in a 50% brine solution which was washed with EtOAc (3x). The combined organic layers were washed with 0.1M HCl (aq.) (2x), brine (3x), dried (MgSO_4) and concentrated *in vacuo*. Purification with silica gel column chromatography (DCM \rightarrow 0.5% MeOH in DCM) yielded compound **33** (0.093 mmol, 0.065 g, 55%). ^1H NMR (400 MHz, Chloroform-*d*) δ = 8.08 – 7.99 (m, 2H), 7.81 (dt, J =8.6, 1.8, 1H), 7.46 (d, J =8.9, 1H), 7.18 – 7.13 (m, 1H), 7.08 – 6.98 (m, 2H), 6.33 (qd, J =6.4, 3.3, 1H), 5.08 (t, J =8.4, 2H), 4.57 (s, 2H), 4.30 – 4.24 (m, 1H), 3.70 (d, J =4.1, 3H), 3.13 (ddq, J =23.7, 12.0, 6.6, 1H), 1.84 – 1.72 (m, 0H), 1.86 – 1.54 (m, 3H), 1.51 (s, 10H), 1.44 (d, J =4.9, 9H), 1.40 – 1.22 (m, 3H). ^{13}C NMR (101 MHz, CDCl_3) δ = 173.29, 168.21, 155.43, 154.79, 154.30, 150.89, 146.62, 140.13, 135.36, 129.28, 125.50, 124.14, 123.08, 115.21, 112.14, 105.11, 104.98, 82.49, 80.00, 68.55, 66.67, 53.14, 52.37, 40.72, 32.53, 29.27, 28.39, 28.14, 22.50, 22.34.

Compound 34



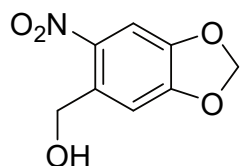
Compound **16** (0.045 mmol, 0.020 g) was dissolved in DMF (1 mL). Boc-Lys-OMe.HOAc (0.076 mmol, 0.020 g) and DiPEA (0.135 mmol, 24 μ L) were added and the mixture was stirred for 16 h at r.t.. TLC analysis indicated complete conversion of the starting material (5% MeOH in DCM, R_f =0.8). The reaction mixture was poured in 0.1M HCl (aq.) and washed with DCM (3x). The combined organic layers were washed with a saturated solution of NaHCO_3 (aq.) (3x), dried (MgSO_4) and concentrated *in vacuo*. Purification with silica gel column chromatography (DCM \rightarrow 0.5% MeOH in DCM) yielded compound **34** (0.035 mmol, 0.020 g, 78%). ^1H NMR (300 MHz, DMSO-*d*₆) δ = 8.14 – 8.02 (m, 2H), 7.87 (dt, J =8.7, 1.5, 1H), 7.66 (d, J =7.7, 1H), 7.59 (d, J =8.2, 1H), 7.45 – 7.15 (m, 4H), 6.42 – 6.31 (m, 1H), 5.06 (d, J =8.4, 1H), 4.99 (s, 1H), 4.28 (d, J =5.6, 1H), 3.72 (d, J =3.3, 3H), 3.15 (tt, J =13.5, 6.8, 2H), 1.71 (d, J =6.5, 3H), 1.68 – 1.50 (m, 1H), 1.46 (d, J =3.6, 10H), 1.27 (s, 5H), 0.95 – 0.82 (m, 2H).

Compound 35



Compound **36** (0.2 mmol, 0.040 g) was dissolved in AcN (1 mL). Boc-Lys-OMe.HOAc (0.3 mmol, 0.08 g), N,N'-disuccinimidyl carbonate (0.4 mmol, 102 mg) and DiPEA (0.50 mmol, 86 μ L) were added and the mixture was stirred for 1 h at r.t.. TLC analysis indicated complete conversion of the starting material (5% MeOH in DCM, R_f =0.5). The reaction mixture was poured in 0.1M HCl (aq.) and washed with DCM (3x). The combined organic layers were washed with a saturated solution of NaHCO₃ (aq.) (3x), dried (MgSO₄) and concentrated *in vacuo*. Purification with silica gel column chromatography (DCM \rightarrow 0.5% MeOH in DCM) yielded compound **43** (0.15 mmol, 0.070 g, 75%). ¹H NMR (400 MHz, CDCl₃) δ 7.62 (s, 1H), 7.00 (s, 1H), 6.14 (s, 2H), 5.45 (s, 2H), 5.18 (d, J = 9.0 Hz, 2H), 4.30 (d, J = 4.8 Hz, 1H), 3.75 (s, 4H), 3.22 (dd, J = 12.9, 6.7 Hz, 3H), 1.90 – 1.76 (m, 2H), 1.71 – 1.51 (m, 4H), 1.48 – 1.32 (m, 14H). ¹³C NMR (101 MHz, CDCl₃) δ 173.27, 155.85, 155.53, 152.52, 147.22, 131.18, 107.28, 105.71, 103.16, 79.95, 63.40, 53.14, 52.33, 40.75, 32.40, 29.24, 28.31, 22.43.

Compound 36



6-nitropiperonal (10 mmol, 1.95 g) was dissolved in EtOH (15 mL) and cooled down to 0°C. NaBH₄ (12 mmol, 0.46 g) was added and the mixture was allowed to stir for 1 hour at 0°C. TLC analysis (20% EtOAc in Pnt, R_f =0.2) indicated complete conversion of the starting material. A saturated solution of NH₄Cl (aq.) was added extremely carefully to quench leftover reagents. The mixture was diluted with H₂O and consequently extracted with DCM (3x). The organic layers were combined, dried (MgSO₄) and concentrated *in vacuo* to afford compound **36** (9.64 mmol, 1.90 g) in a 96% yield.

References

- (1) Maurits, E.; van de Graaff, M. J.; Maiorana, S.; Wander, D. P. A.; Dekker, P. M.; van der Zanden, S. Y.; Florea, B. I.; Neefjes, J. J. C.; Overkleeft, H. S.; van Kasteren, S. I. Immunoproteasome Inhibitor–Doxorubicin Conjugates Target Multiple Myeloma Cells and Release Doxorubicin upon Low-Dose Photon Irradiation. *J. Am. Chem. Soc.* **2020**, *142* (16), 7250–7253.
- (2) Barltrop, J. A.; Plant, P. J.; Schofield, P. Photosensitive Protective Groups. *Chem. Commun. Lond.* **1966**, No. 22, 822.
- (3) Holmes, C. P.; Jones, D. G. Reagents for Combinatorial Organic Synthesis: Development of a New o-Nitrobenzyl Photolabile Linker for Solid Phase Synthesis. *J. Org. Chem.* **1995**, *60* (8), 2318–2319.
- (4) Photolabile Protecting Groups and Linkers. *J. Chem. Soc. Perkin 1* **2002**, No. 2, 125–142.
- (5) Deshpande, R. K.; Waterhouse, G. I. N.; Jameson, G. B.; Telfer, S. G. Photolabile Protecting Groups in Metal–Organic Frameworks: Preventing Interpenetration and Masking Functional Groups. *Chem Commun* **2012**, *48* (10), 1574–1576.
- (6) Klán, P.; Šolomek, T.; Bochet, C. G.; Blanc, A.; Givens, R.; Rubina, M.; Popik, V.; Kostikov, A.; Wirz, J. Photoremovable Protecting Groups in Chemistry and Biology: Reaction Mechanisms and Efficacy. *Chem. Rev.* **2013**, *113* (1), 119–191.
- (7) Šolomek, T.; Mercier, S.; Bally, T.; Bochet, C. G. Photolysis of Ortho-Nitrobenzylic Derivatives: The Importance of the Leaving Group. *Photochem. Photobiol. Sci.* **2012**, *11* (3), 548.
- (8) Rodenko, B.; Toebes, M.; Hadrup, S. R.; van Esch, W. J. E.; Molenaar, A. M.; Schumacher, T. N. M.; Ovaa, H. Generation of Peptide–MHC Class I Complexes through UV-Mediated Ligand Exchange. *Nat. Protoc.* **2006**, *1* (3), 1120–1132.
- (9) Kaplan, J. H.; Forbush, B.; Hoffman, J. F. Rapid Photolytic Release of Adenosine 5'-Triphosphate from a Protected Analogue: Utilization by the Na:K Pump of Human Red Blood Cell Ghosts? *Biochemistry* **1978**, *17* (10), 1929–1935.
- (10) Hasan, A.; Stengele, K.-P.; Giegrich, H.; Cornwell, P.; Isham, K. R.; Sachleben, R. A.; Pfleiderer, W.; Foote, R. S. Photolabile Protecting Groups for Nucleosides: Synthesis and Photodeprotection Rates. *Tetrahedron* **1997**, *53* (12), 4247–4264.
- (11) Engels, J.; Schlaeger, E. J. Synthesis, Structure, and Reactivity of Adenosine Cyclic 3',5'-Phosphate-Benzyltriesters. *J. Med. Chem.* **1977**, *20* (7), 907–911.
- (12) Patterson, D. M.; Nazarova, L. A.; Prescher, J. A. Finding the Right (Bioorthogonal) Chemistry. *ACS Chem. Biol.* **2014**, *9* (3), 592–605.
- (13) Richards, N. G. J.; Cory, M. Computational Methods in the Design of Photocaged Compounds. I. Spectroscopic Calculations upon Substituted Isochromenes. *Int. J. Quantum Chem.* **1992**, *44* (S19), 65–76.
- (14) Silva, J. M.; Silva, E.; Reis, R. L. Light-Triggered Release of Photocaged Therapeutics - Where Are We Now? *J. Controlled Release* **2019**, *298*, 154–176.
- (15) Givens, R. S.; Matuszewski, B.; Athey, P. S.; Stoner, M. R. Photochemistry of Phosphate Esters: An Efficient Method for the Generation of Electrophiles. *J. Am. Chem. Soc.* **1990**, *112* (16), 6016–6021.
- (16) Umeda, N.; Takahashi, H.; Kamiya, M.; Ueno, T.; Komatsu, T.; Terai, T.; Hanaoka, K.; Nagano, T.; Urano, Y. Boron Dipyrromethene As a Fluorescent Caging Group for Single-

- Photon Uncaging with Long-Wavelength Visible Light. *ACS Chem. Biol.* **2014**, 9 (10), 2242–2246.
- (17) Sheehan, J. C.; Umezawa, K. Phenacyl Photosensitive Blocking Groups. *J. Org. Chem.* **1973**, 38 (21), 3771–3774.
 - (18) Zayat, L.; Calero, C.; Alborés, P.; Baraldo, L.; Etchenique, R. A New Strategy for Neurochemical Photodelivery: Metal–Ligand Heterolytic Cleavage. *J. Am. Chem. Soc.* **2003**, 125 (4), 882–883.
 - (19) Wagner, N.; Schuhmacher, M.; Lohmann, A.; Nadler, A. A Coumarin Triflate Reagent Enables One-Step Synthesis of Photo-Caged Lipid Metabolites for Studying Cell Signaling. *Chem. – Eur. J.* **2019**, 25 (68), 15483–15487.
 - (20) Bier, C.; Binder, D.; Drobiez, D.; Loeschcke, A.; Drepper, T.; Jaeger, K.-E.; Pietruszka, J. Photocaged Carbohydrates: Versatile Tools for Controlling Gene Expression by Light. *Synthesis* **2016**, 49 (01), 42–52.
 - (21) Courtney, T.; Deiters, A. Recent Advances in the Optical Control of Protein Function through Genetic Code Expansion. *Curr. Opin. Chem. Biol.* **2018**, 46, 99–107.
 - (22) Ruble, B. K.; Yeldell, S. B.; Dmochowski, I. J. Caged Oligonucleotides for Studying Biological Systems. *J. Inorg. Biochem.* **2015**, 150, 182–188.
 - (23) Liu, Q.; Deiters, A. Optochemical Control of Deoxyoligonucleotide Function via a Nucleobase-Caging Approach. *Acc. Chem. Res.* **2014**, 47 (1), 45–55.
<https://doi.org/10.1021/ar400036a>.
 - (24) Lee, H.-M.; Larson, D. R.; Lawrence, D. S. Illuminating the Chemistry of Life: Design, Synthesis, and Applications of “Caged” and Related Photoresponsive Compounds. *ACS Chem. Biol.* **2009**, 4 (6), 409–427.
 - (25) Amatrudo, J. M.; Olson, J. P.; Agarwal, H. K.; Ellis-Davies, G. C. R. Caged Compounds for Multichromic Optical Interrogation of Neural Systems. *Eur. J. Neurosci.* **2015**, 41 (1), 5–16.
 - (26) Piggott, A. M.; Karuso, P. Synthesis of a New Hydrophilic O-Nitrobenzyl Photocleavable Linker Suitable for Use in Chemical Proteomics. *Tetrahedron Lett.* **2005**, 46 (47), 8241–8244.
 - (27) Sinha, R. P.; Häder, D.-P. UV-Induced DNA Damage and Repair: A Review. *Photochem. Photobiol. Sci.* **2002**, 1 (4), 225–236.
 - (28) Ryu, K. A.; Stutts, L.; Tom, J. K.; Mancini, R. J.; Esser-Kahn, A. P. Stimulation of Innate Immune Cells by Light-Activated TLR7/8 Agonists. *J. Am. Chem. Soc.* **2014**, 136 (31), 10823–10825.
 - (29) Björn, L. O. Light as a Tool for Biologists: Recent Developments. In *Photobiology*; Björn, L. O., Ed.; Springer New York: New York, NY, **2015**; 51–70.
 - (30) Hogenkamp, F.; Hilgers, F.; Knapp, A.; Klaus, O.; Bier, C.; Binder, D.; Jaeger, K.; Drepper, T.; Pietruszka, J. Effect of Photocaged Isopropyl B- D -1-thiogalactopyranoside Solubility on the Light Responsiveness of LacI-controlled Expression Systems in Different Bacteria. *ChemBioChem* **2021**, 22 (3), 539–547.
 - (31) Lusic, H.; Deiters, A. A New Photocaging Group for Aromatic N-Heterocycles. *N. Y.* **2006**, No. 13, 4.
 - (32) Berroy, P.; Viriot, M. L.; CarreÂ, M. C. Photolabile Group for 5H-OH Protection of Nucleosides: Synthesis and Photodeprotection Rate. **2001**, 4.

- (33) Momotake, A.; Lindegger, N.; Niggli, E.; Barsotti, R. J.; Ellis-Davies, G. C. R. The Nitro dibenzofuran Chromophore: A New Caging Group for Ultra-Efficient Photolysis in Living Cells. *Nat. Methods* **2006**, 3 (1), 35–40.
- (34) Komori, N.; Jakkampudi, S.; Motoishi, R.; Abe, M.; Kamada, K.; Furukawa, K.; Katan, C.; Sawada, W.; Takahashi, N.; Kasai, H.; Xue, B.; Kobayashi, T. Design and Synthesis of a New Chromophore, 2-(4-Nitrophenyl)Benzofuran, for Two-Photon Uncaging Using near-IR Light. *Chem. Commun.* **2016**, 52 (2), 331–334.
- (35) Bashkatov, A. N.; Genina, E. A.; Kochubey, V. I.; Tuchin, V. V. Optical Properties of Human Skin, Subcutaneous and Mucous Tissues in the Wavelength Range from 400 to 2000 Nm. *J. Phys. Appl. Phys.* **2005**, 38 (15), 2543–2555.
- (36) Andrasfalvy, B. K.; Zemelman, B. V.; Tang, J.; Vaziri, A. Two-Photon Single-Cell Optogenetic Control of Neuronal Activity by Sculpted Light. *Proc. Natl. Acad. Sci.* **2010**, 107 (26), 11981–11986.
- (37) Brown, E. B.; Shear, J. B.; Adams, S. R.; Tsien, R. Y.; Webb, W. W. Photolysis of Caged Calcium in Femtoliter Volumes Using Two-Photon Excitation. *Biophys. J.* **1999**, 76 (1), 489–499.
- (38) Rumi, M.; Perry, J. W. Two-Photon Absorption: An Overview of Measurements and Principles. *Adv. Opt. Photonics* **2010**, 2 (4), 451.
- (39) Gentil, G. P. P.; Hogervorst, T. P.; Tondini, E.; van de Graaff, M. J.; Overkleeft, H. S.; Codée, J. D. C.; van der Marel, G. A.; Ossendorp, F.; Filippov, D. V. Peptides Conjugated to 2-Alkoxy-8-Oxo-Adenine as Potential Synthetic Vaccines Triggering TLR7. *Bioorg. Med. Chem. Lett.* **2019**, 29 (11), 1340–1344.
- (40) Teague, S. J. Facile Synthesis of a O-Nitrobenzyl Photolabile Linker for Combinatorial Chemistry. *Tetrahedron Lett.* **1996**, 37 (32), 5751–5754.
- (41) Tonga, M. Tunable Optical Properties of Push-Pull Chromophores: End Group Effect. *Tetrahedron Lett.* **2020**, 61 (32), 152205.
- (42) Barker, P.; Finke, P.; Thompson, K. Preparation and Cyclization of Aryloxyacetaldehyde Acetals; A General Synthesis of 2,3-Unsubstituted Benzofurans. *Synth. Commun.* **1989**, 19 (1–2), 257–265.
- (43) Morales, A. R.; Frazer, A.; Woodward, A. W.; Ahn-White, H.-Y.; Fonari, A.; Tongwa, P.; Timofeeva, T.; Belfield, K. D. Design, Synthesis, and Structural and Spectroscopic Studies of Push–Pull Two-Photon Absorbing Chromophores with Acceptor Groups of Varying Strength. *J. Org. Chem.* **2013**, 78 (3), 1014–1025.
- (44) Kosak, T. M.; Conrad, H. A.; Korich, A. L.; Lord, R. L. Ether Cleavage Re-Investigated: Elucidating the Mechanism of BBr₃-Facilitated Demethylation of Aryl Methyl Ethers: Ether Cleavage Re-Investigated. *Eur. J. Org. Chem.* **2015**, 2015 (34), 7460–7467.

Chapter 5

General summary and future prospects^{1,2}

General Summary

Toll-like receptors (TLRs) are important sensors partaking in the initiation and propagation of an immune response. This makes synthetic TLR ligands potential therapeutic targets for diseases in which a correctly mounted immune response is beneficial for host survival, such as in preventing or treating infections.^{3,4} TLRs are also increasingly investigated in the context of immune-based treatment of cancers.⁵ TLR-ligand-based therapies are, however, not without risk: an improperly triggered immune response through TLR activation can lead to excessive inflammation, which in turn can result in sepsis⁶, asthma⁷ and auto-immune disease.⁸ A clear understanding of the signaling pathways that emerge following TLR liganding is therefore vital in rationally designing therapeutics that exploit the TLR system. In this manner, beneficial effects can be invoked, whilst immune-related pathology can be avoided.

Over the past decade, TLRs have been shown to display complex, dynamic behaviour. For example, organelle-specific activation has been described to prevent the detection of self-ligands.^{9–12} Moreover, certain TLRs have been shown to tailor their signaling outcome, depending on the subcellular site of activation. For example, activation of TLR4 when localized on the plasma membrane ultimately results in a pro-inflammatory response, whereas antiviral type I interferons are produced upon activation of TLR4 residing in endosomes.

Various chemical tools have been developed to study spatiotemporal effects on TLR-signaling. For example, TLR ligands immobilized on surfaces through biotin-streptavidin interactions can be used to activate TLRs exclusively at the plasma membrane.¹³ Activating the TLRs at a specific intracellular location has not yet been achieved. In a first step towards achieving this, photolabile protecting groups ('photocages') have been introduced on crucial functionalities within TLR ligands and light has been used to activate the ligands.^{14–17} Whereas this has provided some control over receptor signaling in time, phototoxicity of the UV-light needed to activate these 'pro-ligands' as well as low spatial restriction are current limitations that need to be overcome to obtain spatiotemporal insights.

This thesis has explored the use of less-toxic approaches to induce deprotection of TLR pro-ligands *in vitro*. The aim was to develop methods that would allow the study of TLR-ligands described above, whilst circumventing the limitations set by a photo-irradiation mediated strategy. The first approach that was explored entailed the use of recently-published photocages with superior photochemical properties compared to those previously reported. It was explored whether the use of protecting groups that could be removed by low-dose visible light, and/or two-photon excitation, could upon the previously reported photoprotecting groups. A second approach that was explored in this thesis employed chemically-removable protecting groups. Here, small molecules were used

to remove the protecting groups instead of light, offering an alternative strategy towards sub-cellular activation of TLR-ligands.

Chapter 1 gives a literature overview on the role of pattern-recognition receptors (PRRs) in immune activation. The role of TLRs as a subset of the PRRs is discussed and a short literature review is provided on the signaling biology of these receptors. The chemical structures of the receptor agonists are also described, as well as the concept of caging the activity of these agonists to yield better understanding of the signaling biology. The chapter ends with a brief overview on the currently available photocages and potential chemical caging approaches.

Chapter 2 describes the synthesis of a *trans*-cyclooctene (TCO) protected Pam₂CSK₄, in which the TCO-group could serve as a chemically removable protecting group. This compound was shown to bind to TLR2 similar to the unprotected Pam₂CSK₄ ligand, whilst preventing subsequent dimerization of the bound TLR2 with TLR6 (thereby preventing activation). TLR-signaling could be activated by first priming a mouse macrophage cell line with TCO-Pam₂CSK₄ followed by the subsequent addition of a tetrazine derivative that removes the TCO-group by means of an inverse electron-demand Diels-Alder reaction, followed by retro-Diels-Alder, rearrangement and elimination steps. The activation of immune cells under this condition was visualized by imaging the nuclear translocation of GFP-labelled NF- κ B and further confirmed using a reporter cell line which expressed an alkaline phosphatase reporter under the NF- κ B- promotor.

Interestingly, human cell lines exhibited significant TLR2/6 activation even in the absence of the deprotecting tetrazine. To reduce this background activation, various modifications to the ligand and TCO were explored. It was found that hydrophilic and bulky variants of the TCO protecting group did not reduce this residual activity. Substitution of the tetralysine peptide for a triethylene glycol did reduce background activation of the protected TLR2/6 ligand. This new ligand allowed the precise temporal control over TLR2/6 activation, as near-identical nuclear translocation rates of nuclear NF- κ B were observed by human macrophages cell lines treated with free ligand compared to those pre-treated with caged ligands and activated by the addition of tetrazine.

Chapter 3 describes efforts towards applying the TCO-tetrazine elimination approach to TLR4, 7/8 and 9 ligands. TCO-groups were installed on critical functionalities within each of these TLR's ligand. For TLR9, a CpG-ODN was synthesized in which the cytidine nucleobase was caged with a TCO on its exocyclic amine. To this end, a DMTr/phosphoramidite-protected cytosine building block was synthesized with the TCO installed on its nucleobase. This was used in the on-resin synthesis of ODN. Using this building block, a 12- and 20-meric CpG ODN was synthesized with either an unprotected cytosine or TCO-protected cytosine in the CpG sequence. Its ability to effectively induce TLR9 activation upon co-administering tetrazine is currently awaiting assessment.

The TLR7/8-ligand Resiquimod was also caged with a TCO on its exocyclic amine. This yielded a caged ligand of which the activity could be controlled by tetrazine addition. This was assessed by measuring IL6 and TNF α secretion by bone marrow-derived macrophages (BMDMs). Furthermore, the bis-functionalized TCO-(OSu)₂ reagent was used to synthesize Resiquimod-TCO-OSu, of which its immolative end was appended to the TLR7/8 ligand and the non-

immolative end was appended to the anti-tumour antibody TA99. This reagent was used to deliver TLR ligands to a melanoma *in vivo*, with induced TLR-activity as the result.

Finally, a synthetic pyrimido[5,4-*b*]indole TLR4 ligand was caged with TCO on the endocyclic indole amine, which prevented the activation of TLR4 in BMDMs. The TNF α secretion by BMDMs was blocked by this TCO-modification and could be reactivated upon the addition of tetrazine. IL6 secretion, however, appeared not blocked by TCO-modification.

Chapter 4 describes the application of photocages in the development of light-controllable TLR-ligands. First, the TLR7 ligand 9-benzyl-8-oxo-2-butoxyadenine was protected with the NVOC-photocage on its exocyclic amine. The development of triethylene glycol monomethylether-modified NVOC was necessary to solubilize the construct, as modification with NVOC yielded an insoluble product. The effectivity of the ethylene glycol-modified NVOC to shield the ligand's activity towards TLR7 is currently awaiting assessment.

Next, the TLR2/6 ligand Pam₂CSK₄ was caged on its N-terminal amine with the two-photon-sensitive photocage 4-nitrophenyl(benzofuran) (NPBF). The ability to control ligand activity with this group was verified in THP1 Dual cells. Similar to the experiments outlined in Chapter 2, background activation was a problem with this ligand. The same solution as in Chapter 2 was applied, resulting in the NPBF-caged ligand Pam₂CS(*TEG*), in which the C-terminal tetralysine motif was replaced with a triethylene glycol motif. However, this ligand appeared insoluble in aqueous media and showed high adherence to plastic surfaces. This issue was addressed by the design and synthesis of a phenol-containing NPBF-analogue. The phenol functionality was exploited to include a variety of linkers that can be used to influence the physical-chemical properties of the cage, such as its water solubility. A carboxyl- and propargyl-carrying linker was used to decorate the phenol. Presence of the functionalized phenol also enhanced the molar attenuation efficiency ϵ by 30%.

Future prospects

The new dual cages, particularly the dual-functional NPBF-linker open up a wide range of future experiments, both within and beyond the TLR-field. For example, the NPBF-linked to a TLR-ligand may be used to generate a water-soluble variant of photocaged Pam₂CS(*TEG*), for application in experiments which exploit two-photon absorption to yield a high spatial accuracy. As proposed previously in literature¹⁴, TLR2/6-bearing cells can be primed with a photocaged ligand and subsequently added to a different culture to study the propagation of an immune response (Figure 1) after irradiation of a large group of murine cells. With this next iteration of photocaged TLR2/6 ligands, single-cell, and even single-endosome, activation could be within reach.

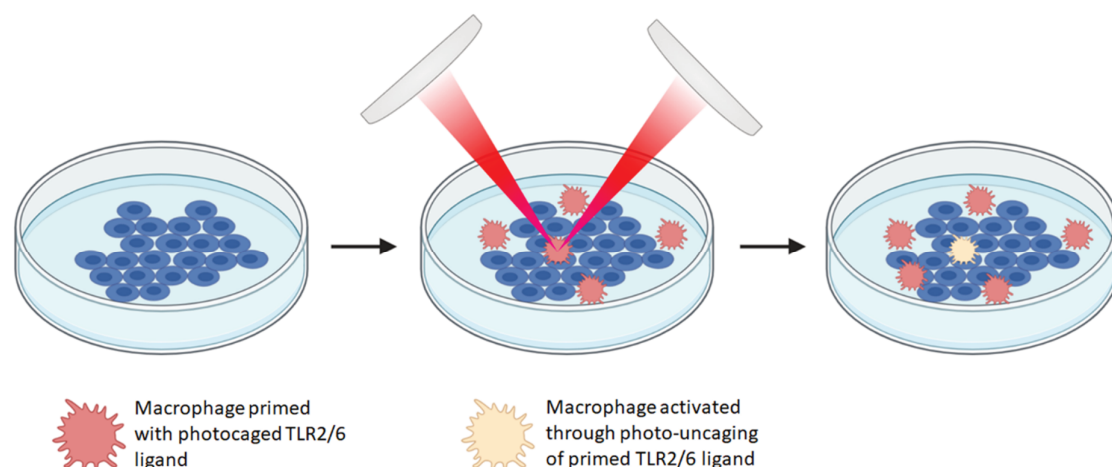


Figure 1. Macrophages primed with human-applicable NPBF-caged ligand can be added to a culture of cells to study the propagation of an immune response. Two-photon excitation enables single-cell activation, whereas the optimization of the TLR2/6 ligand in Chapter 2 enables its use in primary human cells.

The TCO-modified reagents can in future also be used to study spatially restricted activation. For example, by first pre-incubating a macrophage cell line with nanoparticles decorated with tetrazine to saturate their endo-lysosomal system, followed by the addition of the protected ligand, which will then only be deprotected inside the endolysosomal system (Figure 2). Studying the phosphorylation of the signaling adapters under this condition will allow the isolation of only the intracellular signaling of the TLR2/6 receptor complex.

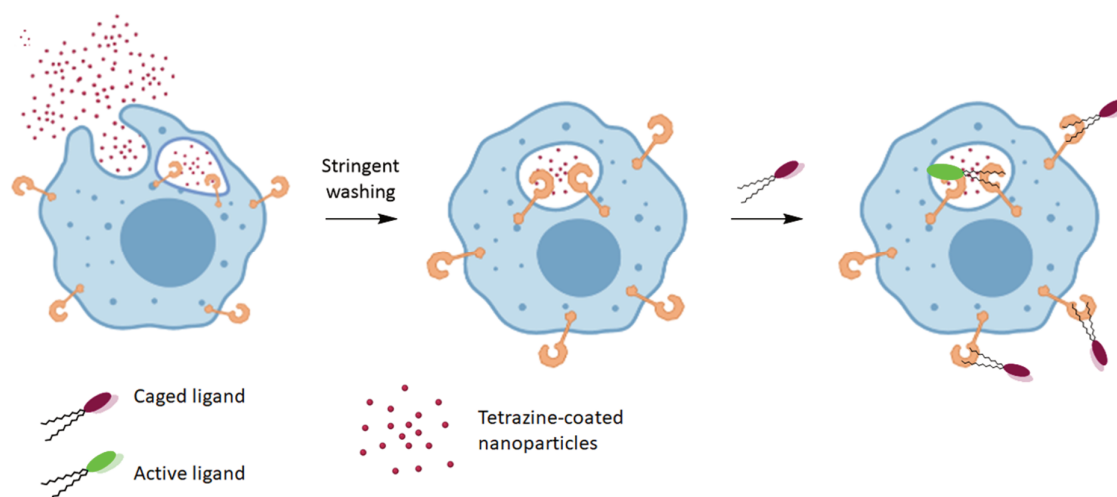


Figure 2. A strategy to activate intracellular TLRs. First the cells are treated with tetrazine-coated nanoparticles which are taken up through phago- and endocytic pathways. After a stringent washing procedure, the cells are treated with TCO-caged TLR-ligand. Liberation of the ligand from its cage should now be prevalent in intracellular vesicles as opposed to the extracellular environment.

Isolating the surface signal is also possible by for example immobilizing a tetrazine-biotin conjugate on a streptavidin-modified surface. Cells that are primed with TCO-caged ligand can then be exposed to this surface, after which the tetrazine will liberate the TCO from the ligand-receptor complex. The advantage of this approach – over the direct immobilization of the TLR-ligand – would be that the internalization of the receptor would not be negatively affected by the approach. After deprotection, the ligated TLR could be taken up as normal (Figure 3).

Finally, in very recent work by the Fox-group¹⁸, subcellular activation of the IEDDA reaction was achieved through the sub-cellular conversion of an unreactive dihydrotetrazine to a tetrazine using a photocatalyst and two-photon-excitation. Applying this approach to the generation of uncaging tetrazines *in vivo* would be an additional powerful tool to study localized TLR signaling.

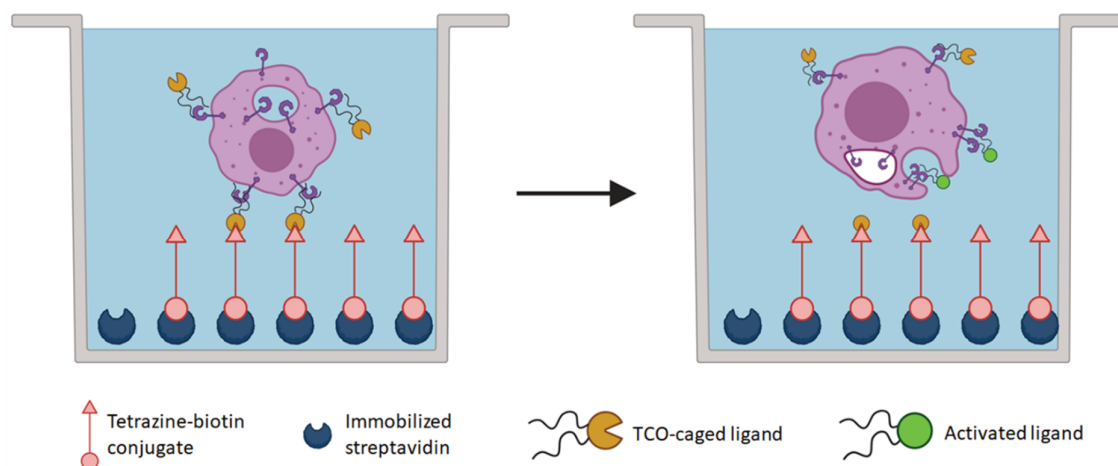


Figure 3. A more natural mode of surface-only TLR2/6 activation. A streptavidin-coated well is treated with a tetrazine-biotin conjugate. Then, cells primed with TCO-caged TLR2/6 ligand are added to the well. The tetrazine reacts with the TCO and liberates the ligand. TLR2/6 dimerization is initiated and endocytosis of the receptor proceeds naturally.

The photo- and chemo-cleavable linkers could in principle also be used to achieve the inverse of photoactivation: photo-*de*activation. This would then allow the study of what happens if TLR-signaling is halted, rather than initiated. For this purpose, a photo-destructible TLR9 ligand may be designed. The palindromic TLR9-ligands reported by the group of Agrawal would for instance be a suitable starting point for this approach.¹⁹ Agrawal and co-workers found that 5'-TCTGACGTTCT-X-TCTTGCAGTCT-5' (where X is a glyceryl linker) is a potent TLR9 agonist, whereas the bissectional sequence 5'-TCTGACGTTCT-3' is not. Substitution of the glyceryl linker by a photocleavable linker, such as the bis-functional TCO or NPBF could give rise to a TLR9 ligand that can effectively be switched off (Figure 4). One possible caveat here is that the TCO-based linker may prove too labile to endure the synthetic cycles required to make the ligand. An NPBF-based linker on the other hand may be too difficult to deprotect quantitatively – a feature which is likely needed to completely terminate a TLR-mediated signaling event.

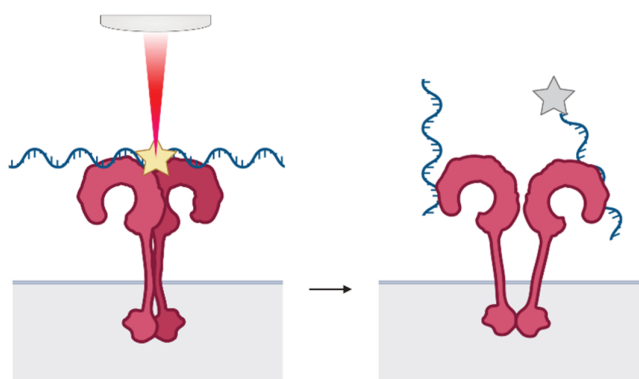
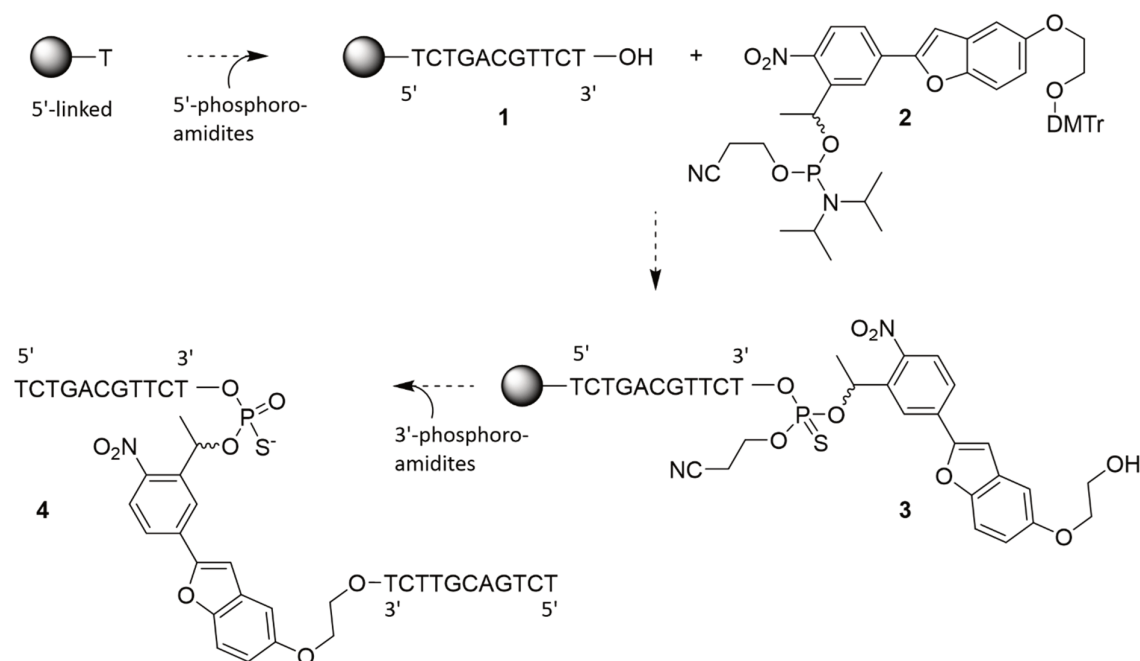


Figure 4. Concept of photodestructible TLR9 ligands. A CpG-containing oligodeoxynucleotide (ODN) is synthesized which possesses a photolabile linker in the appropriate position (fission must lead to non-binding fragments and the linker must not interfere with TLR9 binding). After binding of the conjugate with TLR9, the dimerized complex may be destabilized by cleavage of the photolinker, thus damping the signaling events stemming from the receptor-ligand complex.



Scheme 1. Strategy for the synthesis of a photodestructible TLR9 ligand using the NPBF-linker. Oligonucleotide synthesis is first proceeded in the 5'→3' direction and the NPBF linker is installed in the bisectinonal position. Then, a 3'→5' direction is adopted to ultimately yield the photocleavable palindromic CpG ODN.

Application of photoresponsive linkers beyond TLR-ligands.

This thesis describes the use of the photocage NPBF in the study of TLR-activation.²⁰ However, these bifunctional photocages can also be employed for other purposes. During the work described in this thesis, the first steps in this direction were also taken: namely, through the design of a conjugate composed of a covalent proteasome inhibitor linked to a chemotherapeutic agent. This allowed the specific targeting of the caged toxin to multiple myeloma cells *in vitro*, followed by its

activation with low-dose photo-irradiation. The NPBF-linker was also used as a diagnostic tool in the development of a probe that could be used to mark CD8+ T cells in regions of interest (ROI) in a primary human tumour. This marking then enabled the isolation of the T-cells from the ROI, followed by their single-cell characterization.

Immunoproteasome inhibitor-doxorubicin conjugate¹

Delivering a cytotoxic agent site-selectively to malignant neoplasms is an important strategy to reduce side-effects and to increase efficacy of chemotherapeutics. This is usually done by linking a drug of choice to an antibody. This can even be done in such a way that the drug is deactivated by the attachment of the linker. Localized immolation of the linker then reactivates the drug. This release of the drug can be achieved through either enzymatic activities²¹, pH changes²² or redox potential differences.^{23,24} Alternatively, the release can be induced by an externally applied trigger, such as the addition of a tetrazine to a TCO-linked drug conjugate^{25–27}, or by applying a photon dose to a light-sensitive linker.²⁸ There are two major downsides to the use of antibodies for targeting. Firstly, the choice of target is limited to extracellular proteins only. This excludes many malignancies that do not possess such a unique defining feature. Secondly, surface antigens are usually only present at approximately 100,000 copies per cell. This makes the delivery of a therapeutic dose to the cell difficult.

Many malignancies are characterized by the upregulation of specific enzyme activities. It was envisaged that targeting such an enzyme with irreversible inhibitors could be a valuable alternative strategy, as the number of copies of an enzyme per cell is higher than for surface antigens, and the palette of targets that allow selective tumour targeting can be increased in this manner.

Here such an approach based on the photodestructible NPBF-linker is presented to target multiple myeloma cells *in vitro*. These cells have been shown to upregulate immunoproteasomes, whilst concomitantly downregulating constitutive proteasomes. The immunoproteasome inhibitor LU-035i targets the $\beta 5i$ subunit to induce proteolytic stress and eventually apoptosis in the target cell.²⁹ It is, however, known that these malignancies are able to evolve resistance to such a treatment. It was thus hypothesized that combining the immunoproteasome activity through an irreversible inhibitor with the release of a cytotoxic payload in the cells would reduce the change of resistance emerging. An immunoproteasome inhibitor-doxorubicin conjugate **6** was therefore designed (Figure 5). The LU-035i group was envisaged to serve as both an immunoproteasome inhibitor and targeting group for delivering doxorubicin. This would provide a one-two-punch strategy to the multiple myeloma cells.

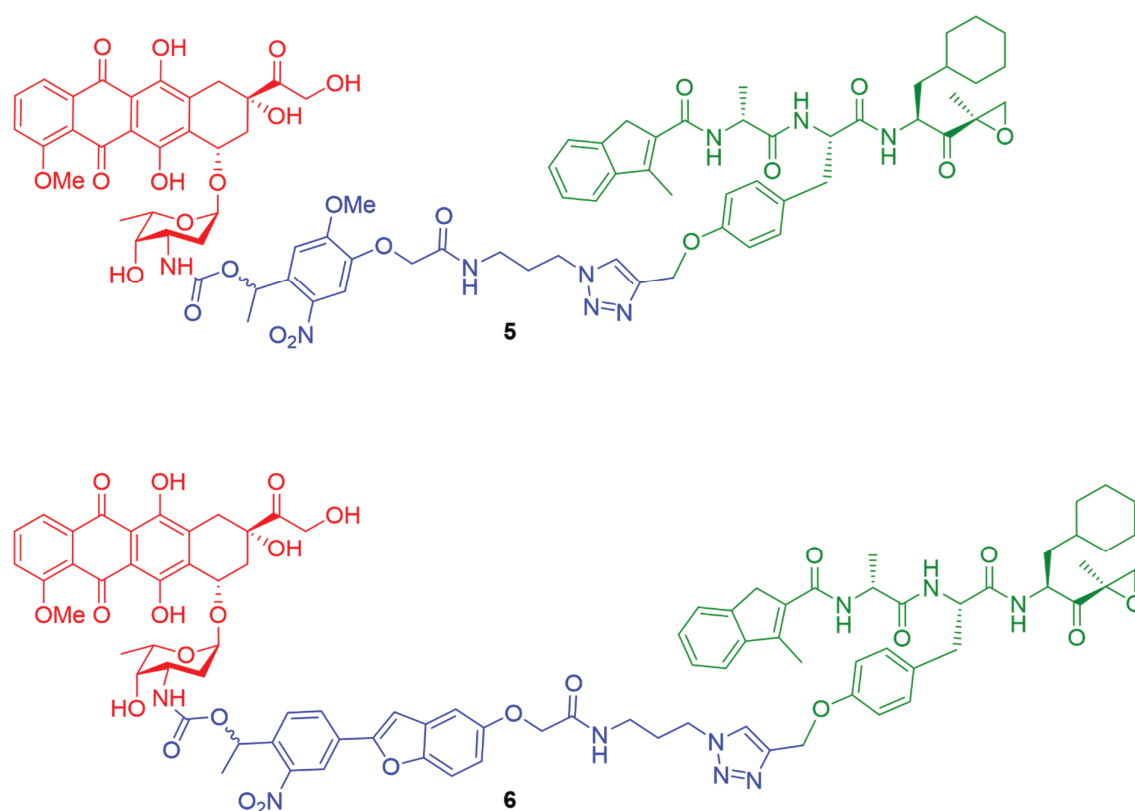


Figure 5. Conjugate consisting of doxorubicin (red) as a cytotoxic payload, bis-functionalized NVOC (blue, 5) or NPBF (blue, 6) as a self-immolative linker and LU-035i (green) as an immunoproteasome-targeting and -inhibiting warhead.

Conjugates **5** and **6** (Figure 5) were made by conjugating the doxorubicin (doxo) amine through a carbamate to either photocleavable linker. It was previously reported that N-acyl derivatives of doxo are non-toxic.²² LU-035i was conjugated to the photocleavable linkers through the tyrosine phenol, which has been shown not to affect its functionality.

A competitive activity-based protein profiling assay confirmed that both conjugates retained their subunit-selectivity (Figure 6A). During initial kinetic experiments it was found that the uncaging rate of conjugate **5** was too low to be viable and was discarded from further assays. The uncaging rate of conjugate **6** at 10 μ M was assessed at 375 nm and 420 nm (Figure 6B) using LC-MS. Quantitative release was observed after 60 s of irradiation with 375 nm light. Phototoxicity of the two wavelengths towards AMO-1 cells was tested in a cell survivability assay (Figure 6C) in which it was clear that the 420 nm light source was more harmful to cell survival. Therefore, further experiments were conducted using the 375 nm light source.

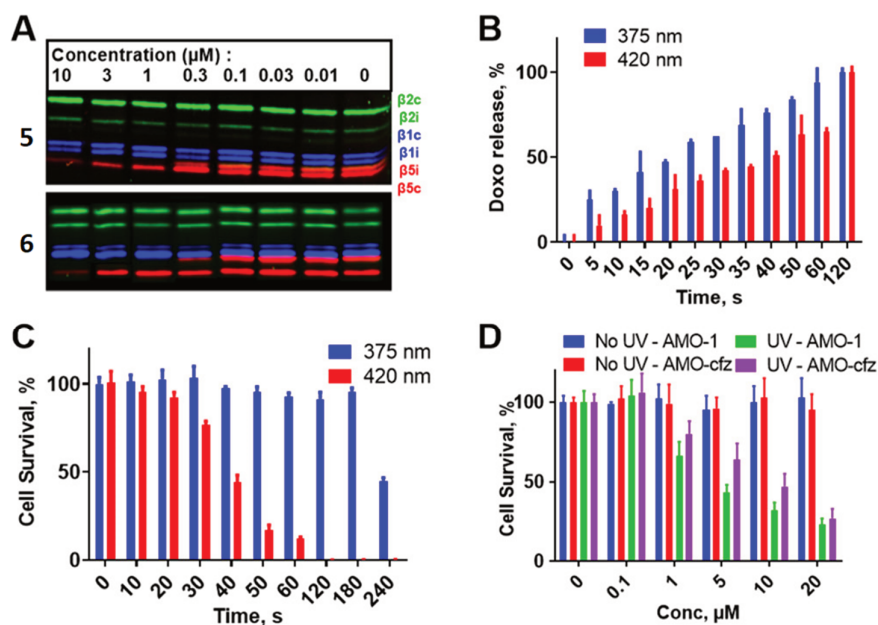


Figure 6. Biological evaluation of conjugates 5 and 6. A) Validation of subunit-selectivity of the conjugates as well as their activity through a competitive activity-based protein profiling assay. B) Release of doxorubicin from conjugate 6 at 10 μM using two different wavelengths as quantified by LC-MS. C) Phototoxicity exhibited by both 375 nm and 420 nm irradiation on AMO-1 cells. D) Dose escalation of conjugate 6 in carfilzomib-sensitive (AMO-1) and carfilzomib-resistant (AMO-cfz) AMO-1 cells in the presence (UV) or absence (No UV) of 375 nm irradiation for 60 seconds. Experiment performed by Elmer Maurits.

The ability of conjugate 6 to induce apoptosis in AMO-1 cells was evaluated next. AMO-1 cells with an acquired resistance for Carfilzomib (an irreversible proteasome inhibitor currently used in the clinic to treat multiple myeloma patients) were also exposed to the conjugate. After treatment of the cells with the conjugate, cells were washed and irradiated for 60 s using 375 nm light. Cell survival was determined three days later (Figure 6D). At a conjugate concentration of 10 μM more than 50% of both cell types were killed when exposed to irradiation.

The combined effect of proteolytic stress induced by LU-035i and poisoning of topoisomerase II by doxorubicin may overcome the resistance that can be acquired by malignant cells that are treated with proteasome inhibitors. This approach can be extended to other mechanism-based hydrolase inhibitors and combinations with highly cytotoxic agents. Although photodynamic therapy is already being applied in oesophageal and lung cancer, this work may aid in broadening the clinical opportunities within this field.³⁰

Photoresponsive OR-gate²

Characterizing individual cells allows the study of functional diversity of a given cell population. Although techniques such as single-cell transcriptomics and proteomics are powerful tools to gain an in-depth understanding of cell states, spatial information is lost upon sample preparation. How environmental signals can influence cell state and differentiation can only be revealed when the spatial context is preserved. In tumours, for example, immune cells can be found in various regions

in the tumour, but how the cell states of these cells correlate to their localization remains poorly understood.³¹

Classical methods that are able to simultaneously determine the localization and phenotypes of individual cells, such as confocal microscopy and immunohistochemistry, are limited by the number of variables analysed. Other, state-of-the-art imaging techniques including multi-ion beam imaging by time of flight (MIBI-TOF)³² and co-detection by indexing (CODEX)³³ do allow analysis of multiple markers on tissue slides. However, these methods are held back by the necessity to decide on which genes or proteins are assessed in advance and their spatial resolution. Analysis of single-cell transcriptomes with a high spatial accuracy has been achieved previously, using tissues from transgenic mouse models that express a photoactivatable green fluorescent protein and consequently switching these only in the regions of interest.³⁴ However, methods that necessitate the use of genetic encoding cannot be translated to analysis of primary human tissues. In response to this several approaches^{35–40}, including Slide-Seq⁴¹, have emerged that enable the correlation of transcriptome data with cellular localization in human tissues. In these types of approaches the transcriptional activity can be analyzed in an unbiased manner, although the data output of gene-expression patterns is often obtained as averages of multiple cells. The specific labeling of cells in a confined region of interest, and consequent single-cell analysis of these cells is not hampered by this limitation, as exemplified by the recently developed ZipSeq method.⁴²

In this work, it was postulated that an NPBF-based reagent could be used to locally ‘mark’ T-cells in a human primary tumour sample to allow for their subsequent single-cell profiling.

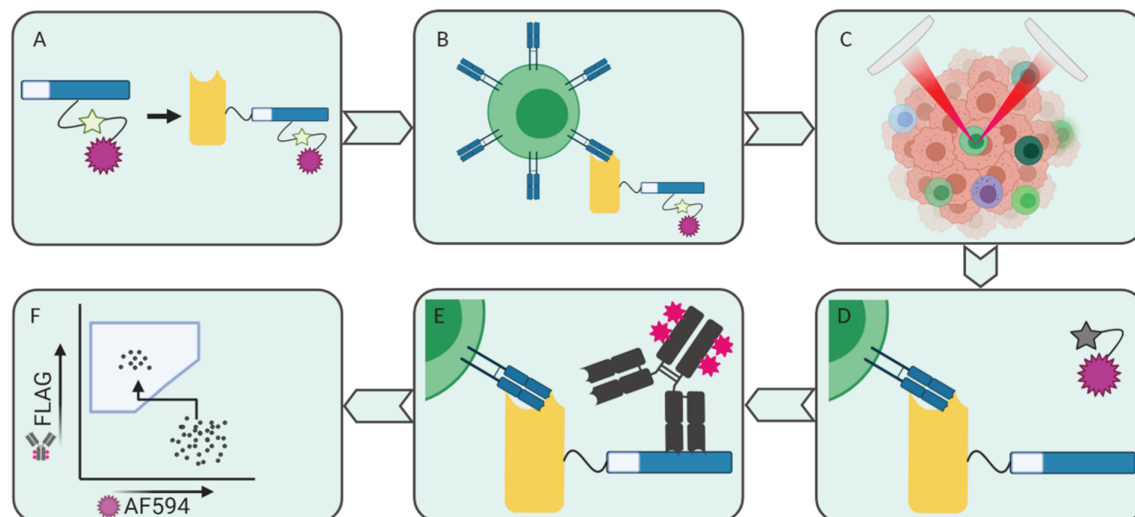


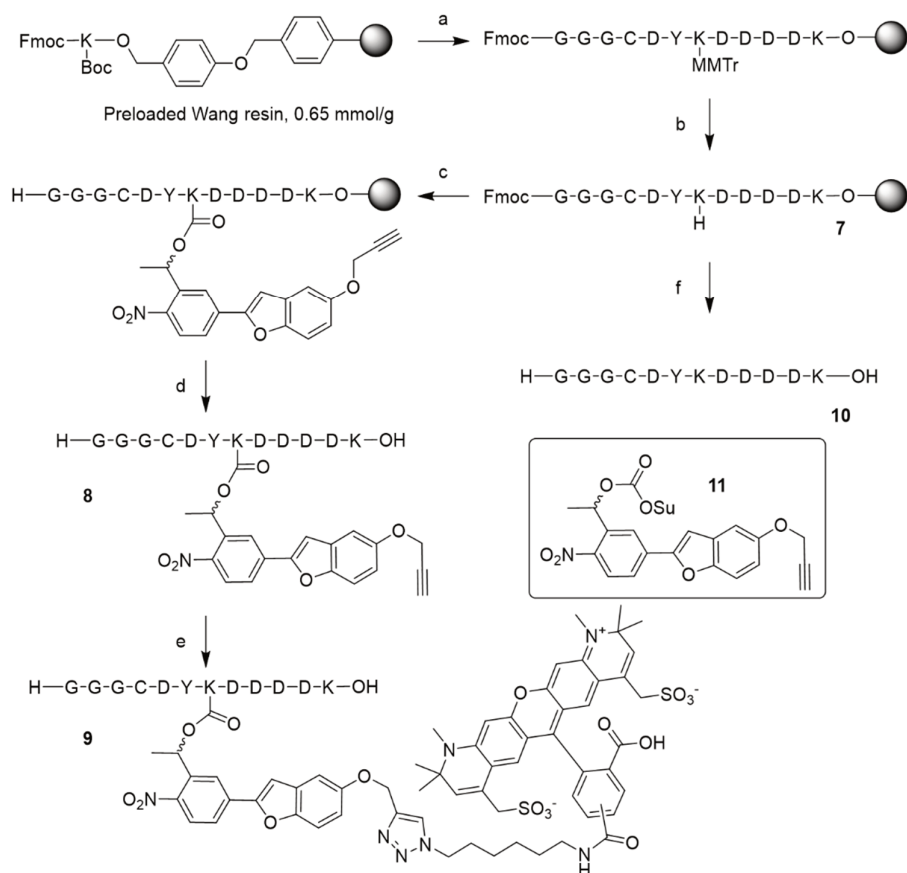
Figure 7. Strategy to tag and identify CD8+ T cells in a tumour sample. A) A peptide fragment containing a sortase recognition sequence (light blue) and a FLAG epitope (dark blue) is caged with a photocleavable linker (green star) containing an AF594 fluorophore (purple badge). This conjugate is ligated to an anti-CD8 nanobody through a sortase-mediated transpeptidation. B) The nanobody conjugate is applied to a tumour block containing CD8+ T cells and binds to CD8-sites. C) The tumour block is spatially-selective photo-irradiated with 405 nm light. D) Irradiation leads to release of the photolinker-fluorophore moiety, thus uncaging the FLAG-epitope. E) The tumour block is treated with fluorescently labeled anti-FLAG antibodies. F) The sample is sorted using FACS. Cells originating from regions-of-interest have been

irradiated and thus their AF594 ‘turned off’ and simultaneously their FLAG signal ‘turned on’, leading to a two-dimensional separation.

The key feature of such a tagging reagent was designed to be a FLAG-tag (DYKDDDDK). This peptide epitope can readily be visualized by staining with a variety of specific antibodies. It also contains multiple lysine residues amenable to protection with an NPBF-group. Most notably, Lys-3 of the epitope, as its protection was found to abolish the selectivity of several FLAG-specific antibodies. The first construct that was made (Scheme 2), contained an N-terminal sortag-motif⁴³ (for conjugating the tag to an anti-CD8 nanobody) followed by an NPBF-caged FLAG-tag. This molecule was next conjugated to an anti-CD8 nanobody dimer and applied to a fresh tumour sample. However, irradiation of the ROIs in the tumour at the phototoxic limit of these primary immune cells did not result in cells that could be distinguished from non-irradiated regions. A second shortcoming in this strategy was that a second fluorescent anti-CD8 antibody had to be added to identify the CD8+ T cell pool in the tumour block. This likely resulted in competition for anti-CD8 binding sites further lowering the maximal signal after deprotection.

To circumvent both of these limitations, a new strategy was devised: the photo-OR-switch (Figure 7). Instead of irradiation leading to an off-to-on-signal, an approach was envisioned in which irradiation would remove one signal whilst simultaneously revealing the FLAG-tag. This would enable the identification of the CD8+ T cell population whilst simultaneously allowing tagging of ROIs within this population, with a single anti-CD8 nanobody dimer conjugate treatment. Furthermore, the disappearance of one signal in conjunction with the appearance of a different signal allows for a two-dimensional separation by flow cytometry.

Scheme 2 depicts the synthesis of the OR-gate probe which was conjugated to an anti-CD8 nanobody dimer. At least three N-terminal glycines were necessary in the OR-gate probe to act as a recognition motif and nucleophile in the sortase-mediated transpeptidation of the probe with a CD8 nanobody dimer. The FLAG-tag was positioned C-terminally in the peptide, of which the center Lys was designated to append the NPBF-linker onto to act as a cage against a suitable anti-FLAG antibody. An alkyne was installed as the second functionality in the NPBF-linker, which was used to click an AlexaFluor 594 group for primary detection of the CD8+ T cells. A cysteine was also included for later conjugation to a second fluorophore. This feature was, however, not exploited in the final construct.



Scheme 2. a) HCTU-mediated Fmoc-based SPPS b) 1% TFA in DCM, r.t., 5 min (10 x) c) i) Compound 11, DiPEA, DCM, r.t., o.n. ii) 20% Piperidine in DMF, r.t., 15 min (3 x) d) TFA, H₂O, TIS, r.t., 2 hr e) AF594 azide, CuI, sodium ascorbate, THPTA, DiPEA, DMSO, r.t., 4 hrs f) i) 20% Piperidine in DMF, r.t., 15 min (3 x) ii) TFA, H₂O, TIS, r.t., 2 hr.

Nonetheless, conjugate **9**, as well as free peptide **10** and photocaged-only peptide **8**, were obtained in sufficient quantities to label anti-CD8 nanobodies ($\alpha\text{CD8}^{\text{D-1}}$). Using a sortase-mediated transpeptidation, $\alpha\text{CD8}^{\text{D-1}}$ nanobodies were conjugated with either **9** (photosensitive tag, 'PsT'), **8** or **10**. Conjugated nanobody PsT was then tested on an in vitro sample of CD8+ T cells (Figure 8). In this manner the feasibility of the approach could be assessed before moving to primary tumour material.

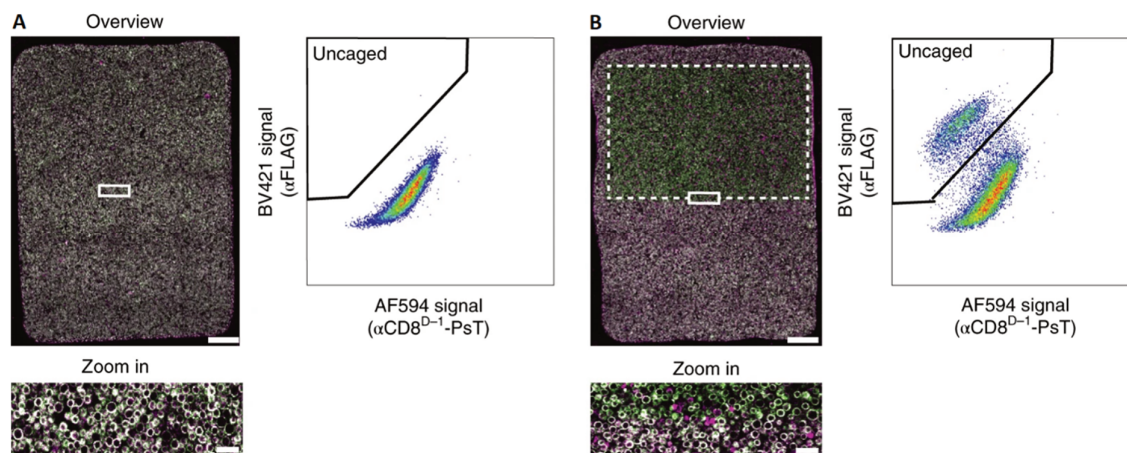


Figure 8. Uncaging of primary human CD8⁺ T cells tagged with PsT. A) Left: Confocal image of CD8⁺ T cells stained with PsT (magenta) and FITC-αCD8^{D-2} (green). Overlapping signals are portrayed as white. The area within the white rectangle is shown at a higher magnification below the image. Scale bars: 100 μm (top), 10 μm (bottom). Right: flow cytometry analysis of the sample after treatment with anti-FLAG antibodies. B) Left: Confocal image of CD8⁺ T cells as in A). The area within the dashed white rectangle has been exposed to 405 nm light. The area within the solid white rectangle is shown at a higher magnification below the image. Scale bars: 100 μm (top), 10 μm (bottom). Right: flow cytometry analysis of the sample after uncaging with 405 nm light and subsequent treatment with anti-FLAG antibodies. Experiment performed by Anne van der Leun, Mirjam Hoekstra and Mireille Toebes.

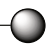
The CD8⁺ T cells were treated with both PsT (exhibiting magenta colour) and FITC-labeled αCD8^{D-2} (exhibiting green colour). Thus, in a non-irradiated sample cells are shown as white due to overlapping signals (Figure 8A, left). Exposure to a 405 nm laser in a designated area led to the loss of the AF594 signal in the exposed area only, causing the T cells to be shown as green only (Figure 8B, left). Flow cytometry analysis of the total sample before (Figure 8A, right) and after (Figure 8B, right) irradiation yields a separate population that can be gated as ‘uncaged’ in a quantitative manner. This probe has subsequently been used to successfully tag and isolate T-cells from ROIs in viable human melanoma and non-squamous cell lung cancer tissues, followed by the sequencing of their transcriptome.²

Experimental section

General methods

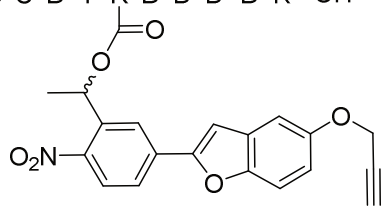
Commercially acquired reagents and solvents were used as received. Anhydrous solvents were prepared with activated 3 Å or 4 Å molecular sieves. All reaction progress was monitored by TLC analysis on Merck aluminum plates pre-coated with silica gel 60 and F254 fluorescent indicator; 254 nm UV light was used to check for compounds, and TLC plates were developed by charring (at approximately 150 °C) plates that were sprayed with permanganate stain (20 g/L KMnO₄ and 10 g/L K₂CO₃ in H₂O), unless stated otherwise. R_f values reported consider the compound being synthesized. Screening Devices silica gel (40-63 µm particle size and 60 Å pore diameter) was used during column chromatography. ¹H and ¹³C NMR spectra were recorded on Bruker AV-400 (400 MHz) and AV-500 (500 MHz) spectrometers. Chemical shifts are reported as δ-values in ppm relative to tetramethylsilane (which was added to CDCl₃) or residual solvent peaks. The ¹³C spectra are proton decoupled. LC-MS checks for all compounds were performed on a Finnigan Surveyor HPLC system with a Gemini C18 50 x 4.60 mm column, which was coupled to a Finnigan LCQ Advantage Max mass spectrometer. LC-MS samples were prepared by dissolving compounds in a tBuOH:ACN:H₂O mixture (1:1:1 by volume).

Compound 7

Fmoc—G—G—C—D—Y—K—D—D—D—K—O— Preloaded Wang resin with Fmoc-Lys(Boc)-OR (0.65 mmol/g; 0.5 mmol, 0.77 g) was used as the starting material in Fmoc SPPS. Fmoc-Asp(*t*-Bu)-OH, Fmoc-Lys(MMTr)-OH, Fmoc-Tyr(*t*-Bu)-OH, Fmoc-Cys(Trt)-OH and Fmoc-Gly-OH were used as the amino acid building blocks. The following automated and repetitive sequence was used: 1) DMF wash and nitrogen purge (1x) 2) Fmoc deprotection using 20% piperidine in DMF (3x5mL) 3) DMF wash (3x) and nitrogen purge 4) Coupling of the amino acid building block (5-fold excess for amino acid, except for Fmoc-Lys(MMTr)-OH for which a 2-fold excess was used) with HCTU (5-fold excess) and DiPEA (10-fold excess) 5) DMF wash (3x) and nitrogen purge 6) Capping of unreacted amines using a mixture of Ac₂O/DiPEA/DMF (20/2/78; v/v/v) 7) DMF wash (3x). A sample (~10 mg) was taken and deprotected by agitation in a mixture of TFA/TIS/H₂O (95/2.5/2.5; v/v/v) for 3 hours. The reaction mixture was filtered and precipitated in Et₂O (-20°C). The precipitate was collected and analyzed by LC-MS (30% AcN in H₂O to 70% AcN in H₂O, C18, TFA, 13 min): R_t = 1.61 min, ESI (m/z): 1509.5 [M+H]⁺. Monomethoxytrityl was removed by swelling the resin in DCM (1 hour), followed by treatment with 1% TFA in DCM (10x3 min.). Completion of the reaction was verified by acetylating a sample (~10 mg) using a mixture of Ac₂O/DiPEA/DMF (20/2/78; v/v/v) after which the peptide was washed with DCM (3x) and deprotected by agitation in a mixture of TFA/TIS/H₂O (95/2.5/2.5; v/v/v) for 3 hours. The reaction mixture was filtered and precipitated in Et₂O (-20°C). The precipitate was collected and analyzed by LC-MS. **LC-MS (3070, C18, H₂O/AcN + TFA, 13 min):** R_t = 2.19 min, ESI (m/z): 1552.3 [M+H]⁺.

Compound 8

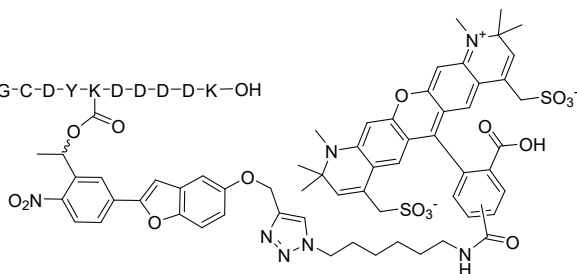
H—G—G—G—C—D—Y—K—D—D—D—K—OH



Compound 7 (25 μmol , 88 mg) was swollen in DCM (1 hour). Compound 11 (30 μmol , 16 mg) and a solution of DiPEA (100 μmol , 17 μL) in DCM (0.5 mL) was added to the resin and the reaction was shaken overnight. A sample (~5 mg) was taken and deprotected by agitation in a mixture of TFA/TIS/ H_2O (95/2.5/2.5; v/v/v) for 3 hours. The reaction mixture was filtered and precipitated in Et_2O (-20°C). The precipitate was collected and analyzed by LC-MS (30% AcN in H_2O to 70% AcN in H_2O , C18, TFA, 13 min): $R_t = 5.78$ min, ESI (m/z): 1873.5 $[\text{M}+\text{H}]^+$. After completion of the reaction was established, the resin was washed with DMF (5x). The resin was treated with a solution of 20% piperidine in DMF (3 x 10min). The resin was washed with DMF (3x) and DCM (5x). A solution of TFA/TIS/ H_2O (95/2.5/2.5; v/v/v) was added and the mixture was shaken for 3 hours. The reaction mixture was filtered and precipitated in Et_2O (-20°C). The precipitate was collected and purified by RP-HPLC. **LC-MS (3070, C18, $\text{H}_2\text{O}/\text{AcN}$ + TFA, 11 min):** $R_t = 4.23$ min, ESI (m/z): 1605.5 $[\text{M}+\text{H}]^+$. **HRMS:** Calculated for $\text{C}_{70}\text{H}_{89}\text{N}_{15}\text{O}_{30}\text{S}$ 1651.56095 $[\text{M}+\text{H}]^+$; found 1651.56094.

Compound 9

H—G—G—G—C—D—Y—K—D—D—D—K—OH



Compound 8 (0.5 μmol , 0.82 mg) was dissolved in DMSO (100 μL). A solution of AFDyeTM594 (0.5 μmol , 0.43 mg (purchased from ClickChemistryTools) in water (100 μL) was added. Solutions of CuSO_4 (0.1 M, 0.5 μmol , 50 μL), THPTA (0.1 M, 0.25 μmol , 2.5 μL) and ascorbic acid (1 M, 5 μmol , 5 μL) in water were purged with N_2 and added. The reaction was shaken under a nitrogen atmosphere for 2 hours. The reaction mixture was diluted with H_2O after which the precipitate was collected by centrifugation. **LC-MS (3070, C18, $\text{H}_2\text{O}/\text{AcN}$ + TFA, 11 min):** $R_t = 2.77$ min, ESI (m/z): 1249.8 $[\text{M}+2\text{H}]^{2+}$

Compound 10

H—G—G—G—C—D—Y—K—D—D—D—K—OH

Compound 7 was swollen in DCM (1 hour) and deprotected by agitation in a mixture of TFA/TIS/ H_2O (95/2.5/2.5; v/v/v) for 3 hours. The reaction mixture was filtered and precipitated in Et_2O (-20°C). The precipitate was collected and purified by RP-HPLC. **LC-MS (3070, C18, $\text{H}_2\text{O}/\text{AcN}$ + TFA, 13 min):** $R_t = 1.61$ min, ESI (m/z): 1509.5 $[\text{M}+\text{H}]^+$.

References

- (1) Maurits, E.; van de Graaff, M. J.; Maiorana, S.; Wander, D. P. A.; Dekker, P. M.; van der Zanden, S. Y.; Florea, B. I.; Neeffes, J. J. C.; Overkleeft, H. S.; van Kasteren, S. I. Immunoproteasome Inhibitor–Doxorubicin Conjugates Target Multiple Myeloma Cells and Release Doxorubicin upon Low-Dose Photon Irradiation. *J. Am. Chem. Soc.* **2020**, *142* (16), 7250–7253.
- (2) van der Leun, A. M.; Hoekstra, M. E.; Reinalda, L.; Scheele, C. L. G. J.; Toebes, M.; van de Graaff, M. J.; Chen, L. Y. Y.; Li, H.; Bercovich, A.; Lubling, Y.; David, E.; Thommen, D. S.; Tanay, A.; van Rheenen, J.; Amit, I.; van Kasteren, S. I.; Schumacher, T. N. Single-Cell Analysis of Regions of Interest (SCARI) Using a Photosensitive Tag. *Nat. Chem. Biol.* **2021**, *17* (11), 1139–1147.
- (3) Savva, A.; Roger, T. Targeting Toll-Like Receptors: Promising Therapeutic Strategies for the Management of Sepsis-Associated Pathology and Infectious Diseases. *Front. Immunol.* **2013**, *4*.
- (4) Hennessy, E. J.; Parker, A. E.; O'Neill, L. A. J. Targeting Toll-like Receptors: Emerging Therapeutics? *Nat. Rev. Drug Discov.* **2010**, *9* (4), 293–307.
- (5) Braunstein, M. J.; Kucharczyk, J.; Adams, S. Targeting Toll-Like Receptors for Cancer Therapy. *Target. Oncol.* **2018**, *13* (5), 583–598.
- (6) Tsujimoto, H.; Ono, S.; Efron, P. A.; Scumpia, P. O.; Moldawer, L. L.; Mochizuki, H. ROLE OF TOLL-LIKE RECEPTORS IN THE DEVELOPMENT OF SEPSIS: *Shock* **2007**, *1*.
- (7) Zuo, L.; Lucas, K.; Fortuna, C. A.; Chuang, C.-C.; Best, T. M. Molecular Regulation of Toll-like Receptors in Asthma and COPD. *Front. Physiol.* **2015**, *6*.
- (8) Lafyatis, R.; Marshak-Rothstein, A. Toll-like Receptors and Innate Immune Responses in Systemic Lupus Erythematosus. *Arthritis Res. Ther.* **2007**, *9* (6), 222.
- (9) Park, B.; Brinkmann, M. M.; Spooner, E.; Lee, C. C.; Kim, Y.-M.; Ploegh, H. L. Proteolytic Cleavage in an Endolysosomal Compartment Is Required for Activation of Toll-like Receptor 9. *Nat. Immunol.* **2008**, *9* (12), 1407–1414.
- (10) Maschalidi, S.; Hässler, S.; Blanc, F.; Sepulveda, F. E.; Tohme, M.; Chignard, M.; van Endert, P.; Si-Tahar, M.; Descamps, D.; Manoury, B. Asparagine Endopeptidase Controls Anti-Influenza Virus Immune Responses through TLR7 Activation. *PLoS Pathog.* **2012**, *8* (8), e1002841.
- (11) Ewald, S. E.; Engel, A.; Lee, J.; Wang, M.; Bogyo, M.; Barton, G. M. Nucleic Acid Recognition by Toll-like Receptors Is Coupled to Stepwise Processing by Cathepsins and Asparagine Endopeptidase. *J. Exp. Med.* **2011**, *208* (4), 643–651.
- (12) Garcia-Cattaneo, A.; Gobert, F.-X.; Muller, M.; Toscano, F.; Flores, M.; Lescure, A.; Del Nery, E.; Benaroch, P. Cleavage of Toll-like Receptor 3 by Cathepsins B and H Is Essential for Signaling. *Proc. Natl. Acad. Sci.* **2012**, *109* (23), 9053–9058.
- (13) Marre, M. L.; Petnicki-Ocwieja, T.; DeFrancesco, A. S.; Darcy, C. T.; Hu, L. T. Human Integrin A3β1 Regulates TLR2 Recognition of Lipopeptides from Endosomal Compartments. *PLoS ONE* **2010**, *5* (9), e12871.
- (14) Mancini, R. J.; Stutts, L.; Moore, T.; Esser-Kahn, A. P. Controlling the Origins of Inflammation with a Photoactive Lipopeptide Immunopotentiator. *Angew. Chem. Int. Ed.* **2015**, *54* (20), 5962–5965.

- (15) Ryu, K. A.; Stutts, L.; Tom, J. K.; Mancini, R. J.; Esser-Kahn, A. P. Stimulation of Innate Immune Cells by Light-Activated TLR7/8 Agonists. *J. Am. Chem. Soc.* **2014**, *136* (31), 10823–10825.
- (16) Stutts, L.; Esser-Kahn, A. P. A Light-Controlled TLR4 Agonist and Selectable Activation of Cell Subpopulations. *ChemBioChem* **2015**, *16* (12), 1744–1748.
- (17) Govan, J. M.; Young, D. D.; Lively, M. O.; Deiters, A. Optically Triggered Immune Response through Photocaged Oligonucleotides. *Tetrahedron Lett.* **2015**, *56* (23), 3639–3642.
- (18) Jemas, A.; Xie, Y.; Pigga, J. E.; Caplan, J. L.; am Ende, C. W.; Fox, J. M. Catalytic Activation of Bioorthogonal Chemistry with Light (CABL) Enables Rapid, Spatiotemporally Controlled Labeling and No-Wash, Subcellular 3D-Patterning in Live Cells Using Long Wavelength Light. *J. Am. Chem. Soc.* **2022**, *144* (4), 1647–1662.
- (19) Yu, D.; Kandimalla, E. R.; Bhagat, L.; Tang, J.-Y.; Cong, Y.; Tang, J.; Agrawal, S. 'Immunomers' novel 3'-3' Linked CpG Oligodeoxyribonucleotides as Potent Immunomodulatory Agents. *Nucleic Acid Res.* **30** (20), 4460–4469.
- (20) Komori, N.; Jakkampudi, S.; Motoishi, R.; Abe, M.; Kamada, K.; Furukawa, K.; Katan, C.; Sawada, W.; Takahashi, N.; Kasai, H.; Xue, B.; Kobayashi, T. Design and Synthesis of a New Chromophore, 2-(4-Nitrophenyl)Benzofuran, for Two-Photon Uncaging Using near-IR Light. *Chem. Commun.* **2016**, *52* (2), 331–334.
- (21) Lu, J.; Jiang, F.; Lu, A.; Zhang, G. Linkers Having a Crucial Role in Antibody–Drug Conjugates. *Int. J. Mol. Sci.* **2016**, *17* (4), 561.
- (22) Trail, P.; Willner, D.; Lasch, S.; Henderson, A.; Hofstead, S.; Casazza, A.; Firestone, R.; Hellstrom, I.; Hellstrom, K. Cure of Xenografted Human Carcinomas by BR96-Doxorubicin Immunoconjugates. *Science* **1993**, *261* (5118), 212–215.
- (23) Kellogg, B. A.; Garrett, L.; Kovtun, Y.; Lai, K. C.; Leece, B.; Miller, M.; Payne, G.; Steeves, R.; Whiteman, K. R.; Widdison, W.; Xie, H.; Singh, R.; Chari, R. V. J.; Lambert, J. M.; Lutz, R. J. Disulfide-Linked Antibody–Maytansinoid Conjugates: Optimization of In Vivo Activity by Varying the Steric Hindrance at Carbon Atoms Adjacent to the Disulfide Linkage. *Bioconjug. Chem.* **2011**, *22* (4), 717–727.
- (24) Spangler, B.; Kline, T.; Hanson, J.; Li, X.; Zhou, S.; Wells, J. A.; Sato, A. K.; Renslo, A. R. Toward a Ferrous Iron-Cleavable Linker for Antibody–Drug Conjugates. *Mol. Pharm.* **2018**, *15* (5), 2054–2059.
- (25) Rossin, R.; van Duijnhoven, S. M. J.; ten Hoeve, W.; Janssen, H. M.; Kleijn, L. H. J.; Hoeben, F. J. M.; Versteegen, R. M.; Robillard, M. S. Triggered Drug Release from an Antibody–Drug Conjugate Using Fast “Click-to-Release” Chemistry in Mice. *Bioconjug. Chem.* **2016**, *27* (7), 1697–1706.
- (26) Versteegen, R. M.; Rossin, R.; ten Hoeve, W.; Janssen, H. M.; Robillard, M. S. Click to Release: Instantaneous Doxorubicin Elimination upon Tetrazine Ligation. *Angew. Chem. Int. Ed.* **2013**, *52* (52), 14112–14116.
- (27) Rossin, R.; Versteegen, R. M.; Wu, J.; Khasanov, A.; Wessels, H. J.; Steenbergen, E. J.; ten Hoeve, W.; Janssen, H. M.; van Onzen, A. H. A. M.; Hudson, P. J.; Robillard, M. S. Chemically Triggered Drug Release from an Antibody–Drug Conjugate Leads to Potent Antitumour Activity in Mice. *Nat. Commun.* **2018**, *9* (1), 1484.

- (28) Wang, Y.; Cheetham, A. G.; Angacian, G.; Su, H.; Xie, L.; Cui, H. Peptide–Drug Conjugates as Effective Prodrug Strategies for Targeted Delivery. *Adv. Drug Deliv. Rev.* **2017**, *110–111*, 112–126.
- (29) de Bruin, G.; Huber, E. M.; Xin, B.-T.; van Rooden, E. J.; Al-Ayed, K.; Kim, K.-B.; Kisselev, A. F.; Driessen, C.; van der Stelt, M.; van der Marel, G. A.; Groll, M.; Overkleeft, H. S. Structure-Based Design of B1i or B5i Specific Inhibitors of Human Immunoproteasomes. *J. Med. Chem.* **2014**, *57* (14), 6197–6209.
- (30) Chen, M.; Pennathur, A.; Luketich, J. D. Role of Photodynamic Therapy in Unresectable Esophageal and Lung Cancer. *Lasers Surg. Med.* **2006**, *38* (5), 396–402.
- (31) Thommen, D. S.; Schumacher, T. N. T Cell Dysfunction in Cancer. *Cancer Cell* **2018**, *33* (4), 547–562.
- (32) Keren, L.; Bosse, M.; Thompson, S.; Risom, T.; Vijayaragavan, K.; McCaffrey, E.; Marquez, D.; Angoshtari, R.; Greenwald, N. F.; Fienberg, H.; Wang, J.; Kambham, N.; Kirkwood, D.; Nolan, G.; Montine, T. J.; Galli, S. J.; West, R.; Bendall, S. C.; Angelo, M. MIBI-TOF: A Multiplexed Imaging Platform Relates Cellular Phenotypes and Tissue Structure. *Sci. Adv.* **2019**, *5* (10), eaax5851.
- (33) Goltsev, Y.; Samusik, N.; Kennedy-Darling, J.; Bhate, S.; Hale, M.; Vazquez, G.; Black, S.; Nolan, G. P. Deep Profiling of Mouse Splenic Architecture with CODEX Multiplexed Imaging. *Cell* **2018**, *174* (4), 968–981.e15.
- (34) Medaglia, C.; Giladi, A.; Stoler-Barak, L.; De Giovanni, M.; Salame, T. M.; Biram, A.; David, E.; Li, H.; Iannacone, M.; Shulman, Z.; Amit, I. Spatial Reconstruction of Immune Niches by Combining Photoactivatable Reporters and ScRNA-Seq. *Science* **2017**, *358* (6370), 1622–1626.
- (35) Moncada, R.; Barkley, D.; Wagner, F.; Chiodin, M.; Devlin, J. C.; Baron, M.; Hajdu, C. H.; Simeone, D. M.; Yanai, I. Integrating Microarray-Based Spatial Transcriptomics and Single-Cell RNA-Seq Reveals Tissue Architecture in Pancreatic Ductal Adenocarcinomas. *Nat. Biotechnol.* **2020**, *38* (3), 333–342.
- (36) Vickovic, S.; Eraslan, G.; Salmén, F.; Klughammer, J.; Stenbeck, L.; Schapiro, D.; Äijö, T.; Bonneau, R.; Bergensträhle, L.; Navarro, J. F.; Gould, J.; Griffin, G. K.; Borg, Å.; Ronaghi, M.; Frisén, J.; Lundeberg, J.; Regev, A.; Ståhl, P. L. High-Definition Spatial Transcriptomics for in Situ Tissue Profiling. *Nat. Methods* **2019**, *16* (10), 987–990.
- (37) Thrane, K.; Eriksson, H.; Maaskola, J.; Hansson, J.; Lundeberg, J. Spatially Resolved Transcriptomics Enables Dissection of Genetic Heterogeneity in Stage III Cutaneous Malignant Melanoma. *Cancer Res.* **2018**, canres.0747.2018.
- (38) Maniatis, S.; Äijö, T.; Vickovic, S.; Braine, C.; Kang, K.; Mollbrink, A.; Fagegaltier, D.; Andrusivová, Ž.; Saarenpää, S.; Saiz-Castro, G.; Cuevas, M.; Watters, A.; Lundeberg, J.; Bonneau, R.; Phatnani, H. Spatiotemporal Dynamics of Molecular Pathology in Amyotrophic Lateral Sclerosis. *Science* **2019**, *364* (6435), 89–93.
- (39) Berglund, E.; Maaskola, J.; Schultz, N.; Friedrich, S.; Marklund, M.; Bergensträhle, J.; Tarish, F.; Tanoglidi, A.; Vickovic, S.; Larsson, L.; Salmén, F.; Ogris, C.; Wallenborg, K.; Lagergren, J.; Ståhl, P.; Sonnhämmer, E.; Helleday, T.; Lundeberg, J. Spatial Maps of Prostate Cancer Transcriptomes Reveal an Unexplored Landscape of Heterogeneity. *Nat. Commun.* **2018**, *9* (1), 2419.
- (40) Ståhl, P. L.; Salmén, F.; Vickovic, S.; Lundmark, A.; Navarro, J. F.; Magnusson, J.; Giacomello, S.; Asp, M.; Westholm, J. O.; Huss, M.; Mollbrink, A.; Linnarsson, S.

- Codeluppi, S.; Borg, Å.; Pontén, F.; Costea, P. I.; Sahlén, P.; Mulder, J.; Bergmann, O.; Lundeberg, J.; Frisén, J. Visualization and Analysis of Gene Expression in Tissue Sections by Spatial Transcriptomics. *Science* **2016**, *353* (6294), 78–82.
- (41) Rodriques, S. G.; Stickels, R. R.; Goeva, A.; Martin, C. A.; Murray, E.; Vanderburg, C. R.; Welch, J.; Chen, L. M.; Chen, F.; Macosko, E. Z. Slide-Seq: A Scalable Technology for Measuring Genome-Wide Expression at High Spatial Resolution. **2019**, 6.
- (42) Hu, K. H.; Eichorst, J. P.; McGinnis, C. S.; Patterson, D. M.; Chow, E. D.; Kersten, K.; Jameson, S. C.; Gartner, Z. J.; Rao, A. A.; Krummel, M. F. ZipSeq: Barcoding for Real-Time Mapping of Single Cell Transcriptomes. *Nat. Methods* **2020**, *17* (8), 833–843.
- (43) Popp, M. W.; Antos, J. M.; Grotenbreg, G. M.; Spooner, E.; Ploegh, H. L. Sortagging: A Versatile Method for Protein Labeling. *Nat. Chem. Biol.* **2007**, *3* (11), 707–708.

Nederlandse Samenvatting

Het immuunsysteem beschikt over de mogelijkheid om onderscheid te kunnen maken tussen cellen van het lichaam zelf en die van indringende pathogene microben. Dat realiseert deze met receptoren die een sterke affiniteit hebben voor moleculaire patronen die zich altijd voordoen op microben. Die patronen liggen ten grondslag van de vitaliteit van de microbe, waardoor mutaties in deze patronen niet vaak voorkomen en de receptor dus altijd functioneel blijft. Een familie van deze receptoren is de Toll-Like Receptor (TLR) familie. Deze TLRs bevinden zich voornamelijk op cellen van het immuunsysteem die door het lichaam patrouilleren, en kunnen de aanwezigheid van bacteriën en virussen waarnemen zowel binnen als buiten hun cel.

Als een TLR geactiveerd wordt, resulteert dit uiteindelijk in twee soorten responsen. De eerste respons is een direct antwoord op de indringer en gebruikt een niet-specifieke aanval die over het algemeen goed werkt tegen pathogenen. Dit wordt het aangeboren immuunsysteem genoemd. Het tweede respons werkt op een langere termijn, en zet het immuunsysteem aan het werk om specifieke antilichamen te maken tegen de indringende microbe. Dit wordt het adaptieve immuunsysteem genoemd, en de kracht van de respons treedt pas na enkele dagen in werking. Wat voor soort respons er gegenereerd wordt, hoe sterk deze is en de robuustheid van de immuniteit die verworven wordt erdoor hangt allemaal af van welke TLRs er op welk moment en in welke locatie van de cel geactiveerd worden. Absolute kennis van hoe deze families van receptoren signalen doorvoeren is daarom van groot belang bij het ontwerpen van moderne vaccins.

Dit proefschrift beschrijft de synthese van moleculen die gebruikt kunnen worden om te onderzoeken hoe TLRs hun signalen doorgeven. Deze moleculen beschikken over de mogelijkheid om te binden aan een TLR zonder een signaal te initiëren. Dit wordt bewerkstelligd door een groep te introduceren op het molecuul die juist dat gedeelte afschermt die cruciaal is voor de receptor om een signaal door te geven. Deze groep wordt ook wel de ‘cage’ genoemd. Pas als er een reagens wordt toegevoegd die de cage eraf haalt, wordt het signaal doorgegeven. Dit geeft de chemisch bioloog controle over waar en wanneer zij bepaalde TLRs wil activeren in de cel, ook wel ‘spatiotemporal control’ genoemd.

Hoofdstuk 1 beschrijft kort hoe het immuunsysteem werkt, welke receptoren daar betrokken bij zijn en de plaats van TLRs daarin. Hierna wordt de focus gelegd op de liganden voor de TLRs, ofwel moleculen die de receptoren kunnen activeren, en welke cages gebruikt kunnen worden om hun activiteit te beheersen. De eigenschappen alsmede de mechanismes waarmee deze cages kunnen worden ontschermd is beschreven in dit hoofdstuk.

Hoofdstuk 2 beschrijft de ontwikkeling van een TLR2/6 ligand waarvan zijn activiteit beheerst kan worden met het gebruik van een *trans*-cyclooctene (TCO) cage. De totstandkoming van dat molecuul is een proces geweest met continue aanpassingen gebaseerd op resultaten uit een nauwe samenwerking met een immunoloog werkend in het LUMC, Timo Oosenbrug. Deze biologische resultaten zijn ook in dit hoofdstuk verwerkt om het proces beter te kunnen beschrijven en illustreren. Uit deze samenwerking is een molecuul verworven die sterk bindt aan TLR2 zonder dat deze een signaal induceert. Pas als een tetrazine reagens wordt toegevoegd, valt de signaalinductie instantaan te volgen door de tijd. Het tetrazine reagens zou aangepast kunnen worden waardoor slechts de intra- of extracellulaire populatie van TLRs wordt geactiveerd.

Hoofdstuk 3 rapporteert de synthese en biologische analyse van conditioneel controleerbare liganden voor de intracellulaire TLRs 4, 7/8 en 9. Voor de TLRs 4 en 7/8 worden twee kleine, synthetische liganden gebruikt om een TCO op een cruciale plek in te bouwen en zo een conditionele controleerbaarheid te bewerkstelligen. Naast het gebruik van een enkel-gefunctionaliseerde TCO als cage, wordt hier ook een dubbel-gefunctionaliseerde TCO gebruikt als cage. Deze beschikt over een tweede positie waar een amine-bevattend molecuul op geïnstalleerd kan worden. In de context van TLR4 wordt deze functionaliteit gebruikt om het oplosbaarheidsvermogen van het product in water te verhogen. In de context van TLR 7/8 wordt deze functionaliteit gebruikt een anti-tumor antilichaam te decoreren met het beschermd ligand. Resultaten hieruit zijn gebruikt in een patentaanvraag voor selectieve levering van TLR-liganden in tumoren: het ligand activeert pas het immuunsysteem nadat de meerderheid zich in de tumor bevindt en het niet-toxische tetrazine wordt toegediend om het ligand te bevrijden. TLR 9 wordt geactiveerd door DNA die 'CpG' motieven bevatten. Omdat er nog geen kleine synthetische liganden bestaan voor TLR 9, is er getracht om een TCO te installeren op een cytosine (de 'C' in CpG) in een enkelstrengs DNA. Hiervoor is een cytosine bouwsteen gemodificeerd met een TCO zodat deze gebruikt kan worden in vaste-dragers DNA-synthese om zo een TCO-beschermde CpG-bevattende enkelstrengs DNA fragment te bekomen.

Hoofdstuk 4 examineert het gebruik van licht-gevoelige cages in de context van TLR-liganden. Waar tetrazine de 'trigger' is voor TCO-cages, is UV-licht de 'trigger' voor deze cages. TLR-liganden die beschermd zijn met de laatstgenoemde bleken over het algemeen compleet onoplosbaar in water. Dit hoofdstuk tracht daarom een extra functionaliteit in deze cages in te brengen, analoog tot de dubbel-gefunctionaliseerde TCO gebruikt in hoofdstuk 3. Deze functionaliteit is gebruikt om moleculaire motieven in te brengen die de oplosbaarheid in water zouden veelvoudigen. Deze strategie is toegepast op klassieke licht-gevoelige cages, maar ook op zeer recent-ontwikkelde cages. Het effect van deze modificatie op de photo-chemische eigenschappen is onderzocht met een in-huis ontwikkelde opstelling en bleek de extinctiecoëfficiënt met 30% te verhogen. De toepasbaarheid van deze nieuwe, dubbel-gefunctionaliseerde cage buiten de context van TLRs is onderzocht in het opvolgend hoofdstuk.

Hoofdstuk 5 geeft een samenvatting van elk hoofdstuk en projecteert potentiële toekomstige experimenten die hun waarde vinden binnen elk onderzoeksgebied. Hiernaast zijn enkele resultaten beschreven die behaald zijn met de dubbel-gefunctionaliseerde licht-gevoelige cage beschreven in hoofdstuk 4. Zo is deze gebruikt om een construct te verwerven die sterk en selectief sub-units van het immunoproteasoom inhibeert waar, na het kort bestralen met laag energetisch UV-licht, het zeer toxische doxorubicin bevrijd wordt. Deze 'one-two-punch' strategie is succesvol in het doden van multiple myeloma cellen die immuniteit hebben ontworpen voor enkel het immunoproteasoom inhibitor. Ook is de cage gebruikt als brug tussen een sortase-tag en fluorophore. Dit construct is geconjugeerd aan een nanolichaam specifiek voor CD8, en is gebruikt om een twee-dimensionale scheiding op de FACS te verkrijgen van laagenergetisch UV-bestraalde CD8⁺ cellen binnen een tumor block. Met deze techniek kunnen individuele cellen binnen specifieke tumorale regio's gesequenced worden, om zo de specifieke immuuncelpopulaties binnen een tumor op te helderen.

List of publications

1) Single-cell analysis of regions of interest (SCARI) using a photosensitive tag

Anne M. van der Leun, Mirjam E. Hoekstra, Luuk Reinalda, Colinda L. G. J. Scheele, Mireille Toebe, Michel J. van de Graaff, Linda Y. Y. Chen, Hanjie Li, Akhiad Bercovich, Yaniv Lubling, Eyal David, Daniela S. Thommen, Amos Tanay, Jacco van Rheenen, Ido Amit, Sander I. van Kasteren, Ton N. Schumacher

Nat. Chem. Biol. **2021**, *17*, 1139-1147

2) Simplified monopalmitoyl Toll-like Receptor 2 ligand mini-UPam for self-adjuvanting neoantigen-based synthetic cancer vaccines

Thomas C. van den Ende, Jeroen M. M. Heuts, Geoffroy P. P. Gentil, Marten Visser, Michel J. van de Graaff, Nataschja I. Ho, Wim Jiskoot, A. Rob P. M. Valentijn, Nico J. Meeuwenoord, Herman S. Overkleeft, Jeroen D. C. Codée, Sjoerd H. van der Burg, Els M. E. Verdegaal, Gijsbert A. van der Marel, Ferry Ossendorp, Dmitri V. Filippov

ChemBioChem **2021**, *22*, 1215-1222

3) Immunoproteasome inhibitor–doxorubicin conjugates target multiple myeloma cells and release doxorubicin upon low-dose photon irradiation

Michel J. van de Graaff, Elmer Maurits, Santina Maiorana, Dennis P. A. Wander, Patrick M. Dekker, Sabina Y. van der Zanden, Bogdan I. Florea, Jacques J. C. Neefjes, Herman S. Overkleeft*, and Sander I. van Kasteren

J. Am. Chem. Soc. **2020**, *142* (16), 7250-7253

4) An alternative model for type I interferon induction downstream of human TLR2

Timo Oosenbrug, Michel J. van de Graaff, Mariëlle C. Haks, Sander I. van Kasteren, Maaïke E. Rensing

J. Biol. Chem. **2020**, *295* (42), 14325-14342

5) Conditionally controlling human TLR2 activity via trans-cyclooctene caged ligands

Michel J. van de Graaff, Timo Oosenbrug, Mikkell H. S. Marqvorsen, Clarissa R. Nascimento, Mark A. R. de Geus, Bénédicte Manoury, Maaïke E. Rensing, and Sander I. van Kasteren

Bioconjug. Chem. **2020**, *31* (6), 1685-1692

6) Peptides conjugated to 2-alkoxy-8-oxo-adenine as potential synthetic vaccines triggering TLR7

Geoffroy P.P. Gential, Tim P. Hogervorst, Elena Tondini, Michel J. van de Graaff, Herman S. Overkleeft, Jeroen D.C. Codée, Gijsbert A. van der Marel, Ferry Ossendorp, Dmitri V. Filippov

Bioorganic Med. Chem. Lett. **2019**, *29* (11), 1340-1344

7) Chemical tools for studying TLR signaling dynamics

Michel J. van de Graaff, Timo Oosenbrug, Maaïke E. Rensing, Sander I. van Kasteren

Cell Chem. Biol. **2017**, *24* (7), 801-812

8) The optimization of bioorthogonal epitope ligation within MHC-I complexes

Joanna B. Pawlak, Brett J. Hos, Michel J. van de Graaff, Otty A. Megantari, Nico Meeuwenoord, Herman S. Overkleeft, Dmitri V. Filippov, Ferry Ossendorp, and Sander I. van Kasteren

ACS Chem. Biol. **2016**, *11* (11), 3172-3178

Curriculum Vitae

Michel Johan van de Graaff was born on the 8th of April 1991 in Delft, the Netherlands. After graduating from the high school Stanislascollege Westplantsoen (VWO) in 2009, he started the bachelor Molecular Science and Technology at the Leiden University and the Delft University of Technology. During his bachelor programme in 2012, he spent one year as a board member of the chemistry study association, Chemisch Dispuut Leiden (CDL).

In 2013 he obtained his bachelor degree and continued his education with the master program Chemistry at the Leiden University. His research internship in the Bio-organic Synthesis group under supervision of dr. Geoffroy Gentil focused on the synthesis of TLR-ligands and their synthetic-long peptide conjugates thereof. In 2015 he obtained his master's degree *cum laude*. From September 2015 until December 2019, he conducted his PhD studies in the Bio-organic Synthesis department of the Leiden Institute of Chemistry, under the supervision of dr. Sander I. van Kasteren. Part of his research was presented orally at NWO CHAINS in Veldhoven (2018) and with posters during NWO CHAINS (2017) and the 4th annual symposium of the Institute of Chemical Immunology in Amsterdam (2018).

Since January 2020, he is working as a Formulation Scientist at SeraNovo B.V. in Leiden.

Acknowledgements

The final days of experimentation in the laboratory marked my 10th anniversary at the Leiden University. It has been an incredible journey: a meandering path carved out by curiosity, with its wearisome hills and invigorating valleys. And although the ultimate goal was always clear, becoming an educated and independent researcher, it turned out to be overshadowed by the sheer joy of being able to spend this chapter of my life with so many gifted and kind people. I am leaving behind not only a workplace, but a wonderful community. I have learned it takes a conscious effort to not take things for granted, and so in light of this, I would like to express my gratitude to everyone who contributed to the culmination of my rewarding experience at the Leiden University.

In particular, I would like to thank Sander van Kasteren and Hermen Overkleef for their roles as promoters and for granting me this wonderful opportunity. Sander, your boundless energy, creativity and enthusiasm proved contagious and was the fuel that drove my engine. You entrusted me with exploring my own ideas which made my time in the fume hood a real pleasure.

A special thanks goes out to Timo Oosenbrug, without whom this thesis would have lacked severely in depth and significance. Timo, you are an excellent and disciplined researcher and I would like to thank you for the fruitful and interactive collaboration we have had over the past years.

Gijs van der Marel, Jeroen Codée, Dmitri Filippov and Mark Overhand I would like to thank for the teachings and lectures during my Bachelor and Master studies. Your passion for organic chemistry made each lecture a luxury to indulge. Gerbrand van der Heden van Noort and Geoffroy Gentil are thanked for their supervision during my Bachelor and Master internships and to have provided me with the practical skills needed to pursue my Ph.D. research. Hans van den Elst and Nico Meeuwenoord I would like to both thank for their help in synthesizing DNA and peptide fragments as well as their purification. A word of apology to them might also be in order, for the persistence of most final compounds to not solubilize in any slightly polar solvent *almost* exceeded my persistence to request yet another purification. Richard van den Berg, Bobby Florea, Rian van den Nieuwendijk, Fons Lefeber and Karthick Sai Sankar Gupta are thanked for all their efforts to keep things running smoothly in and around the laboratories as well as so many of the important facilities that lie at the root of the distinguished research being done here at Leiden.

Interdisciplinary research thrives in its collaborations and so in consideration of this I would like to thank Marc Robillard, Ton Schumacher, Bénédicte Manoury, Maaïke Ressing, Anne van der Leun, Mirjam Hoekstra, Colinda Scheele, Mireille Toebes, Mark de Geus, Elmer Maurits, Mikkell Marqvorsen, Clarissa Nascimento and Joanna Pawlak for the pleasant and rewarding collaborations we have shared over the past years.

The Biosyn group spans several corridors and floors and thus thanking everyone will definitely prove a futile endeavour. However, I would like everyone to know that I sincerely enjoyed every coffee break, Science Club drink, 'tosti lunch', Woo Ping, Beaujolais or any other get-together, albeit under the guise of an intellectual discussion or perhaps rather in the complete absence thereof. Know that I often think back of my time at the University and that so many of you contributed to

this gift I take with me. In particular I would like to thank Thomas, Jerre, Shimrit, Alexi, Ward, Nancy and Mirjam for some of my best memories made and friendships forged.

Finally, I would like to thank my friends, family and my dearest Claudia. Even though I look back on this chapter with bliss, I cannot deny that there have been times defined by hardships and stress. During those times, you were always there to provide a listening ear or plenty of distractions to look forward to instead. Without you, this is all meaningless. And for that you have my deepest gratitude.